

## **General Disclaimer**

### **One or more of the Following Statements may affect this Document**

- This document has been reproduced from the best copy furnished by the organizational source. It is being released in the interest of making available as much information as possible.
- This document may contain data, which exceeds the sheet parameters. It was furnished in this condition by the organizational source and is the best copy available.
- This document may contain tone-on-tone or color graphs, charts and/or pictures, which have been reproduced in black and white.
- This document is paginated as submitted by the original source.
- Portions of this document are not fully legible due to the historical nature of some of the material. However, it is the best reproduction available from the original submission.

NASA CR-135178

DESIGN STUDY OF SUPERCONDUCTING MAGNETS FOR A  
COMBUSTION MAGNETOHYDRODYNAMIC (MHD) GENERATOR

(NASA-CR-135178) DESIGN STUDY OF  
SUPERCONDUCTING MAGNETS FOR A COMBUSTION  
MAGNETOHYDRODYNAMIC (MHD) GENERATOR

N77-20886

(Magnetic Corp. of America, Waltham, Mass.)  
255 p HC A12/MF A01

CSSL 20I G3/75

Unclas  
24642

Richard J. Thome and John W. Ayers

MAGNETIC CORPORATION OF AMERICA

Prepared For

NATIONAL AERONAUTICS AND SPACE ADMINISTRATION

NASA Lewis Research Center

Contract NAS 3-19885



1. Report No. NASA CR-135178		2. Government Accession No.		3. Recipient's Catalog No.	
4. Title and Subtitle Design Study of Superconducting Magnets for a Combustion Magnetohydrodynamic (MHD) Generator				5. Report Date March, 1977	
				6. Performing Organization Code	
7. Author(s) Richard J. Thome and John W. Ayers				8. Performing Organization Report No. NAS-03	
9. Performing Organization Name and Address Magnetic Corporation of America 179 Bear Hill Road Waltham, Massachusetts 02154				10. Work Unit No.	
				11. Contract or Grant No. NAS 3-19885	
12. Sponsoring Agency Name and Address National Aeronautics and Space Administration Washington, D.C. 20546				13. Type of Report and Period Covered Contractor Report	
				14. Sponsoring Agency Code	
15. Supplementary Notes Technical Manager, James A. Burkhart, Plasma Physics Branch, Plasma Flow Section, NASA-Lewis Research Center, Cleveland, Ohio					
16. Abstract  Design trade off studies for 13 different superconducting magnet systems have been carried out. Based on these results, preliminary design characteristics have been prepared for several superconducting magnet systems suitable for use with a Combustion Driven MHD generator. Each magnet generates a field level of 8 T in a volume 1.524 m (60 in.) long with a cross section 0.254 m x 0.254 m (10 in. x 10 in.) at the inlet and 0.406 m x 0.406 m (16 in. x 16 in.) at the outlet. The first design involves a racetrack coil geometry intended for operation at 4.2 K, the second design uses a racetrack geometry at 2.0 K, and the third design utilizes a rectangular saddle geometry at 4.2 K. Each case was oriented differently in terms of MHD channel axis and main field direction relative to gravity in order to evaluate fabrication ease. All cases were designed such that the system could be disassembled to allow for alteration of field gradient in the MHD channel by changing the angle between coils. Preliminary design characteristics and assembly drawings were generated for each case.  <b>ORIGINAL PAGE IS OF POOR QUALITY</b>					
17. Key Words (Suggested by Author(s)) Superconducting Magnet, Magnetohydrodynamic (MHD)			18. Distribution Statement Unclassified		
19. Security Classif. (of this report) Unclassified		20. Security Classif. (of this page) Unclassified		21. No. of Pages 254	22. Price*

FOREWORD

This report was prepared by Magnetic Corporation of America, 179 Bear Hill Road, Waltham, Massachusetts 02154 under NASA Contract No. NAS 3-19885.

The work was administered under the direction of the Plasma Physics Branch, Plasma Flow Section, NASA-Lewis Research Center, Cleveland, Ohio. Mr. James A. Burkhardt served as Technical Manager on the program.

This report describes work performed during the period September 1975 to December 1976. The authors wish to acknowledge contributions to the effort by Z. J. J. Stekly, E. J. Lucas, T. M. Hrycaj, R. J. Camille, F. B. Punched, W. R. Mann, J. Minervini, and P. M. G. Margosian.

TABLE OF CONTENTS

	<u>Page</u>
I. SUMMARY	1
II. INTRODUCTION	3
III. PRELIMINARY DESIGN TRADEOFFS	9
A. State of the Art	9
B. System Configuration and Characteristics	17
C. System Cost Estimates	31
D. Design Considerations	52
E. Selection of Configuration for Analysis	70
IV. 8 T RACETRACK, 4.2 K SYSTEM	73
A. System Description	73
B. Winding Geometry and Field Characteristics	90
C. Structure and Dewar Design	107
V. 8 T RACETRACK, REDUCED TEMPERATURE SYSTEM	129
A. System Description	130
B. Winding Geometry and Field Characteristics	145
C. Structure and Dewar Design	165
VI. 8 T RECTANGULAR SADDLE, 4.2 K SYSTEM	173
A. System Description	173
B. Winding Geometry and Field Characteristics	191
C. Structure and Dewar Design	208
VII. COST ESTIMATES AND DISCUSSION OF RESULTS	221
A. Phase I Results	221
B. Characteristics of Phase II Preliminary Design	222
C. Estimation of Costs for Preliminary Design Nos. 1, 2, and 3	229
VIII. SUMMARY	233
APPENDIX A. EFFECT OF ACCESS PORTS ON THE FIELD IN THE MHD CHANNEL	235
APPENDIX B. STABILITY CRITERIA	241

PRECEDING PAGE BLANK NOT FILMED

## I. SUMMARY

The main goal of this effort was to prepare preliminary designs for three superconducting magnet systems for a combustion driven MHD generator. The program was carried out in two phases. In Phase I alternate design concepts were evaluated to provide sufficient information to allow three to be chosen for the Phase II preliminary design phase.

Phase I concentrated on the relative importance of different winding geometries, superconductors, field levels, operating temperatures, and whether or not iron should be used for field enhancement. Solenoidal, racetrack, rectangular saddle, and annular saddle geometries were evaluated. The rectangular saddle was carried into Phase II because of its efficient use of material and the racetrack was chosen because of its simplicity in fabrication. The 8 T level was selected for all systems, and the decision was made to utilize a limited amount of iron for field enhancement in the MHD channel and for field reduction at the superconducting windings. All systems utilized NbTi since preliminary cost estimates indicated that this material would be most economical for this application.

Preliminary Design No. 1 was based on a racetrack geometry at 4.2 K, No. 2 on a racetrack geometry at 2.0 K, and No. 3 on a rectangular saddle geometry at 4.2 K. Furthermore, each design was carried out such that the system could be disassembled periodically to allow for alteration of field profile on the MHD channel axis by changing the angle between coils. Preliminary design evaluation and preparation of preliminary layout drawings has led to the conclusion that each system is feasible. A program of supporting development will be necessary in any case during final design. One area of particular importance will involve experimental verification of stable superconducting operating conditions for the winding construction finally chosen. This is particularly true if the 2.0 K case (Preliminary Design No. 2) is chosen since little information is available concerning stability criterion in He II.

Results imply that the rectangular saddle (Design No. 3) will be substantially more economical to design and build than any of the racetracks considered. For the racetrack geometry, operation at 2.0 K implies a somewhat less costly system than operation at 4.2 K. The cost of refrigeration or of supporting development was not included, however.

## II. INTRODUCTION

This program involved a trade-off and preliminary design study on concepts for a superconducting magnet system for a Combustion Magnetohydrodynamic (MHD) Generator. This allows an insight to be gained into the magnitude of the project in terms of physical characteristics and cost. It also allows potential interface problem areas to become evident and allows estimates to be made of any development required.

There is no MHD test facility in the U.S. at the present time which utilizes a superconducting magnet system even though the magnetic field provides the coupling mechanism for the power generation process and must be provided by a superconducting magnet if efficient power generation is to take place. The winding geometry required for this application is complex, and the superconducting magnets of interest to this program are among the largest superconducting magnets built to date. Fabrication and installation of an MHD magnet of the type considered in this program would be an important step forward in superconducting magnet development to assure that the technology required for full-scale MHD magnet design and construction will be available when needed.

The dimensional requirements on useful field volume for the system are illustrated in Figure II-1. The main field direction is perpendicular to the axis of a channel which is square in cross section and 1.524 m (60 in.) long. The field at the 10-in. square (0.254 m square) inlet is  $B_1$ , and the field at the 16-in square (0.406 m square) is  $B_0$ . The maximum fields on axis which were considered initially were in the 5 T to 8 T range. A tapered field profile along the channel axis was desired such that  $B_0 = 0.8 B_1$ . Furthermore, the desired field homogeneity was 5 percent.

The effort was divided into two phases. Phase I involved the evaluation of attractive design alternates. Interest centered on the impact of different winding geometries, field level, types of superconductor, operating temperature, and the use of iron for field enhancement. The cases selected for evaluation are summarized in Table II-1.

Figure II-2 defines these geometries by illustrating one quadrant of a transverse section of the coil system. In each case a complete winding cross section would result from reflection of the sketch about both axes. The solenoidal geometry is comparatively simple to design and fabricate; however, the bore size of the solenoid is determined primarily by the length of the MHD channel. A relatively large winding results and magnetic field is generated in large volumes where it is not used. The racetrack uses conductor more efficiently by having windings which lie close to the channel and parallel to the channel axis. The racetrack geometry is, by definition, located "over" and "under" the MHD channel or bore tube with each turn lying in a single plane. The saddle geometries also have turns parallel to the channel axis; however, they require compound bending of the end turns in order to cross over and under the bore tube. Two saddle geometries are illustrated: the rectangular saddle and the annular saddle. The former is better suited to a square bore requirement, and the latter to a round bore; however, both were considered in Phase I.

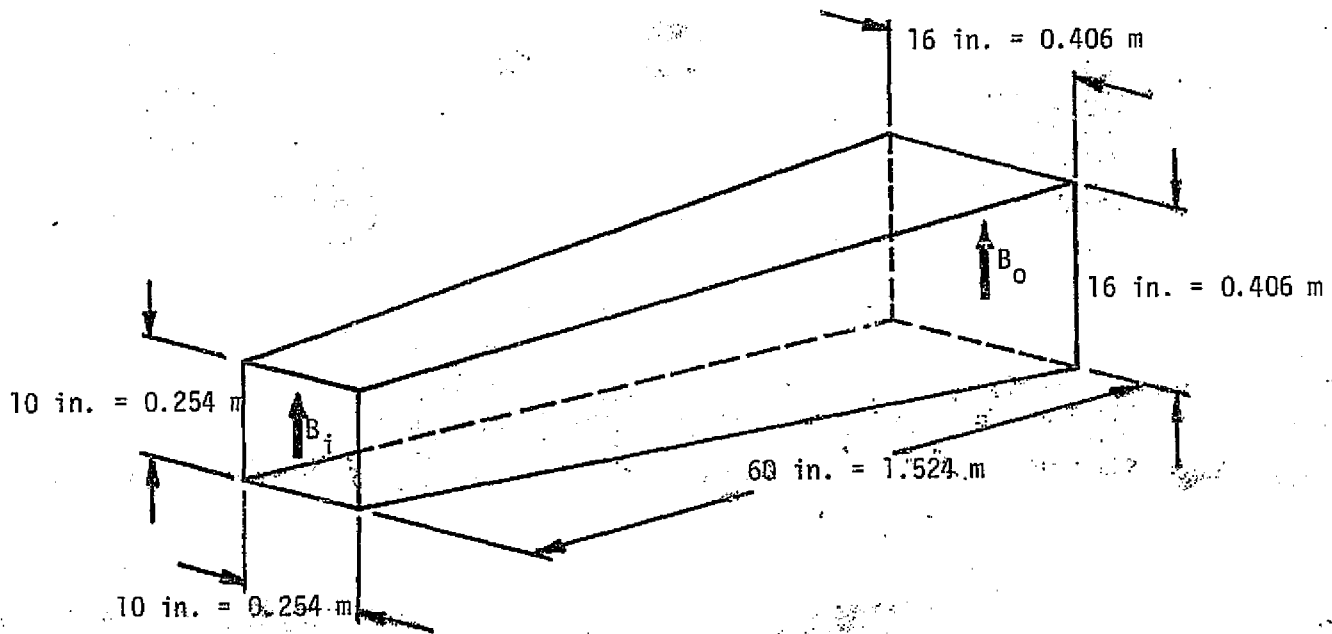


Figure II-1

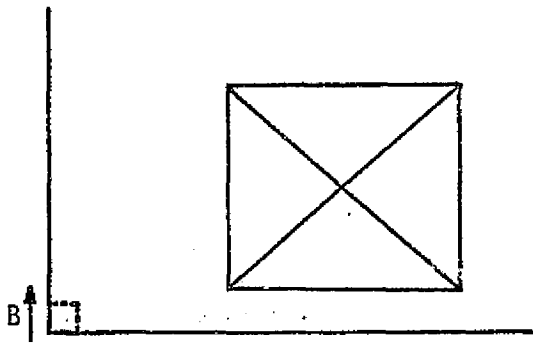
Definition of the Useful Field Volume;  $B_i$  = Field at Inlet;  
 $B_o$  = Field at Outlet.



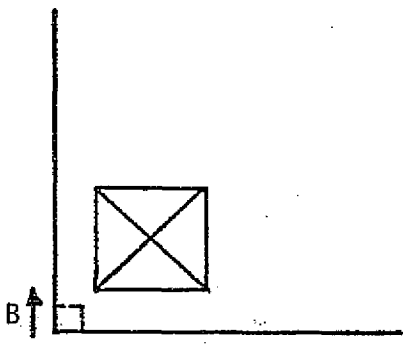
Table II-1

Summary of Magnet Geometries Selected for Investigation in Phase I

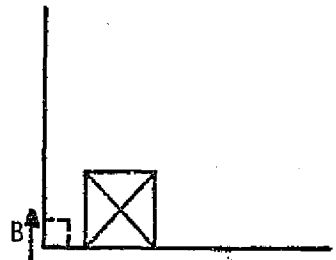
B (Wb/m <sup>2</sup> )	<u>Solenoid</u>		<u>Racetrack</u>		<u>Rectangular Saddle</u>		<u>Annular Saddle</u>
	<u>With Iron</u>	<u>Without Iron</u>	<u>With Iron</u>	<u>Without Iron</u>	<u>With Iron</u>	<u>Without Iron</u>	<u>Without Iron</u>
8	X	X	X	X	X	X	X
6.5							X
5			X	X	X	X	X



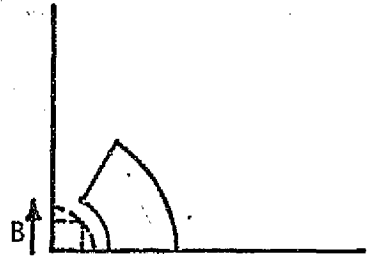
Solenoid



Racetrack



Rectangular Saddle



Annular Section Saddle

Figure II-2

Illustration of Basic Winding Cross Sectional Geometries

In Phase I, estimates were generated which allowed each of the cases in Table II-1 to be optimized from the standpoint of ampere-meter requirement and conductor stress level. Overall winding dimensions and characteristics were determined as well as stored energy and weight estimates for structure and dewar. Labor estimates were made for detail design, fabrication and installation of each system. Consideration was also given to fabrication with three different conductors: NbTi for operation at 4.2 K, NbTi for operation at 3.0 K, and Nb<sub>3</sub>Sn for operation at 10 K. Approximate system costs were then generated for each of the geometries with each conductor for a total of 39 estimates. A review of the results and system characteristics (see Section III) allowed three cases to be chosen to be carried forward into Phase II which involved the generation of a preliminary design for each of the cases.

The net result of Phase I was the decision to concentrate the Phase II effort on: (1) a racetrack geometry with an operating temperature of 4.2 K (Section IV), (2) a racetrack geometry with an operating temperature of 2.0 K (Section V), and (3) a rectangular saddle geometry with an operating temperature of 4.2 K (Section VI). All systems were to produce 8 T, use NbTi superconductor and use iron for field enhancement. It was also decided that the separation of the coils at the downstream end should be adjustable with a mechanical shimming scheme such that the channel exit field would be 6.4 tesla when the coils were positioned closest to the bore tube and 4.5 tesla when the coils were positioned farthest from the bore tube. Furthermore, the goal was for the flux density to deviate from a linear profile  $\pm 5$  percent for the 6.4 tesla channel exit case and  $\pm 8$  percent for the 4.5 tesla channel exit case.

The rectangular channel geometry was chosen because it was the most efficient in terms of material utilization. The racetracks offered simplicity of design and construction. One of the cases was chosen for operation at 2.0 K in order to evaluate the potential advantages of sub-lambda liquid helium as the cooling medium.

Preliminary designs were generated for each case (Sections IV, V, and VI) and then characteristics were compared and cost estimates were prepared (Section VII). All systems satisfied user requirements on field level and field volume. The rectangular saddle was estimated to be substantially less costly than any of the racetrack systems. The saddle is expected to be somewhat more expensive in design, fabrication, and installation labor; however, this was far outweighed by requirements for less material for conductor and structure.

A comparison of the racetrack systems indicated that the 2.0 K systems were somewhat less expensive than their 4.2 K counterpart. Conductor requirements were substantially lower, but this was offset by increased structural requirements to limit the stress level in the windings. No allowance was made for the relative difference in cost of refrigeration or for the additional development which may be necessary because of the lack of data available for magnet design in sub-lambda helium.

The MHD channel axis and the main field direction were oriented differently relative to the gravity vector for each of the three systems. With minor modifications, any of the cryostats could be interchanged with any of the coil subsystems. All orientations appear feasible, and the concept for occasional altera-

tion of the angle between coils was included. In each case, this would involve system warm up, disassembly, replacement of mechanical spacers between coils, re-assembly and cooldown. The concept is suitable for an MHD test facility on this scale where an occasional variation in field profile would be desirable.

The effort has provided preliminary design information on three systems and is suitable as a baseline from which a final design task may be initiated.

### III. PRELIMINARY DESIGN TRADE-OFFS

The first phase of this program involved a preliminary evaluation of alternate magnet design concepts which would satisfy user requirements. Overall magnet system characteristics were estimated, and rough cost estimates were generated for several designs. Three concepts were then selected and investigated in more detail during Phase II. The purpose of this section is to discuss the results of the Phase I effort in which the groundwork was laid for selection of the systems to be carried forward for further study.

#### A. STATE OF THE ART

Before proceeding with a discussion of design concepts, it is useful to consider the general state of development of superconducting MHD magnets and geometrically similar dipoles. Toward this end, several tables and figures were prepared. Figure III-1 is a plot of overall current density versus stored energy with points corresponding to the design or operating points of selected superconducting magnets.

The points shown in Figure III-1 are coded to indicate whether the magnet is operational or is in the design or planning stage. The code also indicates the superconducting material used. The majority of the points are for dipoles or saddle magnets since this is the geometry relevant to applications in MHD and to this program. Certain solenoids are included since they represent the largest superconducting magnets now in existence. These are the bubble chamber magnets at CERN (BEBC), Fermi National Accelerator Laboratory (FNAL), Argonne, and Brookhaven (BNL), and the spark chamber magnet at CERN (Omega). The point labeled "US-USSR" represents the design point for an MHD magnet to be built in the United States for the USSR U25 experimental facility.

Magnets in the lower energy range ( $\sim 1$  MJ or less) often are under development as part of a program seeking to minimize magnet weight for airborne applications or to ultimately minimize magnet cost because of the need for large numbers of magnets. As a result, the overall current density is raised to conserve conductor. This results in designs which are not cryogenically stable but dependent on intrinsic conductor stability criteria and the ability to develop a thermomechanical winding and structural design which will suppress effects which initiate operational perturbations. The understanding of the necessary and sufficient conditions for high current density winding design is not as well developed as the understanding of relatively low current density winding design involving cryostatic stability. As a result, large magnets are conservatively designed at lower current densities because of the large capital investment involved.

The points numerically coded from (1) to (12) in Figure III-1 were specifically designed as part of an MHD-oriented program, with the exception of Nos. (8) and (10). Number (8) is a large bore, low field, iron bound magnet for experiments in high energy physics. Number (10) is a saddle magnet which is typical of present high current density technology and has characteristics which satisfy typical MHD requirements. The characteristics of these magnets are outlined in more detail in Table III-1.

FA 3115

COIL GEOMETRY

- ▽ Dipole in Operation
- ▽ Dipole under Construction
- Solenoid in Operation

CONDUCTOR MATERIAL

- NbTi I
- NbZr III
- Nb<sub>3</sub>Sn II
- Other V

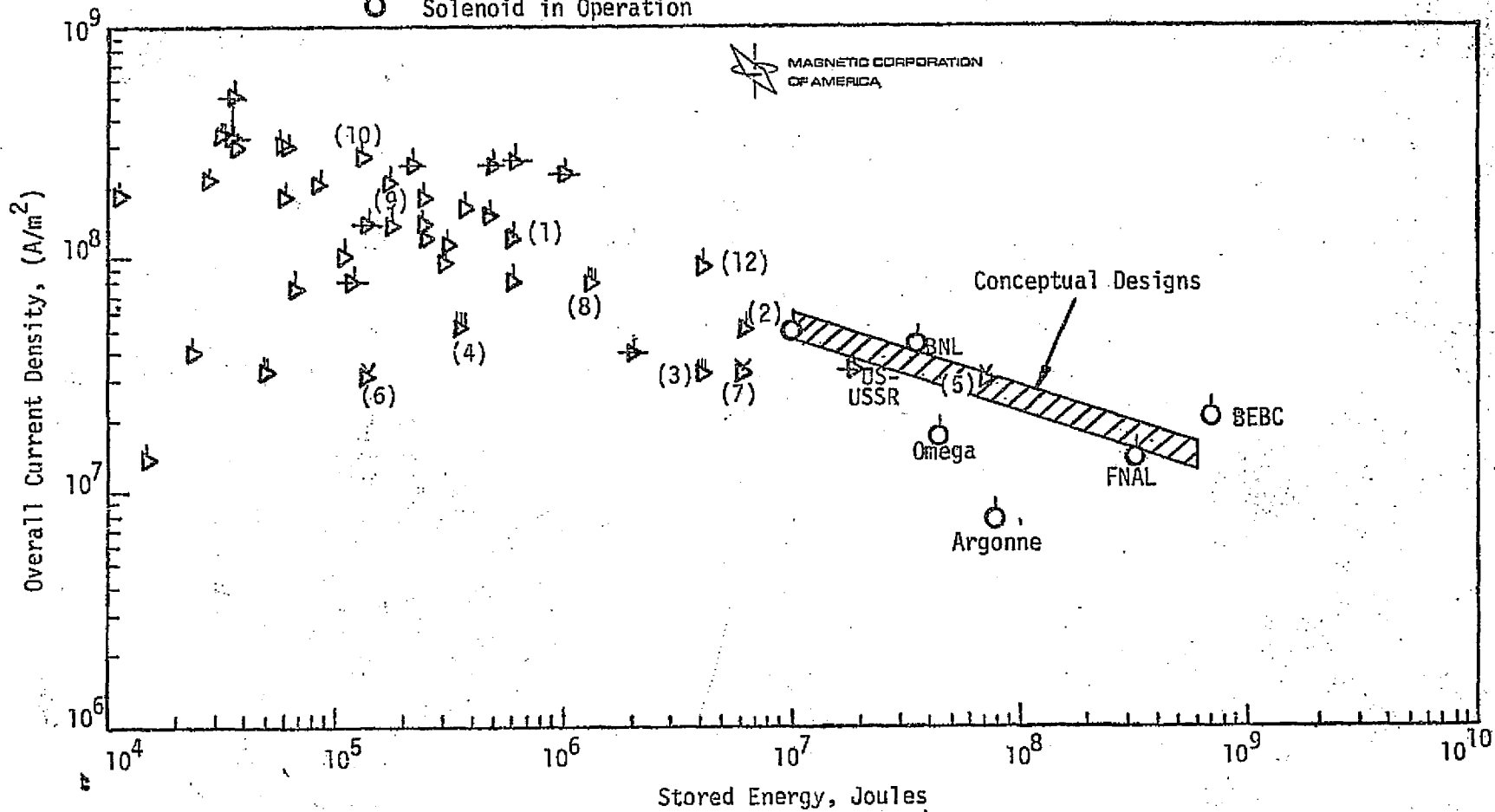


Figure III-1. State of the art of superconducting saddles and dipoles in terms of overall current density and stored energy (the largest superconducting coils in existence are solenoids and are shown as circles).

ORIGINAL PAGE IS  
OF POOR QUALITY

TABLE III-1  
CHARACTERISTICS OF SUPERCONDUCTING MHD-TYPE MAGNETS

	(1)	(2)	(3)	(4)	(5)	(6)	(7)	(8)	(9)	(10)	(11)	(12)
	HCA BUILT FOR WPAFB	GARDNER CRYogenics BUILT FOR KFA-JULICH	AVCO	ELECTRO- TECHNICAL LAB JAPAN	ELECTRO- TECHNICAL LAB JAPAN	MITSUBISHI	HITACHI	LAWRENCE RADIATION LAB LIVERMORE	FERRANTI PACKARD	HCA BUILT FOR FRL	INSTITUTE OF HIGH TEMPERATURE	AI&CO
REMARKS	Saddle MHD	Project ARGAS Racetrack Pair	MHD Model Saddle Magnet	1 kW MHD Saddle Magnet	Racetrack Pair, 1 kW MHD Magnet	MHD Saddle Magnet	MHD Saddle Magnet	High Energy Physics Expts. Saddle Magnet	U.S.A.F.- C.D.R.B. MHD Saddle	1 Meter Muon Saddle Magnet	U.S.S.R. IVTAN MHD Saddle	Saddle MHD Magnet
LENGTH OF UNIFORM FIELD (m)	.98 @ 75% .81 @ 95% Ctr.	1.60	1.2	.34 @ 75%	1.2	.25 @ 90%	.6	----	1	.20	.76	
LENGTH (m)	1.5	1.66	3.05	.85		.84	1.8	2.25	1.05	1.45	.50	1.0
BORE	21.3 cm Magnet Diameter 18 cm Diameter Warm		30.5 cm Cold	33 cm Cold 29 cm Warm	39 x 130 cm Warm	27.8 cm Cold 21.4 cm Warm	38 cm Cold 25 cm Warm	100 cm Room	33 cm Cold	14.6 x 9.5 cm Oval Cold	14 cm Cold	17.5 cm Room Temperature
FIELD (T)	CENTRAL PEAK	3.9 5.46	3.3 6.2	3.7 4.26	2.4 3.2	5 7.5	1.86 2.62	4.5 5.6	.95 2.0	1.55 3.67	2.6* 3.1	3.3
ENERGY (MJ)	.506	6.3	3.9	.37	70	.165	4.5	1.3	.19	.128	.12	4.0
OVERALL CURRENT DENSITY (A/cm <sup>2</sup> )	12,000	5,100	3,270	5,400	2,500/3,000	3,200	3,200	8,000	13,700	25,100		9,300
CONDUCTOR	MF Nb-Ti 1.8:1 CSC 180 Filaments 1" Twist Pitch .064" x .064"	MF Nb-Ti 2.3:1 21 Filaments 3" Twist Pitch .57" x .114"	Nb-Zr 9 Strands .040" x .500" .010" Strand Diameter	Nb-Zr 4 Strands in Cu .010" Dia .040" x .250"	Nb-Ti-Zr 3.5 x 8 cm	Nb-Ti-Ta 10 Cores Soldered .25 mm dia	Nb-Ti-Zr 10 Cores 1.2 x 10 cm	MF Nb-Zr Cable 19 Strands 13 cu.-3 SC .024" dia Strands	Nb-Ti 1.25:1 211 Filaments 5 cm Twist Pitch .080" square	MF Nb-Ti 1.1:1 Flat Cable-11 Strands, .025" Strand Diameter .044" x .144"	Stranded Nb-Ti-Zr Indium Im- preg. Cable 20 Cu - 21 S.C. Strands	121 Strands Nb-Ti in Cu .050" x .125"
CONDUCTOR CURRENT (A)	376	330	725	455	1,275/1,570 2 Sections	1,000	500	800	685	1,625	998	
CONDUCTOR CURRENT DENSITY (A/cm <sup>2</sup> )	14,500		5,900	10,800	4,550/5,600		5,350	----	----	36,500		12,400

\* Produces 3.6 T w/iron core.

Magnet (1) is a superconducting saddle magnet designed and built as part of an Air Force program to develop lightweight MHD magnets. The magnet is shown in Figure III-2. It utilizes a high current density conduction cooled winding and a structure composed of high strength aluminum and titanium. The magnet has been repeatedly operated up to a central field level of 3.9 T at an overall winding current density of  $1.2 \times 10^8$  A/m<sup>2</sup>.

Magnet (2) is a racetrack pair built for an MHD test facility at Julich, West Germany. The design utilizes a relatively low current density. The uniform field length for this magnet is 1.6-m. This is the longest field length for any superconducting MHD magnet that has operated.

Magnet (3) is illustrated in Figure III-3. This magnet was the first superconducting MHD saddle magnet. It utilized a cryostatically stable winding design and aluminum support structure. It has been repeatedly operated to a central field of 3.7 T.

Magnets (4) to (7) were designed and built as part of the MHD R&D effort in Japan. All designs utilize a low current density fully stabilized winding. Magnets (4), (6), and (7) use saddle type windings whereas magnet (5) is a racetrack configuration. The latter has achieved a 5 T central field which is the highest to date for a superconducting MHD magnet.

Magnet (8) is an iron bound saddle type magnet constructed for experiments in high energy physics. It is included here because of its relatively large bore size.

Magnet (9) was designed and built as part of a joint program between the U.S. Air Force and Canadian Defense Research Board to develop lightweight, high current density MHD magnets. It has been operated up to a field level of 1.55 T at an overall current density of  $1.37 \times 10^8$  A/m<sup>2</sup>.

Magnet (10) is shown in Figure III-4. This type of design is representative of the present state of high current density saddle magnet development. It was designed and built for the Fermi National Accelerator Laboratory. The structure is a continuous wrap of high strength stainless steel wire, and each layer is fully impregnated with epoxy as illustrated in Figure III-5. It has been repeatedly operated at a 2.64 T central field level with an overall winding current density of  $2.51 \times 10^8$  A/m<sup>2</sup>.

Magnet (11) is a superconducting saddle magnet built at the Institute of High Temperature in the USSR. It is believed to be a relatively low current density, cryostatically stable winding design.

Magnet (12) is a saddle magnet built as part of the USAF superconducting MHD magnet development program. It has been operated up to a central field level of 3.3 T with an overall winding current density of  $9.3 \times 10^7$  A/m<sup>2</sup>.

In reviewing the information in Table III-1 and Figure III-1, several comments are in order in view of the requirements and alternatives available in the present design program.



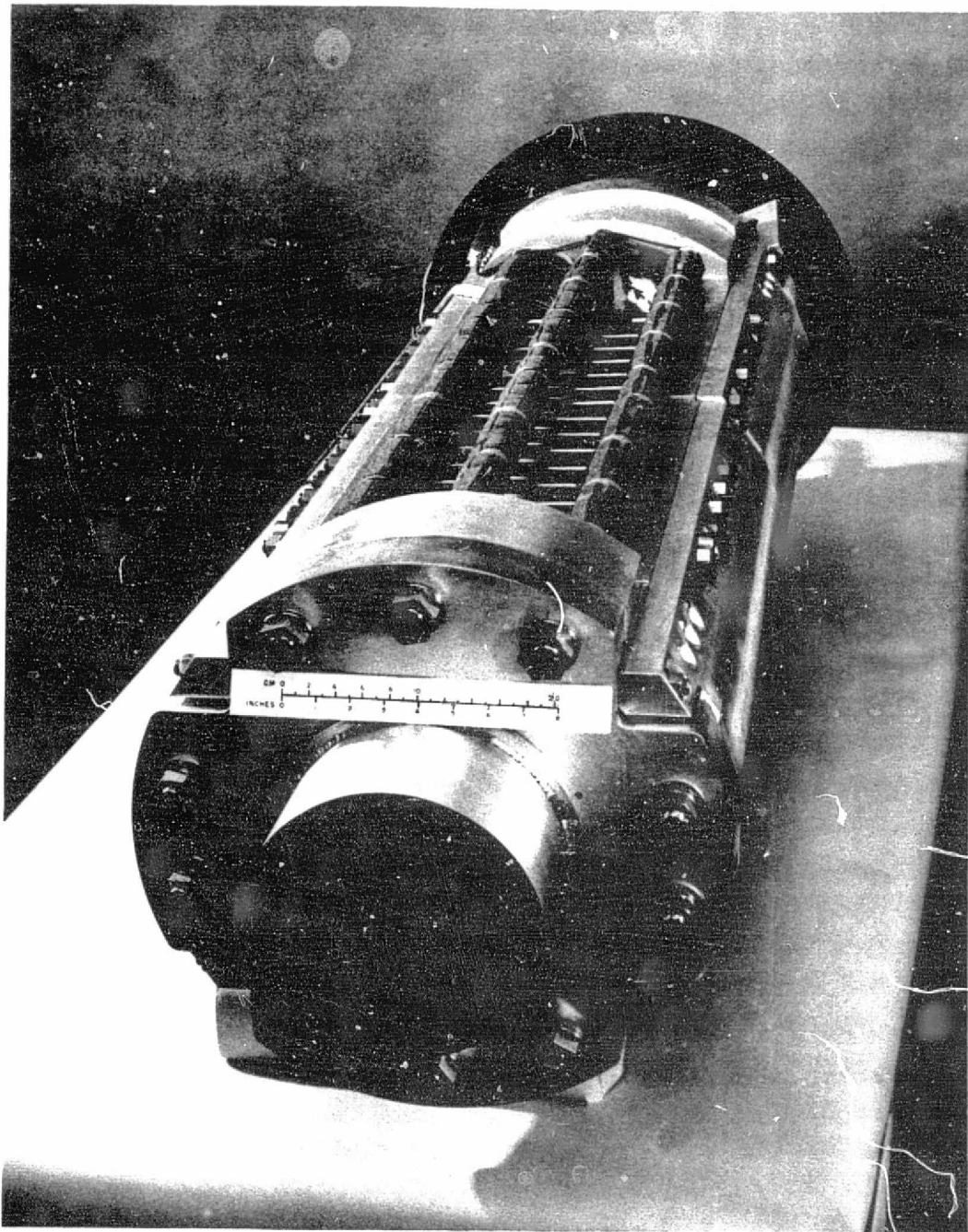


Figure III-2

Assembled superconducting MHD magnet and supporting structure. This magnet has a winding ID of 8 inches, a uniform field length of 40 inches, and has been operated at a central field level of 4.0 T which corresponds to a maximum field at the windings of 5.5 T. This magnet, built by Magnetic Corporation of America and wound entirely with superconducting wire manufactured by our HIconductor Division, is four times lighter than any other similar superconducting magnet.

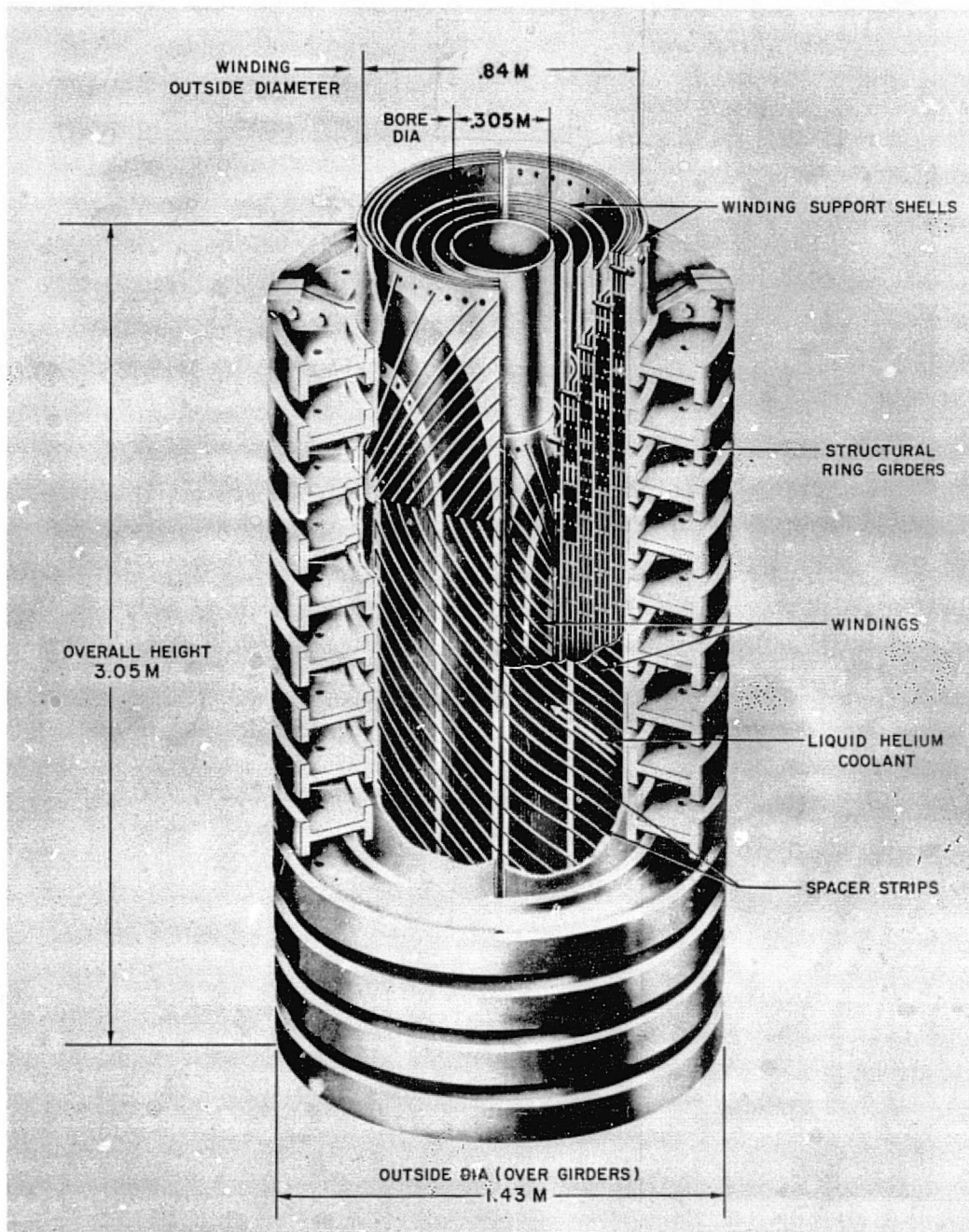


Figure III-3

Cross-section of MHD Saddle Magnet with Bore .305 m and Field Length 3.05 m. The magnet utilizes a cryostatically stable winding design and a structure composed of aluminum ring girders.

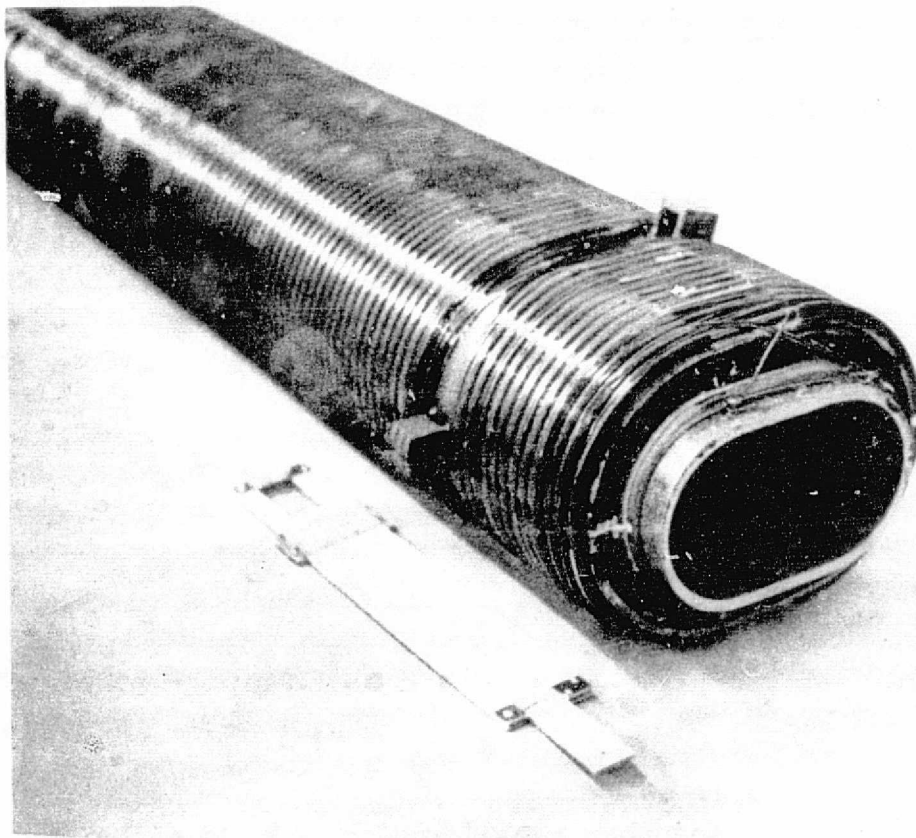


Figure III-4

Fully assembled "saddle" type high current density superconducting beamline dipole. The dipole features a clear bore of 3.6" by 5.8". The main structural components are a stainless steel bore tube and a continuous wrap of stainless steel wire applied under tension to the outer surface.

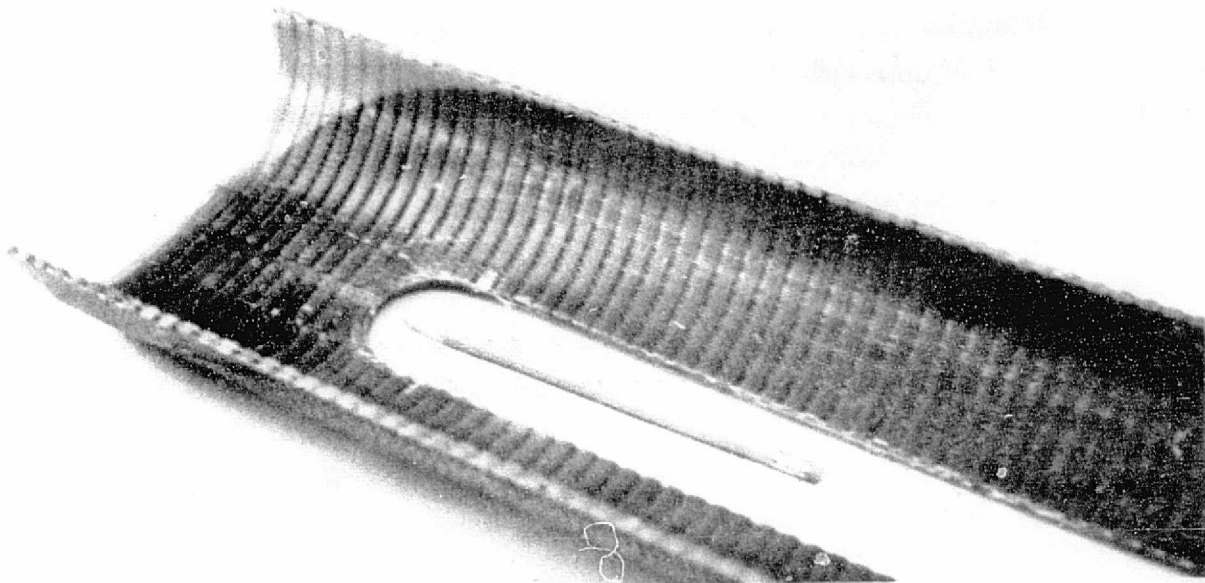


Figure III-5

Epoxy-impregnated "saddle" type layer for a high current density superconducting beamline dipole. Cooling passages between layers are formed on the concave side of the layer by the mold.

1. The present program requires a uniform field length of 1.504 m which is comparable to that of the longest uniform field built to date (Magnet (2)).
2. A tapered bore is required with cross-sectional dimensions in the 0.25 m to 0.41 m range. None of the magnets listed have tapered bore geometries though bore sizes of comparable size have been used.
3. Fields of interest to this program lie in the 5 to 8 T range. The highest central field operated to date is 5 T (Magnet (5)).
4. The conductor utilized in each of the MHD type magnets is a composite conductor of copper and superconductor in the Nb-Ti-Zr alloy family.
5. Large size superconducting magnets ( $\geq 5 \times 10^6$  J) are usually designed at a low overall current density (see Figure III-1) corresponding to cryostatic stability because of the large capital investment involved and the present developmental nature of design at high current densities.

The first task in this design study involved an evaluation of several design alternates. The design points for these alternates in terms of overall current density and stored energy fall in the shaded band in Figure III-1 labeled "conceptual designs." It is clear that the systems of interest to this program are larger than the superconducting MHD type magnets which have been built and among the largest superconducting systems built to date. The shaded band also indicates that the overall current densities used in the program are realistic without excessive conservatism or optimism. The sections which follow will discuss the conceptual design alternates for this program in detail.

## B. SYSTEM CONFIGURATIONS AND CHARACTERISTICS

This section will discuss the basic system configurations which were considered and the initial estimates of system characteristics. The basic coil geometries selected for study are presented first. Overall system size, winding size, and system characteristics are then given for the optimized coil configurations at field levels of 5.0, 6.5, and 8 T. The section closes with estimated field profiles on the channel axis for selected systems.

### 1. Basic Geometry

The basic geometries chosen for study during Phase I are illustrated in Figure III-6. Four sections are shown; each represents one quadrant of a section transverse to the MHD channel. One quarter of the magnet system warm bore is outlined by a dashed line in each case.

A system consisting of a pair of coaxial solenoids is the least complex from the standpoint of design, structural support, and fabrication. Its inner diameter is determined primarily by duct length, however, with the result that a large field volume is available outside of the region of interest. This leads to a winding volume which is relatively large. Solenoid cases were considered in this task with and without the use of iron in the solenoid bore.

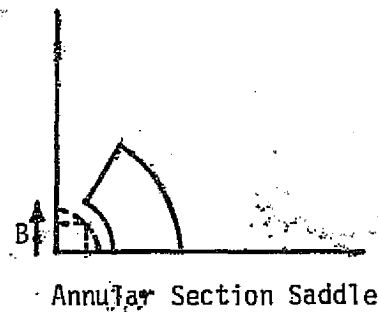
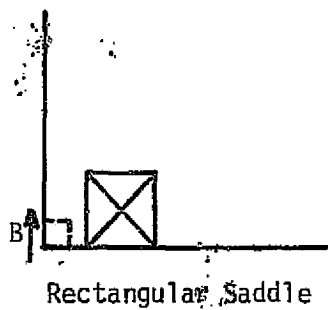
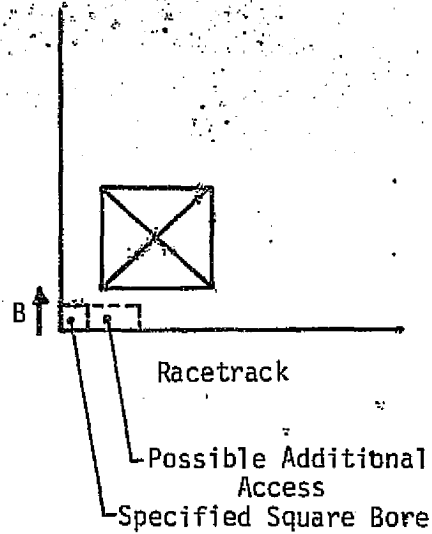
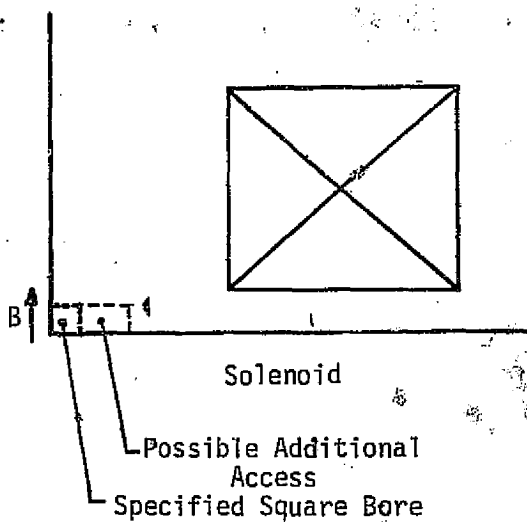


Figure III-6

Illustration of Basic Winding Cross Sectional Geometries

The racetrack geometry consists of two coils with sides essentially parallel to the duct. The overall winding size and volume are reduced relative to the solenoid because the field produced is concentrated in the region of interest. For the purposes of this task, the end turns of the racetrack were assumed to be circular. Furthermore, cases were considered with and without iron in the racetrack bore. The racetrack geometry is more complex from the viewpoint of structure and fabrication than the solenoid but less complex than the geometries which follow.

The rectangular saddle has a cross-sectional shape similar to that of the racetrack except that the two coil halves meet at the midplane between coils. This results in a more effective use of the conductor from the field generation standpoint but increases the complexity since the end turns must be shaped so as to rise up and over (or down and under) the duct on each end. Cases were considered with and without iron in the coil bore.

The annular section saddle is a variation on the saddle geometry and consists of layers of conductor which lie on constant radii. The geometry lends itself to a circular bore which must be sized so as to have a diameter equal to the diagonal of the required square duct. This leads to additional bore volume and represents a major advantage for this case.

Some additional bore access is available with either the solenoid or racetrack as shown in Figure III-6, since the windings do not extend to the midplane. This extended access leads to structural complications, however, because the pair of coils experiences a strong attraction and the windings must be supported as they pass over and under the bore tube.

A qualitative comparison of the winding geometries is outlined in Table III-2 for magnets assumed to have the same field level. Item (1) represents bore access in addition to that required by the square bore specification. This occurs naturally in the case of the annular section saddle because of the round bore for that geometry.

Items (2) and (3) in Table III-2 represent access transverse to the channel in a direction either parallel or perpendicular to the main field direction. This is limited and must be consistent with structural requirements for the coil systems. It is possible for all cases parallel to the main field. Transverse access perpendicular to the main field is most compatible with the solenoid and racetrack.

The fourth item is entrance length which is defined as the distance from the dewar entrance to the MHD channel entrance (i.e., the position of the plane of the maximum field on the channel axis). Early estimates indicated that the shortest entrance length may be expected with the racetrack, followed by the annular section saddle, solenoid, and rectangular saddle in that order.

Items (5) and (6) are overall size and overall weight and are indicative of facility size requirements for the system. Structural weight and ampere-meter requirements are outlined in items (7) and (8) and are a measure of system material costs.

The relative stored energy and charge time for the different configurations

TABLE III-2  
 QUALITATIVE COMPARISON OF WINDING GEOMETRIES

(L=Low; M=Moderate; H=High)

	Solenoid	Racetack	Rectangular Saddle	Annular Section Saddle
1) Additional access around duct	yes	yes	no	yes
2) Possible bore access parallel to B	yes	yes	yes	yes
3) Possible bore access perpendicular to B	yes	yes	no	no
4) Entrance length	med-long	short	long	medium
5) Overall size	H	H-M	L	M-L
6) Overall weight	H	M	L	L
7) Structural weight	H	M	L	M
8) Ampere-meter requirement	H	H	L	M
9) Stored energy	H	M	L	M-L
10) Charge time required	H	M	L	M-L
11) Winding difficulty	L	M	H	H
12) Structural complexity	L	M	M-H	H



is given in items (9) and (10). The energy is a measure of size and also affects charge time assuming the same power supply is used in each instance.

Items (11) and (12) are winding difficulty and structural complexity, respectively, and are a measure of fabrication time and cost.

The list in Table III-2 is intended to provide an insight into some of the overall characteristics of the different systems through a comparison which is strictly qualitative.

## 2. Overall Size Estimates

The overall dimensions for some of the systems considered in Phase I were estimated and are shown in Figures III-7 through III-10. All figures are drawn to the same scale. The approximate dimensions for the 8 T systems are shown in Figures III-7 and III-8. All dimensions are optimistic in overall envelope since they do not include the lengths required for stiffeners on the flat plates of the dewars. Because of the large areas involved, the stiffeners required may be expected to be substantial in size. Three 5 T systems are shown in Figure III-9. Figure III-10 shows 5 T, 6.5 T, and 8 T annular section saddle systems to illustrate the variation in overall size with field level.

In performing the first phase of this program, 13 different designs were carried through the rough cost estimation stage. These cases are listed in Table III-3 together with estimates of the entrance length for each case.

## 3. Winding Size Estimates

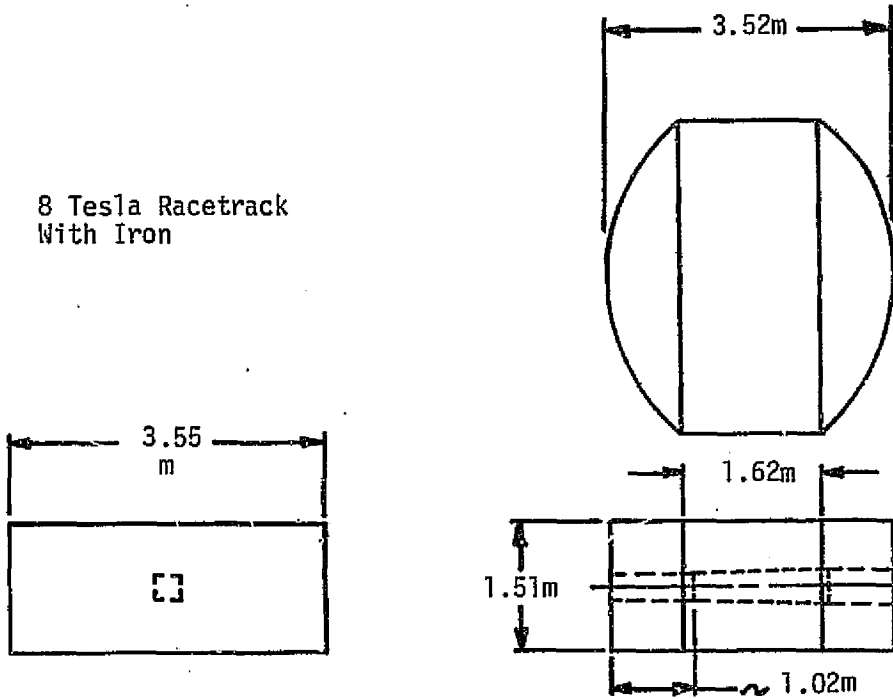
Dimensional estimates for the winding envelopes for each of the 13 cases carried through the first phase are shown in Figures III-11 to III-14. Each case was arrived at through an optimization involving total ampere-meters required, complete cryostatic stabilization, and estimates of conductor stress. The design considerations involved and the trade-off procedure used in Phase I will be described in Section III-D.

Figure III-11 illustrates two 8 T solenoids together with an outline illustrating the position of the duct relative to the windings in a manner consistent with the field profile requirements in the program. It is clear that the use of iron in the solenoid bore has a major impact on winding volume. The iron contributes to the generation of useful field and thus reduces the ampere-meters required. In addition, the iron has a tendency to reduce the peak field at the winding and, therefore, affects the current density chosen in design.

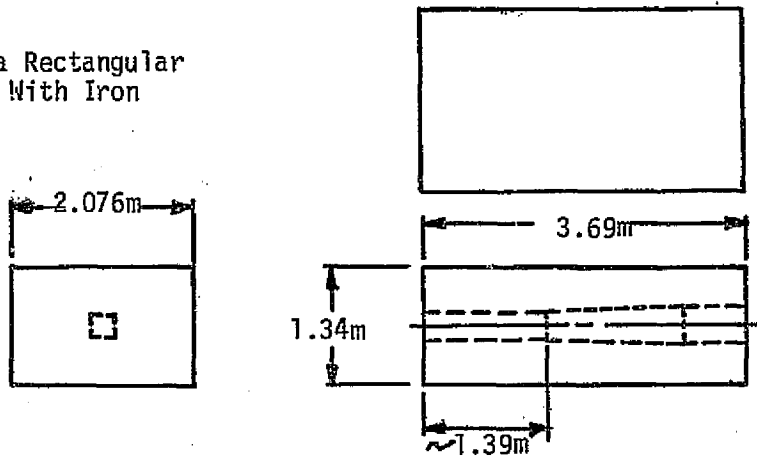
Racetrack winding dimensions are shown in Figure III-12. Both 8 T and 5 T designs are shown with and without iron used in the winding bore. The impact and advantage of the iron is again obvious. Figure III-13 gives similar information for the rectangular saddle geometry. Note that the duct is positioned somewhat further downstream for the saddle than for the racetrack. This arises because of a tendency for the saddle to have a slower rise in field profile than a racetrack.

The relative size of the windings for 5 T, 6.5 T, and 8 T annular section saddle coils is shown in Figure III-14. The dramatic increase in winding volume as field increases is evident.

8 Tesla Racetrack  
With Iron



8 Tesla Rectangular  
Saddle With Iron



8 Tesla Annular  
Saddle

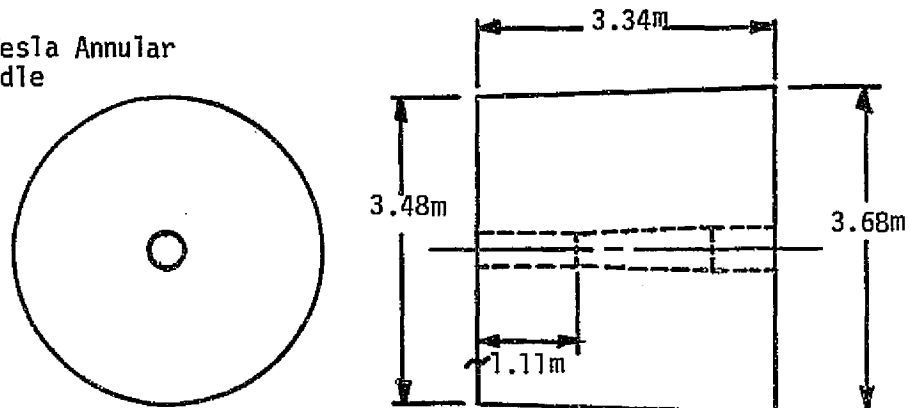
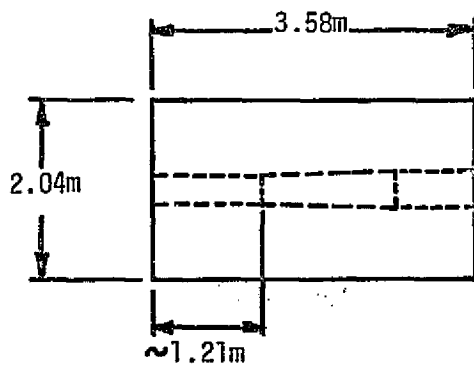
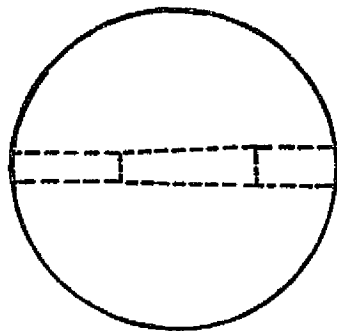


Figure III-7

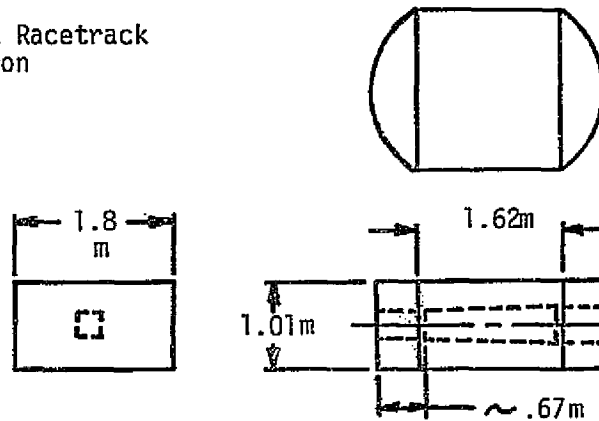


8 Tesla Solenoid With Iron

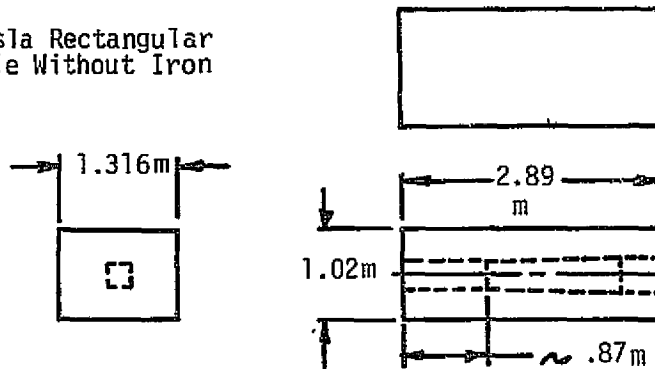
Figure III-8

Approximate Dimensions of Dewar System (in meters)

5 Tesla Racetrack  
With Iron



5 Tesla Rectangular  
Saddle Without Iron



5 Tesla Annular Saddle

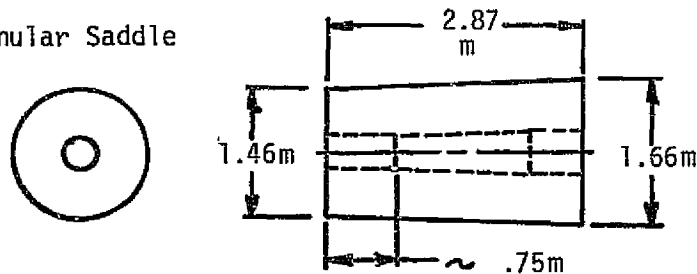
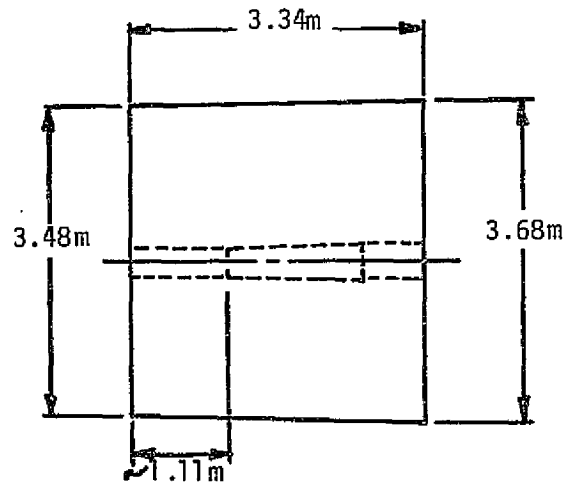
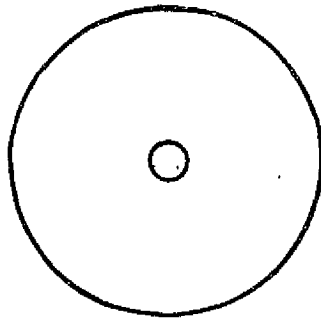


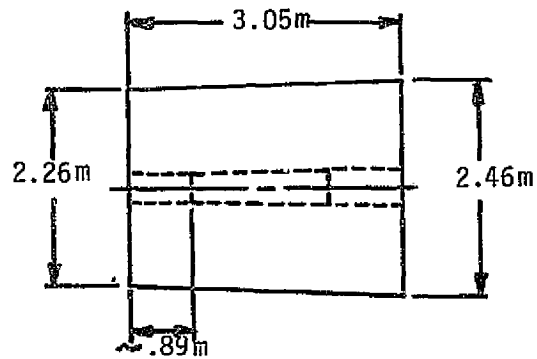
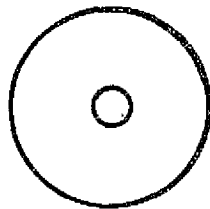
Figure III-9

Approximate Dimensions of 5 T Dewar Systems (in meters)

8.0 Tesla



6.5 Tesla



5 Tesla

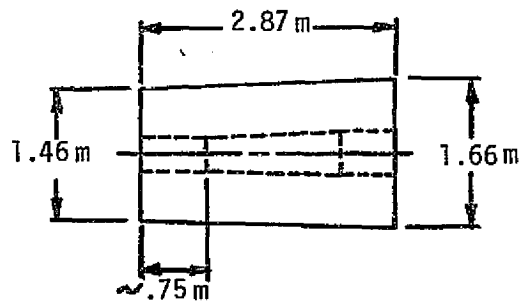


Figure III-10

Approximate Dimensions of Annular Section Dewar Systems (in meters)

Table III-3  
 Estimated Entrance Length (Optimistic)  
 (end of dewar to duct inlet)

$\frac{B}{(\text{wb/m}^2)}$	<u>magnet type</u>	<u>entrance length (m.)</u>
8	solenoid w/iron	1.21
8	solenoid w/o iron	1.67
8	racetrack w/iron	1.02
8	racetrack w/o iron	1.26
8	rectangular saddle w/iron	1.39
8	rectangular saddle w/o iron	1.45
8	annular section saddle	1.11
6.5	annular section saddle	.89
5	annular section saddle	.75
5	racetrack w/iron	.67
5	racetrack w/o iron	.71
5	rectangular saddle w/iron	0.87
5	rectangular saddle w/o iron	0.91

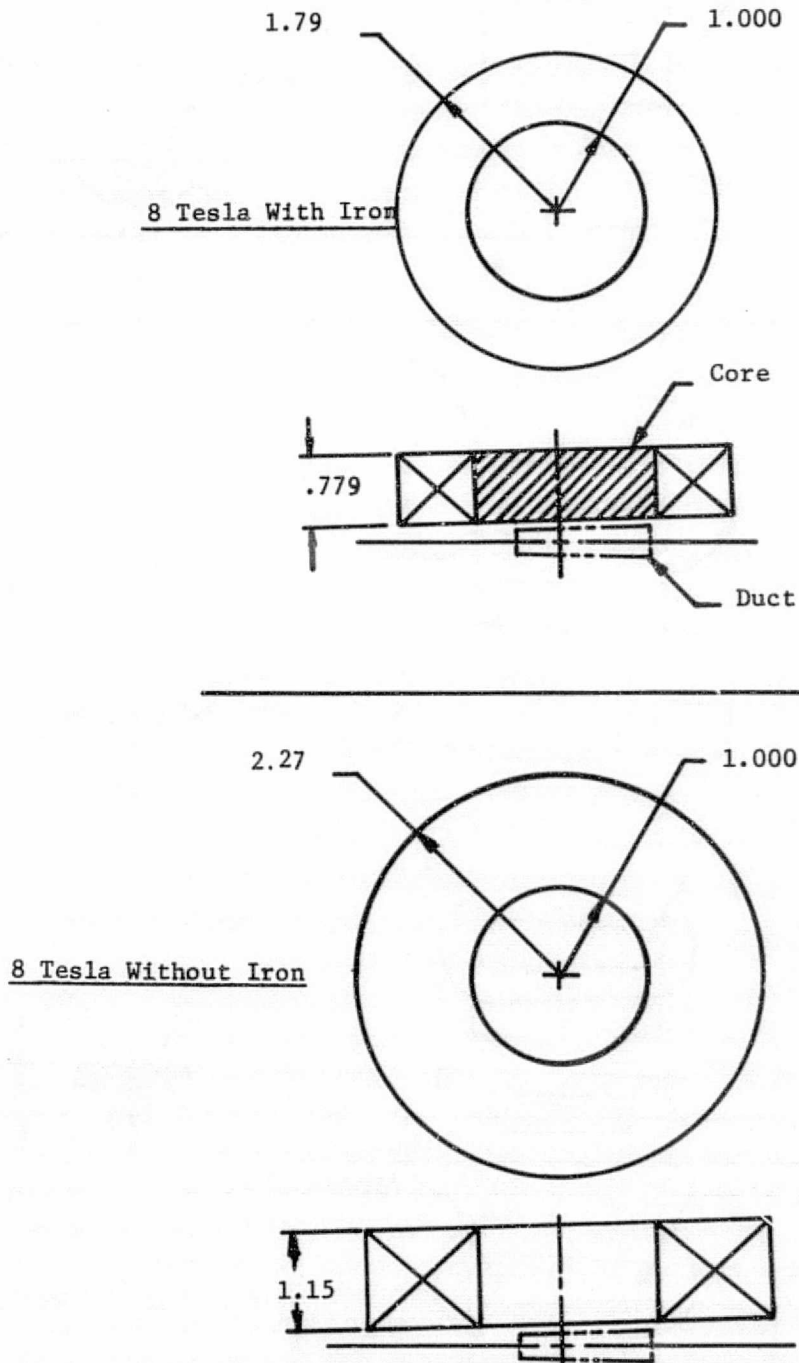


Figure III-11

Illustration of Winding Size for 8 Tesla Solenoids  
 With and Without Iron  
 (one of two windings is shown for each case)

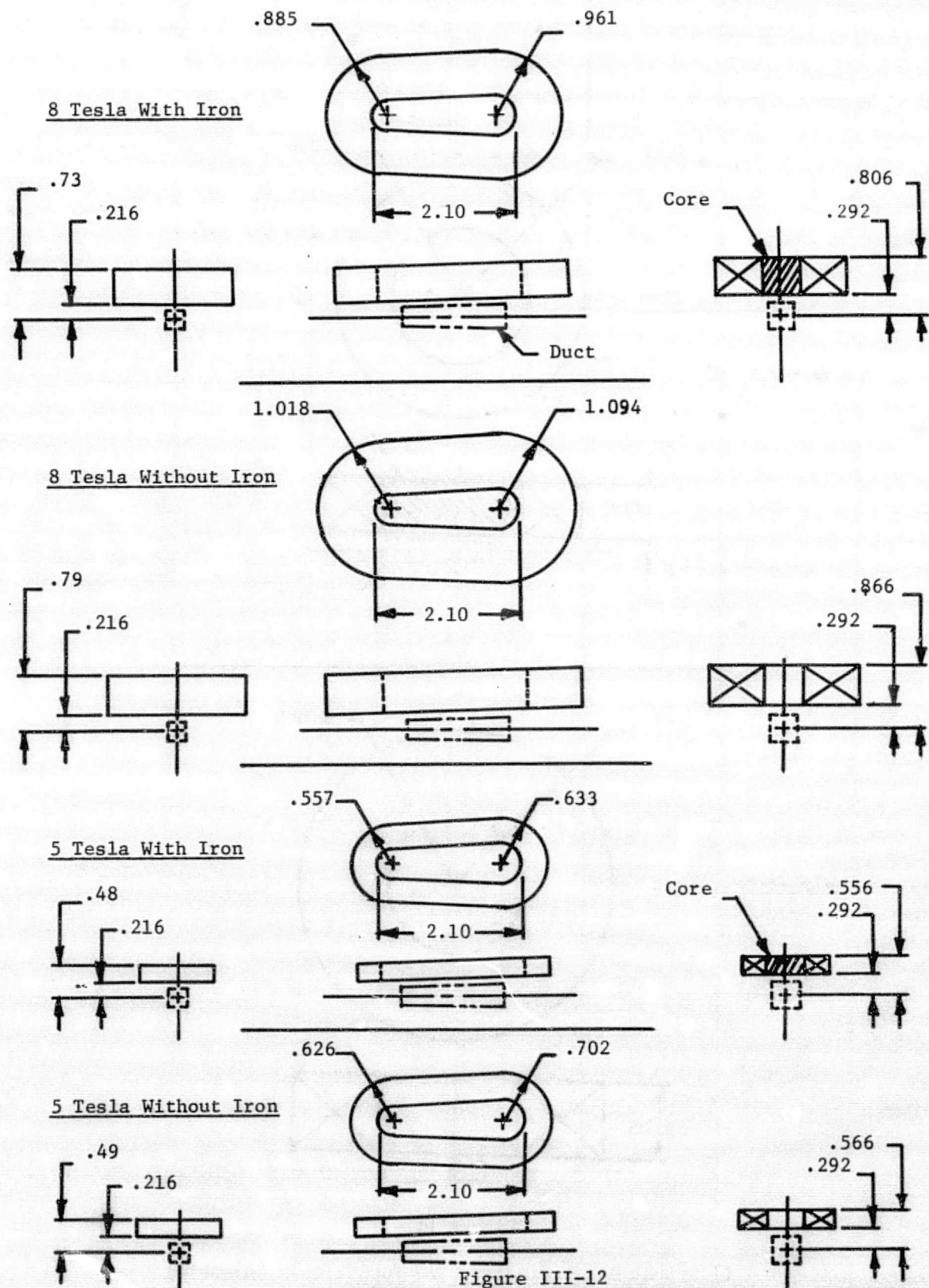


Figure III-12  
 Relative Size of Racetrack Windings for  
 8 and 5 Tesla Systems **With** and **Without** Iron (Dimensions in Meters)  
 (one of two windings is shown for each case)



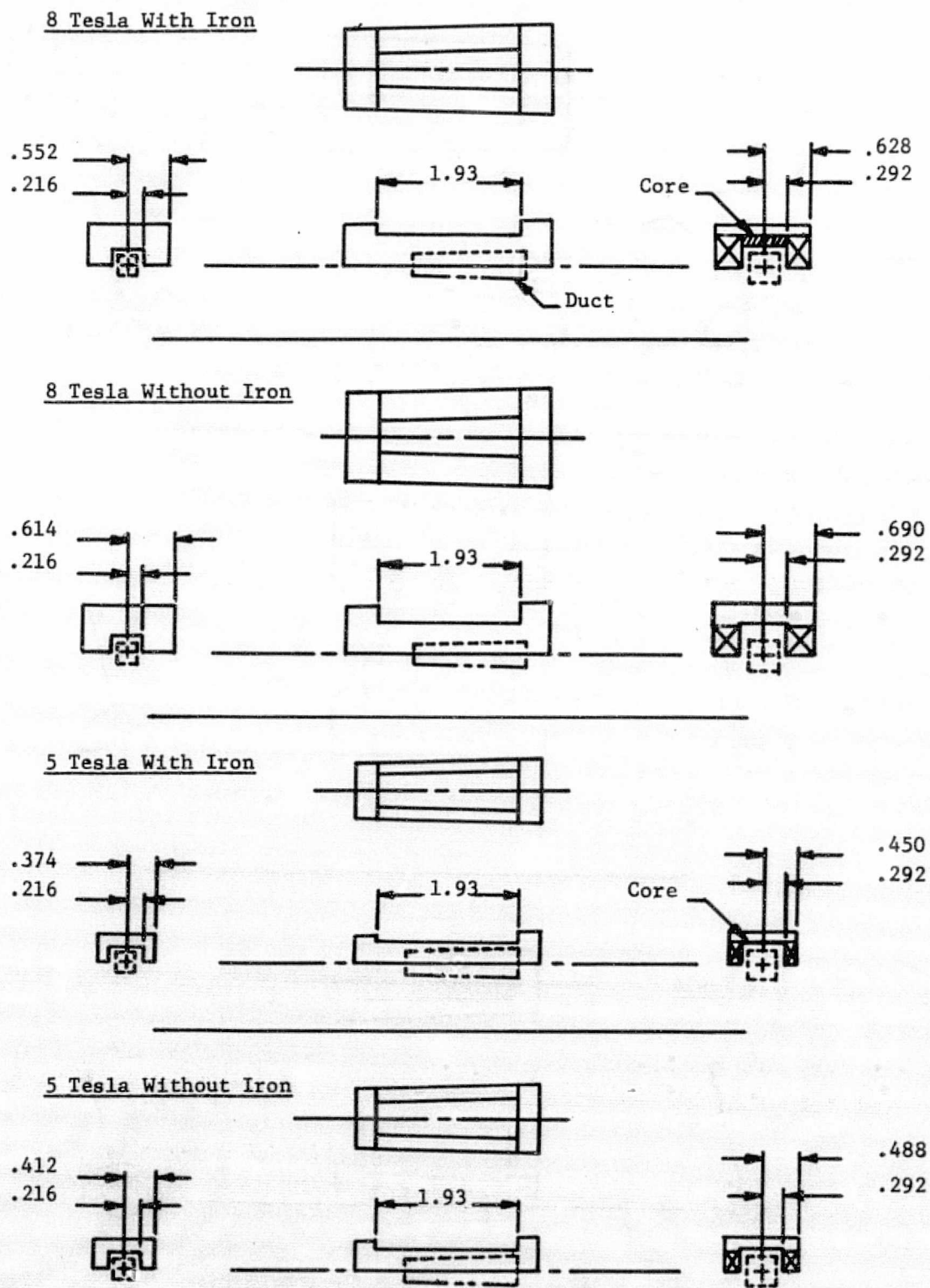


Figure III-13

Relative Size of Rectangular Saddle Windings for 8 and 5 Tesla Systems With and Without Iron (Dimensions in Meters) (one of two windings is shown for each case)

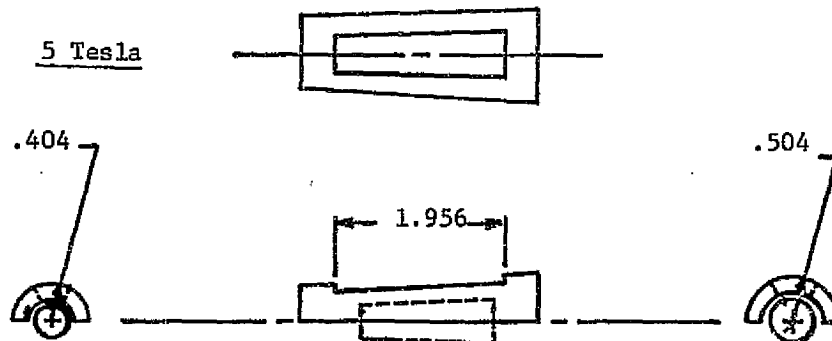
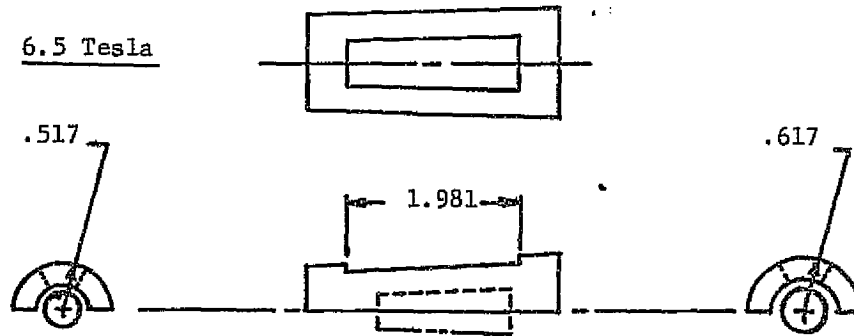
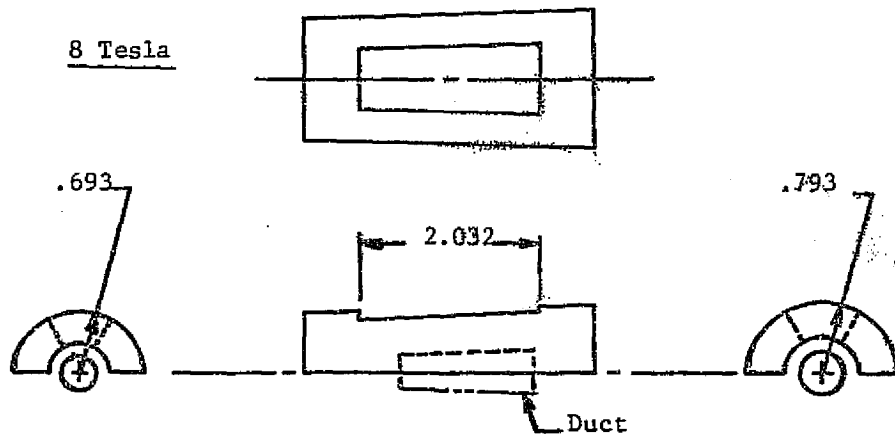


Figure III-14

Relative Size of Annular Section Windings  
for 8, 6.5, and 5 Tesla Systems (Dimensions in Meters)  
(one of two windings is shown for each case)

#### 4. Tabulated System Characteristics

The characteristics of the 13 systems investigated under Phase I of the program are outlined in Tables III-4 through III-7. Each table corresponds to one of the four geometries: solenoid, racetrack, rectangular saddle, and annular saddle. For each case the total central field (i.e., maximum field on duct axis) is given as well as the iron contribution if any. This is followed by the estimated peak field at the windings. Electrical characteristics are then given together with the estimated masses of system components. Each design is based on an overall current density chosen in a manner consistent with complete cryostatic stabilization and a limited conductor stress. Results for comparable systems studied in Phase II may differ somewhat because the design procedures for the latter were more refined.

#### 5. Field Profile Estimates

Figures III-15 to III-21 show field profiles along the axis as estimated in Phase I for several of the designs considered. In each case, two characteristic profile lengths are given. One is based on a length definition such that the useful field is assumed to begin at the maximum field point and end at the point corresponding to 80 percent of maximum. The other is based on a length such that the profile is within  $\pm 5$  percent of a linear profile.

### C. SYSTEM COST ESTIMATES

#### 1. Summary

As part of the comparative system evaluation under this task, rough cost estimates were prepared. These are summarized in Tables III-8 to III-10 in normalized form. Each table contains 13 cases. All cases on a given table utilize a particular type of superconductor operating at a particular temperature; that is, the systems in Table III-8 utilize NbTi at 4.2 K, the systems in Table III-9 utilize NbTi at 3.0 K, and the systems in Table III-10 utilize Nb<sub>3</sub>Sn at 10 K. Following cost estimation, a relative cost was generated by arbitrarily choosing the total cost estimate for the 4.2 K, NbTi, 8 T, annular saddle as a unit cost and dividing all other cost estimates by this value. The approximate cost for the baseline system was  $\$2.27 \times 10^6$ . More detailed analysis and cost estimation may lead to higher values; hence a contingency of the order of 20-25 percent would seem reasonable.

In each table the 13 designs are arranged in columns. The seven columns to the left are designs at an 8 T central field, whereas the five to the right are at 5 T. A design at 6.5 T is given in each table and is bounded by heavy lines. The geometry, whether or not iron is utilized, and central field level are given in the first three lines. Relative cost estimates are then given for labor and for material components. The assumptions and methods used in calculating these Phase I estimates are given in Section III-C-2.

The costs for the system designs reflect the complexity of structural support in that design costs are less for the solenoid and more for the saddle geometries with the racetracks at an intermediate level. The design costs are assumed to be independent of field level or operating temperature. Fabrication and installation costs, on the other hand, are geometry and field level dependent because of the variations in ampere-meters required and in fabrication techniques.

TABLE III-4  
SOLENOID SYSTEM CHARACTERISTICS

Total Central Field (Wb/m <sup>2</sup> )	8.0	8.0
Iron Contribution (Wb/m <sup>2</sup> )	0.96	--
Peak Field (Wb/m <sup>2</sup> )	7.8	9.1
Electrical Characteristics		
Overall Current Density (10 <sup>7</sup> A/m <sup>2</sup> )	1.6	0.99
Operating Current (kA)	4	4
Stored Energy (10 <sup>6</sup> J)	386	607
Ampere-Meters (10 <sup>7</sup> A-m)	16.4	31.8
Ampere-Turns (10 <sup>6</sup> At)	16.1	27.0
Mass of Components		
Conductor (10 <sup>3</sup> kg)	30	64
Structure (10 <sup>3</sup> kg)	59	114
Dewar (10 <sup>3</sup> kg)	27	44
Iron (10 <sup>3</sup> kg)	40	--
Miscellaneous (10 <sup>3</sup> kg)	<u>16</u>	<u>22</u>
TOTAL (10 <sup>3</sup> kg)	172	244

TABLE III-5

## RACETRACK SYSTEM CHARACTERISTICS

Total Central Field (Wb/m <sup>2</sup> )	8.0	8.0	5.0	5.0
Iron Contribution (Wb/m <sup>2</sup> )	0.61	--	0.45	--
Peak Field (Wb/m <sup>2</sup> )	9.6	10.2	7.07	7.9
Electrical Characteristics				
Overall Current Density (10 <sup>7</sup> A/m <sup>2</sup> )	2.55	2.23	4.27	3.9
Operating Current (kA)	4	4	4	4
Stored Energy (10 <sup>6</sup> J)	88.1	120	19.9	26.1
Ampere-Meters (10 <sup>7</sup> A-m)	11.9	14.7	4.5	5.28
Ampere-Turns (10 <sup>6</sup> At)	18	21	8.06	9.1
Mass of Components				
Conductor (10 <sup>3</sup> kg)	25	31	7.7	9.7
Structure (10 <sup>3</sup> kg)	25	39	3.1	4.4
Dewar (10 <sup>3</sup> kg)	56	71	17.4	21.2
Iron (10 <sup>3</sup> kg)	6	--	3.1	--
Miscellaneous (10 <sup>3</sup> kg)	<u>11</u>	<u>14</u>	<u>3.1</u>	<u>3.5</u>
TOTAL (10 <sup>3</sup> kg)	123	155	34.4	38.8

TABLE III-6  
RECTANGULAR SADDLE SYSTEM CHARACTERISTICS

Total Central Field (Wb/m <sup>2</sup> )	8.0	8.0	5.0	5.0
Iron Contribution (Wb/m <sup>2</sup> )	0.41	--	0.21	--
Peak Field (Wb/m <sup>2</sup> )	8.66	9.44	5.35	6.20
Electrical Characteristics				
Overall Current Density (10 <sup>7</sup> A/m <sup>2</sup> )	3.3	3.1	4.73	4.43
Operating Current (kA)	4	4	4	4
Stored Energy (10 <sup>6</sup> J)	37.0	45.5	9.73	11.4
Ampere-Meters (10 <sup>7</sup> A-m)	6.54	7.37	2.77	2.95
Ampere-Turns (10 <sup>6</sup> At)	9.54	10.4	4.50	4.70
Mass of Components				
Conductor (10 <sup>3</sup> kg)	12.7	15.0	4.0	4.6
Structure (10 <sup>3</sup> kg)	13.2	17.0	2.7	2.9
Dewar (10 <sup>3</sup> kg)	35.4	39.6	14.6	14.4
Iron (10 <sup>3</sup> kg)	2.7	--	0.2	--
Miscellaneous (10 <sup>3</sup> kg)	<u>6.4</u>	<u>7.2</u>	<u>2.2</u>	<u>2.2</u>
TOTAL (10 <sup>3</sup> kg)	70.4	78.8	23.7	24.1

TABLE III-7  
ANNULAR SADDLE SYSTEM CHARACTERISTICS

Total Central Field (Wb/m <sup>2</sup> )	8.0	6.5	5.0
Iron Contribution (Wb/m <sup>2</sup> )	--	--	--
Peak Field (Wb/m <sup>2</sup> )	9.44	7.87	6.2
Electrical Characteristics			
Overall Current Density (10 <sup>7</sup> A/m <sup>2</sup> )	3.1	3.75	4.43
Operating Current (kA)	4	4	4
Stored Energy (10 <sup>6</sup> J)	88.8	33.8	13.6
Ampere-Meters (10 <sup>7</sup> A-m)	9.29	5.19	3.05
Ampere-Turns (10 <sup>6</sup> At)	12.3	7.7	4.88
Mass of Components			
Conductor (10 <sup>3</sup> kg)	18.9	9.5	4.8
Structure (10 <sup>3</sup> kg)	26.5	10.9	5.5
Dewar (10 <sup>3</sup> kg)	20.8	9.0	4.5
Iron (10 <sup>3</sup> kg)	--	--	--
Miscellaneous (10 <sup>3</sup> kg)	<u>6.6</u>	<u>2.9</u>	<u>1.5</u>
TOTAL (10 <sup>3</sup> kg)	72.8	32.3	16.3

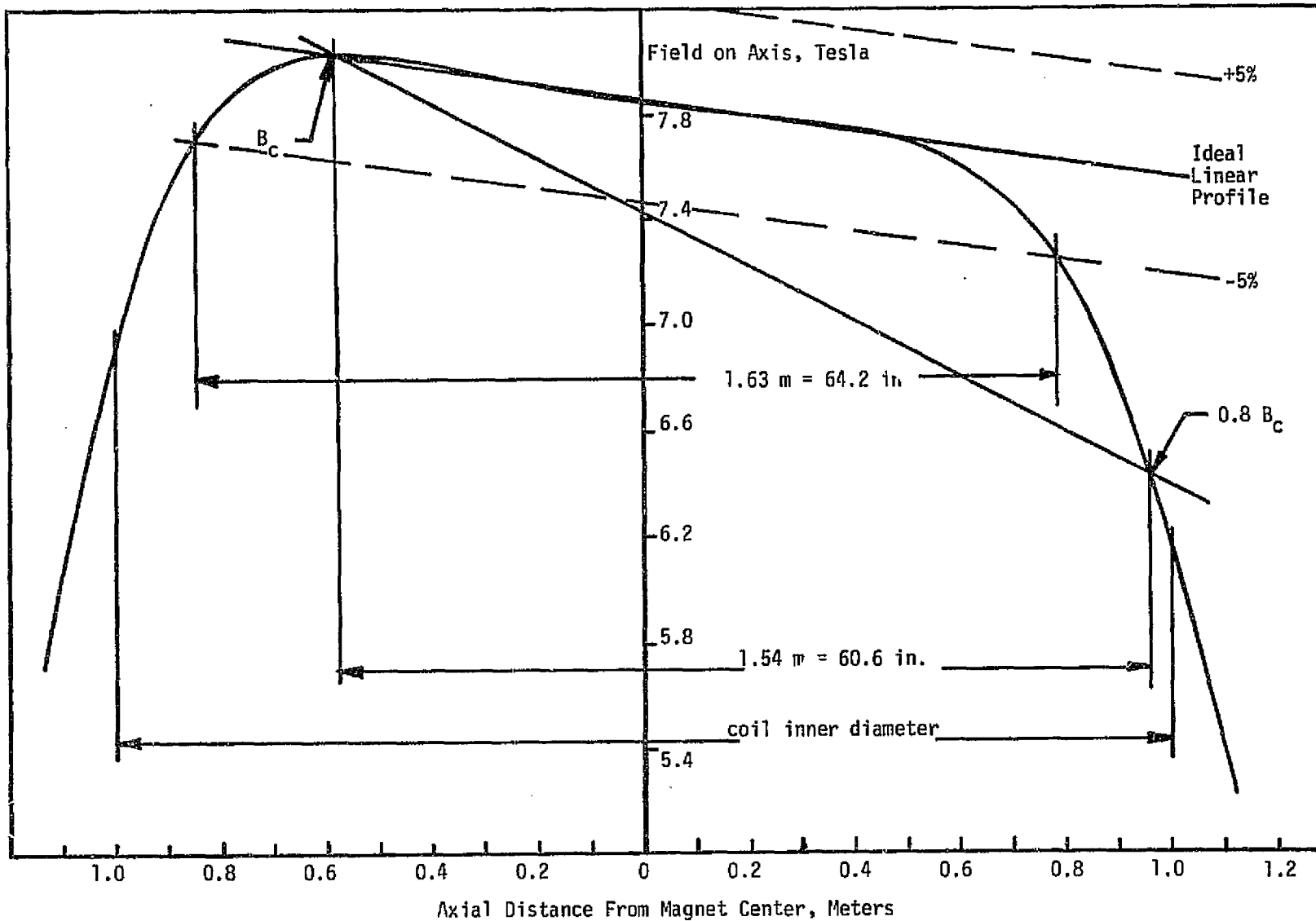


Figure III-15. Field Profile Along Duct Axis for 8 T Solenoid With Iron



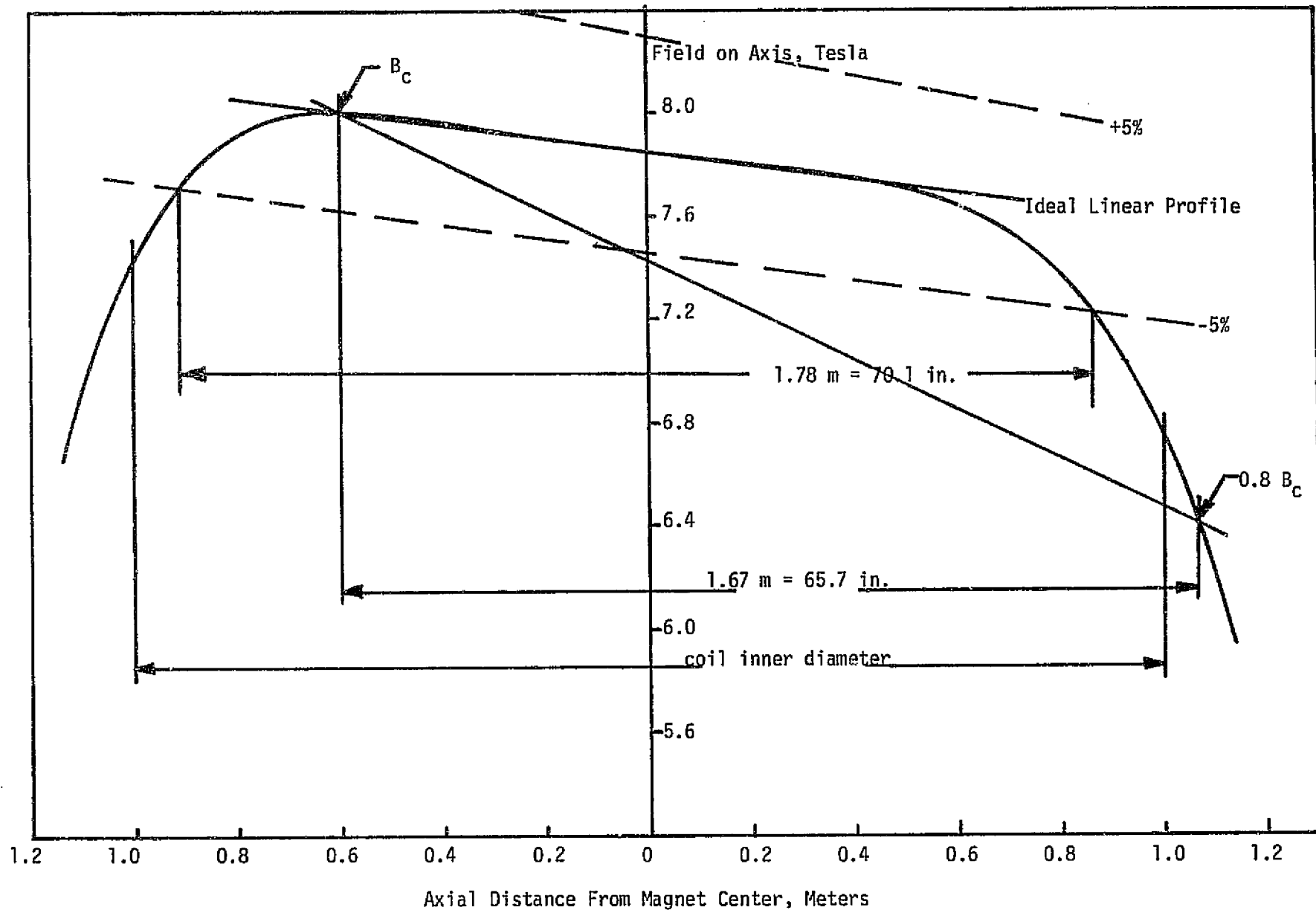


Figure III-16. Field Profile Along Duct Axis For 8 T Solenoid Without Iron

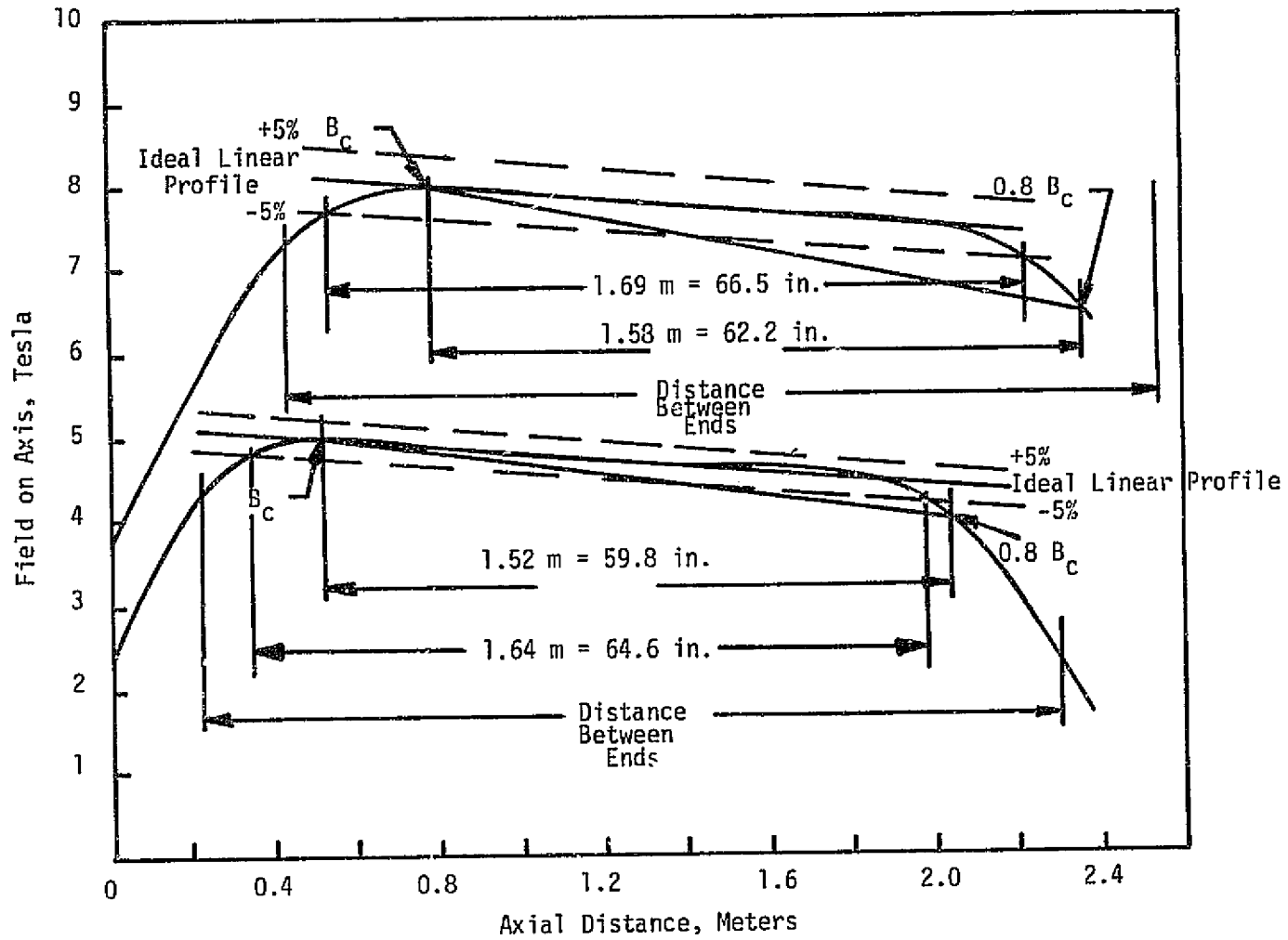


Figure III-17. Axial Field Profiles for Racetracks Without Iron

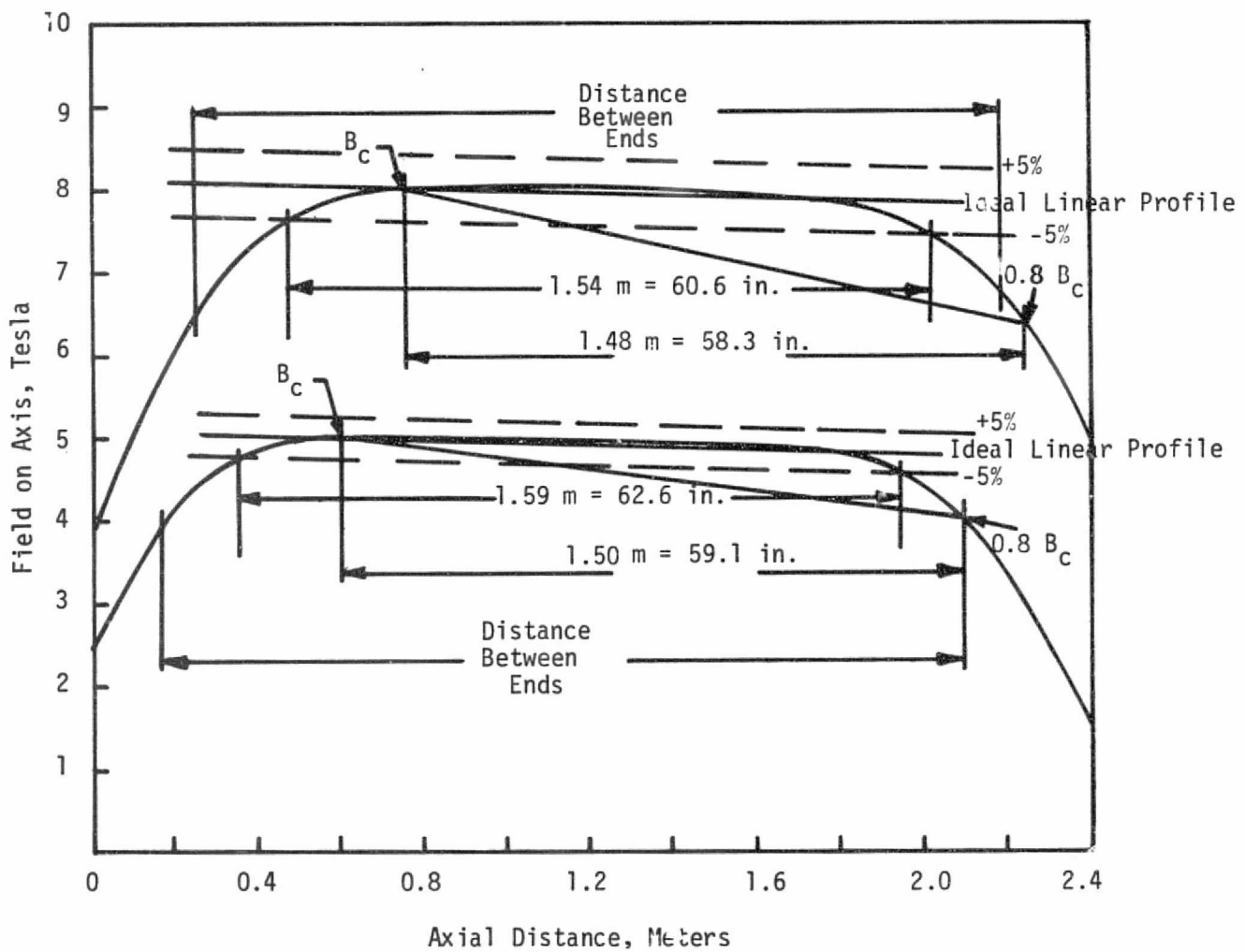


Figure III-18  
 Axial Field Profiles for Rectangular Saddles Without Iron

FA 3110

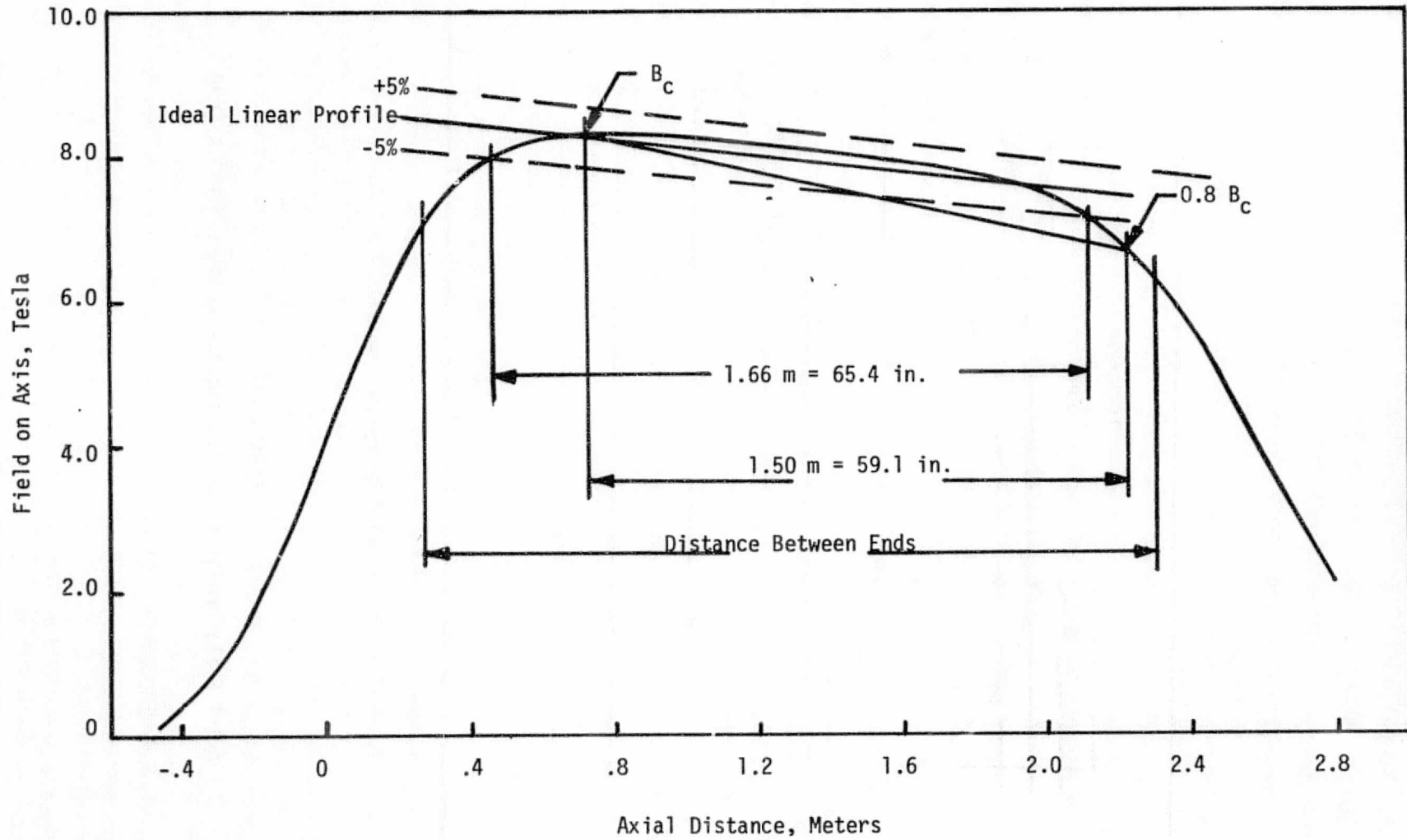


Figure III-19. Axial Field Profile for 8 T Annular Section Saddle Without Iron

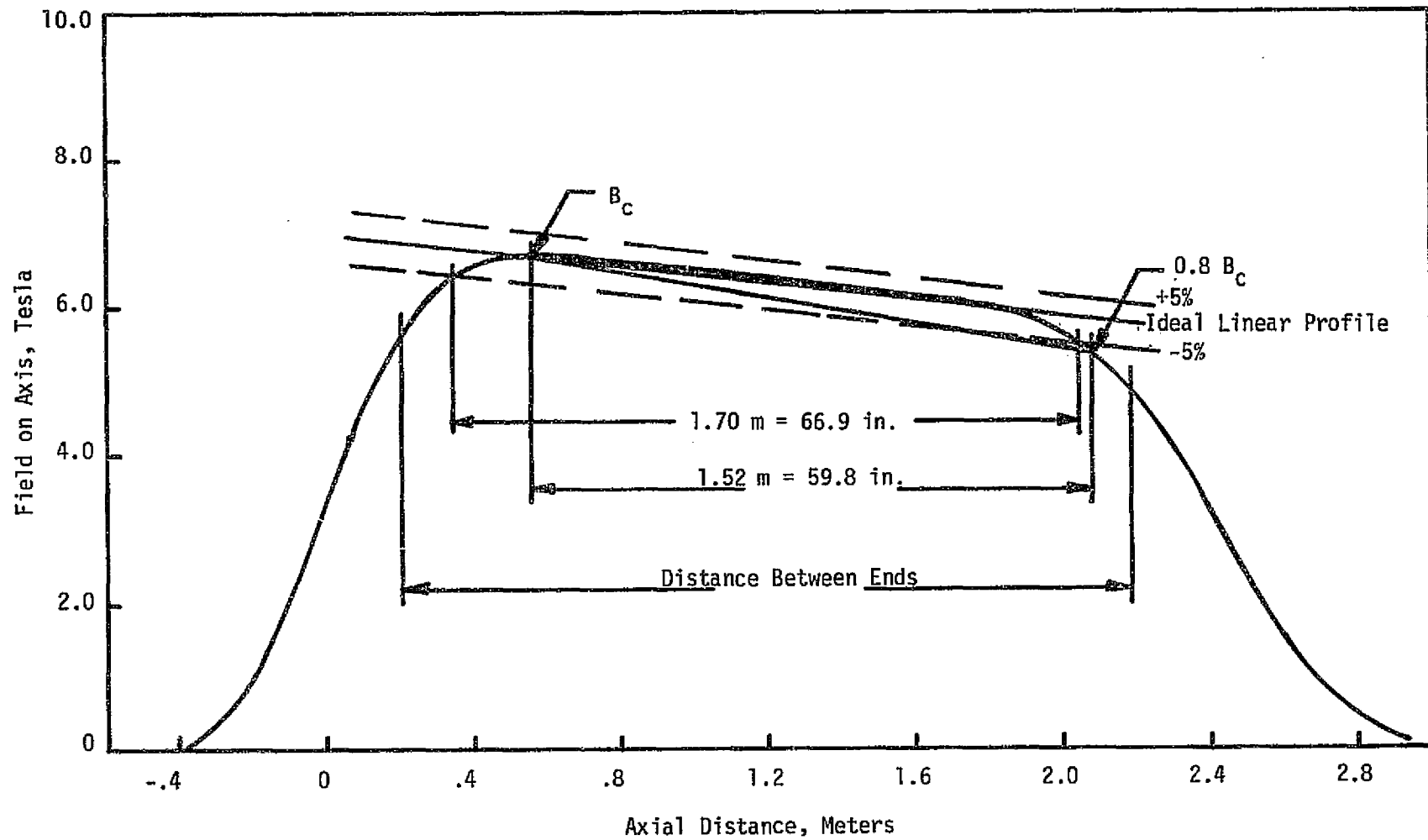


Figure III-20. Axial Field Profile For 6.5 T Annular Section Saddle Without Iron

FA 3112

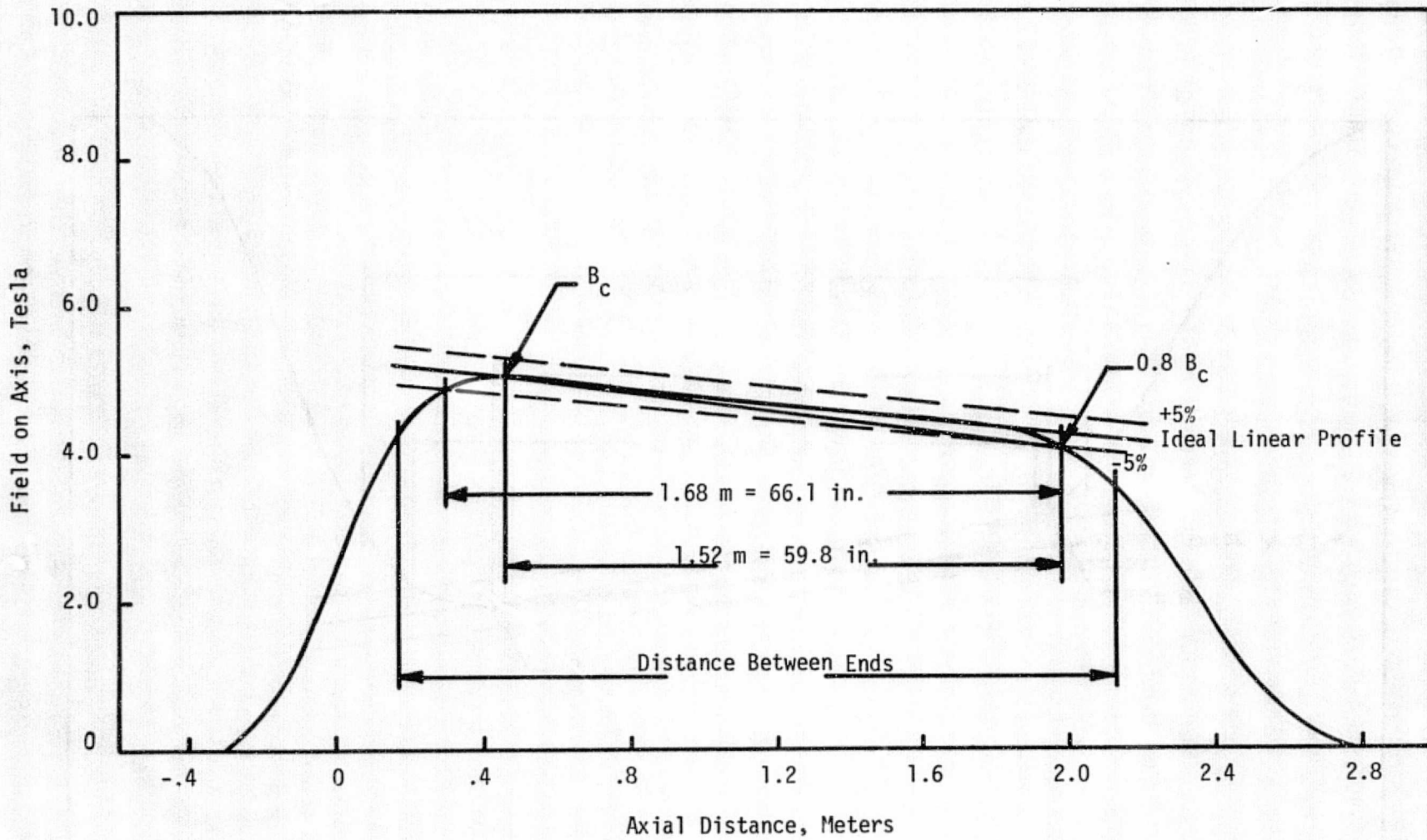


Figure III-21. Axial Field Profile For 5 T Annular Section Saddle Without Iron

Table III-8. Summary of Approximate Relative Cost Estimates for Systems Using NbTi @ 4.2 K

Geometry	Solenoids		Racetracks		Rectangular Saddle		Annular Section Saddle			Racetracks		Rectangular Saddle	
	Yes	No	Yes	No	Yes	No	No	No	No	Yes	No	Yes	No
Iron													
Central Field (Wb/m <sup>2</sup> )	8.0	8.0	8.0	8.0	8.0	8.0	8.0	6.5	5.0	5.0	5.0	5.0	5.0
Labor Costs:													
Design	.04	.04	.05	.05	.06	.06	.06	.06	.06	.05	.05	.06	.06
Fabrication & Installation	.09	.12	.09	.09	.13	.14	.11	.08	.06	.05	.05	.08	.08
Labor Subtotal	.13	.16	.14	.14	.20	.20	.18	.14	.12	.11	.11	.14	.14
Material Costs:													
Conductor	.23	.52	.22	.33	.10	.13	.16	.07	.04	.06	.07	.03	.04
Support Structure	.08	.16	.15	.22	.10	.12	.21	.09	.04	.02	.03	.02	.02
Dewar	.10	.17	.22	.28	.14	.15	.10	.06	.04	.07	.08	.06	.06
Iron Plug	.02	-	.003	-	.001	-	-	-	-	.001	-	<.001	-
Tooling	.06	.06	.06	.06	.07	.07	.07	.07	.06	.05	.05	.05	.05
Miscellaneous	.07	.14	.10	.13	.06	.07	.08	.04	.03	.03	.04	.02	.03
Subtotal	.57	1.06	.74	1.02	.46	.55	.63	.32	.20	.23	.27	.19	.19
Administrative Expenses	.17	.32	.22	.31	.14	.16	.19	.10	.06	.07	.08	.06	.06
Material Subtotal	.74	1.37	.97	1.33	.60	.71	.82	.42	.27	.30	.36	.24	.25
TOTAL COST	.87	1.53	1.11	1.47	.80	.91	1.00	.56	.39	.40	.46	.39	.39

Table III-9. Summary of Approximate Relative Cost Estimates for Systems Using NbTi @ 3 K

Geometry	Solenoids		Racetracks		Rectangular Saddle		Annular Section Saddle			Racetracks		Rectangular Saddle	
	Yes	No	Yes	No	Yes	No	No	No	No	Yes	No	Yes	No
Iron													
Central Field (Wb/m <sup>2</sup> )	8.0	8.0	8.0	8.0	8.0	8.0	8.0	6.5	5.0	5.0	5.0	5.0	5.0
Labor Costs:													
Design	.04	.04	.05	.05	.06	.06	.06	.06	.06	.05	.05	.06	.06
Fabrication & Installation	.09	.12	.09	.09	.13	.14	.11	.08	.06	.05	.05	.08	.08
Labor Subtotal	.13	.16	.14	.14	.20	.20	.18	.12	.12	.11	.11	.14	.14
Material Costs:													
Conductor	.18	.40	.16	.22	.08	.10	.12	.06	.03	.05	.06	.03	.03
Support Structure	.08	.16	.15	.22	.10	.12	.21	.09	.04	.02	.03	.02	.02
Dewar	.10	.17	.22	.28	.14	.15	.10	.06	.04	.07	.08	.06	.06
Iron Plug	.02	-	.003	-	.001	-	-	-	-	.001	-	<.001	-
Tooling	.06	.06	.06	.06	.07	.07	.07	.07	.06	.05	.05	.05	.05
Miscellaneous	.07	.12	.09	.12	.06	.07	.08	.04	.03	.03	.03	.02	.02
Subtotal	.52	.92	.68	.89	.44	.51	.58	.31	.20	.22	.26	.18	.19
Administrative Expenses	.15	.28	.20	.27	.13	.15	.18	.09	.06	.06	.08	.06	.06
Material Subtotal	.67	1.20	.88	1.16	.57	.66	.76	.40	.26	.28	.33	.24	.24
TOTAL COST	.80	1.36	1.02	1.30	.77	.86	.94	.54	.38	.39	.44	.38	.38



Table III-10. Summary of Approximate Relative Cost Estimates for Systems Using Nb<sub>3</sub>Sn @ 10 K

Geometry	Solenoids		Racetracks		Rectangular Saddle		Annular Section Saddle			Racetracks		Rectangular Saddle	
	Yes	No	Yes	No	Yes	No	No	No	No	Yes	No	Yes	No
Iron													
Central Field (Wb/m <sup>2</sup> )	8.0	8.0	8.0	8.0	8.0	8.0	8.0	6.5	5.0	5.0	5.0	5.0	5.0
Labor Costs:													
Design	.04	.04	.05	.05	.06	.06	.06	.06	.06	.05	.05	.06	.06
Fabrication & Installation	.09	.12	.09	.09	.13	.14	.11	.08	.06	.05	.05	.08	.08
Labor Subtotal	.13	.16	.14	.14	.20	.20	.18	.14	.12	.11	.11	.14	.14
Material Costs:													
Conductor	1.90	4.46	1.81	2.53	.85	1.09	1.38	.60	.30	.48	.62	.25	.29
Support Structure	.08	.16	.15	.22	.10	.12	.21	.09	.04	.02	.03	.02	.02
Dewar	.10	.17	.22	.28	.14	.15	.10	.06	.04	.07	.08	.06	.06
Iron Plug	.02	-	.003	-	.001	-	-	-	-	.001	-	<.001	-
Tooling	.06	.06	.06	.06	.07	.07	.07	.07	.06	.05	.05	.05	.05
Miscellaneous	.32	.73	.34	.46	.17	.22	.26	.12	.07	.09	.12	.06	.06
Subtotal	2.48	5.58	2.58	3.54	1.33	1.65	2.03	.94	.50	.71	.90	.44	.48
Administrative Expenses	.74	1.68	.77	1.06	.40	.49	.61	.28	.15	.21	.27	.13	.14
Material Subtotal	3.22	7.26	3.35	4.61	1.73	2.14	2.64	1.22	.65	.92	1.17	.57	.63
TOTAL COST	3.35	7.42	3.49	4.75	1.92	2.35	2.81	1.36	.78	1.03	1.28	.71	.77

The cost for conductor is dependent on field level, geometry and whether or not iron is utilized. The impact of the latter is dramatic at the high field levels. Generally speaking, the solenoid requires the most conductor, followed by the racetrack, the annular saddle, and the rectangular saddle. The geometry of the conductor in the annular saddle is more efficient for field production than that in the rectangular saddle; however, the conductor for the rectangular saddle lies closer to the axis in this case because the desired cross section is square, and the annular saddle must be positioned on the basis of the diagonal rather than the side of the square.

Support structure was divided into that which could be wound into the coils (e.g., a stainless steel strip wound into a solenoid) and that which must be applied externally or between coils. Size and weight of structure were computed on the basis of stress and load estimates and then multiplied by a chosen cost per pound factor for cost estimation purposes.

Cost estimates for the dewar in each case were based on size, weight, and structural requirements. Tooling cost is determined by both geometry and field level since the latter has a major effect on coil size and weight which must be handled. The manner in which each component cost was estimated is given in the section which follows.

The format for the three tables is similar, and the major difference is conductor cost. A comparison of the total system cost estimates indicates a cost advantage for a system at reduced temperature. Cost estimates for Nb<sub>3</sub>Sn systems at 10 K were generated because of an expressed interest in the possibility of operation at high temperature. As indicated, this leads to substantial cost increases.

## 2. Component Cost Estimates

The purpose of this section is to outline the manner in which the approximate cost components were estimated for use in Phase I in preparation of the relative costs given in Tables III-8, III-9, and III-10.

### a. Labor Costs

#### 1) Design

In generating labor costs for the design of the different systems under consideration, it was assumed that the design effort required was independent of field level over the field range of interest and primarily dependent on basic geometry. The design effort was broken into a list of design tasks for the solenoid, racetrack, and saddle systems. For each task the manhours were estimated for engineering, drafting, and engineering assistant labor categories. Total manhours in each category were totaled for each system geometry, and a total design cost was generated under the assumption that the unit labor cost to the program was \$30/manhour for engineering, \$20/manhour for drafting, and \$12/manhour for engineering assistants. An allowance was also included for a direct material charge for computer time. The latter was relatively low for the solenoid system because of its symmetry and relatively high for the saddle systems because of their complexity (racetracks were midway between the two).

## 2) Fabrication and Installation

In generating labor costs for fabrication and installation, manhours were estimated for engineering and technician labor categories for four general tasks for each system. The four tasks included: superconducting coil module fabrication, module and structural assembly, coil-dewar assembly, and assembly to subsystems (e.g., power supply, quench protection circuitry, refrigeration system, etc.). No allowance was made for initial system shakedown and test nor for site preparation (e.g., foundation, building, utilities, etc.). Manhours were totaled and costs were generated under the assumption that the unit labor cost to the program was \$30/manhour for engineering and \$12/manhour for technicians.

### b. Material Costs

#### 1) Conductor

Early in the program conductor designs were generated on the basis of typical current density vs. field characteristics and an approximate criterion for cryostatic stabilization. Conductor dimensions were determined as well as the required copper to superconductor ratio for several operating current levels as a function of magnetic field level (see Section III-D-1). Consideration was given to multifilament NbTi at temperatures of 2, 3, and 4.2 K; to multifilament Nb<sub>3</sub>Sn at 4.2 and 10 K; and to Nb<sub>3</sub>Sn tape type conductor at 4.2 K. An operating current level of 4,000 A was chosen as well as a type of conductor construction.

Figure III-22 illustrates the "built-up" construction which was chosen. This may be expected to be economical for the high copper to superconductor ratios and large quantities required for the magnets under consideration. It consists of a basic multifilament or tape type conductor which is then soldered to sufficient copper to achieve the necessary total copper to superconductor ratios. A cost estimate for a unit length of conductor was determined as a function of magnetic field by first estimating the cost per kiloamp-meter for the basic conductor and then incrementing the cost to allow for the additional copper required and for the soldering operation. The cost per kiloamp-meter for the base conductors was estimated following discussions with conductor manufacturers\* and scaled to different field values. The assumed values are given in Table III-11. The values in Table III-11 are approximate but suitable for use in generation of rough system cost estimates. No attempt was made to consider the cost or fabrication implications of large quantity production or the need to develop handling techniques.

On the basis of approximate stability criteria, the amount of copper needed to stabilize each of the base conductors in Table III-11 was found. It was then estimated that the final conductor cost would be determined by the base conductor cost from Table III-11, an incremental cost of 2.3 \$/lb. for the additional copper required, and an incremental cost of 0.85 \$/lb. of total conductor weight

---

\* Manufacturers contacted were: Intermagnetics General Corp. for Nb<sub>3</sub>Sn tape, Harwell Superconductors for Nb<sub>3</sub>Sn multifilament, and Magnetic Corporation of America for NbTi multifilament.

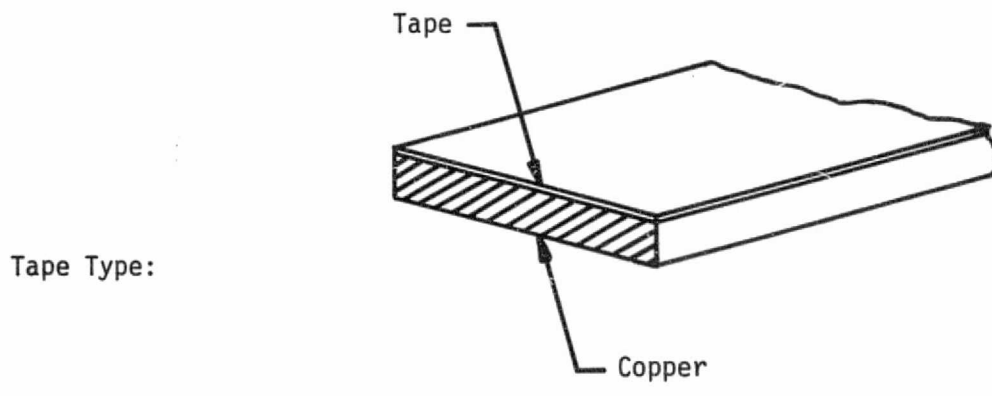
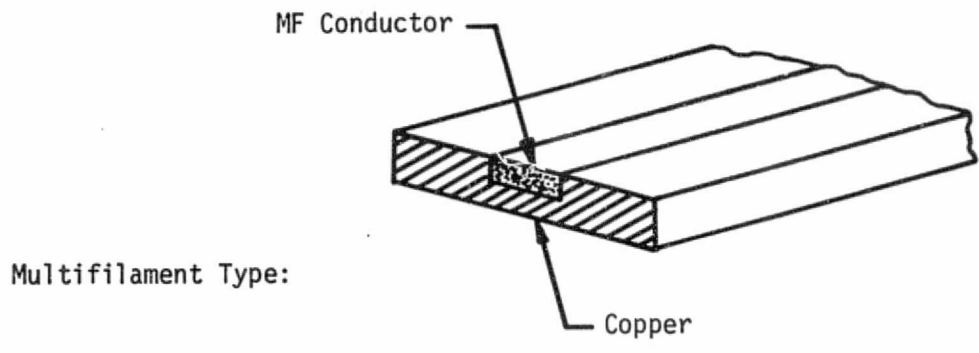


Figure III-22  
"Built-up" Conductor Construction for Multifilament and  
Tape Type Superconductors

TABLE III-11

ASSUMED COST PER UNIT LENGTH: (\$/kAm) FOR BASE CONDUCTORS

<u>Magnetic Field (Tesla)</u>	<u>5</u>	<u>8</u>	<u>10</u>	<u>11</u>	<u>12</u>
Nb <sub>3</sub> Sn (tape) @ 4.2 K	5.95	11.13	17.25	--	28.75
Nb <sub>3</sub> Sn (MF) @ 4.2 K	10.87	16.22	25.30	--	38.93
Nb <sub>3</sub> Sn (MF) @ 10 K	21.57	37.12	67.47	--	133.32
NbTi (MF) @ 4.2 K	2.3	4.4	11.1	68.8	--
NbTi (MF) @ 3 K	1.58	2.82	4.69	7.12	--
NbTi (MF) @ 2 K	1.25	1.91	2.92	3.94	--

for forming the "built-up" conductor through soldering. The resulting estimated conductor cost in \$/m for the six conductors considered is shown in Figure III-23 as a function of magnetic field. The curves clearly indicate the cost advantage at 4.2 K of NbTi relative to Nb<sub>3</sub>Sn tape or relative to Nb<sub>3</sub>Sn multifilament from low fields to field levels in excess of 10 T. Results also indicate a substantial cost savings for NbTi if the temperature is reduced below 4.2 K. The effect arises from the increase in critical current density as temperature decreases and is most pronounced at the high field levels. Nb<sub>3</sub>Sn multifilament was also considered at 10 K because of a possible interest in high temperature operation; however, results indicate that the cost may be prohibitive. The overriding effect is the decrease in critical current density at the high temperatures.

Figure III-23 now forms the basis for generating the conductor cost estimates for the systems considered. For each system the total conductor length and the peak magnetic field at the windings were estimated. It was then assumed that a graded construction would be utilized with three different conductors. These were chosen for operation at the peak field, at 0.8 times the peak field, and at 0.6 times the peak field. Furthermore, it was assumed that 20 percent of the total conductor required would be purchased with properties suitable for peak field operation, 20 percent with properties suitable for operation at 0.8 times the peak field, and 60 percent with properties suitable for operation at 0.6 times the peak field. This then specified the quantity required at each of three fields for each system and combined with the unit costs from Figure III-23 determined the total conductor cost for the purposes of the Phase I system comparison.

## 2) Support Structure

Costs for support structure were determined by estimating the weight of structural components and then multiplying by an estimated cost/unit weight. Structural weights were based on conceptual designs for support (see Section III-D-2) sized on the basis of calculated loads of electromagnetic origin for each case. Components were divided into external structure and internal structure. External structure was defined as tie rods and built-up stainless steel sections such as I-beams and ring girders applied to the outside of the winding envelope. Internal structure was defined as stainless steel strip wound within the windings in parallel with the conductor for internal winding support. Following estimation of weights for external and internal structure, total structural costs were generated assuming unit costs of 8.1 \$/lb. for external structure and 1.5 \$/lb. for internal structure.

## 3) Dewar

Dewar weights were estimated on the basis of the overall size of the windings plus support structure together with approximate calculations involving the necessary shell, plate, and rib thicknesses to support the atmospheric loads with a suitable safety factor (see Section III-D-3). Dewar costs were then determined by multiplying the estimated dewar weight by a unit cost assumed to be 4.40 \$/lb.

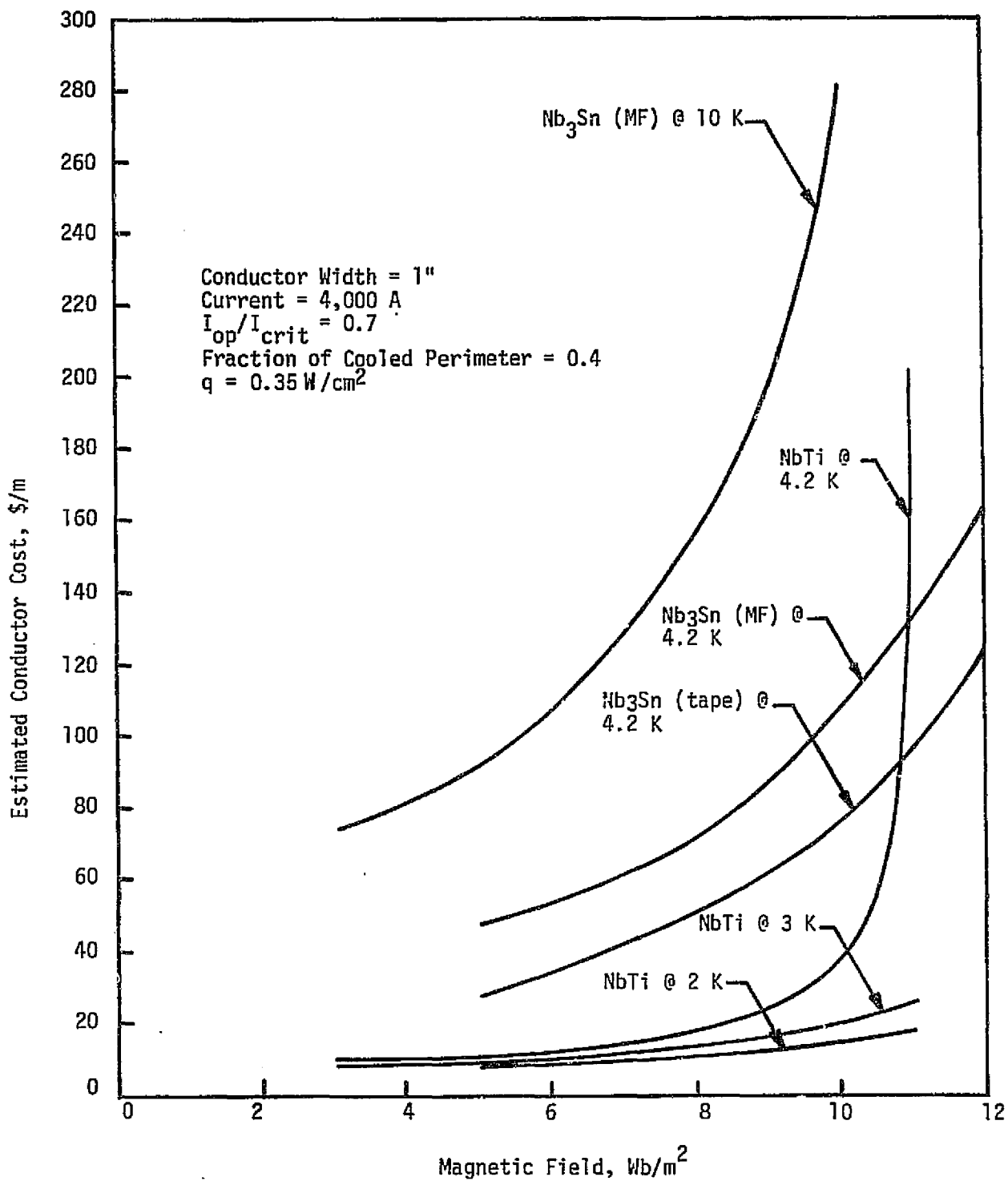


Figure III-23

Estimated Conductor Cost Vs. Field for Fully Stable Conductors

#### 4) Iron Plug

For each case involving the use of iron, the weight of the iron plugs was determined on the basis of the optimized system dimensions. A cost estimate was then found on the basis of a unit cost assumed to be 0.45 \$/lb.

#### 5) Tooling

To determine the tooling cost for the systems, the effort focused on the characteristics of the 8 T systems. For each case (i.e., solenoid, racetrack, rectangular saddle, and annular saddle), estimates were made for the cost of tooling in four categories. This included winding fixtures, coil and module handling fixtures, winding machine requirements, and on-site handling and dewar assembly fixtures. The total tooling cost for each 8 T geometry was then reduced by 10 percent to arrive at a tooling cost for the 6.5 T case, and the tooling cost for each 8 T geometry was reduced by 20 percent to arrive at a corresponding value for the 5 T case.

#### 6) Miscellaneous

The cost for miscellaneous material items was assumed to be 15 percent of the sum of the material cost estimates for conductor, support structure, dewar, iron plugs, and tooling.

#### 7) Administrative Expenses

Administrative expenses are those costs which arise in procurement of the material and in administering the contracts for each material item. These were assumed to be 30 percent of the subtotal for conductor, support structure, dewar, iron plugs, tooling and miscellaneous.

### D. DESIGN CONSIDERATIONS

This section will present a discussion of the methods used in developing and evaluating the design concepts for Phase I of this program. The methods and techniques are approximate but suitable for use in overall systems and trade-off analyses and in the generation of approximate cost estimates.

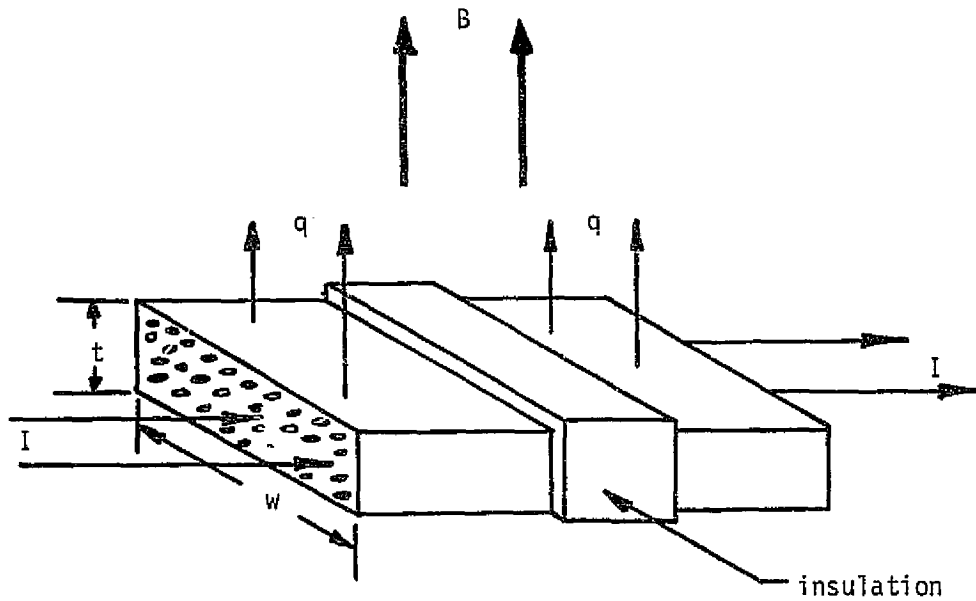
#### 1. Conductor

The basic component in any superconducting magnet is the conductor. The characteristics of the conductor are dependent on the operating current level, field to be experienced, operating temperature, and stability criterion used in design. Because of the large size and capital investment required for the systems of interest to this program, a design involving full cryostatic stabilization is justified. Typical conductor size and copper to superconductor ratios were determined early in the program for use in finding the overall current density and quantity of conductor necessary for each magnet concept considered.

The model used for conductor design is illustrated in Figure III-24. The figure illustrates a conductor with cross-sectional dimensions,  $t \times w$ , carrying a current  $I$  in the presence of a magnetic field  $B$ . A fraction,  $f$ , of the



SCHEMATIC ILLUSTRATING MODEL USED FOR DETERMINING CONDUCTOR SIZE  
AND COPPER TO SUPERCONDUCTOR RATIO



Heat Balance:  $\rho j_{sc} I = 2fq(t+w)(csc)$

Geometry:  $j_{sc} tw = I(1+csc)$

$\rho$  = resistivity =  $\rho(B,T)$

$B$  = magnetic flux density

$T$  = temperature

$j_{sc}$  = superconductor current density =  $j_{sc}(B,T)$

$I$  = operating current

$q$  = heat flux per unit area

$f$  = fraction of exposed area

$csc$  = copper to superconductor ratio

Figure III-24

surface area is exposed to liquid helium which is assumed to be able to accept a heat flux per unit area,  $q$ . The critical current density of the superconductor,  $j_{sc}$ , and the resistivity of the substrate,  $\rho$ , are known functions of field and temperature. Two equations can then be written on the basis of a heat balance assuming all current flow in the substrate (note: substrate to superconductor ratio = csc) and on the basis of a geometrical constraint.

The decision was made to concentrate on multifilament NbTi and Nb<sub>3</sub>Sn tape type conductor because of their commercial availability in large quantities and application experience. Consideration was also given to multifilament Nb<sub>3</sub>Sn because of its potential for availability and application in the future.

The critical surface for a superconducting wire is illustrated in Figure III-25. The so-called "short sample" characteristic is shown at the temperature  $T_b$ . Note that temperature reduction below  $T_b$  leads to increased current carrying capacity, and temperature increase above  $T_b$  leads to a decrease in capacity. For this program we are particularly interested in operation at  $T_b = 4.2$  K; consequently, conductor designs were generated for multifilament NbTi, for multifilament Nb<sub>3</sub>Sn, and for tape type Nb<sub>3</sub>Sn. Interest was also expressed in an advanced design for operation at  $T_b = 10$  K; consequently, multifilament Nb<sub>3</sub>Sn designs were determined at this temperature. Finally, the decision was made to consider operation at a reduced temperature to take advantage of possible cost savings in the conductor required. As a result, conductor designs were generated for NbTi at 3.0 K and at 2.0 K. The impact of low temperature operation on current carrying capacity is indicated in Figure III-26, which shows superconductor current density as a function of magnetic flux density and temperature for NbTi. The effect is particularly important at the high field level where the percentage gain in critical current density as temperature is reduced is most dramatic. Reduced temperature operation leads to increased refrigeration costs; however, these may be offset by substantial savings in the conductor required.

Figure III-27 gives the conductor thickness as a function of magnetic field for the six superconductor-temperature combinations considered. All conductors have a width of one inch and operate at 4,000 A, which is 70 percent of the critical current for the conductor. All designs are fully stabilized assuming a fraction of cooled conductor perimeter of 0.4 and an allowable heat flux from the conductor surface of 0.35 W/cm<sup>2</sup>. Note that the variation in conductor thickness for the six combinations is relatively small at a given field over most of the field range even though the superconductor current density may be vastly different. This results from the relatively large amount of copper required for cryostatic stabilization. In effect, the conductor cross section is determined primarily by the quantity of copper necessary and not by the quantity of superconductor. This argument holds for fields up to about 10 Wb/m<sup>2</sup>. Above this field, the conductor thickness curve for NbTi at 4.2 K begins to increase rapidly. This arises because of the rapid decrease in critical current density of NbTi at these high field levels for  $T_b = 4.2$  K. When the temperature is decreased to 3.0 K and 2.0 K, the effect is cancelled.

The conductor current density for the six conductor-temperature combinations is shown in Figure III-28. For fields up to about 10 T, there is relatively little variation between conductors at the 2 K, 3 K, and 4.2 K levels. The

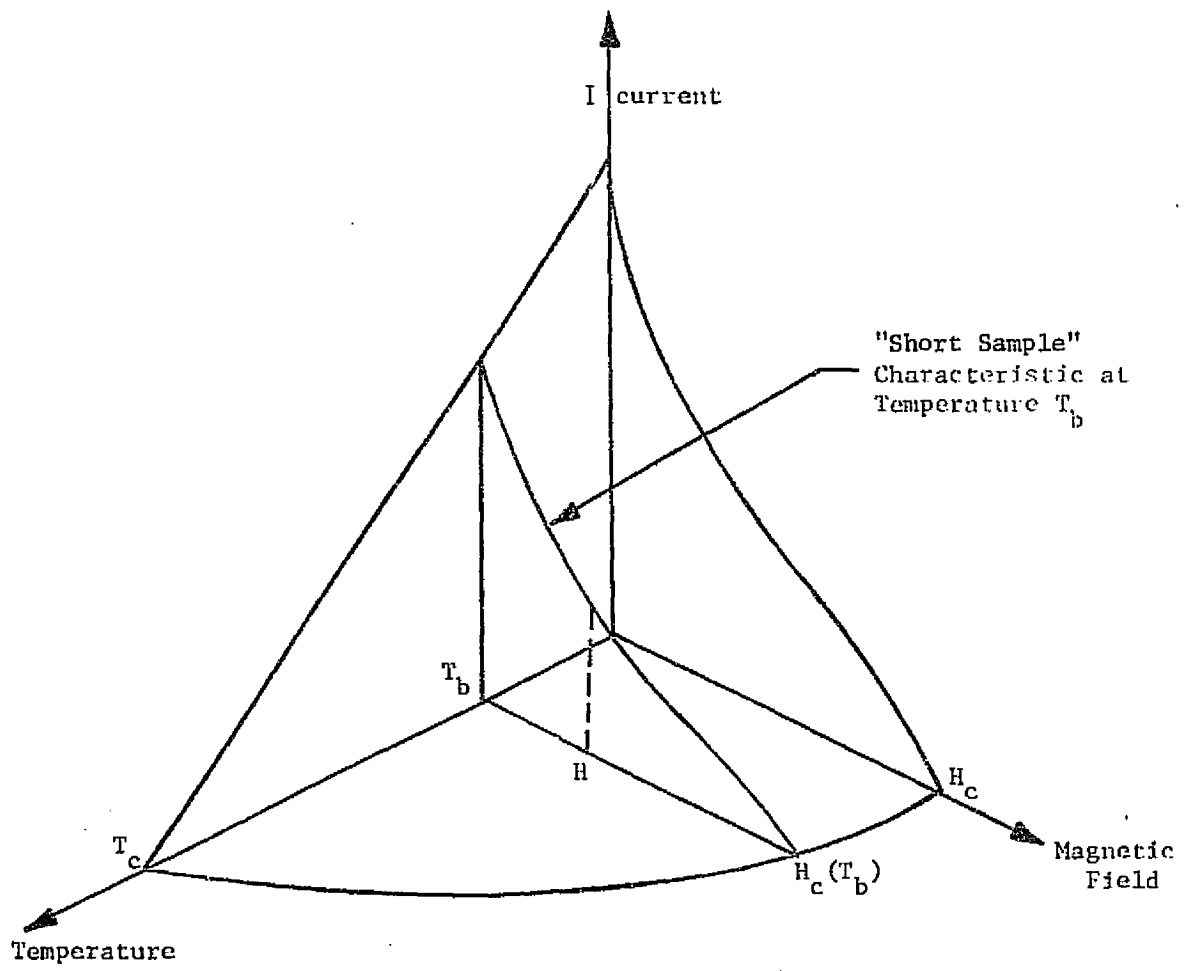


Figure III-25

Illustration of the Critical Surface of a Superconductor

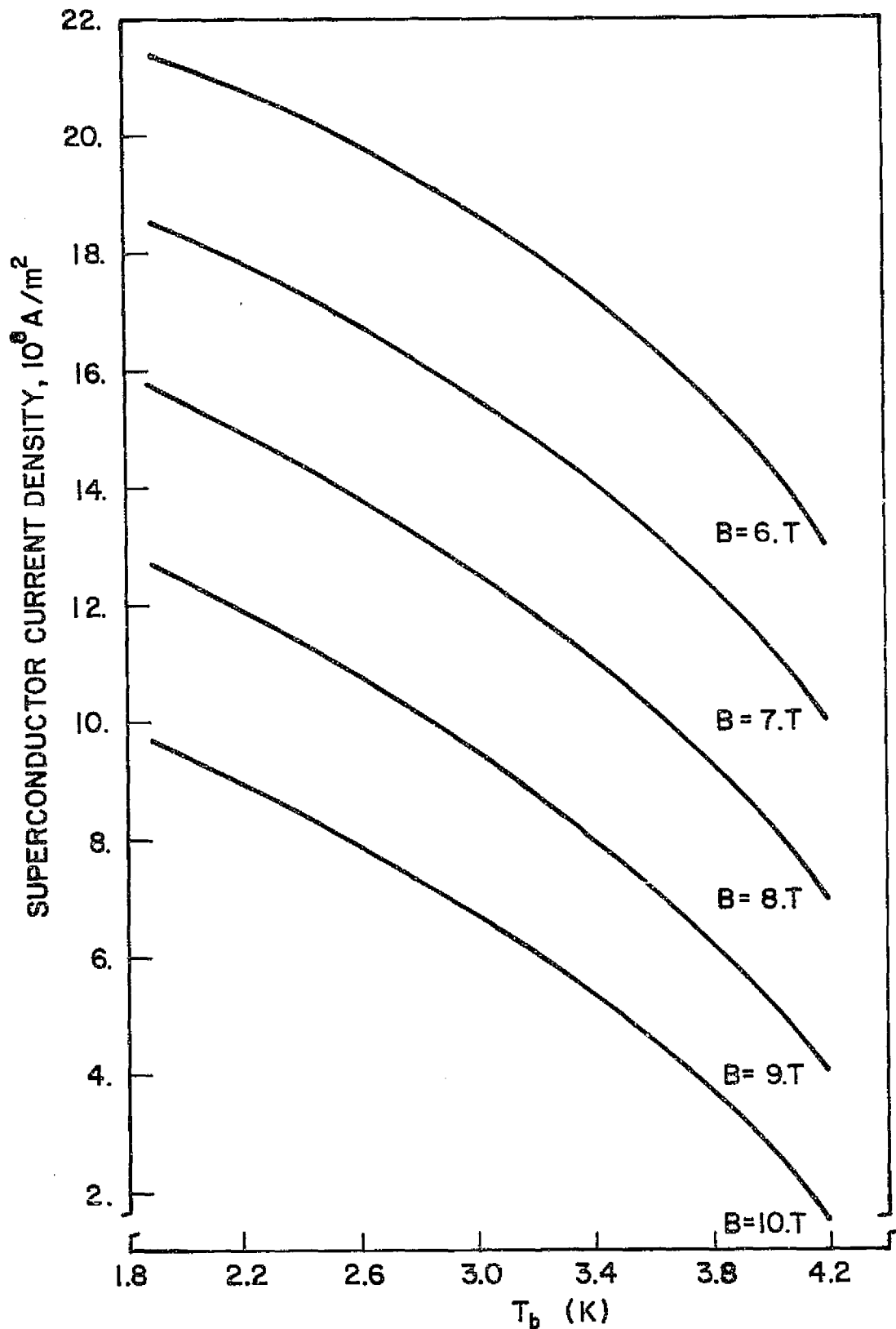


Figure III-26. SUPERCONDUCTOR CURRENT DENSITY AS A FUNCTION OF MAGNETIC FLUX DENSITY AND TEMPERATURE FOR NbTi.

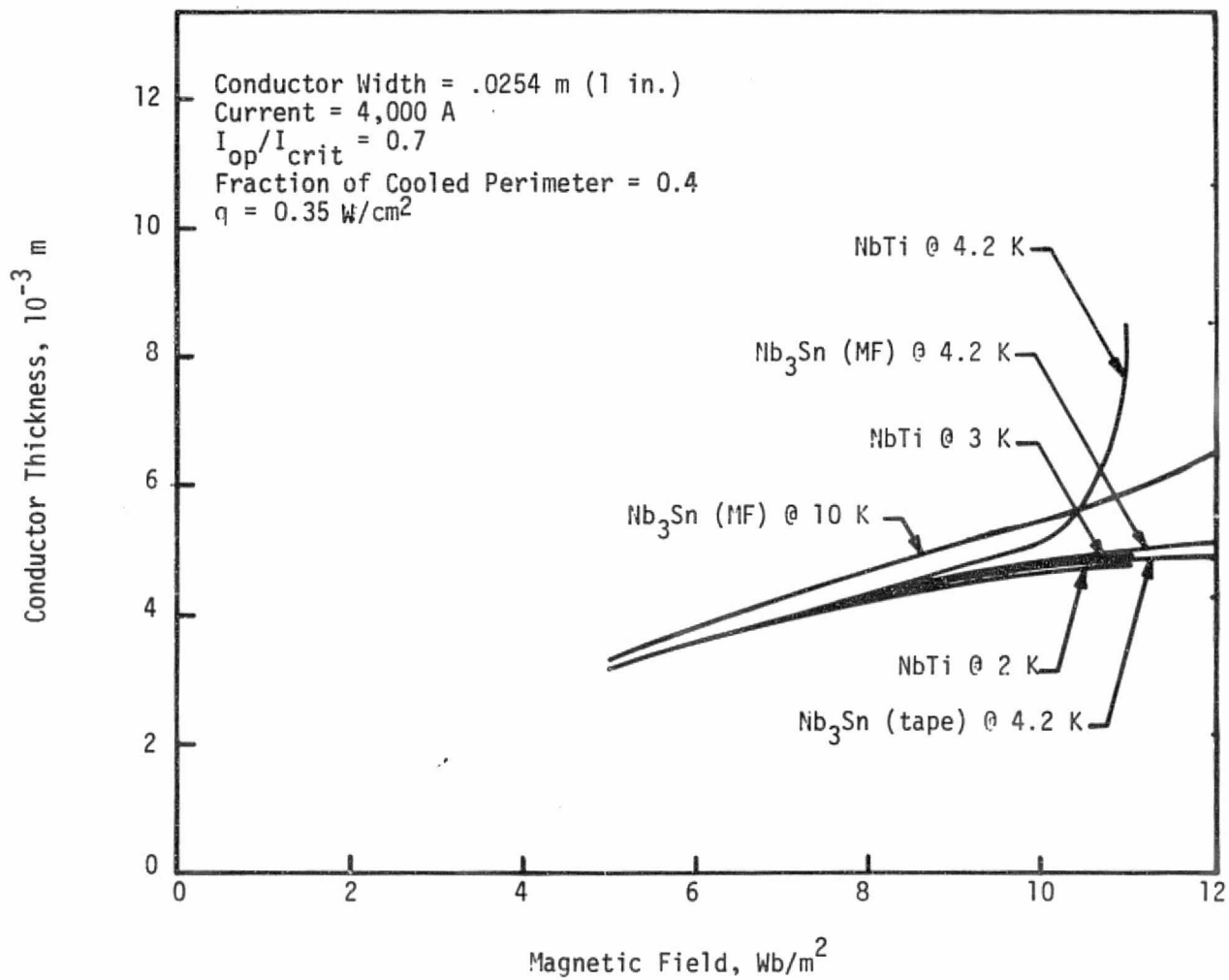


Figure III-27

Conductor Thickness Vs. Field for Fully Stable Conductors

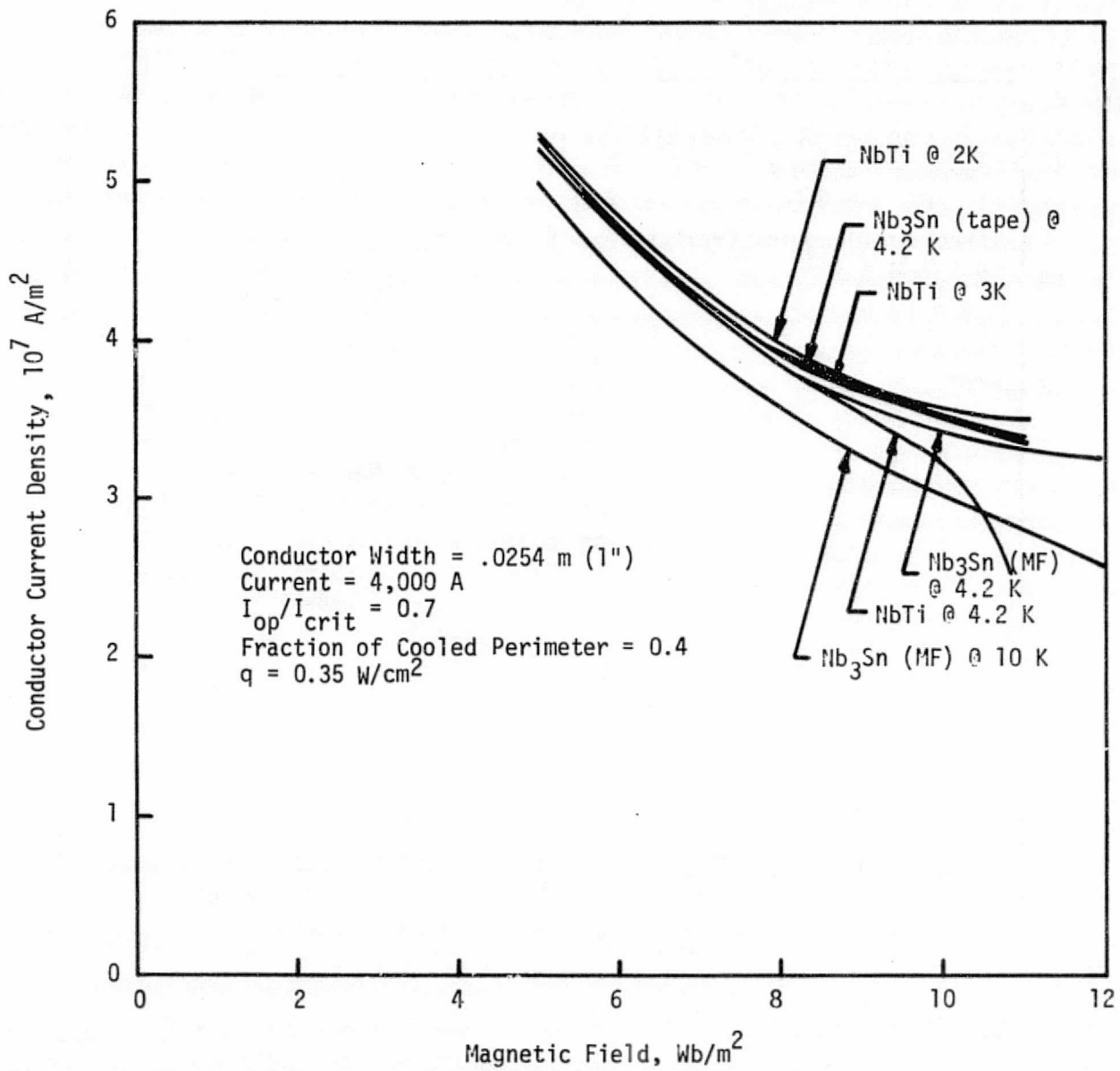


Figure III-2.

Conductor Current Density Vs. Magnetic Field for Fully Stable Conductors

conductor at 10 K operates at somewhat lower current densities but is still in the same general range. The weights per unit length for these conductors are given in Figure III-29.

Figure III-30 gives the overall current density attainable with the conductor assuming a spiral wrap insulation 0.006 inches thick on each turn and assuming a 0.032-inch thick spacer between layers. This is the maximum attainable overall current density since it does not include a loss in packing factor attributable to internal winding structure if it is needed.

Each of the curves described above corresponds to fully stabilized, high copper to superconductor ratio conductors with an operating current of 4,000 A. Generally speaking, the advantage of a high operating current is a reduced cost. As higher currents are considered, however, overall current density is eventually penalized because of limitations on heat transfer from the conductor surface. Conductor characteristics were run at the 3,000 A and 5,000 A levels as well as at 4,000 A. The latter was eventually chosen for the Phase I conceptual design effort because it was high enough to reduce the total turns involved to a reasonable level and yet not so high as to substantially penalize the attainable overall current density.

## 2. Support Structure

Cost estimates for magnet support structure were arrived at by determining loads of electromagnetic origin for each system, estimating the weight of the structure required to support the loads, and multiplying the weight by a suitable unit cost.

Figure III-31 illustrates the main loads in a solenoid system and the mode of support assumed in the Phase I conceptual design trade-off. In the lower figure,  $F_c$  represents the attractive load between coils,  $F_i$  represents the attractive load between iron plugs, and  $F_r$  represents the radially directed load on the windings. The weight of the compressive structure was determined on the basis of stainless steel loaded to a working stress of  $2.8 \times 10^4$  psi with sufficient length to bridge the space between coils and sufficient cross-sectional area to carry the total load  $F_c$  and  $F_i$ . The radial load  $F_r$  was assumed to be supported by "hoop" stresses generated in the conductor and in stainless steel banding wound within the winding. In order to size the banding, the average hoop stress across the winding was computed and then multiplied by a geometry dependent factor to estimate the maximum hoop stress. Sufficient stainless steel was then added to the winding to limit the stress in the conductor to 10,000 psi. The top sketch in Figure III-31 illustrates a section of a single turn in parallel with a structural band and the manner in which the radial stresses are supported by hoop stresses in the conductor and structural band. The division of the hoop load between the conductor and band is dependent on their relative cross-sectional area and moduli of elasticity. For the cases considered, the band was sized to limit conductor stress to a pre-determined level.

The main loads of em origin in a transverse section of magnets with the racetrack or saddle geometries are illustrated in Figure III-32. The top figure is a racetrack section.  $F_c$  represents the attractive force between the magnet

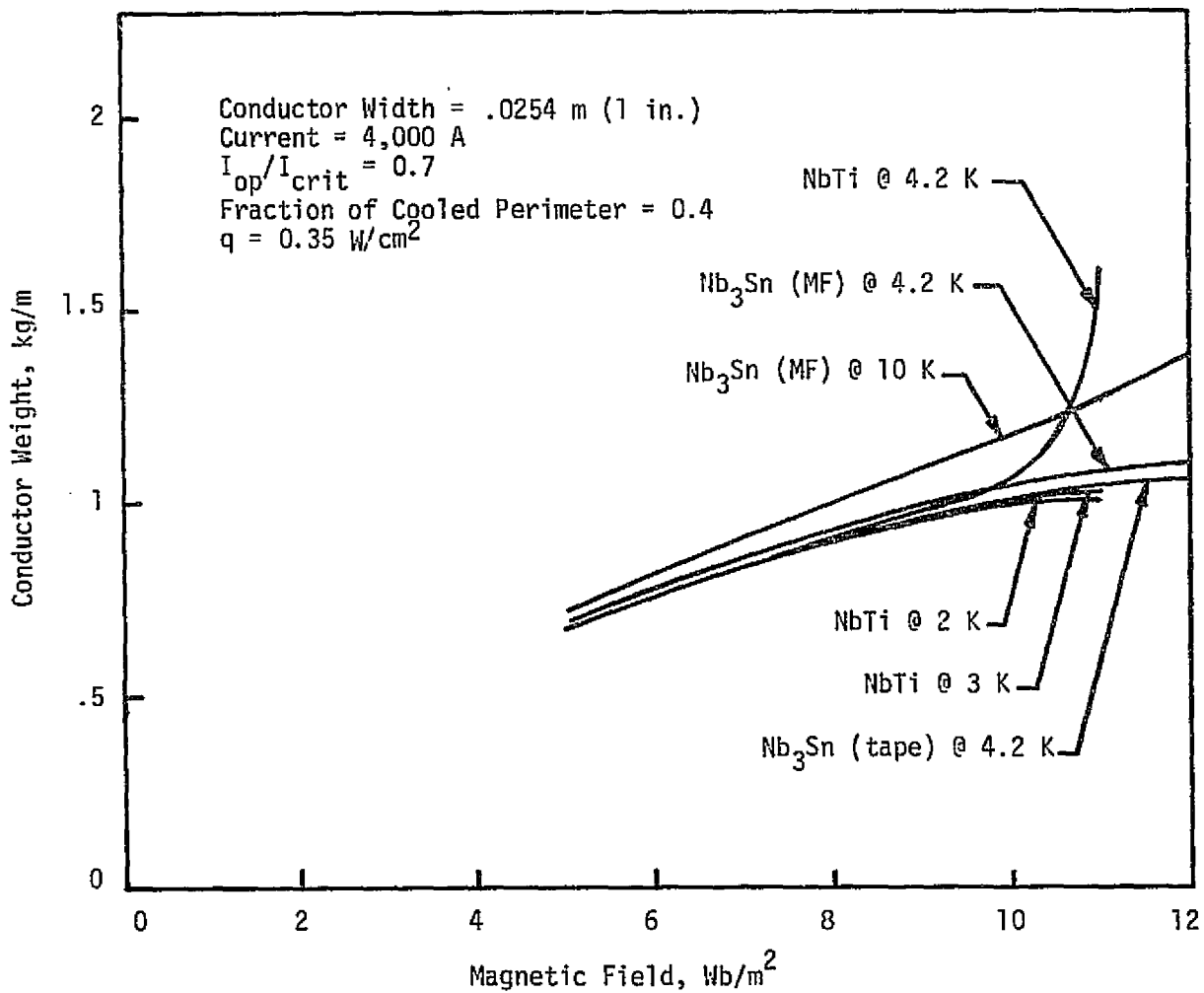


Figure III-29

Conductor Weight Vs. Magnetic Field for Fully Stable Conductors

FA 3088



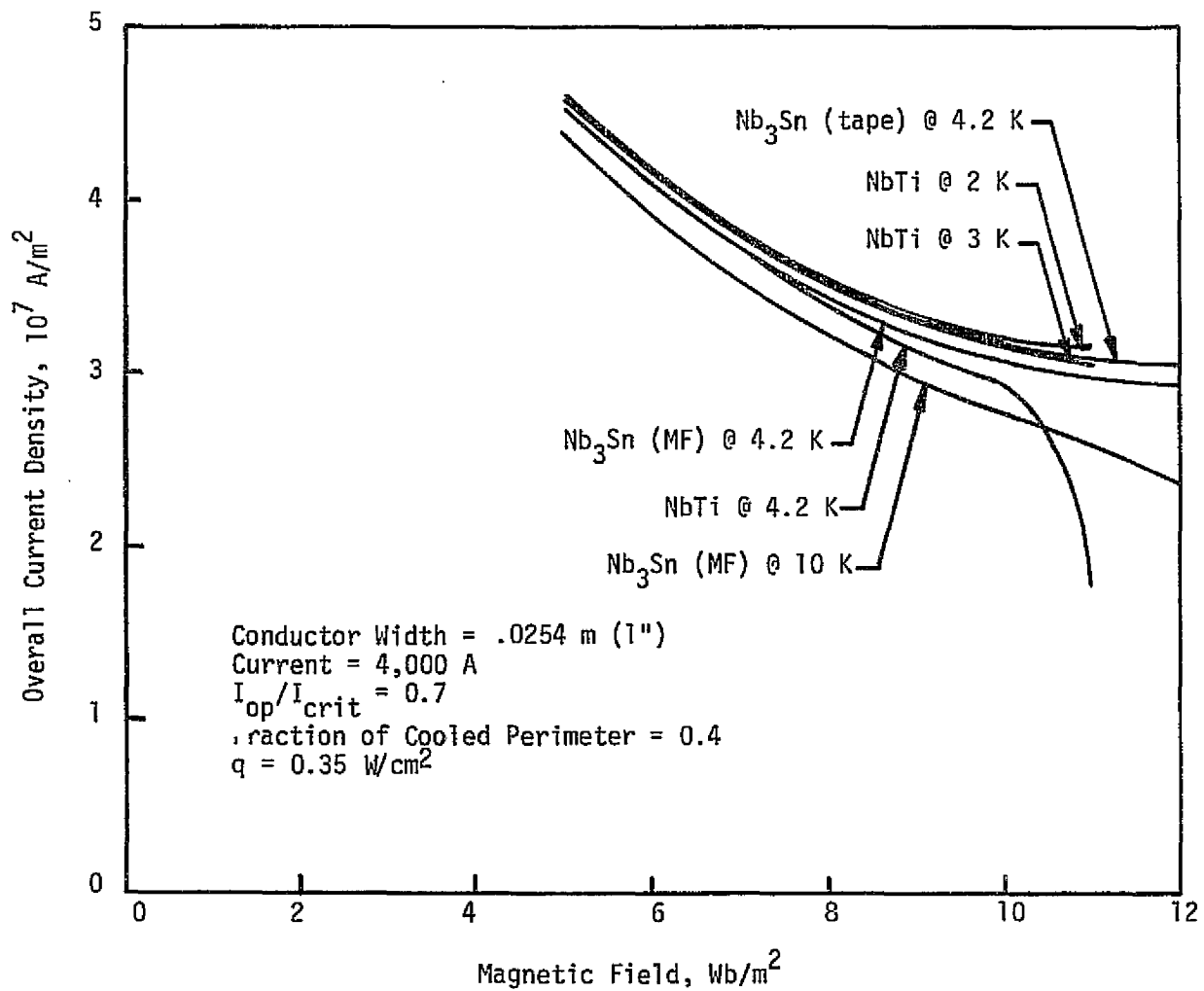
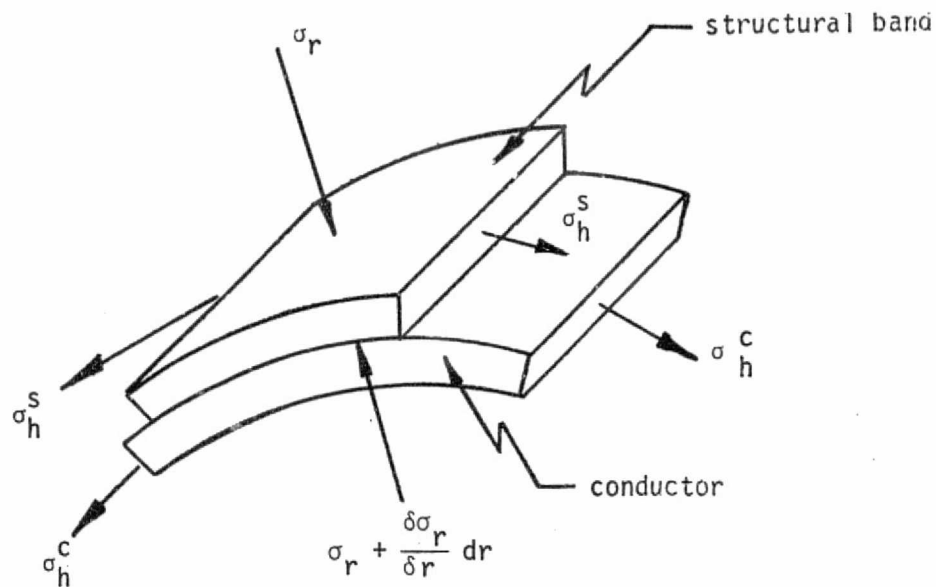


Figure III-30

Overall Current Density (No Allowance for Structure) Vs. Magnetic Field for Fully Stable Conductors



$F_r$  - Radial force

$F_h$  - Hoop force

$F_c$  - Compressive (attractive) force

$F_i$  - Attractive force in the iron

$\sigma_r$  = Radial Stress

$\sigma_h$  = Hoop Stress

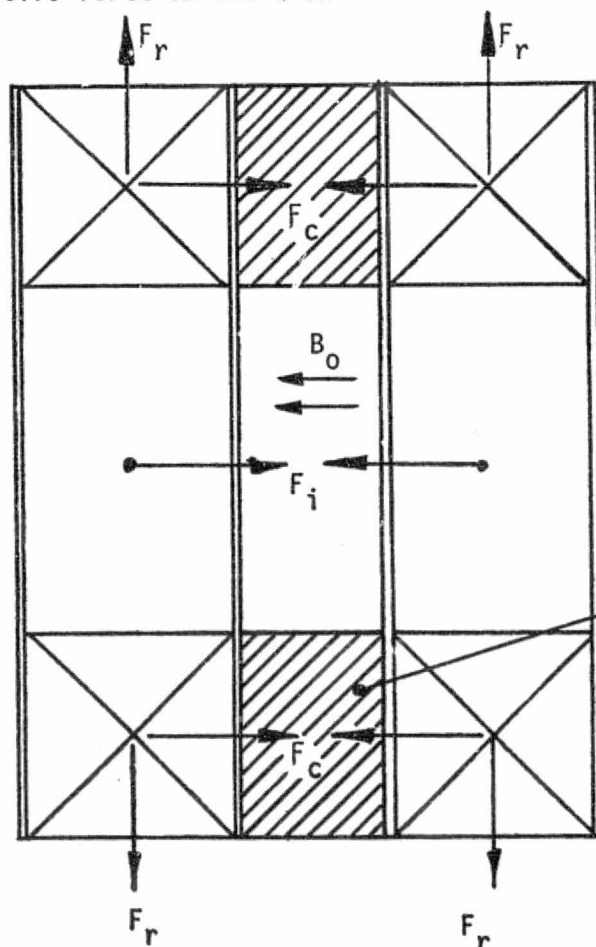


Figure III-31

Illustration of the loads of electromagnetic origin in a split solenoid and of the stresses carried by a winding segment.

Compressive Structure

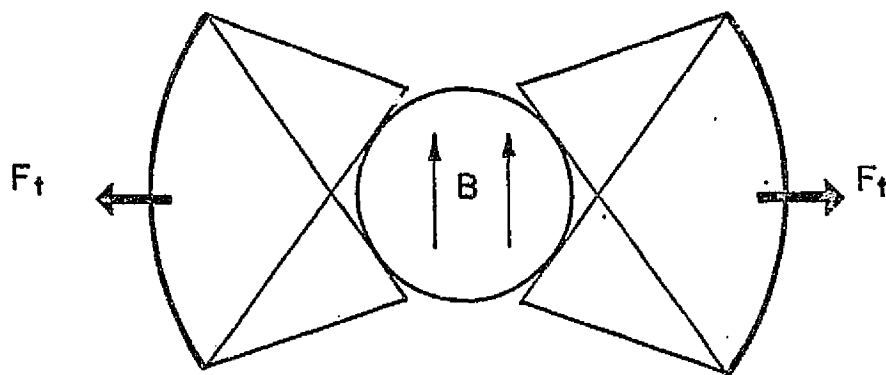
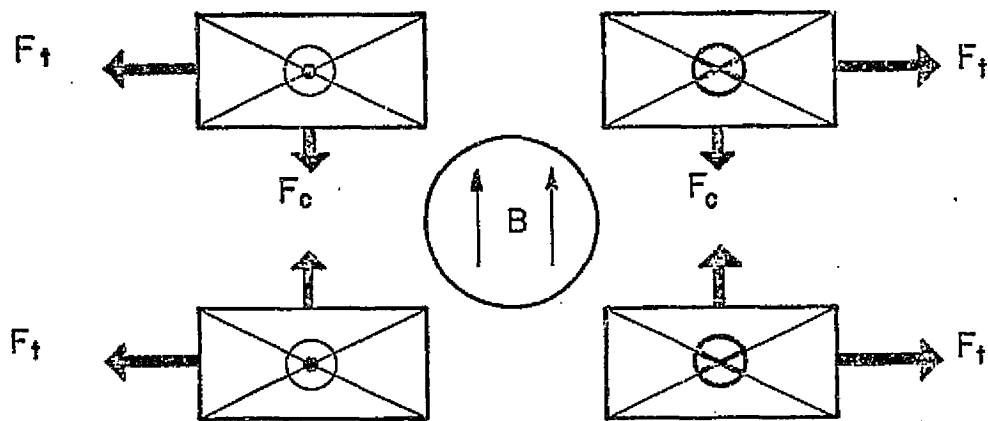


Figure III-32

Transverse sections of racetrack and saddle magnets showing loads of electromagnetic origin. In addition an axial load exists which tends to stretch the windings perpendicular to the sketches.

halves. The weight of the compressive structure which supports this load was determined on the basis of stainless steel loaded to a working stress of  $2.8 \times 10^4$  psi with sufficient length to span the distance between coils and sufficient cross-sectional area to carry the total load  $F_c$ . For the purposes of estimating the structural weight necessary to support the loads  $F_t$ , the concept illustrated in Figure III-33 was utilized. This consists of I-beams which span both coils and which transmit the load from one side of the coil to the other via tie rods. Stainless steel loaded to a working stress of  $2.8 \times 10^4$  psi was utilized. A similar structure was assumed for transverse support in the rectangular saddle geometry. Somewhat different structural concepts were used in the Phase II design phase. The concepts illustrated served as a basis for comparison involving sufficient structure in a trade-off for several field levels and geometries for the purposes of Phase I.

The lower sketch in Figure III-32 illustrates the main load in a transverse section of an annular saddle type magnet. This is comparable to the load  $F_t$  in the racetrack. The load in the saddle which is comparable to  $F_c$  in the racetrack is supported within the windings and may require internal structure. To estimate a transverse structural weight for the annular saddle, a stainless steel ring girder structure similar to that illustrated in Figure III-34 was assumed.

In addition to the loads illustrated in Figure III-32, the racetrack, rectangular saddle, and annular saddle experience loads on the end turns which tend to "stretch" the coils parallel to the axis. In the racetrack and annular saddle geometries, weight estimates were generated for sufficient stainless steel strips to carry this load component under the assumption that it would be wrapped within the windings. For the rectangular saddle, weight estimates were generated assuming I-beams and tie rods for load transmittal between ends.

The purpose of the structural concepts described above was to provide a basis for computing structural weights sufficient to carry the loads of em origin and, in turn, to allow rough cost estimates to be generated. The techniques for load support were all subject to review and change in Phase II.

### 3. Dewar

Dewar weights were determined for cost estimation purposes by sizing individual shells and walls with stiffeners where applicable. For the cylindrical shells envisioned for the annular section saddle and for the cylindrical shell components of the solenoid and racetrack systems, weight optimization computer programs were utilized. These programs are used to size the thicknesses, diameters, and lengths of a cylindrical magnet dewar in a preliminary fashion to yield the optimum weight design based upon safe structural strength criteria. The dewar consists of helium can, radiation shield, and room temperature container. It was assumed that the radiation shield was cooled by liquid helium boiloff and that the radiation shield and cold vessel were wrapped with superinsulation. No allowance was made for cryogenic support equipment such as vacuum pumps, transfer lines, etc.

The magnet size was determined by the MHD field-volume requirement and the assumed overall current density. Estimates of em loads were used to size structure. This then determined the radii of the helium can, radiation shield

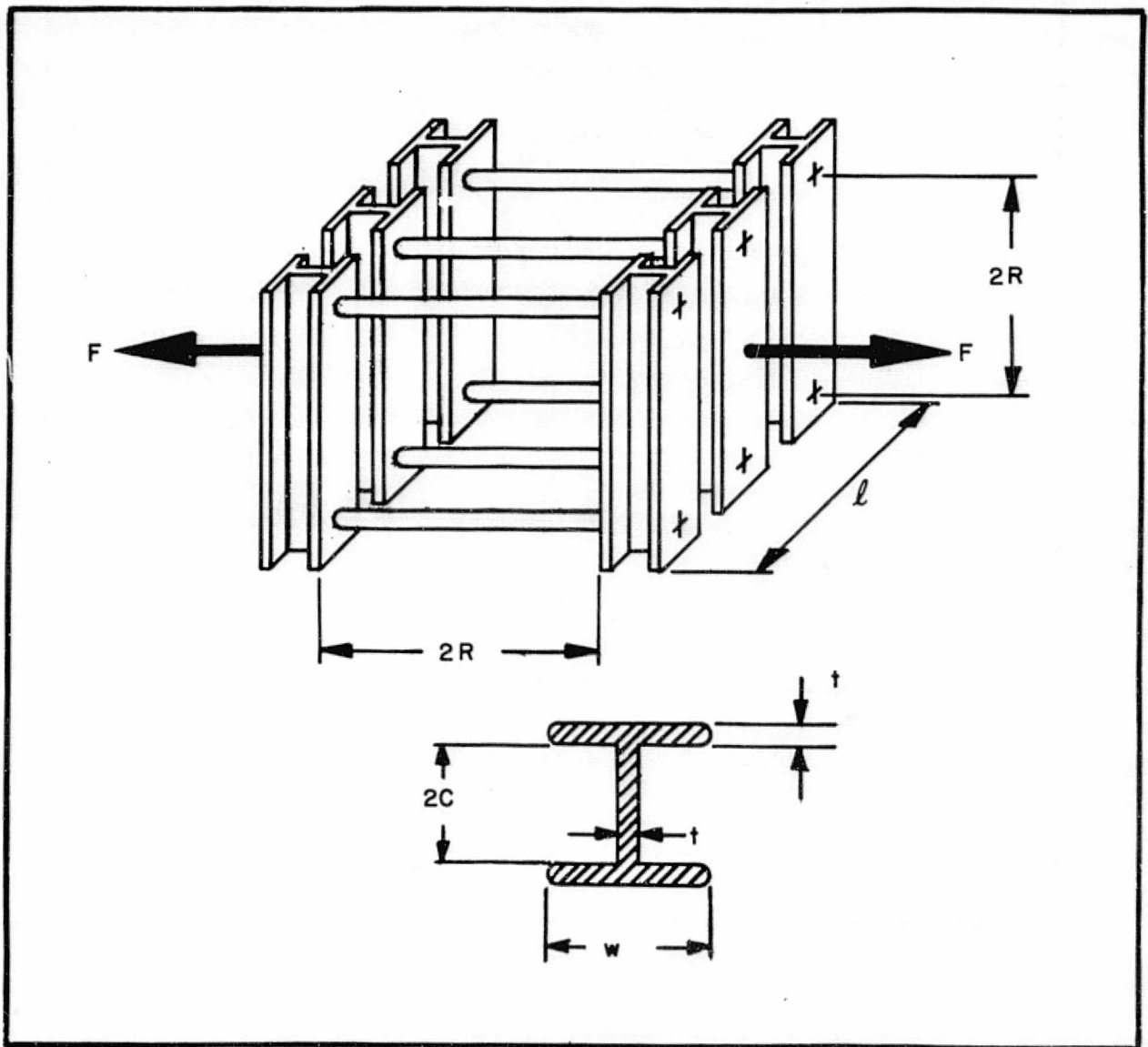


Figure III-33

Tension Rod and Straight Beam Structure for Transverse Support  
of Racetrack or Rectangular Saddle Configuration

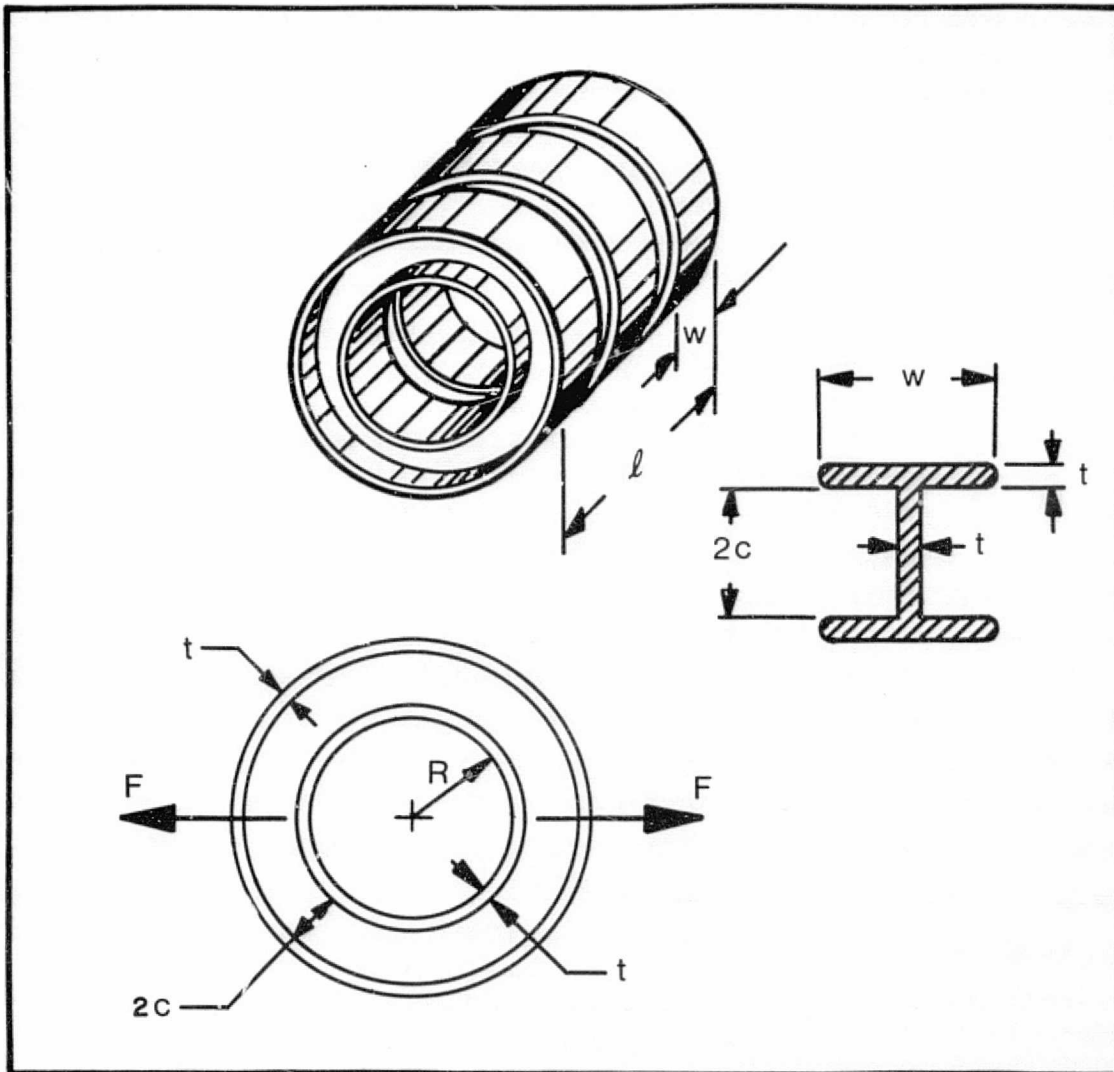


Figure III-34

Ring Girder Structure for Transverse Support of the  
Annular Section Saddle Geometry

and room temperature container in the region of the magnet. Reasonable engineering tolerances were assumed for distances between walls.

The criteria for determining the shell thicknesses depended upon the type of shell loading, there being two different types of loading to be considered in dewar construction.

The helium can is subjected to an internal pressure, and the thickness was calculated from a maximum working stress criteria with a constraint set on minimum allowable thickness based on past experience in shell handling and fabrication.

A safety factor was incorporated by taking the pressure to be larger than expected over-pressures and/or in the choice of working stress. The outer shell is subjected to an external pressure, and the criteria for preventing buckling are usually more stringent than those determining the compressive stress in the walls. The outer shell is subject to buckling both radially and axially, and there are different criteria for each of these in the computer program. Which one is the most stringent depends upon the lengths, diameters, material thicknesses, and material properties. A ribbed structure was assumed. The number of ribs required for stability and the weight of the configuration were calculated on the basis of the appropriate stability criterion.

Flat plates were assumed to be subjected to a uniform pressure and ribbed with stiffeners. Figure III-35 illustrates typical results for weight estimates for flat plates as a function of dimension and aspect ratio (i.e., ratio of plate width to length) for a load of 45 psi and a working stress of  $2 \times 10^4$  psi.

Shells sized in the above fashion by subroutines were then combined by a main program to determine dewar weight.

#### 4. Iron

The use of iron offers two advantages in a superconducting magnet system: (1) it can contribute to magnetic field production and, therefore, reduce the total ampere-meter requirement and (2) it can be positioned so as to create a reverse field in the vicinity of the maximum field region near the winding and thus reduce the maximum field experienced by the superconductor.

To gain an insight into the field production capability of the iron, consider Figure III-36. The sketch represents the cross section of one quadrant of a rectangular saddle system with dimensions suitable for production of a central field of about 8 T. Three different locations for iron slabs are illustrated. The table indicates estimates for the central field production capability of each type. The type 1 slab or pole piece is the most effective and contributes approximately  $0.5 \text{ Wb/m}^2$  to the central field. Type 2 and type 3 locations are comparable in field production capability but only 70 percent as effective as the type 1 location. The table also indicates the respective masses per unit length for iron in the three locations. Assuming that cost is dependent on weight, it is clear that the type 1 location is most cost effective.

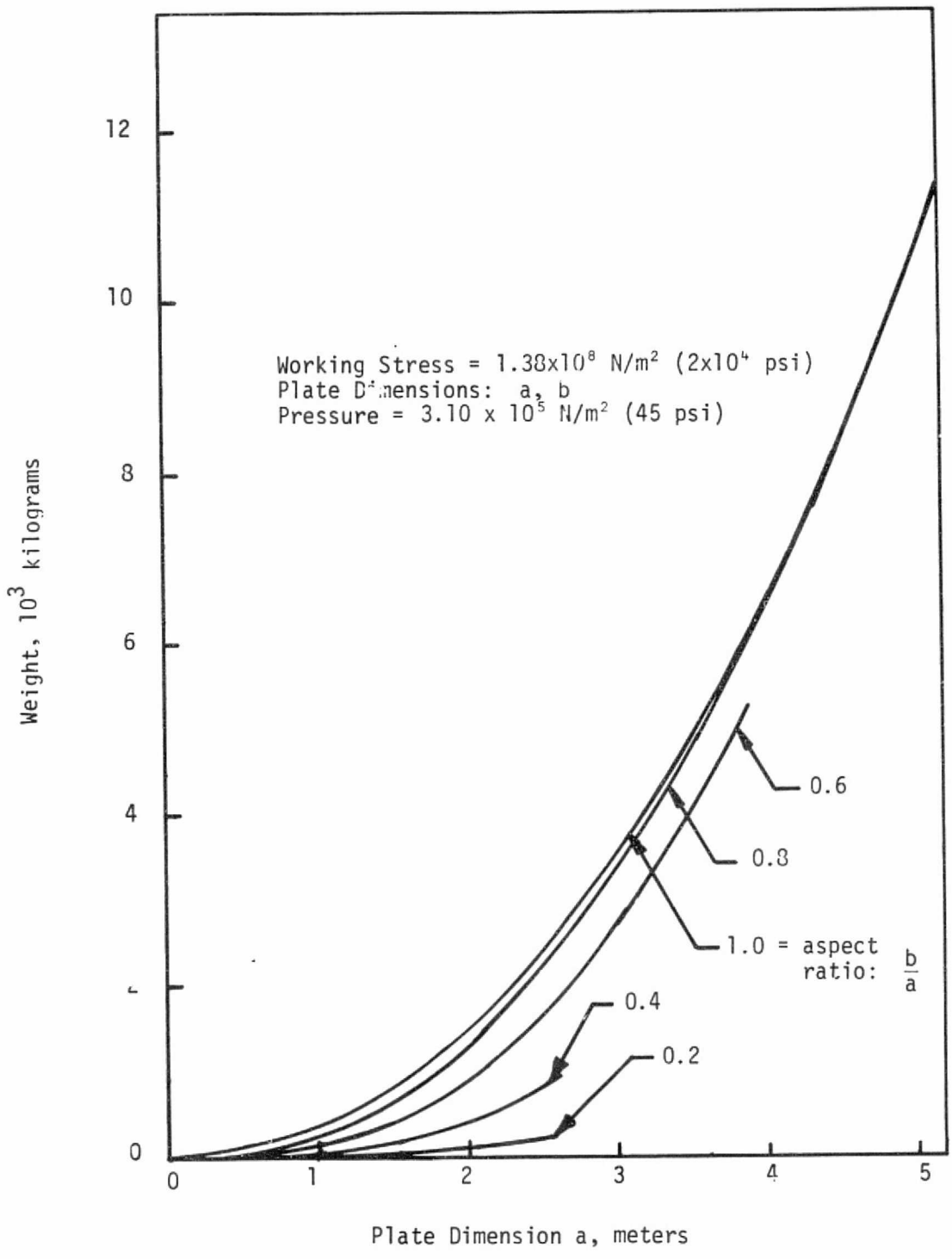
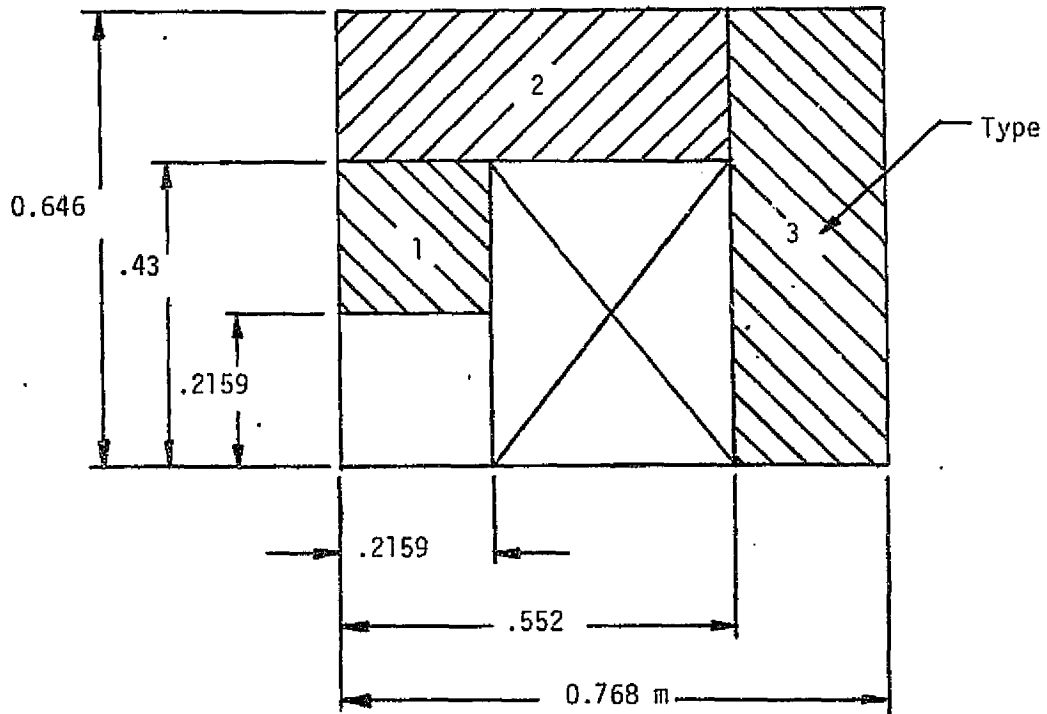


Figure III-35  
 Estimated Weights for Reinforced Plates Under Uniform Load





Type	B* (Tesla)	Mass per unit length (kg/m)
1	0.52	360
2	0.36	930
3	0.34	1100

\* Assume saturation  $B = 2$  tesla and optimum magnetization of all iron

Figure III-36

Magnetic Field at Axis of MHD Duct Generated by Different Types of Iron Slabs with Optimum Magnetization

Furthermore, iron with good magnetic properties is not suited for use as structure at liquid helium temperatures; consequently, iron in the type 2 and type 3 locations would not serve as structural support but would complicate the design and application of the structure required. As a result, the decision was made to consider the type 1 location for iron position in the solenoids, racetracks, and rectangular saddles in Phase I. Iron was not considered for use with the annular saddle geometry because the winding window was expected to be filled with structural material.

The field contribution on the channel axis by iron in the type 1 location for four cases considered in Phase I was estimated and is shown in Figure III-37. The field is normalized to the saturation flux density for the iron and decreases along the length because of the taper of the pole pieces arising from the channel divergence.

#### E. SELECTION OF CONFIGURATIONS FOR ANALYSIS

After completion of Phase I, the material discussed in this section was presented to and reviewed with NASA personnel. Three configurations were then chosen for further investigation in Phase II. These consisted of: (1) an 8.0 T racetrack with iron pole pieces to be operated at 4.2 K, (2) at 8.0 T racetrack with iron pole pieces to be operated at  $T < 4.2$  K, and (3) an 8.0 T rectangular saddle with iron pole pieces to be operated at 4.2 K. Considerable interest was also expressed in a design which could allow the magnetic field to be changed by system shutdown, warm up, and alteration of winding position. This was included in the three designs which will be discussed in the sections which follow. Each of the three designs uses a different coil-dewar orientation. Minor modifications would allow any of the coil system concepts to be merged with any of the dewars.

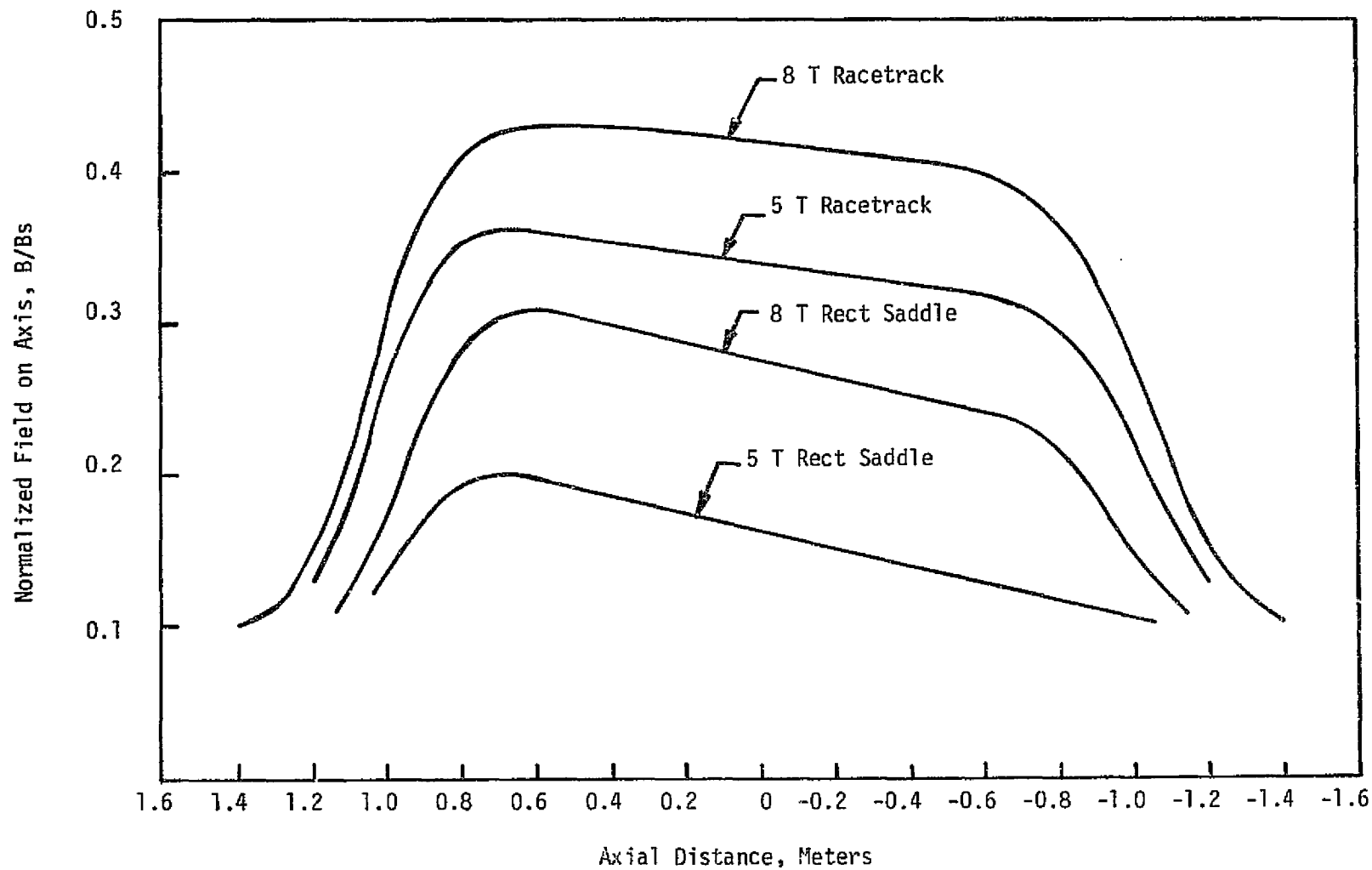


Figure III-37. Normalized Field Produced by Iron Core

#### IV. 8 T RACETRACK, 4.2 K SYSTEM

This section will present results on the first of the three preliminary designs considered in Phase II of the program. This consisted of a cryostat-ically stable, 8 T, 4.2 K magnet-dewar system. The magnet was mounted with MHD channel axis horizontal and main field direction vertical. A split racetrack pair geometry was utilized, and the system was designed to allow the included angle between the coil pair to be altered so as to provide for variation of the field gradient along the MHD channel. The subsection which follows will present an overall description of the system. This will then be followed by a discussion of the winding geometry and conductor characteristics. The section will close with a discussion of the structure and dewar design.

##### A. SYSTEM DESCRIPTION

###### 1. Overall Characteristics

The preliminary design characteristics for Design No. 1 are given in Table IV-1. The overall system dimensions are given in the top section of the table. This is followed by electrical characteristics. Two modes are indicated and correspond to operation of the two racetrack coils with a  $5^\circ$  included half-angle (low gradient mode) or  $15^\circ$  included half-angle (high gradient mode). The maximum field at the winding is 10.3 T. This level may be reduced somewhat upon further iteration of the graded design during a future detail design phase. The range of overall current density and conductor current density are given. Weights are summarized and indicate that conductor is the heaviest component and represents about half of the total weight of 80,970 kg. At the MHD channel inlet, the magnetic flux density is 7.6 T for the low gradient operating mode and 7.9 T for the high gradient mode. At the exit, the magnetic flux density is 6.08 T for the low gradient mode and 4.65 T for the high gradient mode.

Top and side views of the racetrack coils are given in Figures IV-1 and IV-2, respectively. Figure IV-2 also shows the two extreme coil positions from the standpoint of field profile variation. Calculated field profiles along the channel axis for these coil positions are shown in Figures IV-3 and IV-4. The flux density variation from a linear profile is  $\pm 5\%$  for the low gradient mode and  $\pm 8\%$  for the high gradient mode.

Figure IV-5 shows one quadrant of the cross section of the MHD channel at the channel inlet, channel exit, and at planes 0.508 m (20 inches) in from each end. Two numbers are given at each point in the sections. One number is the Y component of field (i.e., main field direction) when the maximum field on axis is 8 T, and the other number (in parentheses) is the ratio of the local Y component of field to the Y component of the field on axis in that plane. Table IV-2 gives results for the computed field components and magnitude with corresponding coordinates in the channel.

An assembly drawing of the magnet-dewar system is shown in Figure IV-6 (Drawing No. E-2703).

Preliminary Design Characteristics for System No. 1

- 8T Racetrack with Iron - 4.2K -

Dewar Dimensions

Inlet	0.254 m. x 0.254 m. (10 in. x 10 in.)
Outlet	0.4064 m. x 0.508 m. (16 in. x 20 in.)
Overall Length	4.3 m. (169 in.)
Outside Diameter	4.09 m. (161 in.)
Overall Height	6.41 m. (253 in.)

Electrical Characteristics

Field at Channel Inlet	
5° Mode	7.60 T.
15° Mode	7.90 T.
Field at Channel Outlet	
5° Mode	6.08 T.
15° Mode	4.65 T.
Max. Field on Channel Axis	
5° Mode	8 T.
15° Mode	8 T.
Max. Field at Winding*	10.3 T.
Active Field Length	1.524 m. (60 in.)
Stored Energy*	$171 \times 10^6$ J.
Inductance*	21.4 H.
Operating Current*	4000 A.
Overall Current Density*	$1.97 \times 10^7$ A/m <sup>2</sup> - $4.52 \times 10^7$ A/m <sup>2</sup>
Conductor Current Density*	$5.21 \times 10^7$ A/m <sup>2</sup> - $8.16 \times 10^7$ A/m <sup>2</sup>
Total Turns	4894
Ampere-Meters	$12.70 \times 10^7$

Weights

Conductor (Kg)	15,900
Structure (Kg)	39,866
Dewar (Kg)	25,204
TOTAL (Kg)	80,970

\* Values for 5° Mode

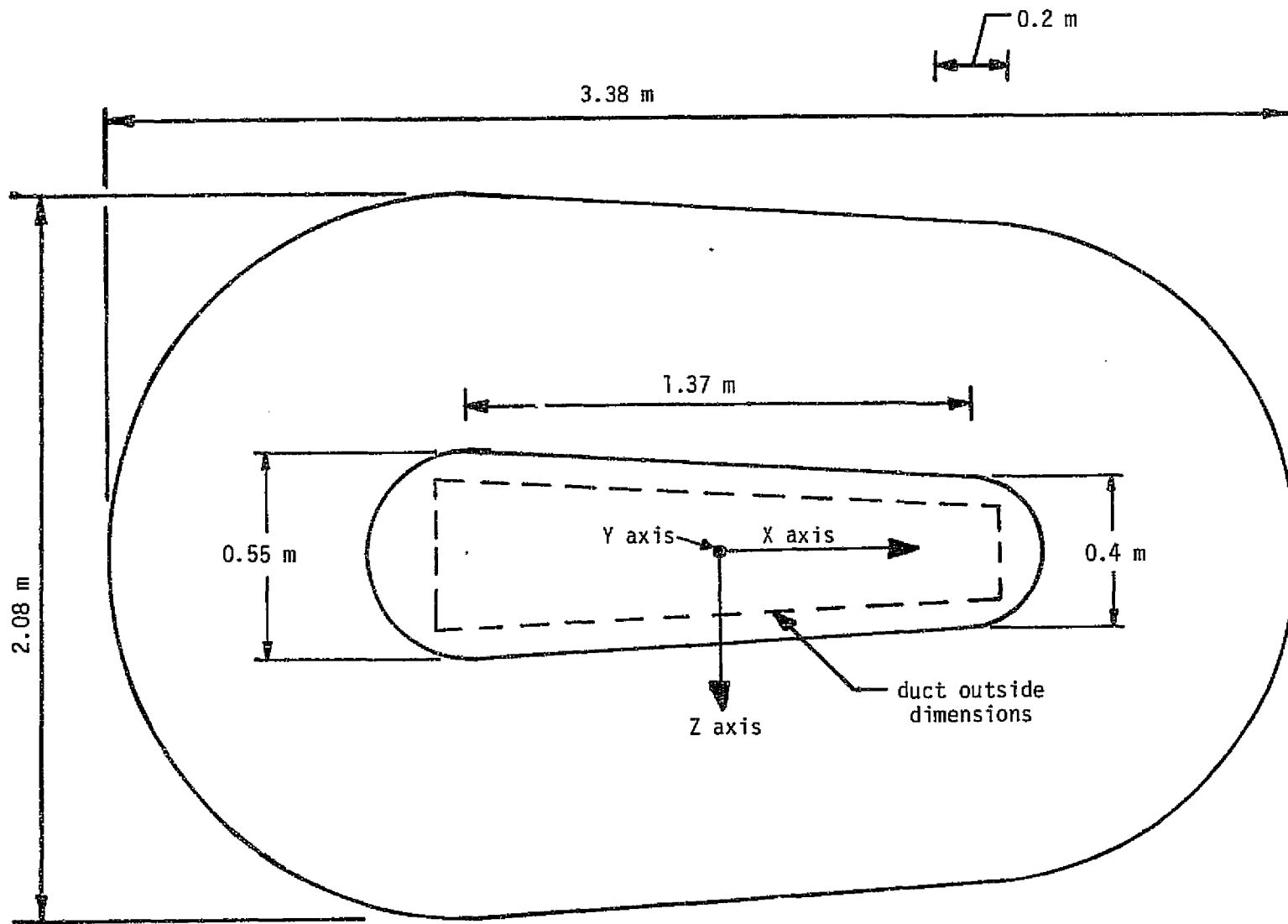


Figure IV-1. Top View of Racetrack Coil for Design No. 1

FA 3298

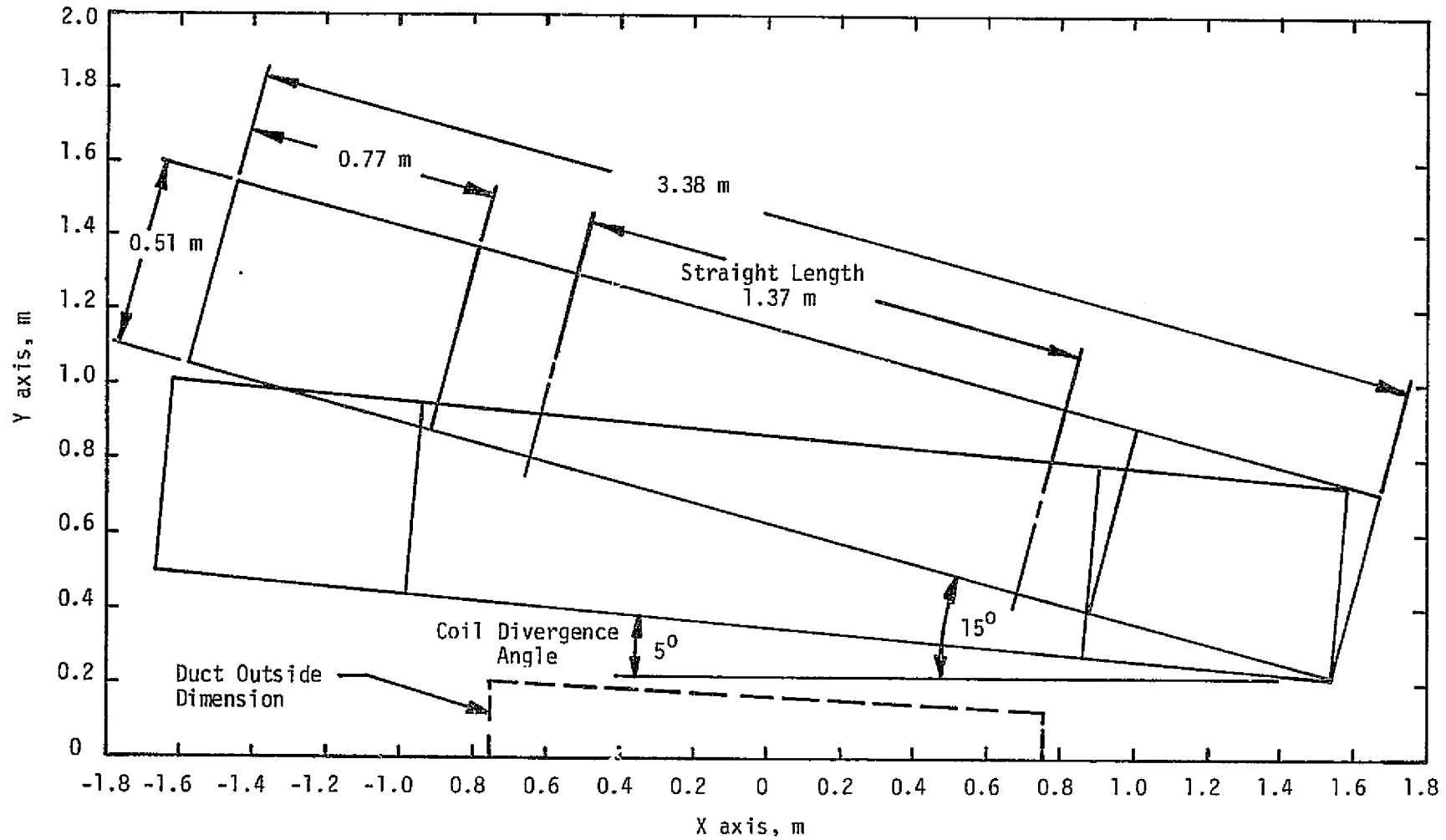


Figure IV-2

Sketch of Extreme Coil Positions Necessary to Satisfy Design Limits on Field Profile (Design No. 1)

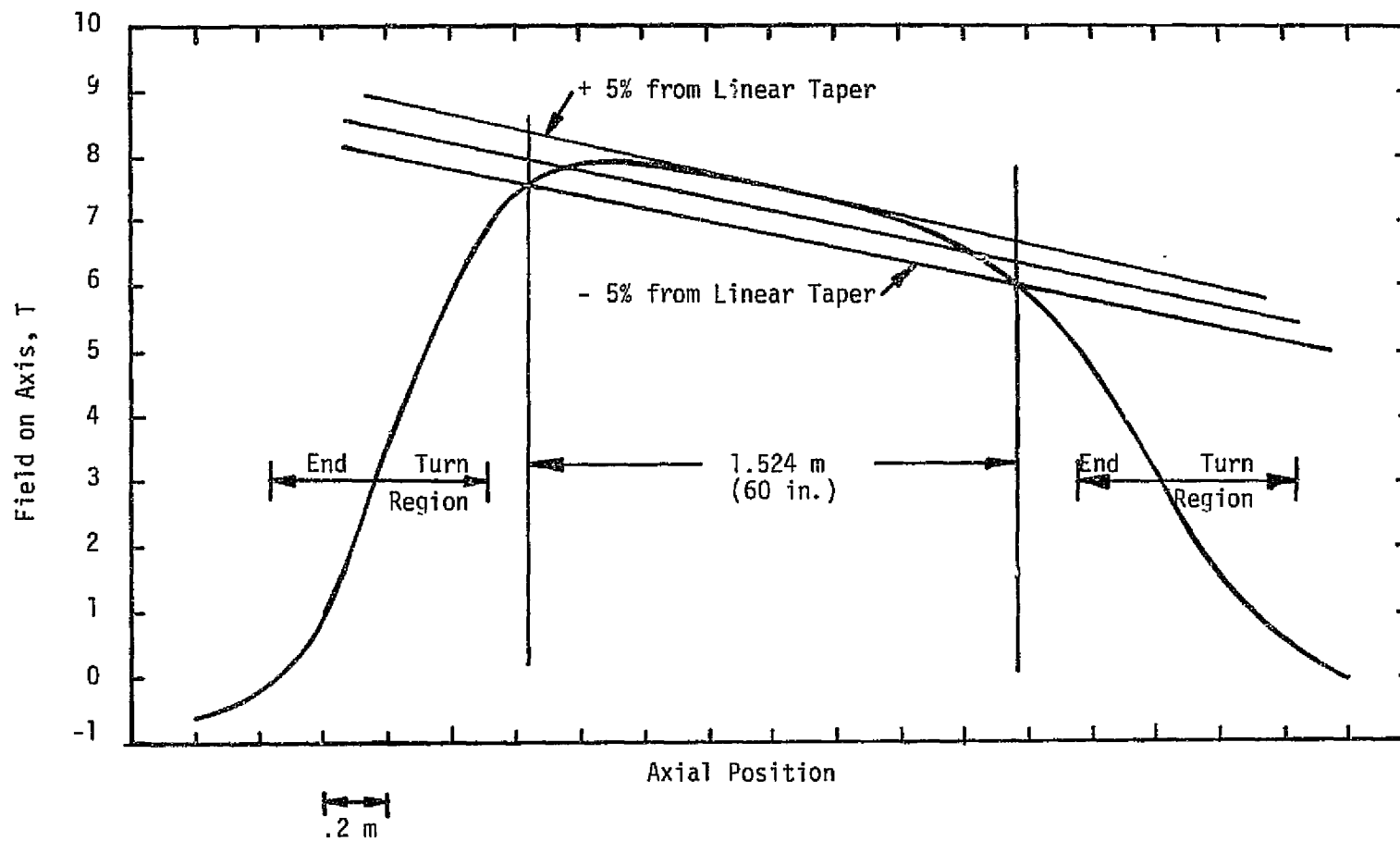


Figure IV-3

Computed Field Profile on Axis for Design No. 1 with Coil Divergence Angle =  $5^{\circ}$   
 (Low Gradient Operating Mode)



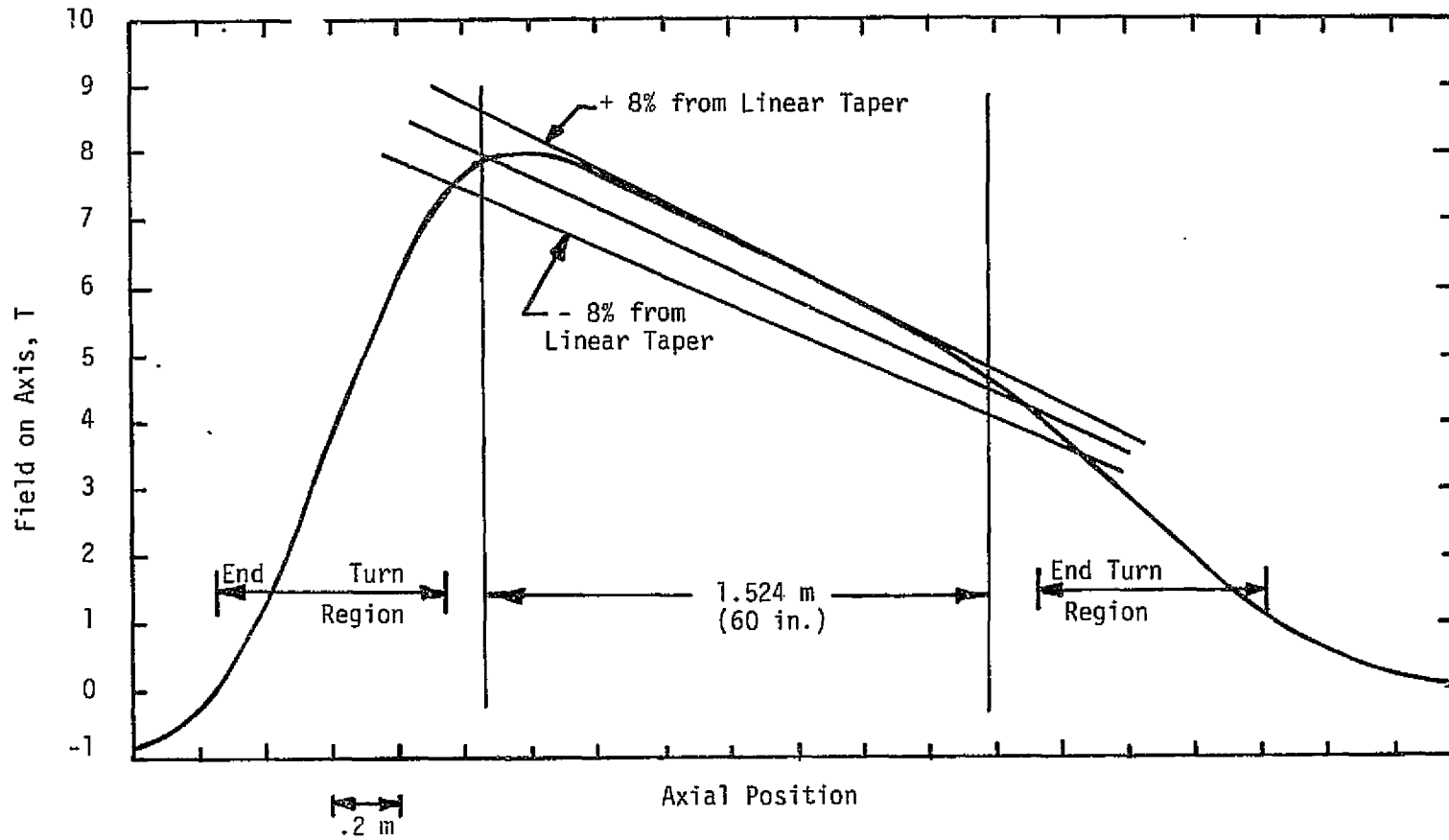


Figure IV-4

Estimated Field Profile on Axis for Design No. 1 with Coil Divergence Angle =  $15^\circ$   
(High Gradient Operating Mode)

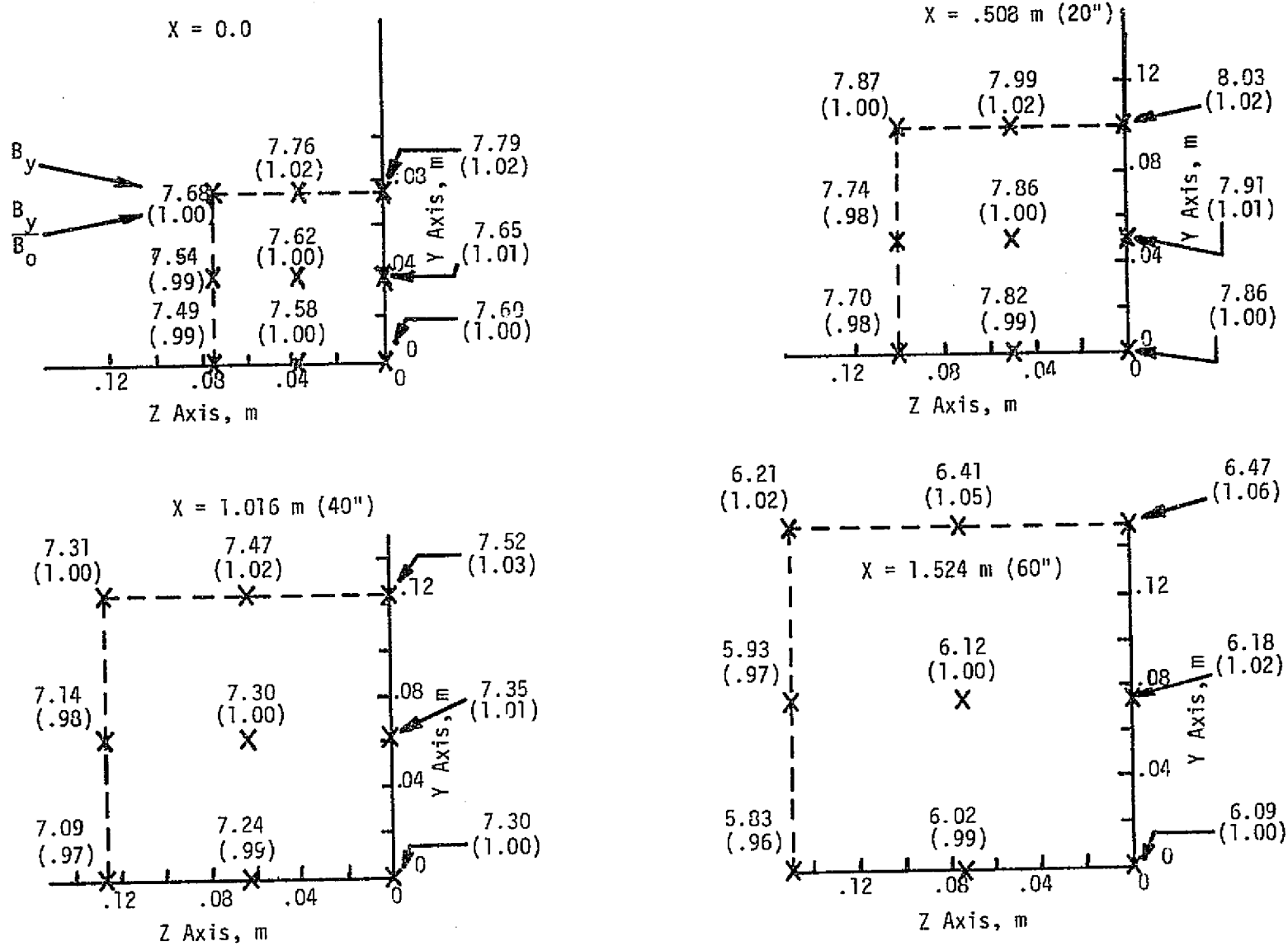


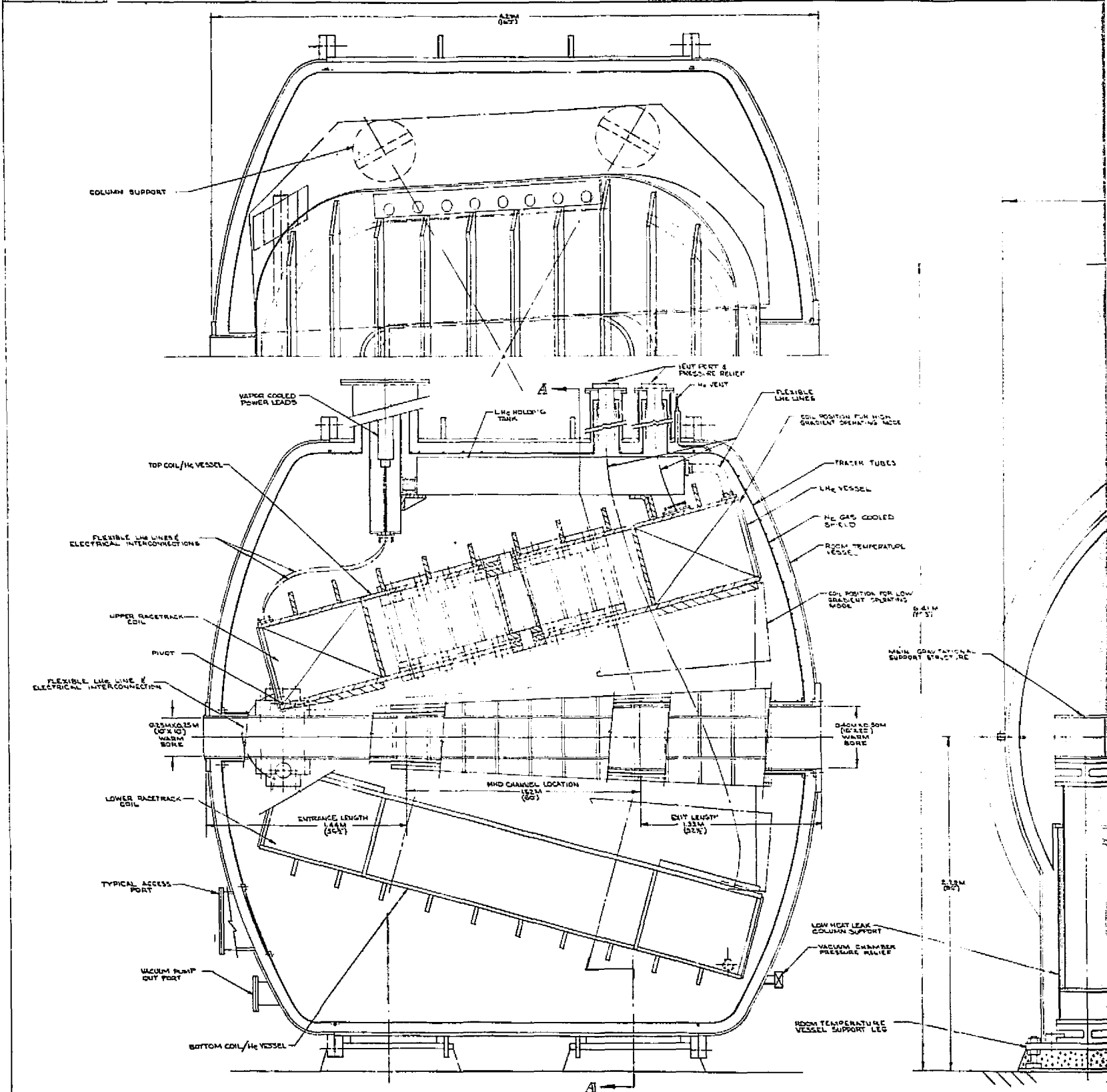
Figure IV-5  
 Calculated Main Component of Field and Homogeneity in One Quadrant of the MHD Channel at  
 Four Planes Along the Axis for the Low Gradient Operating Mode

Table IV-2

Computed Field Components at Selected Points Throughout  
MHD Channel Volume for 5<sup>0</sup> Mode

Coordinate (m)			Field Component (T)			Field Magnitude (T)	
X	Y	Z	B <sub>X</sub>	B <sub>Y</sub>	B <sub>Z</sub>	/B/	
0.00	0.00	0.00	0.00	7.55	0.00	7.55	Points on Axis
.400	0.00	0.00	0.00	7.95	0.00	7.95	
.500	0.00	0.00	0.00	8.00	0.00	8.00	
.600	0.00	0.00	0.00	7.96	0.00	7.96	
-0.764	0.00	0.00	0.00	6.09	0.00	6.09	Field Points at Duct Outlet
-0.764	0.00	0.076	0.00	6.02	0.00	6.02	
-0.764	0.00	0.152	0.00	5.83	0.00	5.83	
-0.764	0.076	0.00	0.33	6.18	0.00	6.19	
-0.764	0.076	0.076	0.33	6.12	-0.13	6.13	
-0.764	0.076	0.152	0.32	5.93	-0.25	5.94	
-0.764	0.152	0.00	0.66	6.47	0.00	6.50	
-0.764	0.152	0.076	0.65	6.41	-0.26	6.45	
-0.764	0.152	0.152	0.64	6.21	-0.51	6.26	
-0.256	0.00	0.00	0.00	7.30	0.00	7.30	
-0.256	0.00	0.064	0.00	7.24	0.00	7.24	
-0.256	0.00	0.127	0.00	7.09	0.00	7.09	
-0.256	0.064	0.00	0.08	7.35	0.00	7.35	
-0.256	0.064	0.064	0.08	7.30	-0.10	7.30	
-0.256	0.064	0.127	0.08	7.14	-0.21	7.14	
-0.256	0.127	0.00	0.16	7.52	0.00	7.52	
-0.256	0.127	0.064	0.16	7.47	-0.21	7.47	
-0.256	0.127	0.127	0.15	7.31	-0.42	7.32	
0.252	0.00	0.00	0.00	7.86	0.00	7.86	Field Points 20" from Duct Inlet
0.252	0.00	0.051	0.00	7.82	0.00	7.82	
0.252	0.00	0.102	0.00	7.70	0.00	7.70	
0.252	0.051	0.00	0.05	7.91	0.00	7.91	
0.252	0.051	0.051	0.05	7.86	-0.08	7.86	
0.252	0.051	0.102	0.05	7.74	-0.16	7.74	
0.252	0.102	0.00	0.11	8.03	0.00	8.03	
0.252	0.102	0.051	0.11	7.99	-0.16	7.99	
0.252	0.102	0.102	0.10	7.87	-0.33	7.88	
0.760	0.00	0.00	0.00	7.60	0.00	7.60	
0.760	0.00	0.038	0.00	7.58	0.00	7.58	
0.760	0.00	0.076	0.00	7.49	0.00	7.49	
0.760	0.038	0.00	-0.16	7.65	0.00	7.67	
0.760	0.038	0.038	-0.16	7.62	-0.06	7.62	
0.760	0.038	0.076	-0.16	7.54	-0.11	7.54	
0.760	0.076	0.00	-0.32	7.79	0.00	7.80	
0.760	0.076	0.038	-0.32	7.76	-0.11	7.77	
0.760	0.076	0.076	-0.32	7.68	-0.22	7.69	

ORIGINAL PAGE IS  
OF POOR QUALITY



BOBOT FRAME |

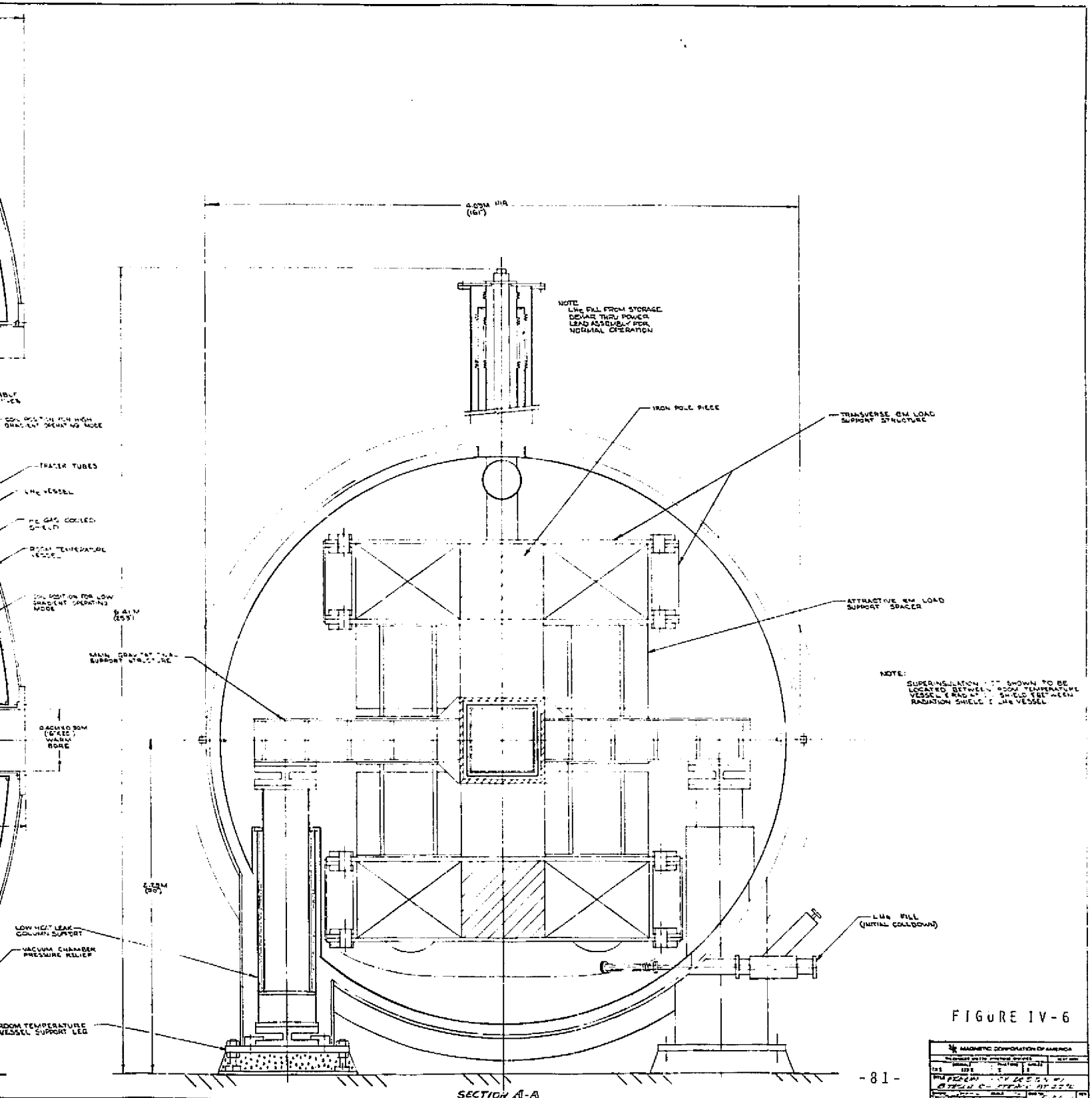


FIGURE IV-6

MAGNETIC COILS OF AMERICA			
NO.	DATE	BY	CHKD.
101	11/15/54	J. H. H.	J. H. H.
102	11/15/54	J. H. H.	J. H. H.
103	11/15/54	J. H. H.	J. H. H.
104	11/15/54	J. H. H.	J. H. H.
105	11/15/54	J. H. H.	J. H. H.
106	11/15/54	J. H. H.	J. H. H.
107	11/15/54	J. H. H.	J. H. H.
108	11/15/54	J. H. H.	J. H. H.
109	11/15/54	J. H. H.	J. H. H.
110	11/15/54	J. H. H.	J. H. H.

2

The main components of the magnet system consist of the upper and lower superconducting racetrack coils, internal and external coil support structure, iron pole pieces and LHe dewar. The MHD channel would have its axis coincident with the axis of the warm bore tube of the LHe dewar, which is located approximately 2.29 m (90 inches) above the ground level. The magnetic field is perpendicular to the axis of the dewar bore and the main field direction is vertical. The warm bore tube measures 0.254 m x 0.254 m (10" x 10") at the inlet and tapers to 0.406 m x 0.508 m (16" x 20") at the outlet over an "active" MHD channel length of 1.524 m (60"). The distance from the upstream end of the dewar to channel inlet (entrance length) is 1.42 m (56"), and the distance from the channel outlet to the downstream end of the dewar (exit length) is 1.35 m (53"). Because the design affords additional clearance at the outlet end of the magnet over that required, the warm bore outlet dimensions given above are purposely larger than those specified. This allows one to utilize the additional space in the warm bore if desired.

For the completed assembly, the highest point (vapor-cooled power leads) measures approximately 6.41 m (212") above the floor. The dewar has an outer diameter of 4.37 m (172") with an approximate overall length of 4.29 m (169"). It bolts to the floor at four locations and weighs a total of approximately 80,970 kg (178,500 lbs.). A cryogenic valve is located near the bottom of the magnet and is used for initial fill of the magnet with LHe. During normal operation, a fill port which is located in the power lead assembly is used to maintain a constant LHe level. Vent ports, which are used to vent the LHe boiloff, and a pressure relief valve, which is used to protect the magnet from a pressure overload, are located on top of the dewar. In addition, a vacuum port with a pressure relief valve is located near the bottom of the magnet and is used to evacuate the dewar. The dewar utilizes a helium vapor-cooled radiation shield between the warm vessel and cold vessel walls. Superinsulation is used between the radiation shield and cold vessel at all locations except where penetrations are necessary for the gravitational supports or fill and vent lines. The warm bore tube and bore radiation shield are concentric and supported by connection to their corresponding elements at the ends.

The magnet coils are of a racetrack geometry and are designed to operate in the superconducting state at a temperature of 4.2° K and a pressure of about one atmosphere. The axial loads of electromagnetic origin are supported internally by the conductor and a strip of stainless steel wound in parallel with the conductor during fabrication. The liquid helium vessel doubles as external support structure. Transverse loads of em origin are supported by built-up stainless steel sections along the sides of each coil and by plates which are placed over and under each coil. These plates also restrain iron pole pieces which are located in the winding window for each coil. The attractive load between coils and between iron "plugs" is supported by built-up stainless steel wedge-shaped spacers. The latter also determines the coil angle and transmits the weight of the coils to the main gravitational support structure.

The main gravitational support structure is stationary within the dewar and held in place by four low heat leak column supports. The coils are pivoted on one end to allow the angle between them to be changed by disassembly of one end of the dewar and replacement of the wedges between the coils and main gravitational support.

The coils are electrically in series with the interconnection between coils located within a flexible LHe line or bellows at the pivot end. Flexible

vent lines at the downstream end of the magnet are intended to be replaced if the angle is changed whereas the power lead and helium lines at the upstream end are permanent. The liquid helium holdup tank and vapor-cooled lead cryostat section are connected via a coupling.

## 2. Power Lead Assembly

The vapor-cooled lead assembly is a high current coaxial design similar to those designed and fabricated by MCA for use in the Argonne National Laboratory bubble chamber magnet. A typical construction for these leads is shown in Figure IV-7. Current enters via buss-bars connected to the warm end A and then passes through the walls of a bundle of copper tubes in the center of the assembly to the cold end terminal A'. This bundle of tubes is electrically isolated from another tube bundle located in the annulus between large concentric, non-conducting tubes. The return current enters the cold end terminal at B', passes through the walls of the copper tubes in the annulus, and exits at the warm end terminal B.

## 3. Alteration of Field Gradient

Each coil is located inside a stainless steel structure which has been designed to pivot about a fixed shaft mounted on the main gravitational support structure and dewar. An outline of the steps in the procedure for changing the coil angle from high gradient mode (wide angle) to the low gradient mode (low angle) is shown in Table IV-3. This is intended as an outline of the procedure and must be expanded to include a detailed step-by-step procedure and QC when a detailed design effort is performed. At present it illustrates feasibility of the concept.

## 4. Outline of System Assembly

Table IV-4 presents an outline of an assembly procedure for the magnet system described above. It shows the basic sequence of events that is required and indicates the complexity of the task and scope of the major erection equipment needed. A final procedure is beyond the scope of the present effort and would result from a detailed design program.

The procedure assumes that each racetrack coil and its main structure/LHe dewar are subassembled off site. The main components of the dewar are also assumed to be subassembled off site. In addition, it is assumed that the facility, foundation, utilities, and component handling fixtures are available. It is essential that measures be taken to ensure a "clean room" atmosphere about the immediate area in which the final assembly takes place. This will minimize the possibility of foreign matter, dust, etc. getting onto the superinsulation and other sensitive components of the magnet system.

Several ports for viewing or accessibility will be necessary. The quantity, size, and location of these ports will be determined during the final design phase.

~~PRECEDING PAGE BLANK NOT FILMED~~

NOTE: DIMENSIONS OF A AND B ARE 1/2" AND 1/4"  
 DENOTES INSULATING MATH

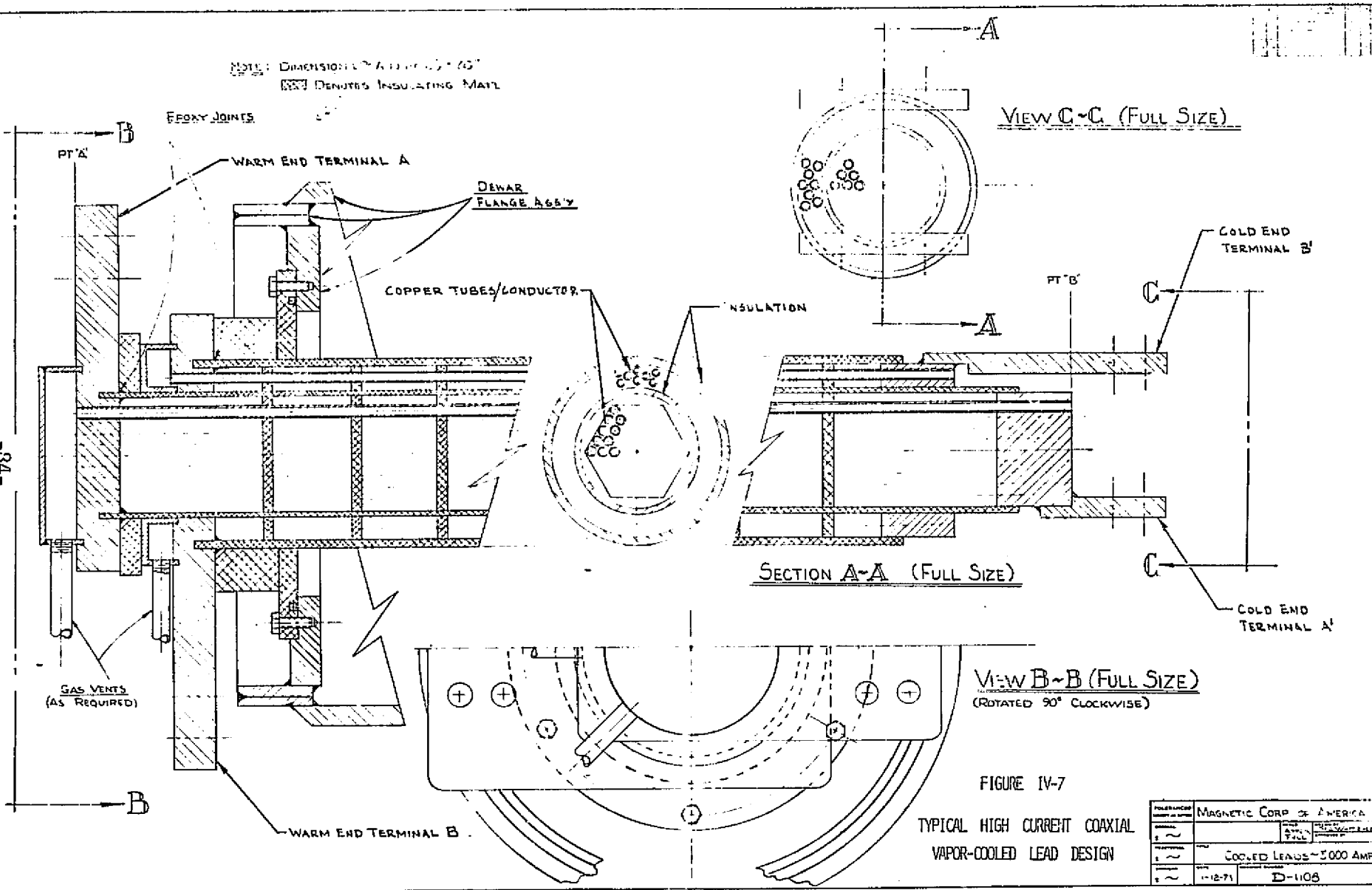


FIGURE IV-7  
 TYPICAL HIGH CURRENT COAXIAL  
 VAPOR-COOLED LEAD DESIGN

DESIGNED BY	MAGNETIC CORP OF AMERICA
DRAWN BY	
CHECKED BY	
DATE	
TITLE	COOLED LEADS - 5000 AMPS
NO.	D-1108
REV.	
DATE	11-12-71

IF THIS PAGE IS  
 OF POOR QUALITY



Table IV-3

Outline of Procedure to Alter Field Gradient

De-energize the magnet, remove the LHe and allow the system to warm up to room temperature.

Apply a fixture to support the downstream end of the warm bore tube.

Release the dewar vacuum, unbolt the warm bore tube from the downstream room temperature vessel end cover, and remove the end cover.

Apply a fixture to support the downstream end of the bore tube radiation shield.

Remove superinsulation and de-couple radiation shield cooling tubes as necessary.

Unbolt the bore tube radiation shield from the downstream radiation shield end cover and remove the latter.

Remove superinsulation as necessary and remove flexible helium lines from each coil to the vent ports, initial fill port and from the upper coil to the hold-up tank.

Attach a mechanical or hydraulic jack between each coil/LHe vessel and the main gravitational structural support.

Remove the attractive em load support spacers.

Change the angle of the coils by jacking each coil/LHe vessel into place.

Position the new intercoil support spacers.

Bolt the He vessels to the main gravitation structural support and to the spacers. Remove the jacks.

Replace flexible helium lines to vent ports, initial fill port and between upper coil and hold-up tank. Replace superinsulation as required.

Replace downstream radiation shield end cover and bolt to bore tube radiation shield and outer radiation shield.

Connect radiation shield cooling tubes, replace superinsulation, and remove support fixture for downstream end of bore tube radiation shield.

Replace room temperature vessel end cover, bolt cover to main shell and to bore tube. Remove warm bore tube end support fixture.

Evacuate vessel and prepare for cooldown.

Table IV-4

Outline of Assembly Procedure\*

Place the bottom half of the room temperature vessel in position on the foundation (Reference Figure IV-8a).

Place the low heat leak columns inside the legs of the room temperature vessel and fasten them to the base of the legs (Reference: Figure IV-8a).

Attach the preassembled multilayered superinsulation blankets to the entire inside surface of the room temperature vessel (Reference: Figure IV-8a).

Place the lower half of the radiation shield in position and attach it to the low heat leak columns. Attach the multilayered superinsulation blankets to the entire inside surface of the radiation shield (Reference: Figure IV-8b).

Preassemble the bottom spacers and the coil/He vessel to the main gravitational support structure. Lift and position the entire subassembly on the low heat leak columns and fasten it in place (Reference: Figure IV-8c).

Preassemble the upper coil and spacer. Lift and position the subassembly onto the main gravitational support structure and fasten in place (Reference: Figure IV-8d).

Attach the preassembled multilayered superinsulation blankets to the entire inside surface of the upper half of the room temperature vessel. Place the latter in position on top of the lower half and weld them together along the mating surfaces (Reference: Figure IV-8d).

Position and dress the multilayered superinsulation blanket along the inside of the mating surfaces of the room temperature vessel halves (Reference: Figure IV-8d).

Attach the multilayered superinsulation blanket to the inside of the upper half of the radiation shield. Slide it into position from the upstream end of the assembly and fasten it to the lower half of the radiation shield (Reference: Figure IV-8e).

Place the helium hold-up tank into position, temporarily support it at the inlet end of the magnet with a fixture, and fasten it to the bracket at the outlet end of the magnet (Reference: Figure IV-8f).

Insert power lead assembly and connect to helium hold-up tank. Complete all electrical and plumbing connections. Complete assembly of power lead housing (Reference: Figure IV-8f).

Using a fixture to support one end, feed the warm bore tube radiation shield, which has multilayered superinsulation blankets attached to its outer wall, through the rectangular opening in the main gravitational support, position it in place, and support it at each end (Reference: Figure IV-8g).

---

\* Occasional reference to the assembly drawing, which is shown in Figure IV-6, will aid in visualization of the procedure.

Table IV-4 (Concluded)

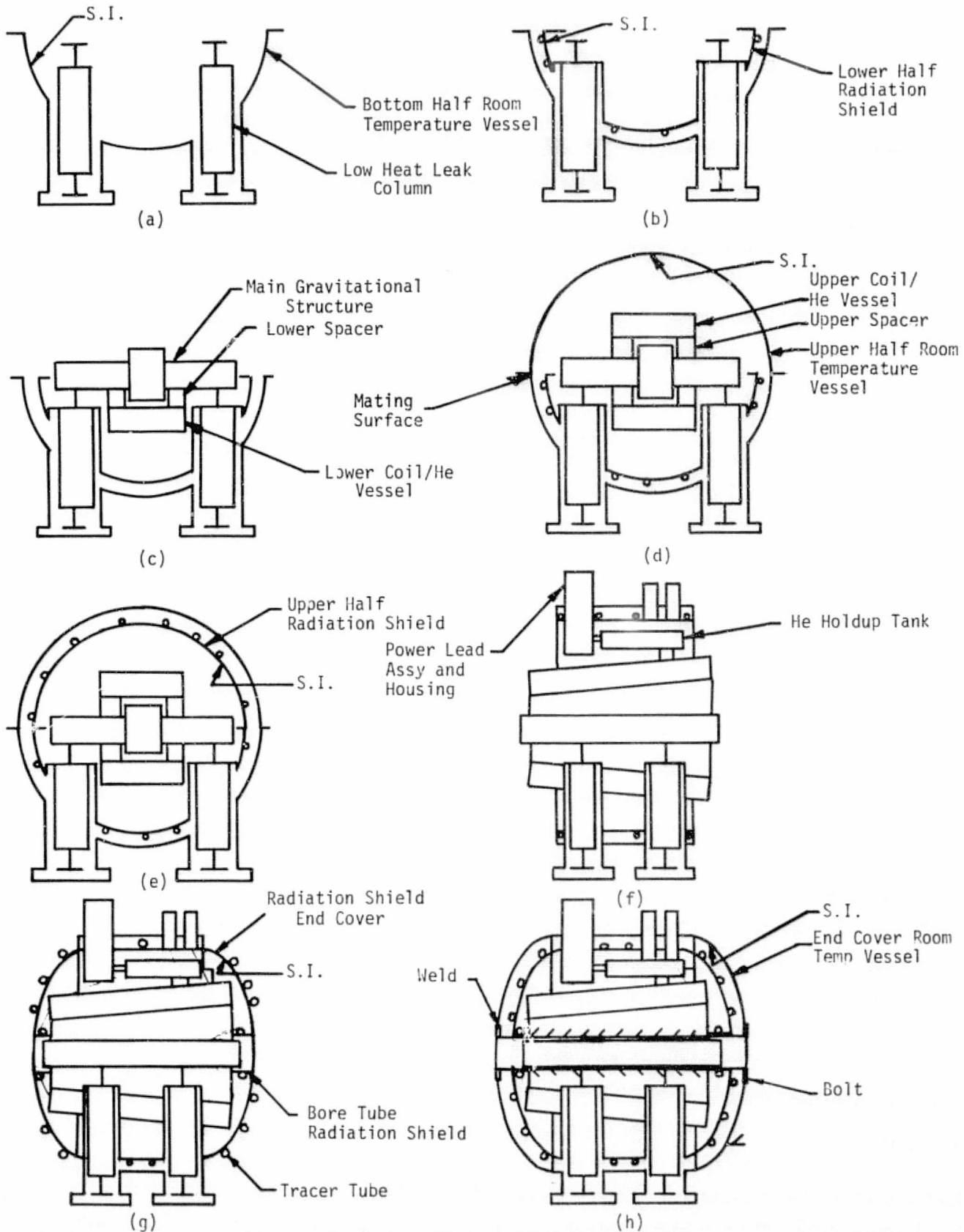
Assemble the radiation shield end covers, which have multilayered superinsulation blankets attached to their inside surface, to each end of the magnet and bolt to bore tube radiation shield (Reference: Figure IV-8g).

Connect the tracer tubes of the end covers to the warm bore tube radiation shield and to the outer radiation shield at each end of the magnet as required (Reference: Figure IV-8g).

Position the room temperature vessel end covers, which have multilayered superinsulation blankets attached to their inside surfaces, in place and fasten them to the flanges of the center portion of the room temperature vessel (Reference: Figure IV-8h).

Using the same procedure as that used for installation of the warm bore tube radiation shield, feed the warm bore tube, which has multilayered superinsulation blankets attached to its outer wall, through the rectangular opening in the bore tube radiation shield and position it in place (Reference: Figure IV-8h).

Bolt the warm bore tube to the downstream end cover and weld the warm bore tube to upstream end cover (Reference: Figure IV-8h).



FA 3671

Figure IV-3. Assembly Sequence for Design No. 1

After dewar evacuation and successful completion of the steps in Table IV-4, the magnet is ready to be cooled down and energized. This assumes that appropriate tests and quality control checks have been performed during the final assembly stage.

## B. WINDING GEOMETRY AND CONDUCTOR CHARACTERISTICS

During Phase I, racetrack coil systems were considered at different field levels with and without iron pole pieces. The dimensions of the coils were optimized according to a procedure involving estimation of certain characteristics which are critical from a magnet design standpoint. This procedure consisted of the following four parts:

- a. Select a realistic range of current densities and determine the effect of overall winding geometry and dimensions on the total conductor volume and total ampere-meters required for a specified central magnetic field,
- b. For the more promising configurations found in a, estimate the stress levels in the windings,
- c. For designs that are realistic with respect to a and b above, calculate the peak fields in the windings, and
- d. Evaluate results and repeat.

The "best" initial design point was taken as that which had the minimum value of ampere-meters consistent with realistic stress level estimates and a realistic peak field estimate in the windings. The dimensions of the coil system found in this fashion were the starting point for the Phase II analysis. The latter proceeded iteratively through a process of:

1. Assume an overall current density.
2. Calculate fields along the axis and throughout the winding.
3. Adjust the geometry and/or current density and repeat 1-3.
4. Size the conductor, insulation, and internal structural components.
5. Calculate an overall current density, compare with the value assumed initially, and repeat steps 1 to 5.

The initial optimization was done on the basis of the low gradient profile, and then during step 2 the winding geometry was altered slightly to achieve the high gradient field profile. The information which follows represents the result of several iterations leading to a set of preliminary design specifications.

As mentioned earlier, the starting point for the iterative design loop was the set of coil dimensions and uniform overall current density found for the 8 T racetrack, 4.2 K, design with iron in Phase I. The cross section for each coil in this case was rectangular. The Phase II analysis began by calculating the field distribution in the windings. It was concluded that this simple cross-sectional shape resulted in a peak field which was quite high; hence a "notch" of conductor was removed from the inner section of the winding and the conductor was "graded" or tailored to the field distribution experienced in the

winding. Grading was limited to four sizes of conductor since it was felt that extension of the concept beyond four would not offer an economic advantage in total conductor cost. It would, in addition, necessitate more joints in fabrication.

The dimensional characteristics of the four conductors and required stainless steel banding are given in Tables IV-5 and IV-6, respectively. Lengths and weights are also given. Conductor was sized to be cryostatically stable by using the design technique discussed in Appendix B. The size was also based on calculated values of maximum field determined in each of the winding sections. The manner in which the conductor and stainless band are used in the winding is shown in Figure IV-9 together with the final overall dimensions. Insulation and winding spacer thicknesses are given and consist of a spiral wrap of  $1.524 \times 10^{-4}$  m (0.006 in.), turn-to-turn insulation and a distribution of  $2.286 \times 10^{-3}$  m (0.090 in.) thick insulating slats between "pancakes".

The design assumes that the conductor will be insulated with a 60 percent spiral wrap of insulation and then wound in parallel with the stainless steel channel into "pancakes". Pancakes would then be stacked with slats between them and joints made at the inside and outside to electrically connect the pancakes in series and form the coil. The main purpose of the stainless steel is to carry the axial load of electromagnetic origin. In addition, the width of the stainless steel is equal to that of the conductor plus the spiral wrap insulation. This allows the compressive load parallel to the wide face of the conductor to be carried, transmitted, and accumulated pancake to pancake by the stainless steel rather than to accumulate conductor to conductor. Similarly, the sides of the channel section are wide enough to prevent conductor to conductor accumulation of load perpendicular to the conductor face.

Figure IV-10 again shows a cross-section of the winding for Design No. 1 in the end turn region. The solid lines indicate the winding boundary assumed for field computation purposes to provide input information to size conductor and steel requirements. The dashed lines indicate the winding boundary for Design No. 1 on the basis of the conductor and steel chosen as a result of the previous step. The next step in the iterative design process would be to recompute field distributions in the new winding envelope and relax the shape of the notch. This, however, is part of the final design process and may be considered as "fine tuning" from the standpoint of preliminary design.

The model used for field calculation purposes in the windings for Design No. 1 is illustrated in Figure IV-11, which shows a cross section of the racetrack in the midplane of the end turn region. The location of the iron relative to the coil is shown as well as the 11 current filaments used to model the coil to generate field profiles for use in grading studies. The model used a rectangular notch for the purpose of maximum field reduction. Further development of this concept during the detailed design of the coil would use more filaments in the coil model and eventually replace the rectangular notch with a triangular shape (see dashed line in Figure IV-11) with the "depth" adjusted so as to minimize the field concentration ratio. For the purposes of this program, the rectangular notch is suitable to generate the preliminary design requirements.

Table IV-5

Estimated Conductor Requirements for Design No. 1

q=0.7 w/cm<sup>2</sup>; Conductor Width=0.0254 m=1.0 in.; (Also See Figure IV-9)

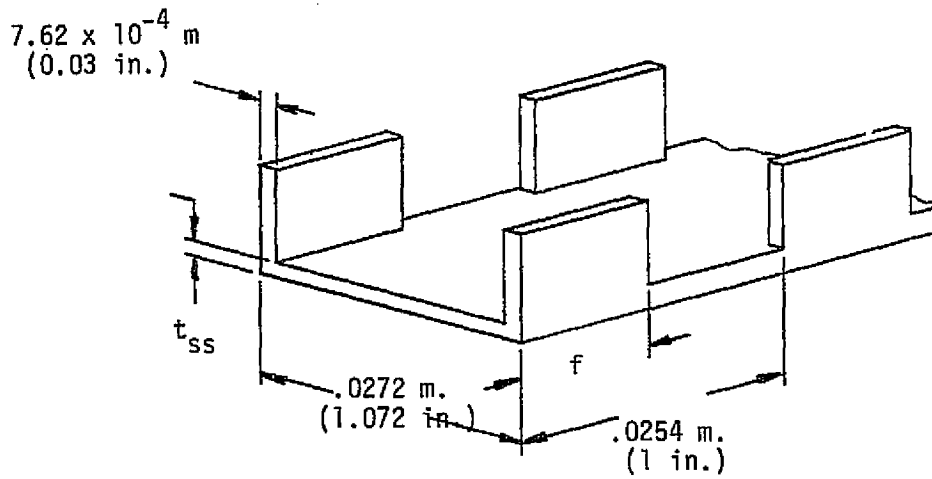
Conductor Type	Region Where Used	Conductor Thickness, t m. (in.)	Copper	Length (m.)	Weight (kg)
			Superconductor		
1	a,f,i	$3.02 \times 10^{-3}$ (0.119)	4.3	3963	2595
2	b,j	$2.77 \times 10^{-3}$ (0.109)	6.3	4161	2460
3	c,g,k	$2.29 \times 10^{-3}$ (0.090)	11.4	9121	4605
4	d,h,l	$1.93 \times 10^{-3}$ (0.076)	14.3	14,515	6240
			TOTAL =	<u>31,760</u>	<u>15,900</u>



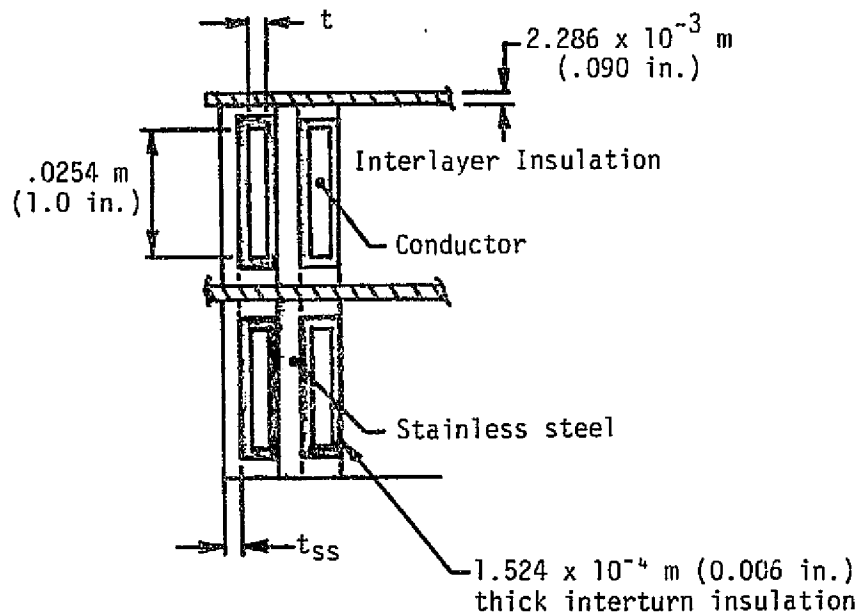
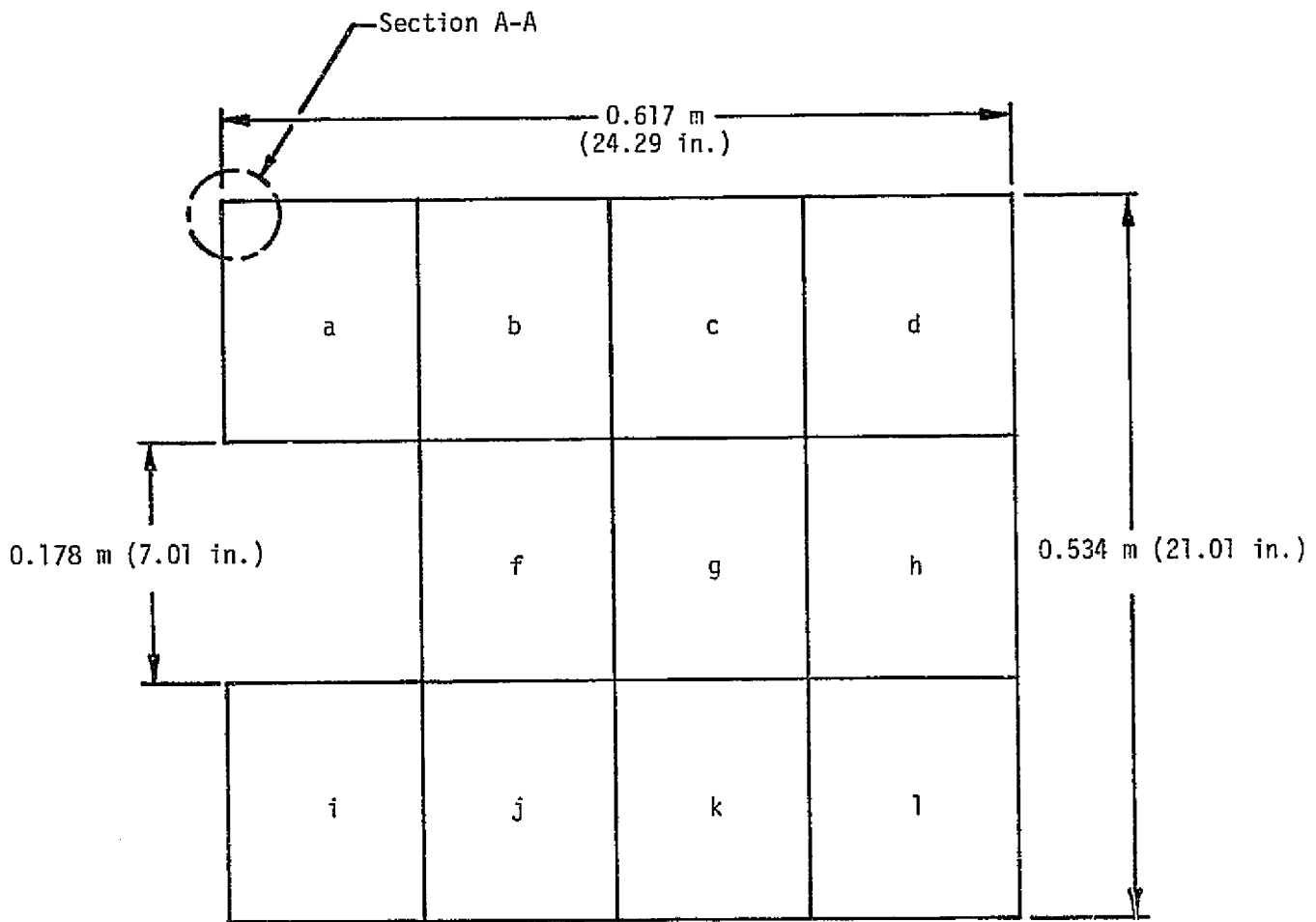
Table IV-6

Internal Structural Requirements for Design No. 1;

$q=0.7 \text{ w/cm}^2$ ;  $f=0.6$  (Also See Figure IV-9)



ss Type	Region Where Used	$t_{ss}$ m. (in.)	Length (m.)	Weight (kg)
1	a,i	$3.56 \times 10^{-3}$ (0.140)	2490	1940
2	b,j	$1.75 \times 10^{-3}$ (0.069)	4161	1640
3	f	$2.97 \times 10^{-3}$ (0.117)	1473	965
4	c,g,k	$7.62 \times 10^{-4}$ (0.030)	9121	1640
5	d,h,l	$7.62 \times 10^{-4}$ (0.030)	14,515	2585
TOTAL:			31,760	8770



FA 3658

Section A-A

Figure IV-9. Winding Final Dimensions and Constructional Detail for Design No. 1

C-2

0.1 m

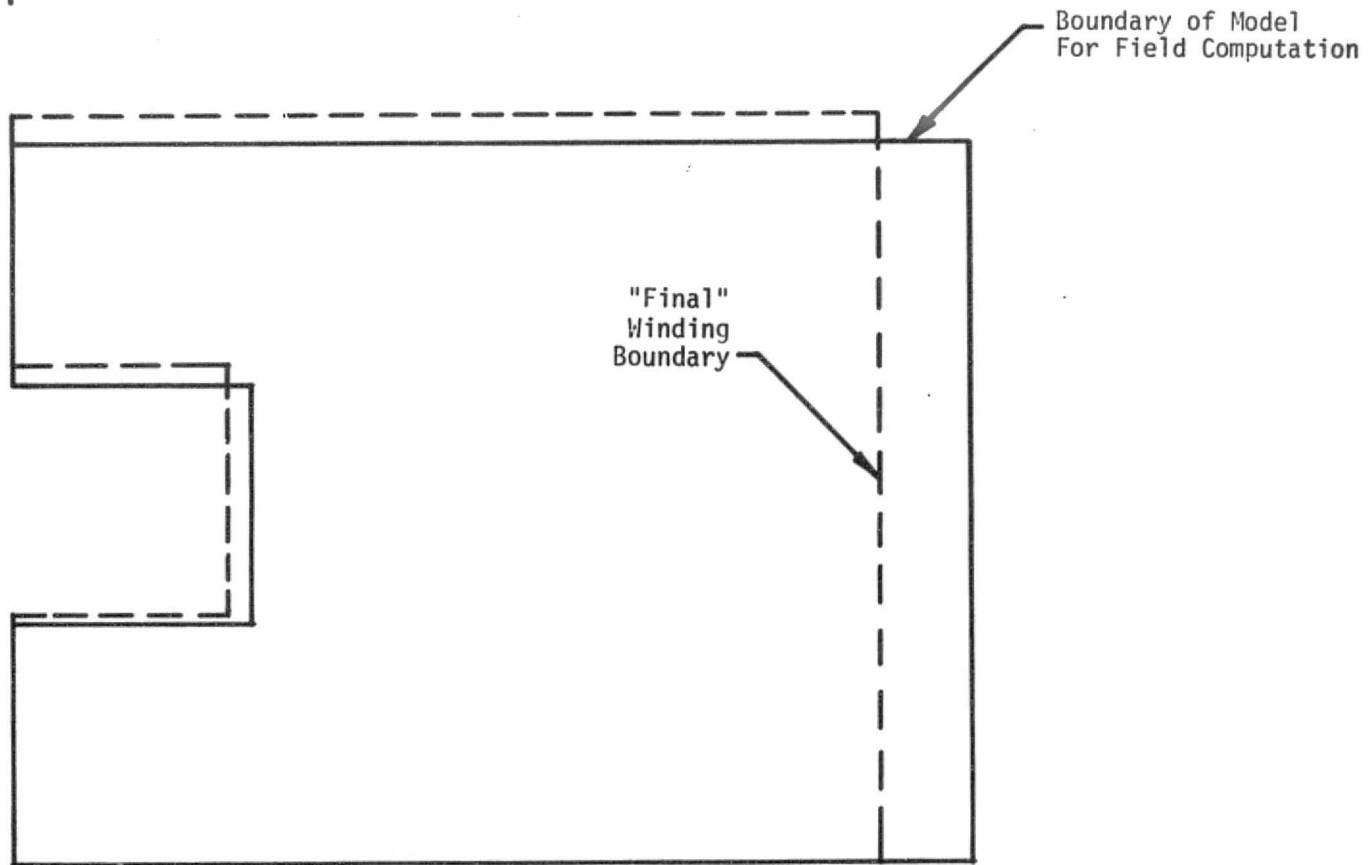
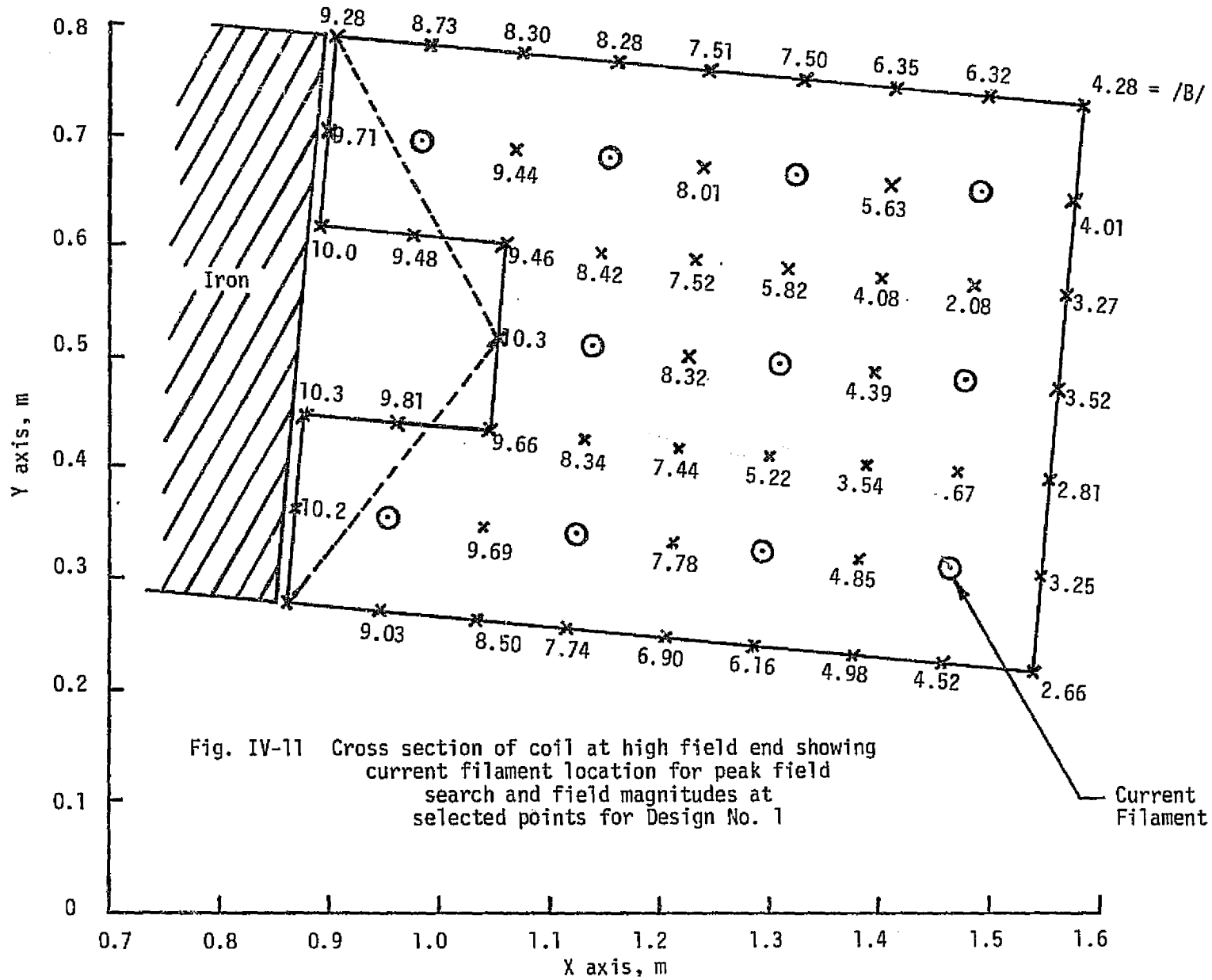


Figure IV-10 Cross Section of Coil End Turn Region Showing Winding Envelope Calculated for an Allowable Surface Heat Flux from Conductor ( $q$ ) of 0.7 Watts/cm<sup>2</sup> for Design No. 1



The calculated field distribution is indicated for the graded construction chosen. Note that the modeling process tends to overestimate the field calculated at points on the boundary adjacent to current filaments and underestimate the field at points between filaments. The actual field may be approximated by averaging the values at adjacent points.

Figure IV-12 shows the calculated field concentration ratios along lines through the winding as illustrated in the sketch above the plot. This illustrates the basic reason why conductor grading can be performed; that is, the field becomes progressively lower as the outer coil boundary is approached.

Figure IV-13 illustrates the manner in which grading helps to reduce the peak field concentration ratio. This is a plot of the calculated field concentration ratio at the points illustrated in the sketch above the plot. The calculated values are given; however, the actual profile may be approximated by averaging values at adjacent points. This leads to a smoother profile, but the character is similar. Line "a" represents results without grading and shows a peak ratio in the vicinity of points 5 and 6 at a level of about 1.35. Line "b" shows the first attempt at grading and illustrates how the field concentration around points 5 and 6 was drastically reduced; however, it became more severe in the vicinity of 8, 9, and 10 which then becomes the governing location. Line "c" shows the results for the grading chosen for Design No. 1 and illustrates how the results have progressed to a situation where the variation along the boundary (points 5-13) and the level of concentration is reduced. This was deemed sufficient for the purposes of this preliminary design. Further iterations during detail design may alter the shape of the notch and specify the boundaries between conductor grades somewhat differently, but the general character and complexity may be expected to be similar.

Following specification of the coil and conductor characteristics, a preliminary investigation into the quench characteristics for magnet design one was begun. A computer model was used which carries out a forward integration in time to estimate the current, temperature and voltage transients within the coil system.

Basically, the model begins with the assumption that the coil becomes normal at a single point. Ohmic heating at this point leads to a temperature rise in its vicinity with subsequent growth of the normal region. Since the winding thermal properties are not isotropic, the normal region does not grow with equal speed in all directions. This is modeled and transformed into an equivalent resistance to be used in a circuit equation in finite difference form which allows calculation of current during the next time increment. The effects of temperature on the resistance of successive normal volume increments is taken into account. The circuit used is shown in Figure IV-14 which assumes that the power supply is disconnected during the discharge transient and that the superconducting coil dissipates its energy internally in the normal region  $R(t)$  and in "dump" resistor,  $RFS$ , located outside the dewar.

Results of the quench calculations are shown in Figures IV-15, IV-16 and IV-17.

Three values for the circuit dump resistor,  $RES$  (Figure IV-14) were considered. Figure IV-15 shows the current in the coil as a function of time assuming quench initiation at  $t=0$  from an initial current equal to the operating current level of 4000 A. As expected, the larger the dump resistor, the faster the discharge rate.

The maximum temperature in the coil occurs at the point of quench initiation. Figure IV-16 shows the maximum temperature as it develops in time during

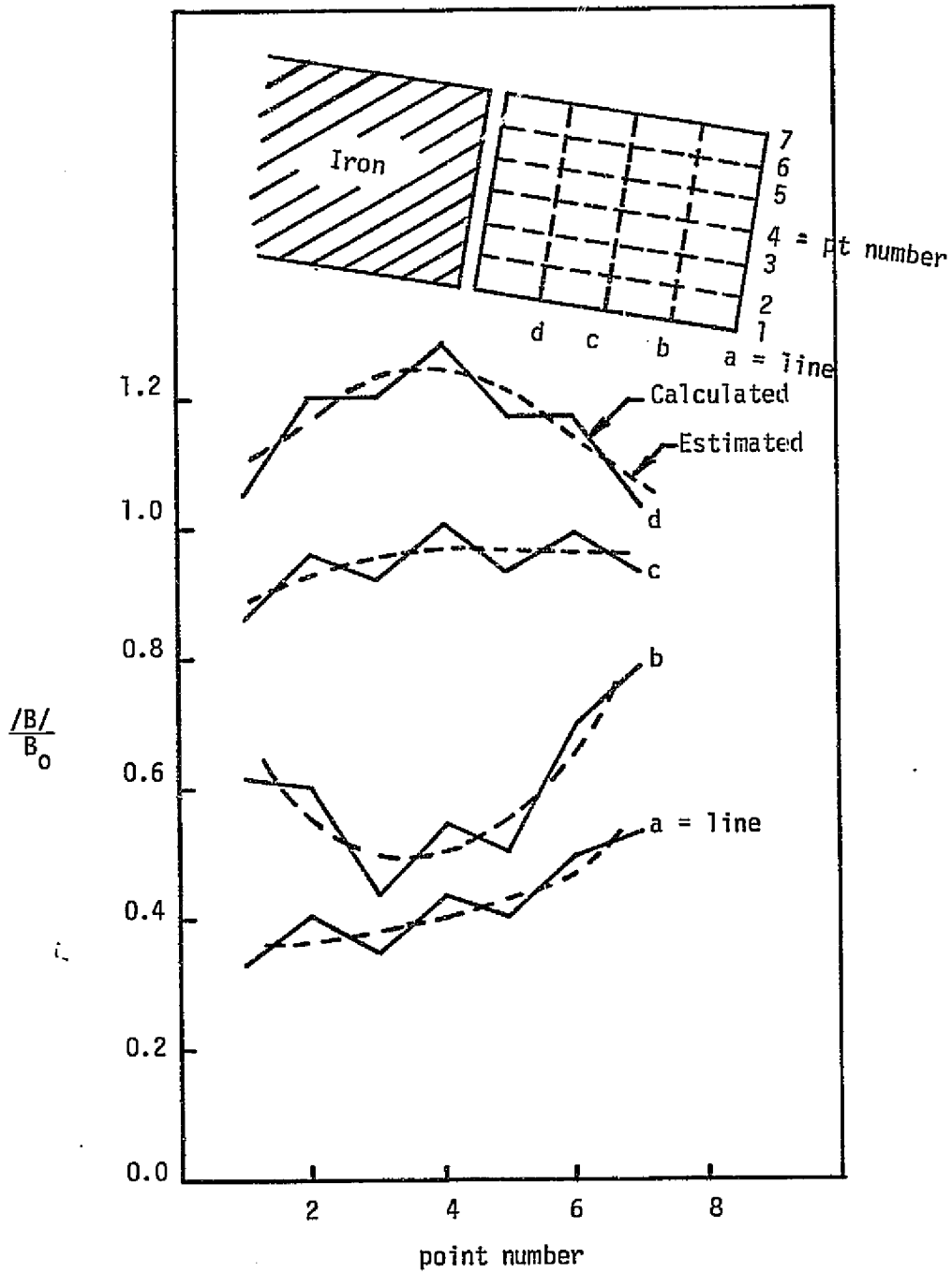
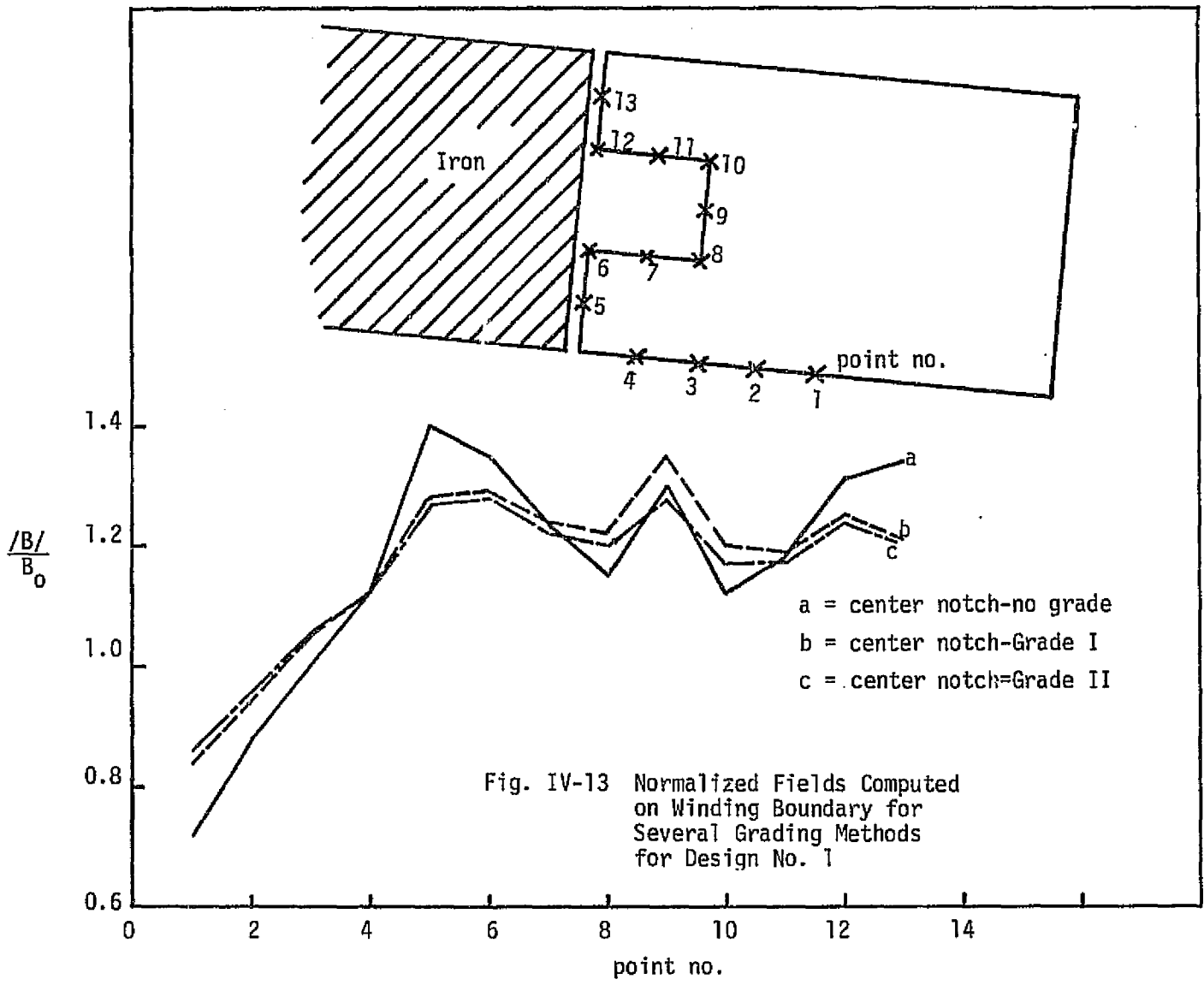


Figure IV-12 Normalized Fields Computed Throughout End Turn Cross Section for Coil Design No. 1





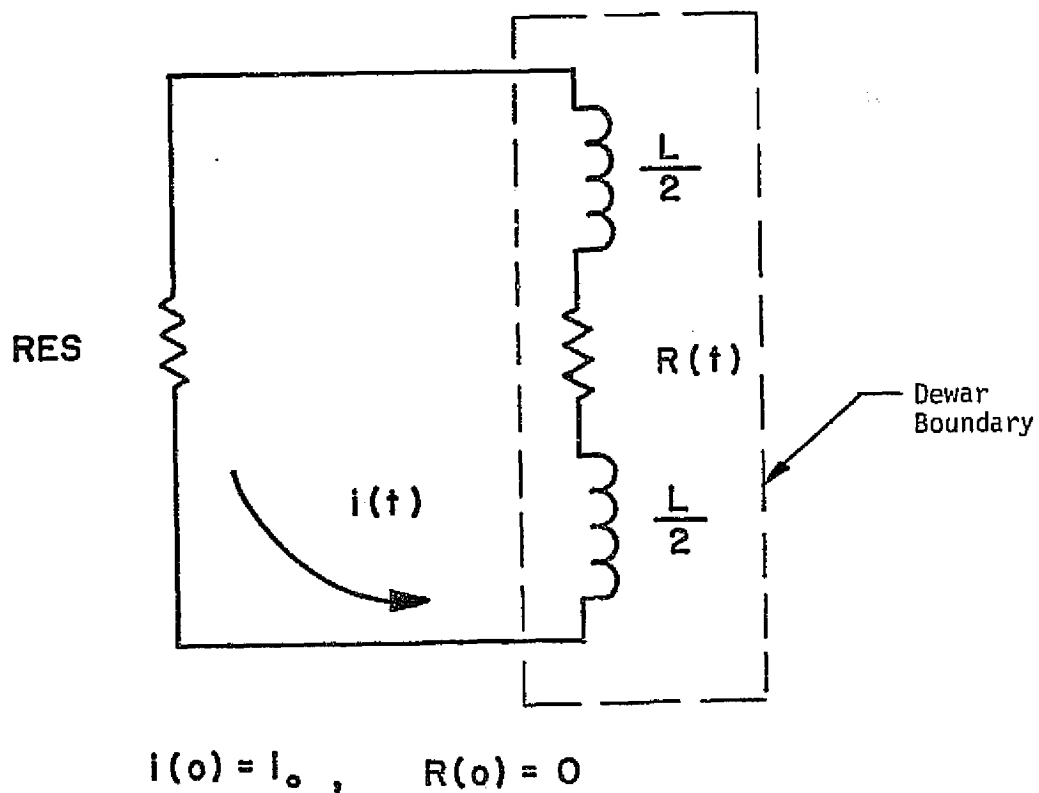


Figure IV-14 Circuit representing a superconducting coil of inductance  $L$  dissipating its energy in an external resistor,  $RES$ , and in a propagating normal region,  $R(t)$ , located near midcoil

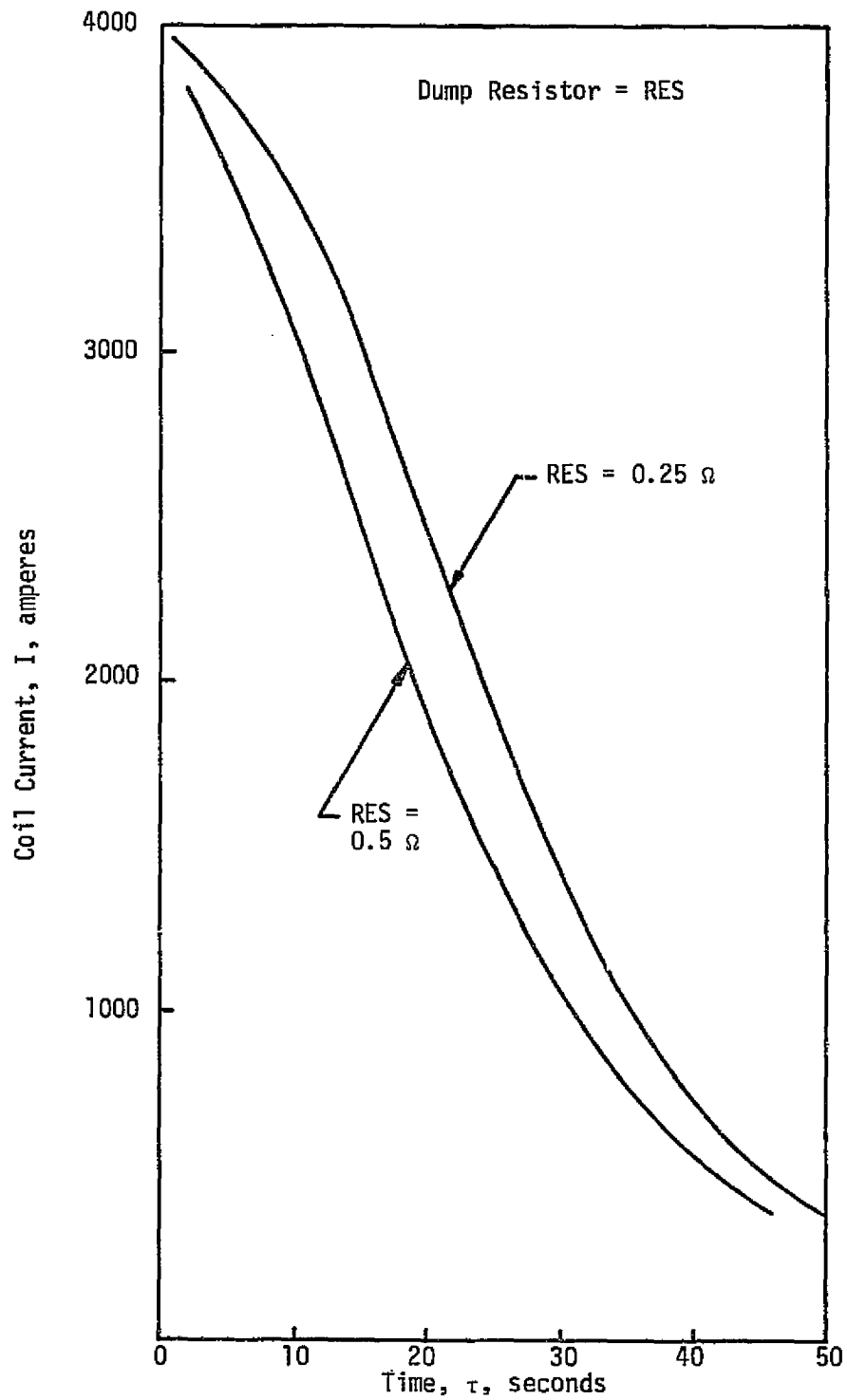


Figure IV-15. Computed Current Vs. Time Quench Transients for Design No. 1

Dump Resistor = RES

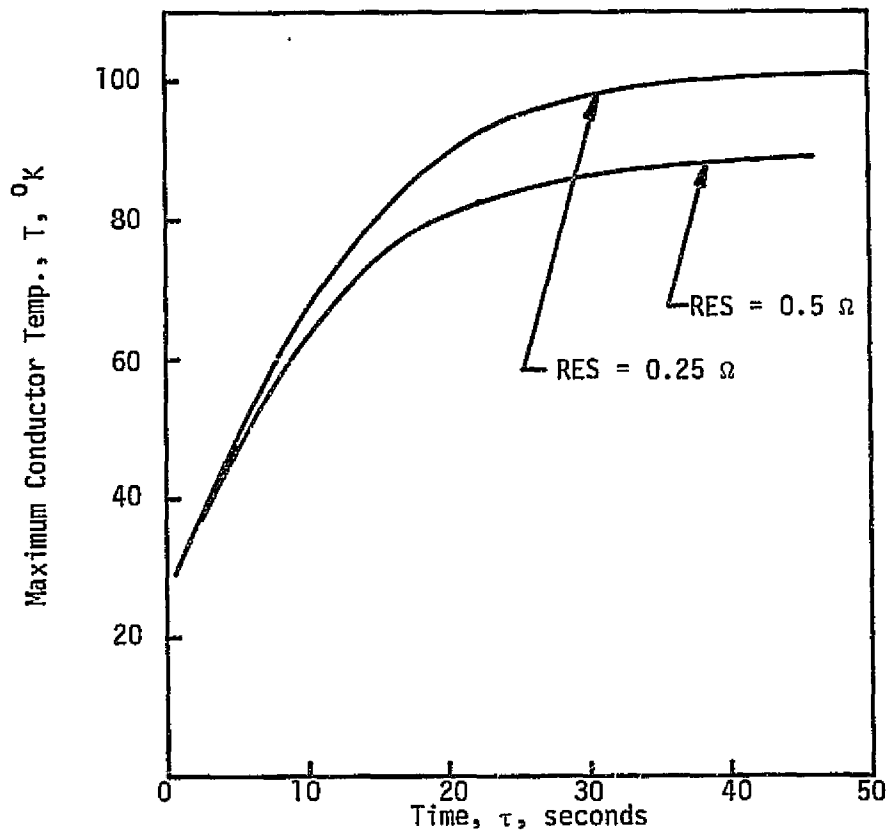


Figure IV-16

Computed Maximum Conductor Temperature During Quench Transient for Design No. 1

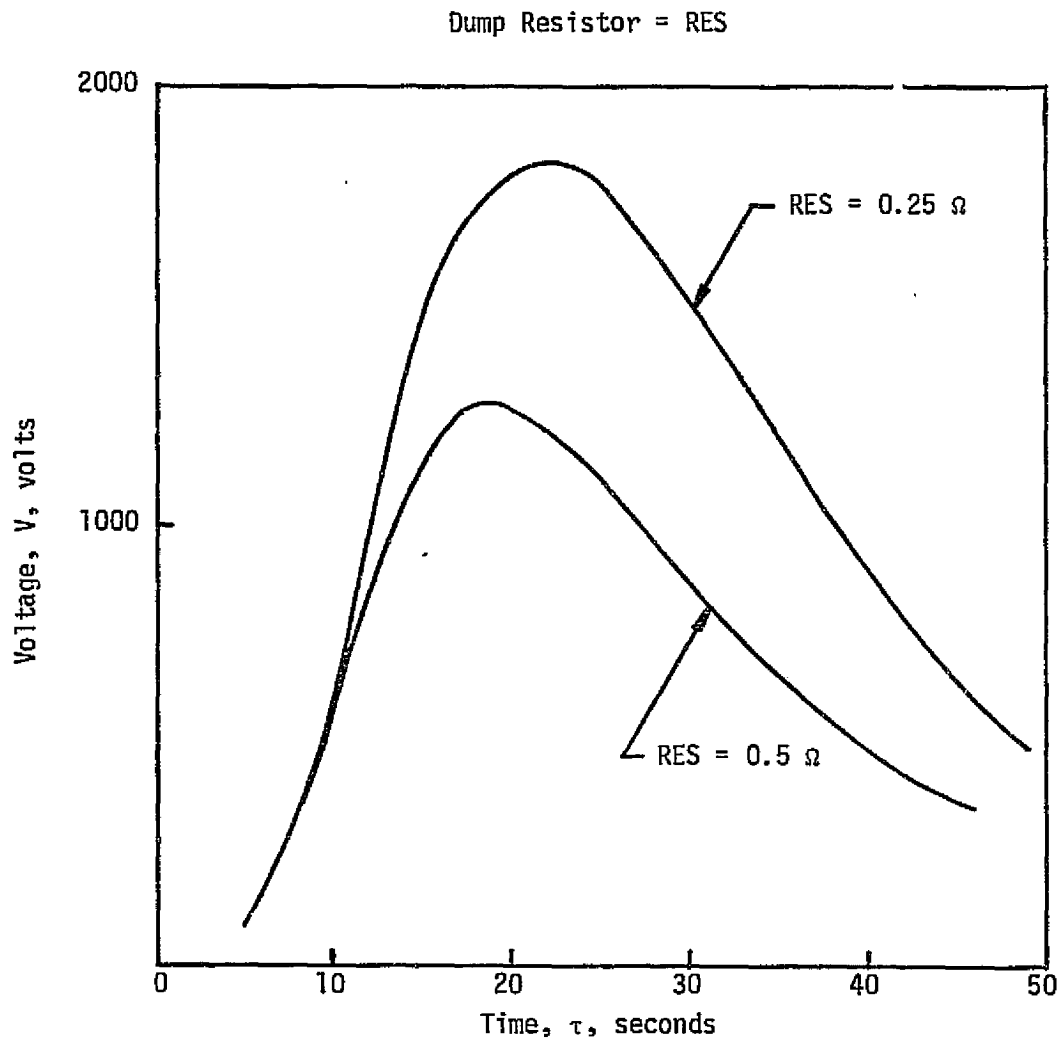
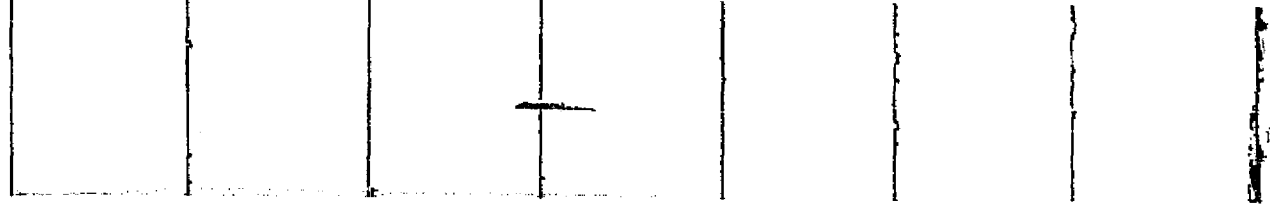


Figure IV-17  
Computed Voltage Across Normal Region for Design No. 1



the quench transient for the two cases corresponding to the different dump resistors. The rapid initial climb in temperature arises from the low specific heat at reduced temperatures and the high energy dissipation rates during the initial part of the transient. Note that the higher value for the dump resistor leads to a reduced maximum temperature since less energy is dissipated in the coil.

The voltage across the normal region in the coil is plotted in Figure IV-17. This is defined as the current times the resistance of the normal region and is a measure of the voltage levels experienced within the magnet. As shown in the figure, the voltage rises to a peak and then decays. A summary of the results is given in Table IV-7. Note that the larger dump resistance leads to a faster decay rate, a lower maximum temperature, a lower internal voltage, and a higher terminal voltage.

The layer to layer voltage that corresponds to the 0.5 ohm external dump resistor was estimated at less than 145 volts for the resistive voltage component alone. This will be reduced by the inductive voltage component. The voltage across the coil terminals is high but acceptable, though special precautions will be necessary in design and construction.

On the basis of these preliminary results, a simple protection scheme consisting of a dump resistor at about the 0.25 to 0.5 ohm level seems reasonable for this system. Reevaluation and more detailed analysis will be necessary during a detailed design phase.

Table IV-7

Summary of Estimated Quench Characteristics for Design No. 1

Dump Resistor (ohm)	Decay Time Constant (sec)	Maximum Temperature ( $^{\circ}$ K)	Max. Voltage Across Normal Region (V)	Max. Voltage At Coil Terminals (V)
0.25	20.99	101	1877	977
0.5	16.85	89	1281	2000

### C. STRUCTURE AND DEWAR DESIGN

This section begins with a discussion of the applied forces of electromagnetic origin which are induced in the windings and the manner in which they were computed. It continues with a description of the structure and dewar and of the design criteria utilized in their design. The section ends with a discussion of the heat leak estimates for the magnet system

#### 1. Applied Forces

Several different types of loadings must be considered in the design of a superconducting magnet. These include: gravity loads, thermal loads, thermally induced loads, loads by electrical transients, and electromagnetic (em) loads experienced in operation. The em loads are by far the greatest and are discussed in this section in detail. The remaining loads, which must be taken into consideration ultimately, are considered beyond the scope of this program and would be dealt with in depth during a detailed design phase. The overall characteristics of the preliminary design as presented in this report should not change to any large extent as a result of the consideration of these other loads.

The total force on a section of current carrying conductor(s)--for example, a portion of a magnet winding--may be found by integrating the Lorentz force over the volume of the section of interest. To obtain an analytical result in closed mathematical form, it must be possible to perform the following operations in the region:

1. Express  $\vec{J}$  mathematically
2. Express  $\vec{B}$  mathematically
3. Integrate  $\vec{J} \times \vec{B}$

The procedure outlined by steps 1, 2, and 3 is tractable only in situations with particularly simple geometry. In most cases, one or more of these steps must be replaced by an approximating procedure.

For the racetrack and rectangular saddle geometries, all of the above steps must be carried out numerically. The basis for the computation is that it is possible to express in closed form the magnetic field generated by a straight current filament of finite length. The above procedure is then replaced by:

1. Represent the entire current carrying winding by a model composed of current carrying "sticks" of finite length. This requires a specification of the end points of each stick in a suitable coordinate system and of the magnitude and direction of the current carried by each stick.
2. Select the coordinates of points at which the magnetic field is to be determined and calculate the field at each of these points by a vectorial sum of the contributions from each current "stick." If a point lies outside the winding model, then contributions from all of the sticks are summed. However, if a point is located on a stick (as is

necessary if the goal is the determination of the force at that point), then it is necessary to sum all contributions except for that due to the stick which passes through the point of interest. The latter is necessary to avoid the fact that the zero cross-sectional area of a given stick together with its finite current leads to an infinite magnetic field on the stick itself.

3. Determine the local components of the force per unit volume at a given point by forming the vector cross product of the current carried by the stick and total magnetic field calculated at that point and dividing by the winding cross-sectional area which the stick represents.
4. Find the total force in a selected direction on a section of winding by summing the proper components of the forces per unit volume multiplied by the incremental volumes they model over the section.

In general, the larger the number of sticks in the current filament model, the better the approximation; however, computational time increases rapidly and even the initial task of merely specifying the coordinates of the sticks may become formidable.

The current filament model used for force computation in this preliminary design is illustrated in Figure IV-18. This is again a coil cross section in the end turn region. Forces of electromagnetic origin for the purposes of this preliminary design were computed using four current filaments in each coil. The amp-turns for each filament are indicated. Two views of the current sticks for the model are given in Figures IV-19 through IV-22 together with force vectors drawn to scale to illustrate the load distribution and magnitude at rated field.

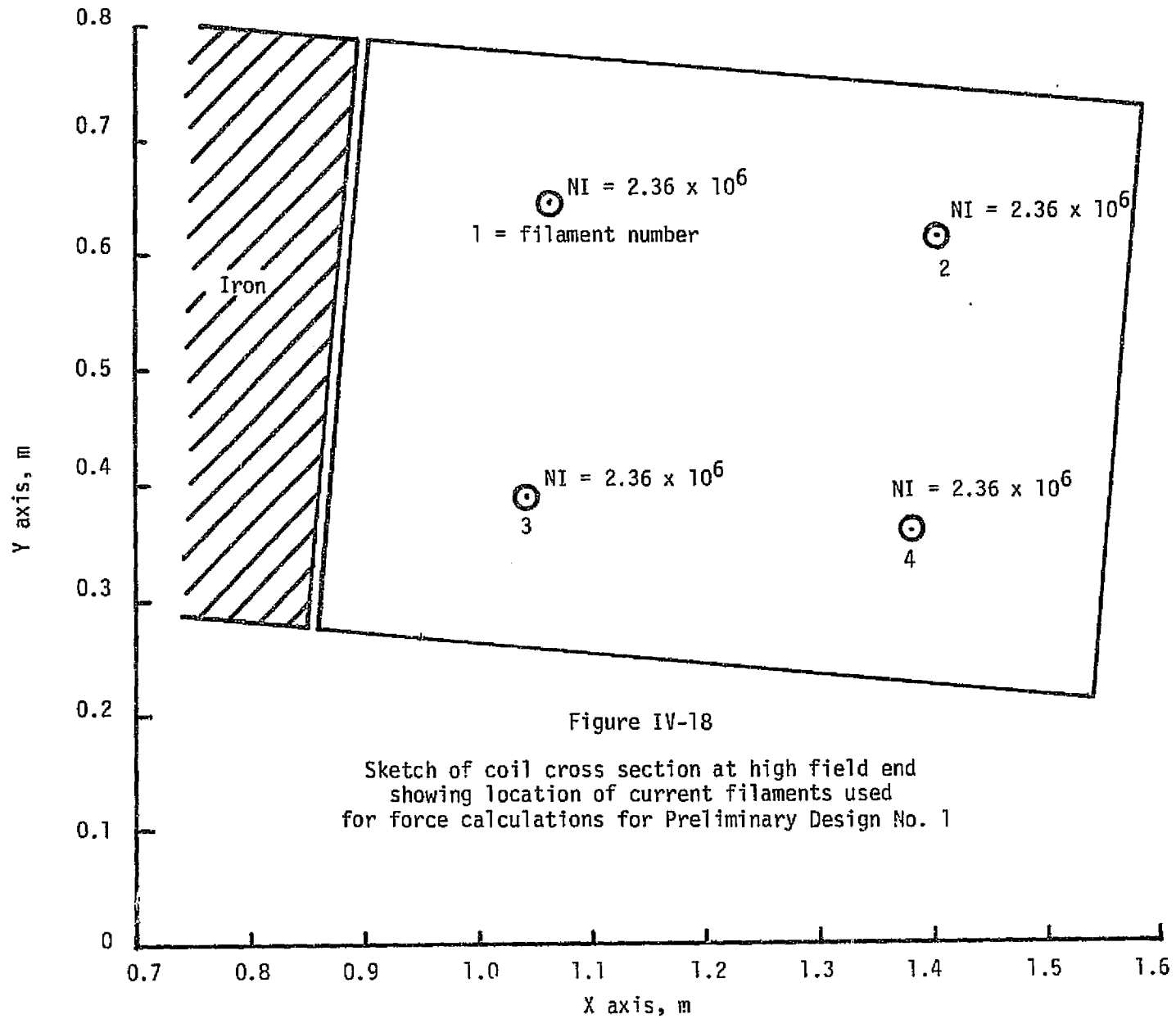
The X and Z force components in the end turn regions were used to design the stainless steel bands that are integrally wound in parallel with the conductor as described in Section IV-A of this report. The Z force components along the straight section or sides of the coil were used in designing the transverse support structure of the coil, and the Y force components were used to design the support spacers for the attractive load between the coils.

## 2. Structure Description and Design Criteria

A summary of the mechanical characteristics of the external structural components for Design No. 1 is given in Table IV-8. This gives the design pressure, weight, materials, and overall size of the major structural components of the magnet system which include the coil/He vessel, the attractive em load support spacers, and the main gravitational support structure. The design of the structure was based on a maximum allowable working stress of  $2.75 \times 10^8$  N/m<sup>2</sup> (40,000 psi), which allows for a margin of safety of two (2) applied to the allowable yield strength of stainless steel.

The above represents external support structure. In addition, there is structure internal to the winding. This consists of the stainless steel channel that is wound in parallel with the conductor and which, in conjunction with the conductor, supports the axial em loads in the coil windings.





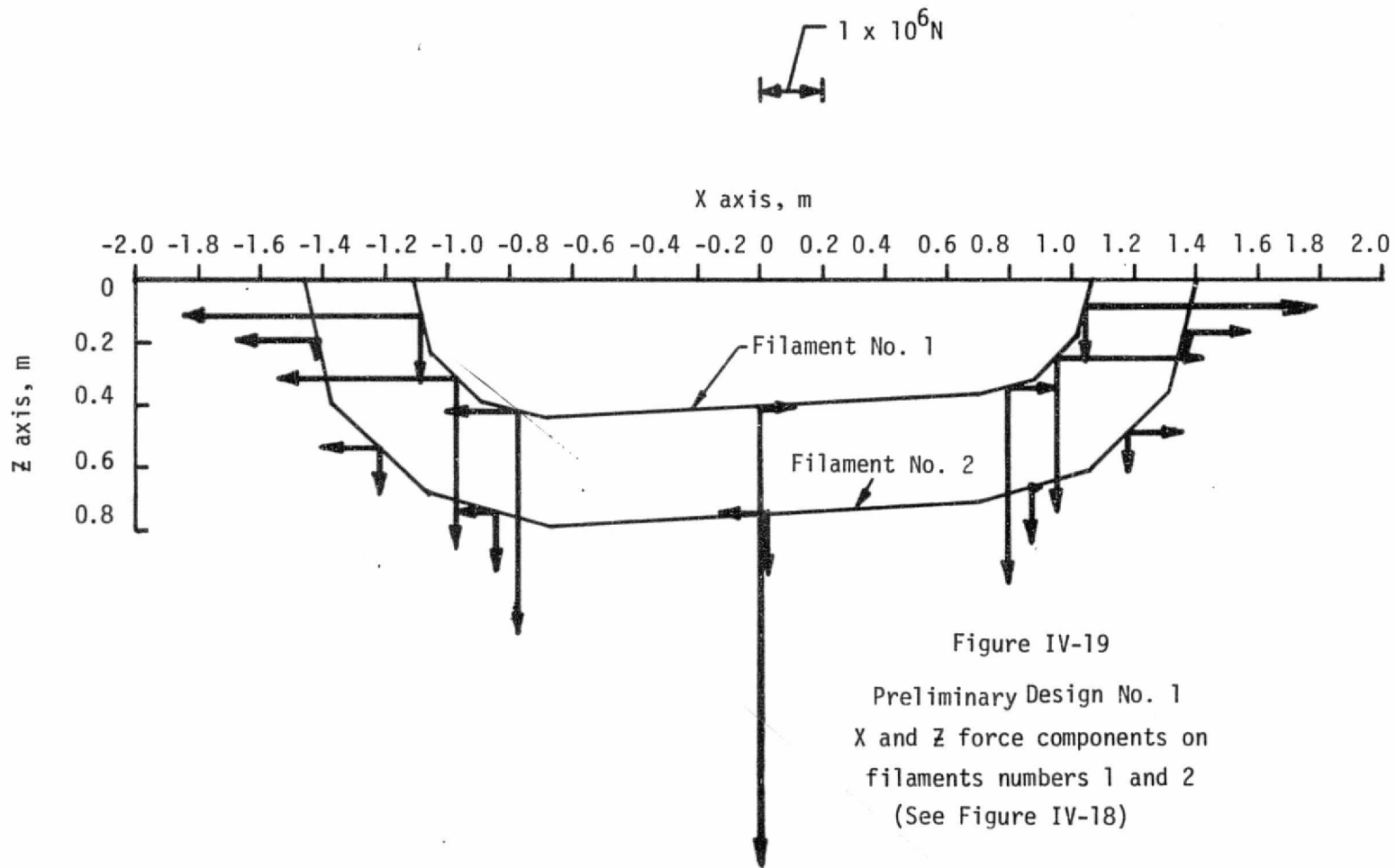


Figure IV-19  
Preliminary Design No. 1  
X and Z force components on  
filaments numbers 1 and 2  
(See Figure IV-18)

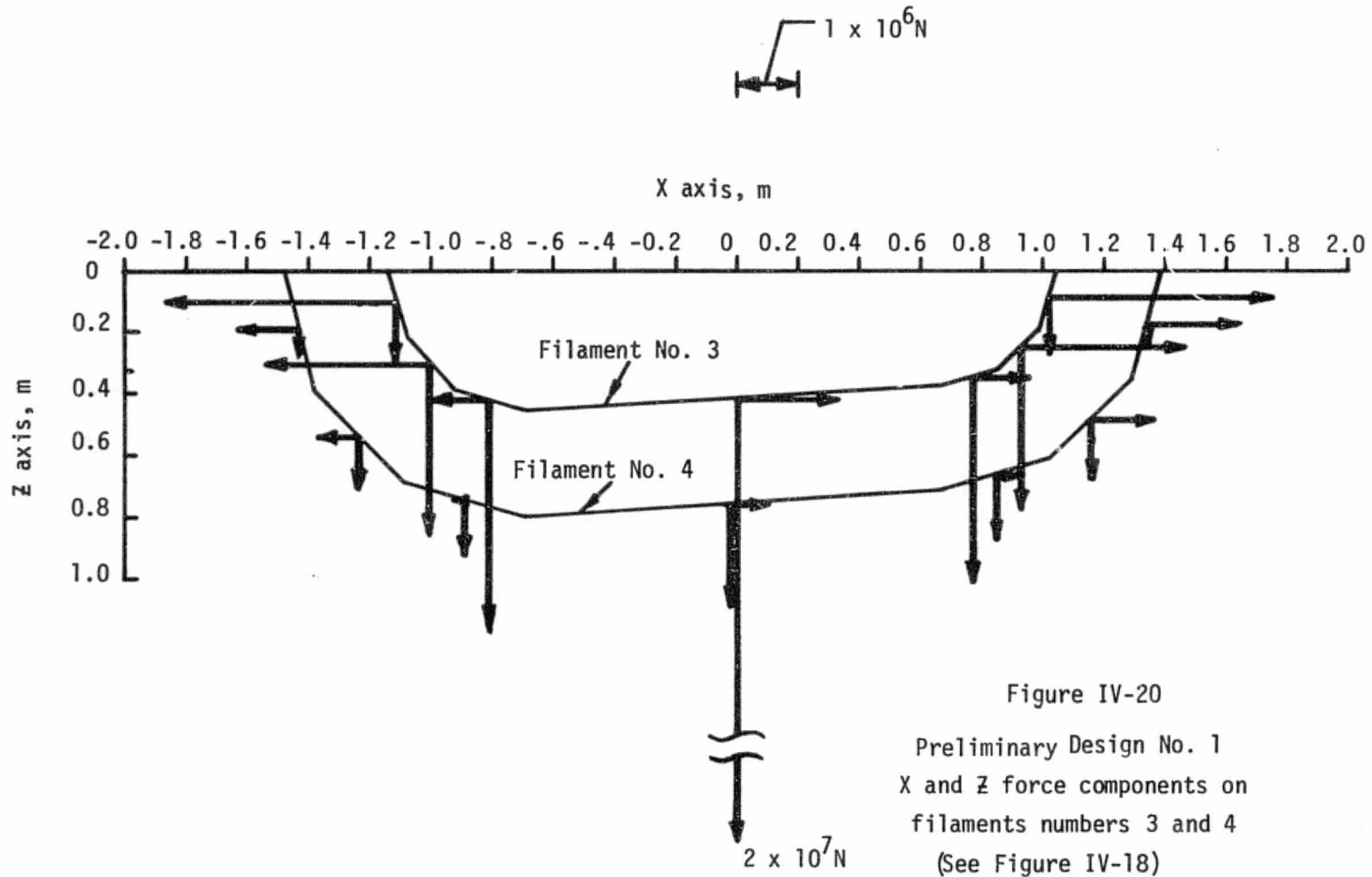


Figure IV-20  
 Preliminary Design No. 1  
 X and Z force components on  
 filaments numbers 3 and 4  
 (See Figure IV-18)

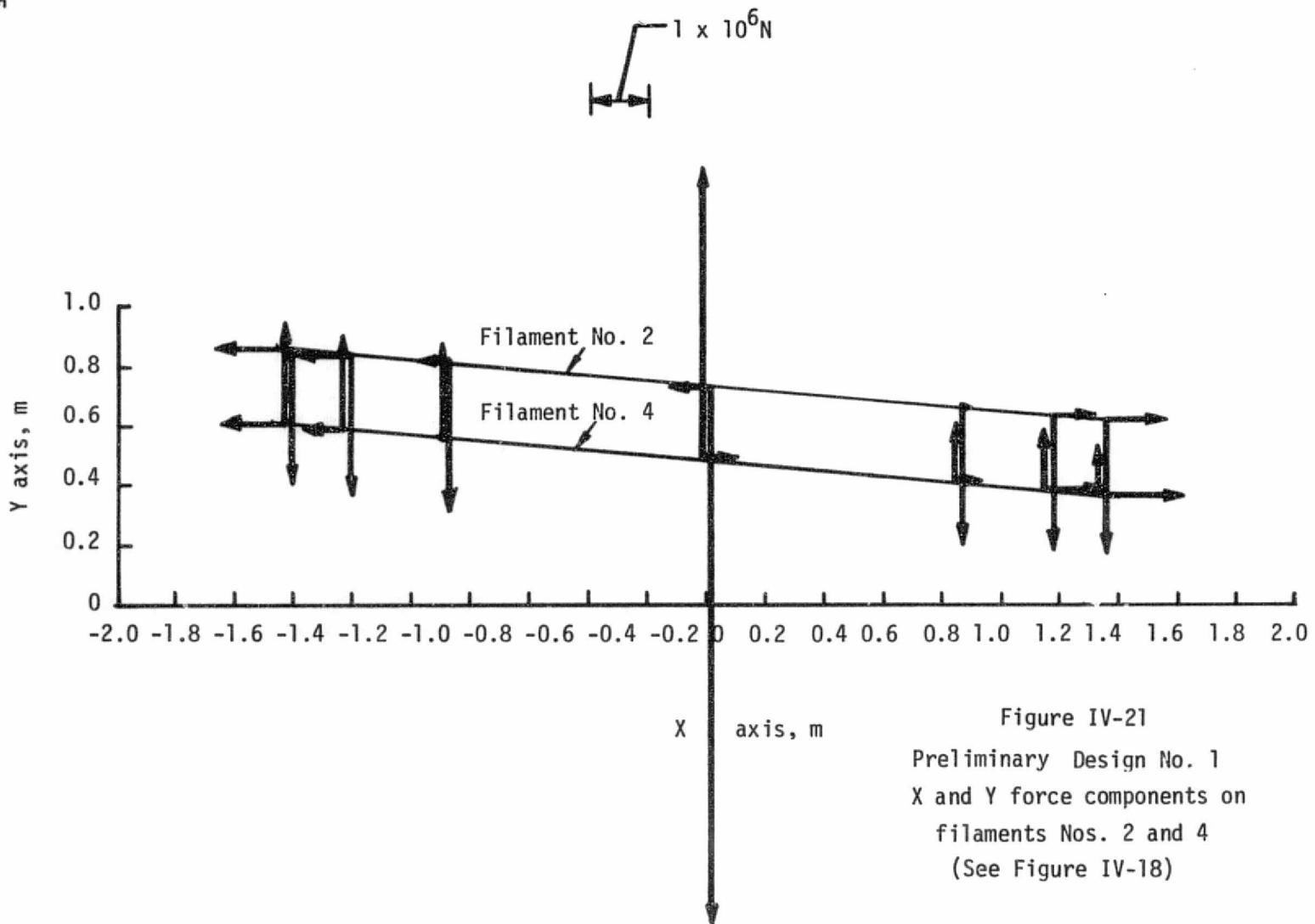


Figure IV-21  
Preliminary Design No. 1  
X and Y force components on  
filaments Nos. 2 and 4  
(See Figure IV-18)

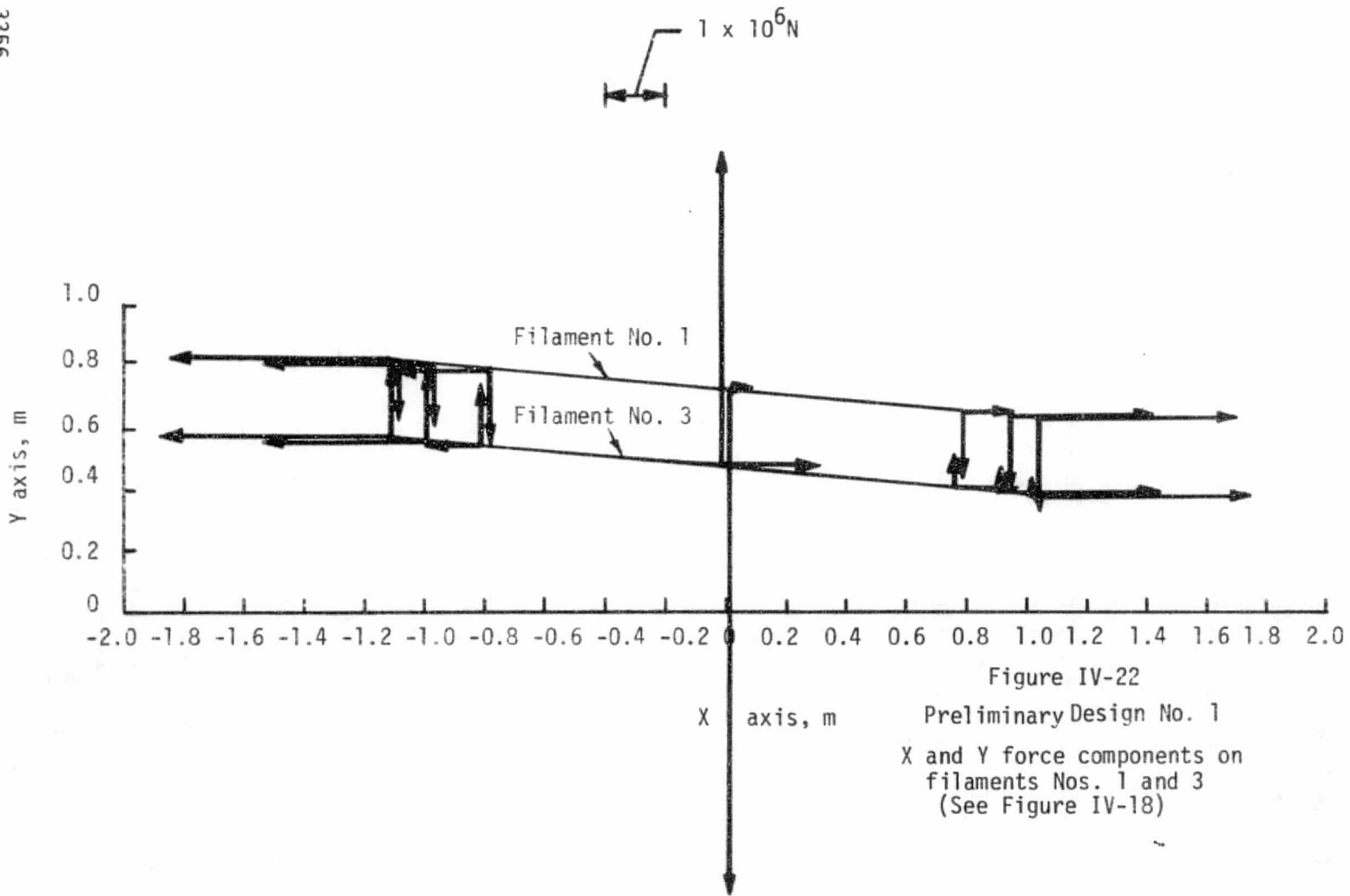


Figure IV-22  
 Preliminary Design No. 1  
 X and Y force components on  
 filaments Nos. 1 and 3  
 (See Figure IV-18)

Table IV-8

Summary of Mechanical Characteristics of the Major  
Structural Components for Design No. 1

I. Coil/He Vessel

A. Design Pressure

1.  $2.07 \times 10^5$  N/m<sup>2</sup> (30 psia) Internal
2.  $1.03 \times 10^5$  N/m<sup>2</sup> (15 psia) External

B. Weight

1. Conductor = 15,900 kg (34,980 lbs.) (2)
  2. Iron = 6,773 kg (14,900 lbs.) (2)
  3. Structure = 18,182 kg (40,000 lbs.) (2)
- TOTAL = 40,855 kg (89,880 lbs.)

C. Material

1. Conductor - MF NbTi/Copper
2. Iron - AISI 1008
3. Structure - 310S SS

D. Overall Size of Each Vessel

1. Length = 3.30 m (130 in.)
2. Width = 2.39 m (94 in.)
3. Height = .76 m (30 in.)

II. Support Spacers for Attractive em Load (Low Gradient Profile Mode)

A. Weight (Low Gradient)

1,205 kg (2,650 lbs.) ea; total - 4,820 kg (10,600 lbs.)

B. Weight (High Gradient)

568 kg (1,250 lbs.) ea; total - 2,273 kg (5,000 lbs.)

C. Material - 310S SS

D. Overall Size

	High	Low
1. Length =	2.48 m (98 in.)	2.48 m (98 in.)
2. Width =	1.91 m (75 in.)	1.91 m (75 in.)
3. Inlet Height =	0.18 m (7 in.)	0.10 m (4 in.)
4. Outlet Height =	0.71 m (28 in.)	0.18 m (7 in.)

III. Main Gravitational Support Structure

A. Weight - 7,818 kg (17,200 lbs.)

B. Material - 310S SS

C. Overall Size

1. Length = 3.38 m (133 in.)
2. Width = 3.25 m (128 in.)
3. Height = 0.56 m (22 in.)

#### a. Stainless Steel Channel (Internal Structure)

The dimensional characteristics of the required stainless steel banding are given in Table IV-6. Estimated lengths and weights are also included. The manner in which this material is used in the winding is shown in Figure IV-9. Insulation and winding spacer thicknesses are given and consist of a spiral wrap  $1.52 \times 10^{-4}$  m (0.006 in.) turn-to-turn insulation and a distribution of  $2.286 \times 10^{-3}$  (0.090 in.) thick insulating slats between "pancakes". The estimated hoop stress distribution in the winding is shown in Figure IV-23. As indicated, the average hoop stress attains a peak level of about  $7.49 \times 10^7$  N/m<sup>2</sup> (11,000 psi) in the windings. The windings experience zero radial stress on the inside turns and a compressive radial stress in those turns outside of the peak hoop stress location. For the purposes of this program, this stress distribution was calculated based on the assumption that the end turn region acts as a solenoid. This is a reasonable assumption as long as the boundary conditions are valid; i.e., as long as the radial deflections of the point of tangency between the straight portion of the coil and the round portion of the end turns of the coil are consistent with that of a solenoid having the same dimension. In order to do this, the transverse structure should be designed with suitable stiffness at that point.

The size of the stainless steel banding required in each subregion (see Figure IV-9) of the coil cross section was chosen to limit the axial stress in the conductor to  $6.90 \times 10^7$  N/m<sup>2</sup> (10,000 psi). Results of the analysis indicated stainless steel banding was required only in regions a, b, f, i, and j based on this criterion. However, the stainless steel banding must also transmit the attractive em loads parallel to the wide face of the conductor and prevent load accumulation between conductors in adjacent pancakes. As a result of this criterion, it is required in the remaining regions and was included with a wall thickness of  $7.62 \times 10^{-4}$  m. (0.030 in.).

#### b. Coil/He Vessel (See Figure IV-6)

The coil/He vessel, which contains the iron pole pieces, coil windings, and LHe, consists of a top plate, bottom plate, center section, side beams, and seal plate, all of which are fabricated from 310S stainless steel. Ribs are welded to the top plate for additional stiffness, and doubler plates are welded to the bottom plate for added strength for the section of the coil end turns that passes over the bore tube; i.e., that portion which is not supported directly by the attractive em load support spacers. The center section is welded to the bottom plate after the coil and iron pole piece have been assembled, and it is plug welded to the top plate. Several stainless steel rods, which are threaded through clearance holes in the iron plug, connect the center of the top plate with the center of the bottom plate to minimize local bulging due to the internal pressure of the LHe. Shear pins connect the top plate and bottom plates to the side plates. The seal plate is the last part to be added and is seal welded about the perimeter of the vessel to provide a vacuum tight container.

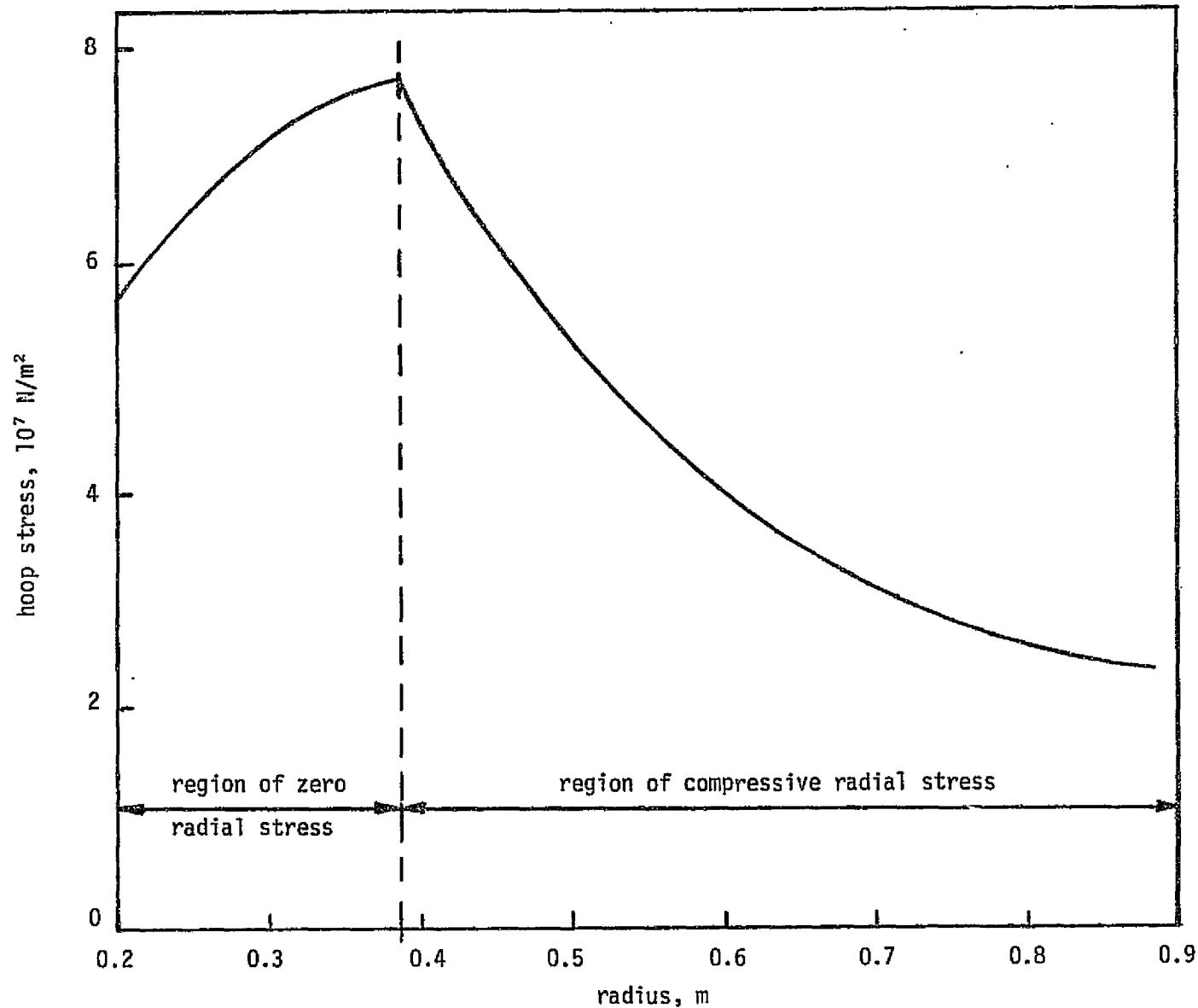


Figure IV-23 Estimated Average Hoop Stress Distribution for Design No. 1



The top and bottom plates were designed to support the transverse em loads in tension. In addition, the top plate has been designed to withstand the internal pressure of  $1.03 \times 10^5 \text{ N/m}^2$  (15 psia), which can increase to a maximum value of  $2.07 \times 10^5 \text{ N/m}^2$  (30 psia = pressure at which relief valves are assumed to open) under a fault condition. The bottom plate has been designed to support the coil in the end turn region where it spans the gap between the attractive em load support spacers. The bottom plate has also been designed to support the em loading that is applied by the iron pole piece. The seal plate has been designed to withstand the maximum expected internal pressure of the coil/He vessel. The pivot shaft, which is an integral part of the coil/He vessel, has been sized to support one half of the gross weight of the coil/He vessel.

#### c. Attractive em Load Support Spacers

The attractive em support spacers fasten between the coil/He vessel and the main gravitational structure and have been designed to support the high attractive loads which exist between the upper and lower coil/He vessels during normal operation. Two sets of four spacers per set are required per magnet system; i.e., one set for the high field profile design case and one set for the low field profile design case. The wedge-shaped spacers are fabricated from 310S stainless steel plate and consist of a top plate, bottom plate, and two center webs. The top and bottom plates have been designed from a bearing stress point of view, while the center webs have been analyzed from a compressive stress and elastic stability viewpoint. The bolts which fasten the bottom spacers to the coil/He vessel and the main gravitational support have been designed to support the weight of the coil/He vessel. The bolts for top spacers have been designed to support the shear forces that develop due to the attractive em loads acting on the wedge-shaped spacers. They have also been designed to support the weight of the coil/He vessel in tension.

#### d. Main Gravitational Support Structure

The main gravitational support structure has a twofold purpose; i.e., it supports the attractive em loads between coil/He vessels and the combined weight of the coil/He vessels and attractive em load support spacers. It has been designed to transmit these loads to the column support system which in turn transfers them to the ground. Basically speaking, the main support consists of longitudinal and transverse beams with a gusseted, rectangular beam encircling the warm bore tube and radiation shield. The longitudinal and transverse beams have been designed to support the gravitational loads as a beam in bending at room temperature even though its yield strength will increase at cryogenic temperatures. The rectangular box beam in the center has been designed to transmit the loads across the warm bore tube and radiation shield. The deflection of the inner wall of the rectangular box beam has been limited to avoid any contact with the superinsulation around the outer surface of the radiation shield. The pillow block bearings which support the shaft of the coil/He vessel have been designed with slots which provide some adjustment for final alignment purposes and allow the coil/He vessel to be positioned accurately at final assembly.

The main gravitational support structure will be fabricated from 310S stainless steel and is of welded construction. In addition, it will be made in

two pieces off site to satisfy shipping requirements and then transported to the site and field welded together to form a single weldment.

### 3. Dewar Description and Design Criteria

From a structural standpoint the dewar must be designed to carry the gravitational loads of the magnet, the induced electromagnetic loadings, and the thermally induced loads. In addition, it must insulate the cold space sufficiently well to maintain the heat leak into the system at an acceptable level. The dewar consists of a warm bore tube, warm bore tube radiation shield, outer room temperature vessel, outer radiation shield, and the column support system. The liquid helium vessel has been incorporated into the coil support structure and was discussed earlier.

A summary of the mechanical characteristics of the dewar for Design No. 1 is given in Table IV-9. This gives the design pressures, weights, materials, and overall sizes of the major dewar components for the magnet system. These components are the room temperature vessel, the radiation shield, the column support system, and the vapor-cooled power lead assembly. This section describes the major components of the dewar and discusses the criteria that were the basis for the design.

#### a. Warm Bore Tube and Warm Bore Radiation Shield

The most important and significant characteristic resulting from the design of a warm bore tube and warm bore radiation shield is the distance from the center of the bore to the coil. This dimension impacts the quantity of conductor used, the size and weight of the magnet, the cost, and other aspects of the design. It is essential that this dimension be kept to a minimum. In order to do this, the warm bore tube and radiation shield must be designed to be as thin as possible and as close to each other as can be tolerated. This implies solid plate design without ribs or corrugations, which would normally be used for stiffness.

The warm bore tube is located at the center of the magnet and surrounds the MHD channel. Superinsulation is wound around the warm bore tube to reduce the radiation heat load from room temperature to the radiation shield and helium vessel. A small gap separates the superinsulation from the radiation shield and is sized to compensate for any assembly or manufacturing tolerances as well as thermal contraction during cooldown. If the superinsulation comes in contact with the radiation shield, a conduction path is established which acts to increase the boiloff rate of the magnet, which is highly undesirable. The radiation shield intercepts the radiation heat load that reaches it and conducts it to a suitable heat sink. Around the radiation shield is placed additional superinsulation which minimizes the radiation heat load from the radiation shield to the helium vessel. There is also a small gap between the superinsulation and the helium vessel.

Figure IV-24 shows the cross section of the warm bore tube and radiation shield at the inlet of the magnet and gives the clearance between the warm bore tube and the radiation shield and the distance from the center of the warm bore tube to the innermost surface of the coil. These clearances remain the same as

Table IV-9

Summary of Mechanical Characteristics of Dewar for Design No. 1

I. Room Temperature Vessel

A. Design Pressure

1.  $1.03 \times 10^5 \text{ N/m}^2$  (15 psia) Internal
2.  $1.03 \times 10^5 \text{ N/m}^2$  (15 psia) External

B. Weight = 18,636 kg (41,000 lbs.)

C. Material = 304L SS

II. Radiation Shield

A. Design Pressure

1.  $0 \text{ N/m}^2$  (0 psia) Internal
2.  $0 \text{ N/m}^2$  (0 psia) External

B. Weight = 5,909 kg (13,000 lbs.)

C. Material = ETP Copper Annealed

III. Column Support System

A. Configuration

1. Four legs consisting of three concentric cylinders
2. All columns have flexural hinges and are designed to compensate for thermal contraction of the He vessel and main support

B. Type

1. Inner Cylinder = G10
2. Intermediate Cylinder = Aluminum
3. Outer Cylinder = G10
4. Hinge Material = 6Al4V ELI Titanium

C. Weight = 142 kg (312 lbs.) ea x 4 = 568 kg (1250 lbs.) total

IV. 4,000 A Lead Assembly

A. Weight = 91 kg (200 lbs.)

B. Material = OFHC Copper and G10

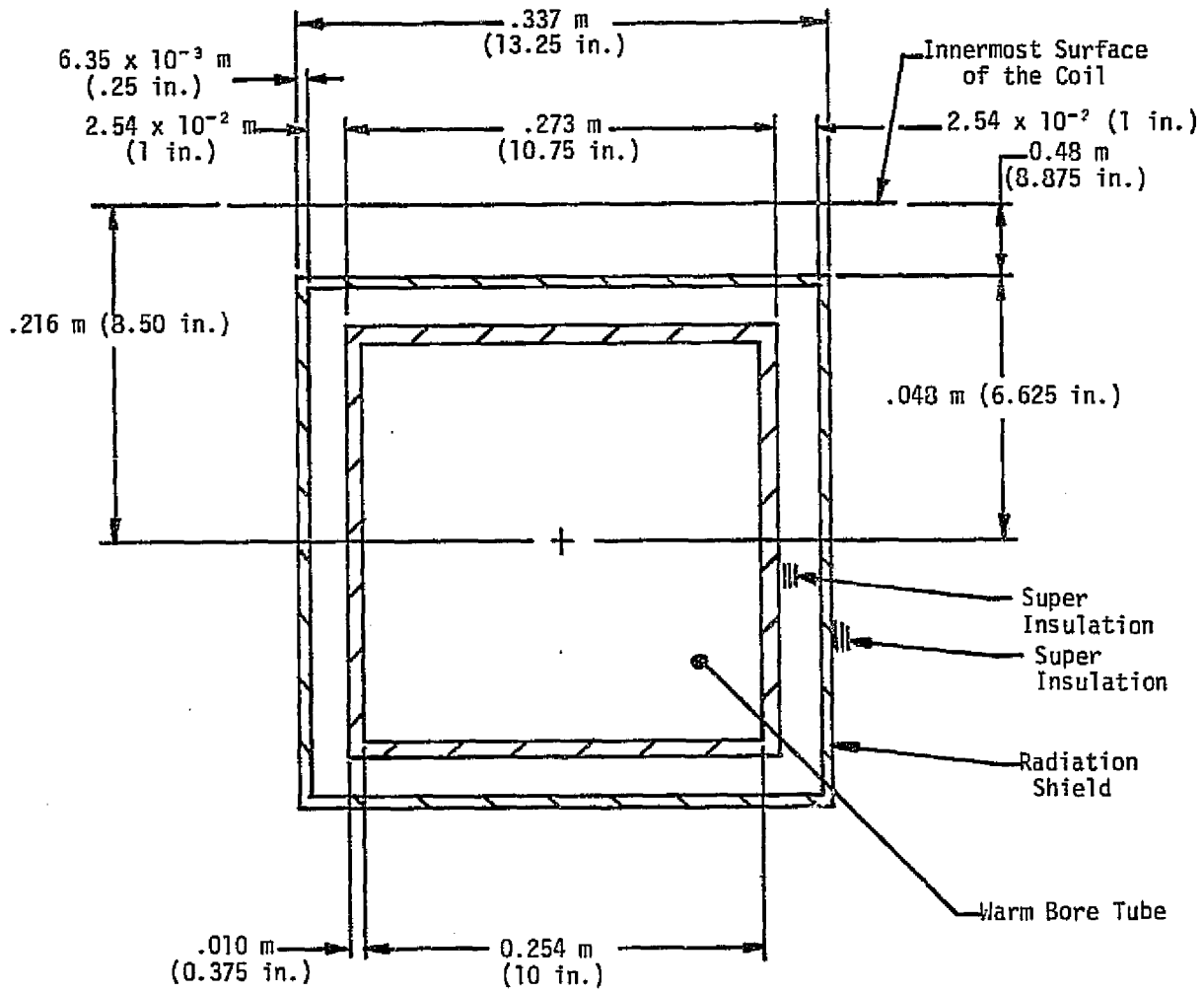


Figure IV-24 Warm Bore Tube and Radiation Shield at Duct

the warm bore tube, and the radiation shield tapers to 0.406 m x 0.508 m (16 in. x 20 in.) at the outlet of the magnet.

The warm bore tube, which is at a temperature of 300° K and subjected to an internal pressure of  $1.03 \times 10^5$  N/m<sup>2</sup> (15 psia) during normal operation, was analyzed for stress and deflection as a simple beam supporting its own weight uniformly over its length. It was also analyzed as a square, flat sided tube having an internal pressure of  $1.03 \times 10^5$  N/m<sup>2</sup> (15 psia). The flat plates were assumed to be uniformly loaded and supported on all edges. Based on a maximum allowable deflection of  $7.6 \times 10^{-4}$  m (0.03 in.), the design of the warm bore tube proved to be deflection controlled. The clearance space between the warm bore tube and the radiation shield takes into consideration the following areas: superinsulation thickness, deflection under gravitational and internal pressures, manufacturing tolerances, and a clearance space.

The radiation shield in the bore was analyzed so as to support its own weight when held at the ends. In the course of the design of the radiation shield, it was found that its size is controlled by manufacturing, handling, and shipping considerations. Stress and deflection are small and consequently do not govern the design. As a matter of judgment, the minimum practical thickness based on these considerations is  $6.35 \times 10^{-3}$  m (.25 in.) for a tube of the size required for this magnet system.

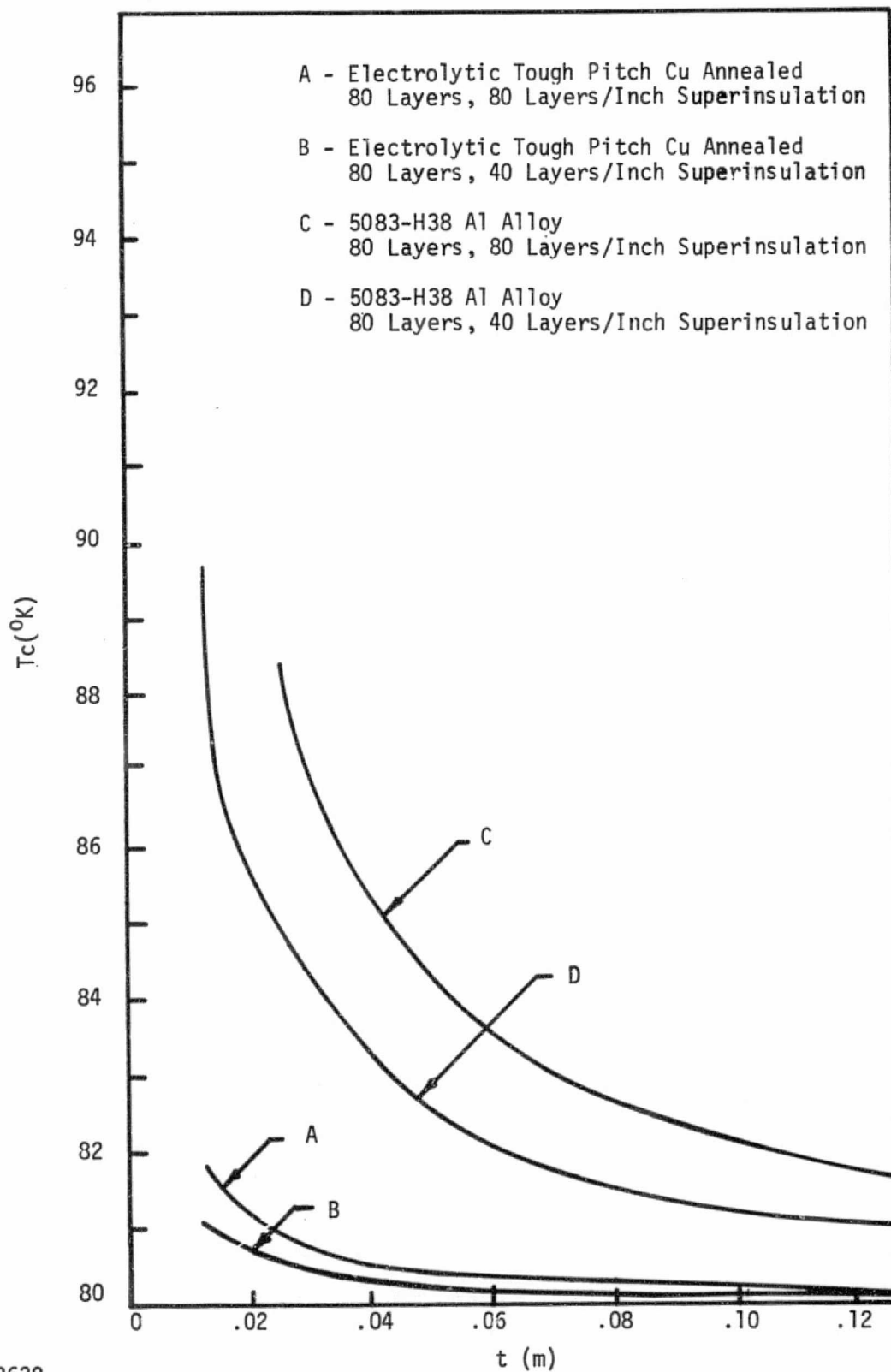
Figure IV-25 shows the radiation shield temperature rise as a function of thickness for 5083-H38 aluminum alloy and Electrolytic Tough Pitch (ETP) copper for two different packing densities of superinsulation. The temperature rise in this case was calculated based on the radiation shield conducting the radiation heat load input to a cold sink. It is clear from this figure that from a heat transfer point of view the ETP copper should be used to minimize the temperature rise and consequently the LHe boiloff. A more detailed analysis may, however, indicate that aluminum is suitable though less attractive thermally.

Both the warm bore tube and the warm bore radiation shield are made as single weldments and shipped to the site for final assembly.

#### b. Room Temperature Vessel and Outer Radiation Shield

The room temperature vessel consists of a center section, which is fabricated from welded 304L stainless steel plate and rolled into final shape, and two dished end covers which are spun into shape. The center section is made in two sections with a flange at the mating surfaces; i.e., a top half section and bottom half section. The structural design of a vacuum vessel of this size is controlled by the external pressure; i.e., that pressure that would cause the vessel to become elastically unstable (local buckling). Stiffening rings are required about the center tube at the location of the support legs to prevent localized bending and buckling failures. The support legs have been designed with a large inside diameter to accept the low heat leak columns. The room temperature vessel was also analyzed as a beam and for elastic instability when supporting its own weight. In the final design, consideration should also be given to mild steel as material for the room temperature vessel.

The radiation shield is situated in a vacuum and is not pressure loaded; consequently, it must only be designed to withstand its own weight. It was



FA 3628

Figure IV-25 Radiation Shield Temp. Rise as a Function of Thickness

analyzed as a beam and for elastic instability. Manufacturing, handling, and shipping considerations controlled the design. In performing the analysis, the additional stiffness supplied by the tracer tubes was neglected. The radiation shield is fabricated in the same manner as the room temperature vessel. As with the warm bore radiation shield, the material was chosen as ETP copper.

### c. Column Support System

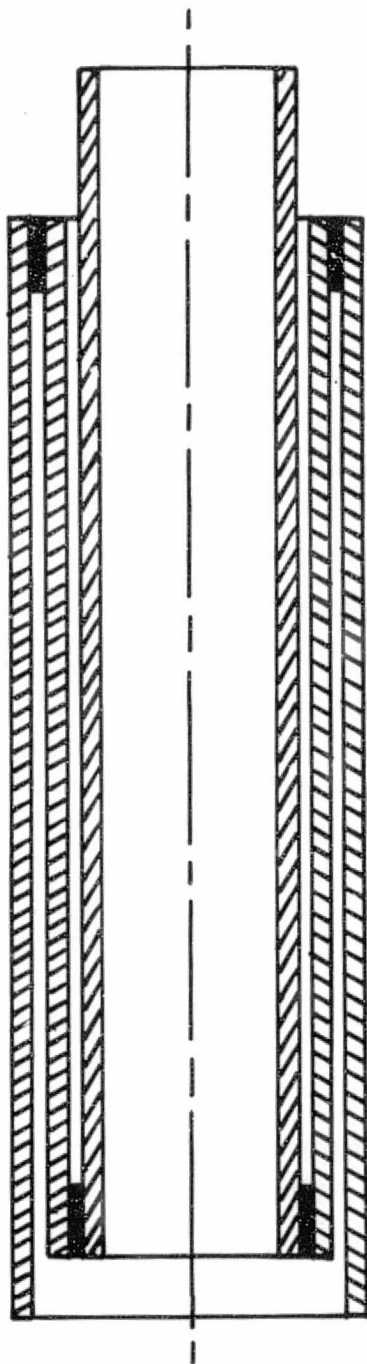
The column support system must transmit the gravitational load of the structure and coils to the foundation. For a given structural configuration, the heat load is directly proportional to the cross-sectional area of the support and inversely proportional to its length. It is desirable, therefore, to use long, slender members to support the gravitational loads. If these members are to be used in tension, the design is relatively simple, and an efficient structure is obtained. If the loads must be borne in compression, the buckling load of the support often becomes a limiting factor before the material is loaded to its design stress level.

The column support system chosen for this program consists of a collection of nested cylinders of epoxy-glass composite and aluminum materials which has been discussed and analyzed by J. R. Heim, Cryogenics, December 1972. This type of support has been successfully tested and has been incorporated in the design of some large superconducting magnets which are either operating or under construction presently. As Figure IV-26 shows, this type of support consists of three or more concentric cylinders. If materials are selected such that the thermal contraction of the intermediate tube (for a three-column design) is equal to the sum of the contractions of the inner and outer tubes, the overall height will not change when the column is cooled down to operating conditions. Consequently, all alignments can be made at room temperature during final assembly and will not be lost when the magnet system is cooled down. For a three-tube configuration, the middle tube can be made from aluminum, and the outer tube and inner tube can be made from epoxy-glass composite. This results in a low heat leak temperature stabilized column type support. At the top and bottom of the support are located hinges which are fabricated from 6Al4V (ELI) titanium. Titanium is chosen because it can withstand large deflections without exceeding its yield point. At final assembly the webs of the hinges are aligned perpendicular to the line of action which connects the centers of diagonal supports (see the assembly drawing, Figure IV-6). When the magnet cools down, the hinges bend to compensate for the thermal contraction of the system in a plane parallel to the ground. This is shown in Figure IV-27.

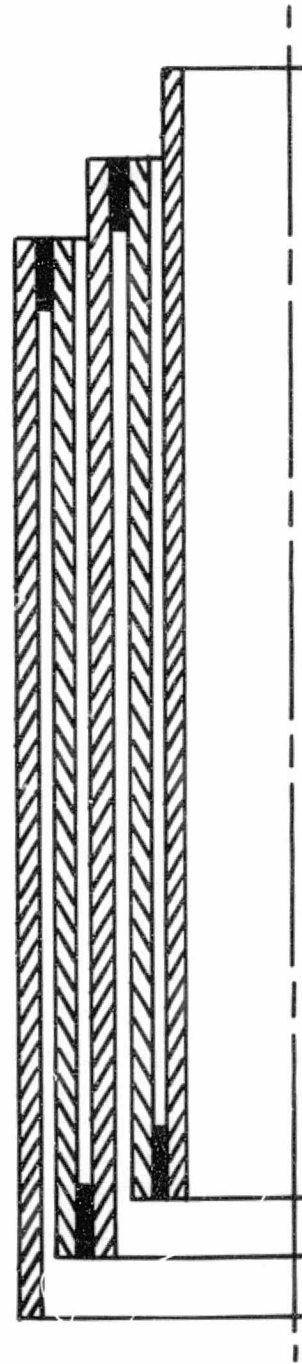
The column support has been analyzed for compression, tension (inner cylinder), buckling, and elastic stability modes of failure. The hinge has been analyzed to ensure the yield strength is not exceeded based on the calculated angle of tilt which occurs on cooldown. It has also been designed to withstand a lateral force approximately equal to  $2.2 \times 10^3$  N (500 lbs.) applied at the top of the column. This is in anticipation of a possible side force that might be applied to it during installation.

### 4. Radiation Heat Load Estimates

The total heat load on the magnet system consists of the sum of the conduction heat leak through the supports, the radiation heat leak, resistive



**3 MEMBER  
LOW CONDUCTION  
HEAT LEAK SUPPORT**

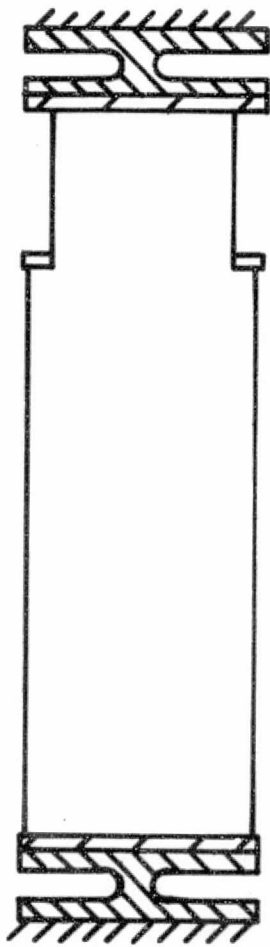


**5 MEMBER  
LOW CONDUCTION  
HEAT LEAK SUPPORT**

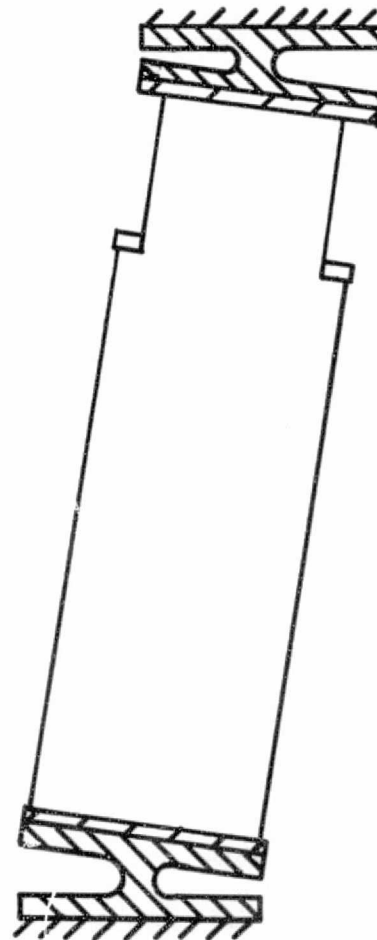
Figure IV-26

Illustration of Low Heat Leak Supports Consisting of Three and Five Members





Room Temperature:  
Before Cooldown  
of System



4.2° K:  
After Cooldown of  
System (Exaggerated)

Figure IV-27 Illustration of Column Support Hinge  
Action (Exaggerated) When System is  
Cooled Down.

heating in nonsuperconducting electrical joints, and the heat loss due to conduction through and heat generation in the energized leads. For the scale of magnet systems under consideration, thermal radiation and the vapor-cooled power leads are the largest heat load on the system.

The radiative heat load from the room temperature container to the radiation shield and from the radiation shield to the liquid helium container can be easily estimated by calculating the surface area exposed to thermal radiation and by estimating an equivalent heat flux per unit surface area for these two temperature ranges. Estimates have been performed for Design No. 1, and the results are presented in Table IV-10. It was assumed that the radiation shield is cooled by LHe boiloff and the equivalent heat flux through the superinsulation from room temperature was 100 milliwatts per square foot. The heat flux from the radiation shield to the superinsulated liquid helium container was assumed to be 5 milliwatts per square foot.

Table IV-10

Estimated Cryogenic Characteristics for 8 T Racetrack  
with Iron - 4.2 K

- I. Temperature He Vessel - 4.2<sup>o</sup> K
- II. Temperature Radiation Shield - 98<sup>o</sup> K
- III. Total He Inventory - 359 liters
- IV. Boiloff Rate
  - A. Leads - 12 ℓ/hr.
  - B. Radiation Shield, Column Supports, He Vessel - 8 ℓ/hr.
- V. Superinsulation
  - A. Bore
    - 1. Cold Side -  $1.91 \times 10^{-2}$  m (.75 in.)
    - 2. Warm Side -  $2.54 \times 10^{-2}$  m (1.0 in.)
  - B. Outside
    - 1. Cold Side -  $5.08 \times 10^{-2}$  m (2.0 in.)
    - 2. Warm Side -  $5.08 \times 10^{-2}$  m (2.0 in.)

## V. 8 T RACETRACK, 2 K SYSTEM

The second system considered under Phase II of this program was similar to the first in that it involved an 8 T magnetic field level in a system utilizing a racetrack geometry. The operating temperature, however, was selected as 2 K (nominal) to allow the impact of sub-lambda operation to be considered. Reduced temperature operation (i.e.,  $T < 4.2$  K) offers two potential advantages: (1) the critical current density of the superconductor increases as temperature decreases; hence less superconducting material cross section is required for a given current and field level and (2) the liquid helium experiences a change in state below 2.2 K (approximately) and exhibits an infinite apparent thermal conductivity. The latter may lead to the equivalent of a very high allowable heat flux from the surface of the conductor for stability purposes with a corresponding decrease in the amount of copper substrate required. This may translate into a substantial reduction in conductor cost. The latter would ultimately have to be weighed against the increased cost and complexity of providing a 2 K environment for the coils.

In considering the design of the conductor, little empirical information was found which could be directly translated and applied to the design of a 2° K fully stabilized conductor. There is little doubt that a theoretical and experimental program oriented directly toward stable superconducting magnet design in sub-lambda helium would be desirable. The main question surrounds the determination of an allowable heat flux from the surface of the conductor (or an equivalent condition). Since the information was not available, cases were considered for two selected values for this variable. Two sets of conductor designs resulted with two sets of winding envelope dimensions. These results are presented in tabular form and indicate the impact on the design of different allowable heat flux levels in the fluid. The determination of the level which may actually be achieved will require an experimental program.

System No. 2 was designed such that the MHD channel axis was horizontal and the main magnetic field horizontal. The dewar and magnet are, therefore, similar to those in Design No. 1 with the magnet, however, rotated 90° about the channel axis. This led to a somewhat less complicated procedure for variation of angle between the coils for this system which was also designed to allow variation of field gradient along the channel axis.

The dewar utilizes a radiation shield cooled by bulk liquid nitrogen. Each coil is enclosed in its own LHe dewar which is integrated into the structure for support of the axial and transverse forces of em origin. The cryogenic support subsystem envisioned for this system would involve a liquefier which maintains liquid helium in a 1,000 g storage dewar at 2-4 psig and about 4.5 K. This liquid is then pumped and used in a 2 K (nominal) heat exchanger which cools the main magnet-dewar system. The vapor-cooled power leads would not use coolant from the main magnet-dewar but would be supplied with LHe I directly from the pressurized storage dewar. Providing the coolant for the leads would, therefore, be independent of the subsystem providing the 2 K environment for the coils.

The subsections which follow will present an overall description of the system, a discussion of the winding geometry and conductor characteristics, and a description of the structure and dewar design.

## A. SYSTEM DESCRIPTION

### 1. Overall Characteristics

The preliminary design characteristics for Design No. 2 are given in Table V-1. The overall system dimensions and electrical characteristics are presented. Two modes are indicated and correspond to operation of the two race-track coils with a  $5^\circ$  included half-angle (low gradient mode) or  $15^\circ$  included half-angle (high gradient mode). The maximum magnetic field at the winding is 11.4 T. This level may be reduced somewhat upon further iteration of the graded design during a future detail design phase. In addition, the range of overall current density and conductor current density is given. Weights are summarized in Table V-2, as a function of the allowable heat flux from the surface of the conductor from a stability standpoint. The value which can actually be achieved must be determined in an experimental program. Note the dramatic effect on conductor weight. As is the case with Design No. 1, the conductor comprises a substantial portion of the overall weight of the magnet systems.

The magnetic flux densities required at the inlet and outlet for the low gradient mode and the high gradient mode for Design No. 2 are the same as Design No. 1; i.e., 8.0 T (inlet) and 6.4 T (outlet) for the low gradient mode and 8.0 T (inlet) and 4.5 T (outlet) for the high gradient mode with allowed variations of  $\pm 5\%$  and  $\pm 8\%$ , respectively.

Top and side views of the racetrack coils are given in Figures V-1 and V-2, respectively. Figure V-2 also shows the extreme coil positions from the viewpoint of field profile variation. Calculated field profiles along the channel axis for these coil positions are shown in Figures V-3 and V-4. The flux density variation from a linear profile is  $\pm 5\%$  for the low gradient mode and  $\pm 8\%$  for the high gradient mode.

Figure V-5 shows one quadrant of the cross section of the MHD channel at the channel inlet, channel exit, and at planes 0.508 m (20 in.) in from each end. Two numbers are given at each point in the sections. One number is the Y component of field (i.e., main field direction) when the maximum field on axis is 8 T, and the other number (in parentheses) is the ratio of the local Y component of field to the Y component of the field on axis in that plane. Table V-3 gives results for the computed field components and magnitude with corresponding coordinates in the channel.

An assembly drawing of the magnet-dewar system is shown in Figure V-6 (MCA Drawing E-2808).

The main components of the system consist of the left and right superconducting racetrack coils (as viewed from the downstream end of the system), internal and external coil support structures, iron pole pieces, and LHe dewar. The MHD channel would have its axis coincident with that of the warm bore tube of the LHe dewar which is located approximately 2.46 m (97 in.) above the foundation. The magnetic field is perpendicular to the axis of the dewar, and the

Table V-1

Preliminary Design Characteristics for Design No. 2  
8 T Racetrack with Iron - 2 K

Dewar Dimensions

Inlet	0.2540 m x 0.2540 m (10 in. x 10 in.)
Outlet	0.4064 m x 0.508 m (16 in. x 20 in.)
Overall Height	6.33 m (250 in.)
Outside Diameter	4.37 m (172 in.)
Overall Length	4.01 m (158 in.)

Magnetic Field Characteristics

Field at Channel Inlet	
5° Mode	7.60 T
15° Mode	7.85 T
Field at Channel Outlet	
5° Mode	6.29 T
15° Mode	4.50 T
Max. Field on Channel Axis	
5° Mode	8 T
15° Mode	8 T
Max. Field at Winding*	11.4 T
Active Field Length	1.524 m (60 in.)

Electrical Characteristics

	<u>Design 2.1</u>	<u>Design 2.2</u>
Stored Energy*	138 x 10 <sup>6</sup> J	138 x 10 <sup>6</sup> J
Inductance*	17.3 H	17.3 H
Operating Current*	4000 A	4000 A
Overall Current Density*	1.78 x 10 <sup>7</sup> A/m <sup>2</sup> - 6.79 x 10 <sup>7</sup> A/m <sup>2</sup>	1.84 x 10 <sup>7</sup> A/m <sup>2</sup> - 9.66 x 10 <sup>7</sup> A/m <sup>2</sup>
Conductor Current Density*	9.39 x 10 <sup>7</sup> A/m <sup>2</sup> - 11.7 x 10 <sup>7</sup> A/m <sup>2</sup>	14.9 x 10 <sup>7</sup> A/m <sup>2</sup> - 20.0 x 10 <sup>7</sup> A/m <sup>2</sup>
Total Turns	4824	4824
Ampere-Meters	13.03 x 10 <sup>7</sup>	12.73 x 10 <sup>7</sup>

\* Values for 5° Mode.

Table V-2

Summary of Weights for Preliminary Design  
Characteristics for Design No. 2  
8 T Racetrack with Iron - 2 K

<u>Weights</u>	<u>Design 2.1</u>	<u>Design 2.2</u>
Conductor (kg)	10,960	6,020
Structure (kg)	30,455	26,585
Dewar (kg)	<u>24,920</u>	<u>24,920</u>
TOTAL (kg)	66,335	57,525

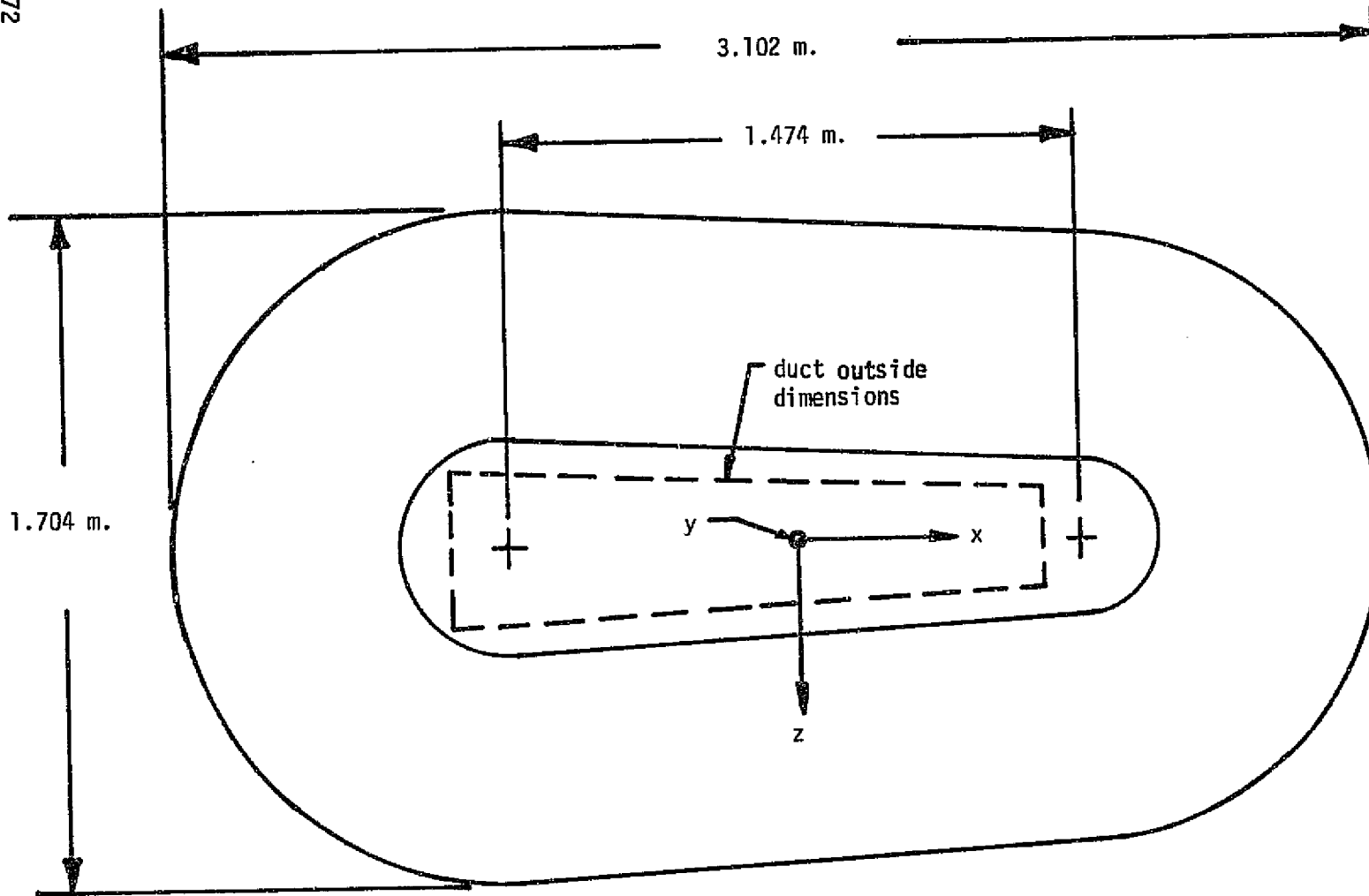


Figure V-1

Top View of Racetrack Coil for Preliminary Design No. 2



FA 3476

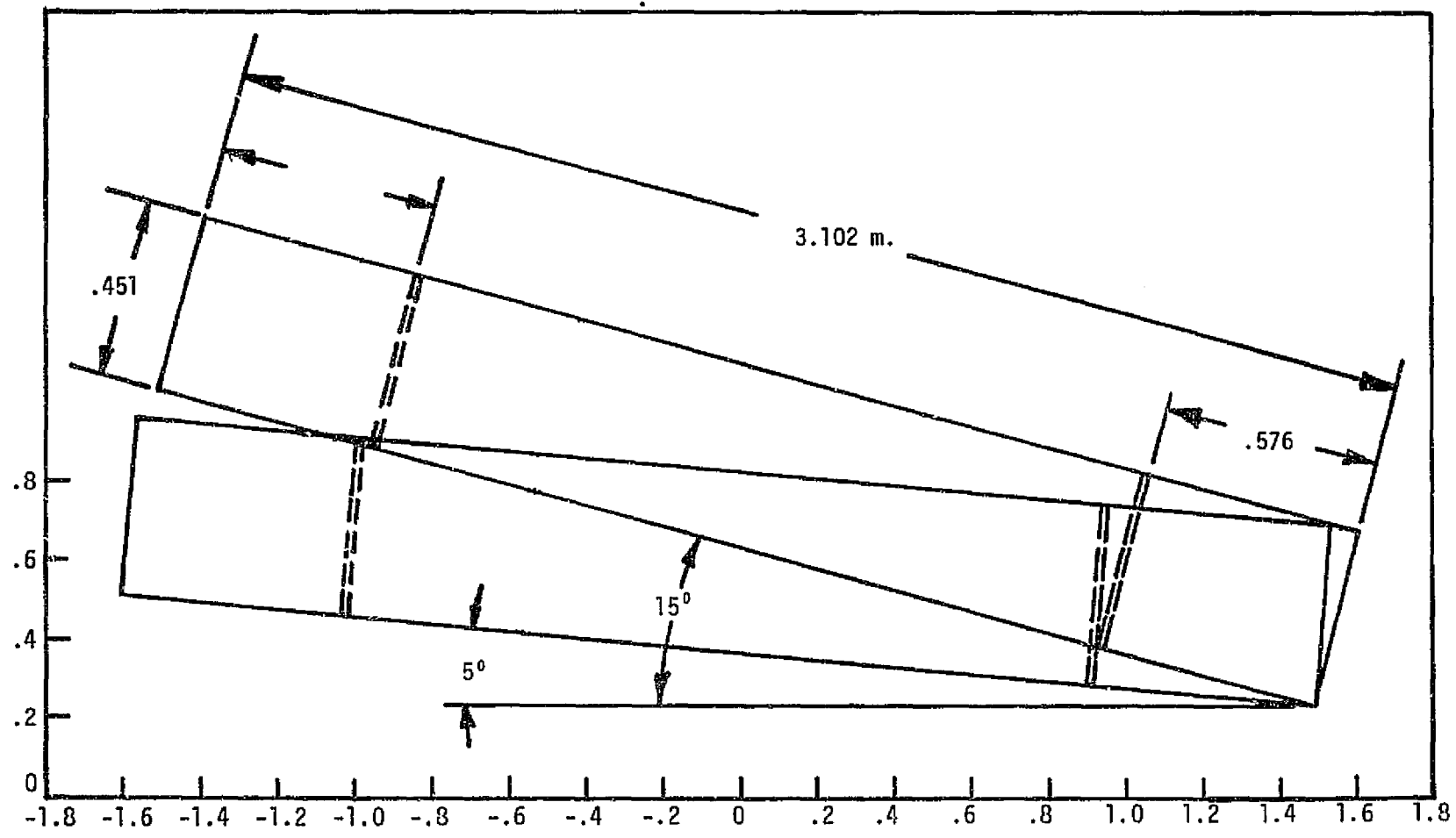


Figure V-2

Side View of Racetrack Coil for Preliminary Design No. 2 showing Extreme Coil Positions Necessary to Satisfy Design Limits on Field Profile.

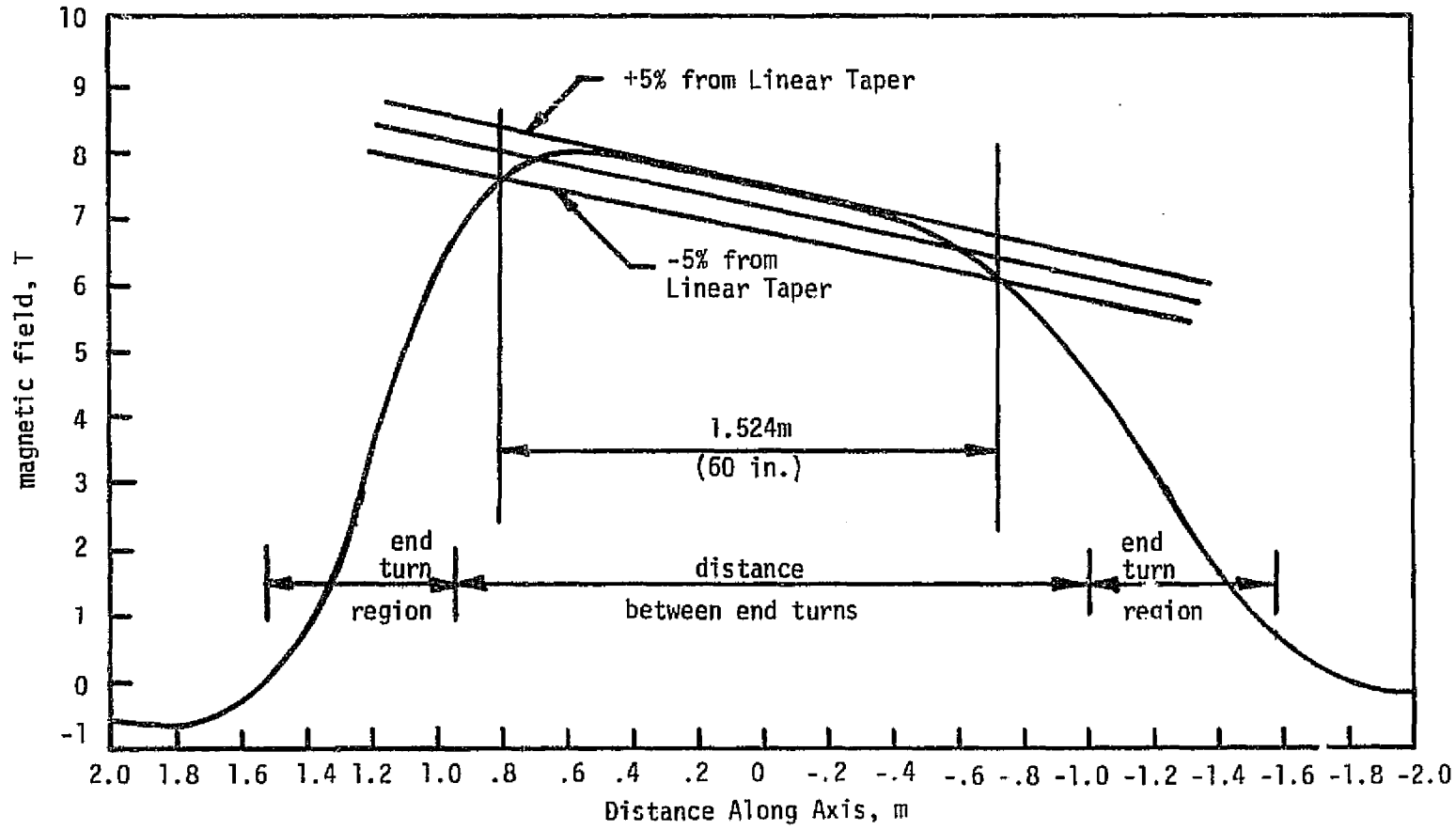


Figure V-3  
Field Profile for Design No. 2 (low gradient mode)

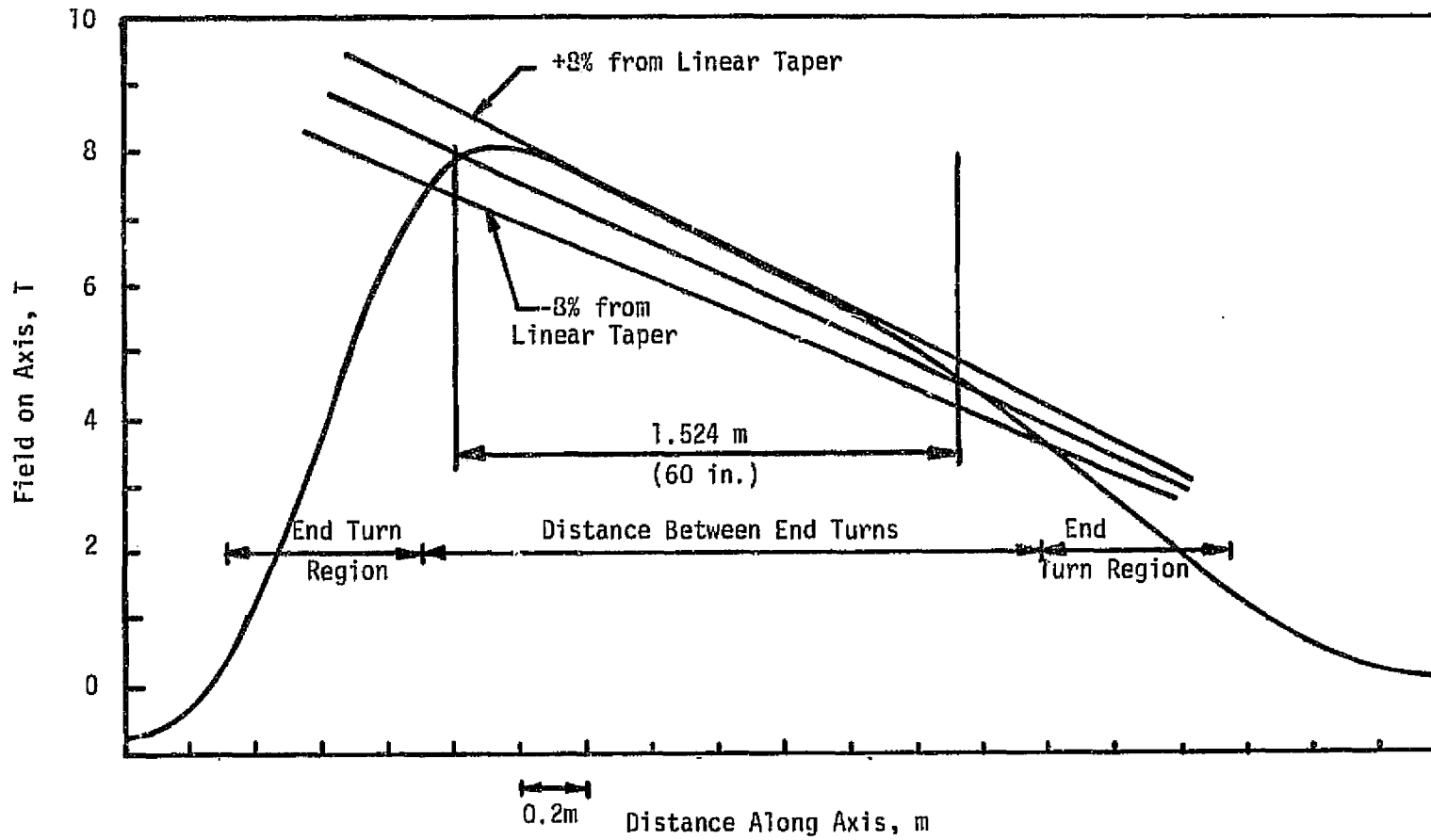


Figure V-4

Computed Field Profile on Axis for Preliminary Design No. 2  
for a Coil Divergence Angle of  $15^\circ$   
(High Gradient Mode)

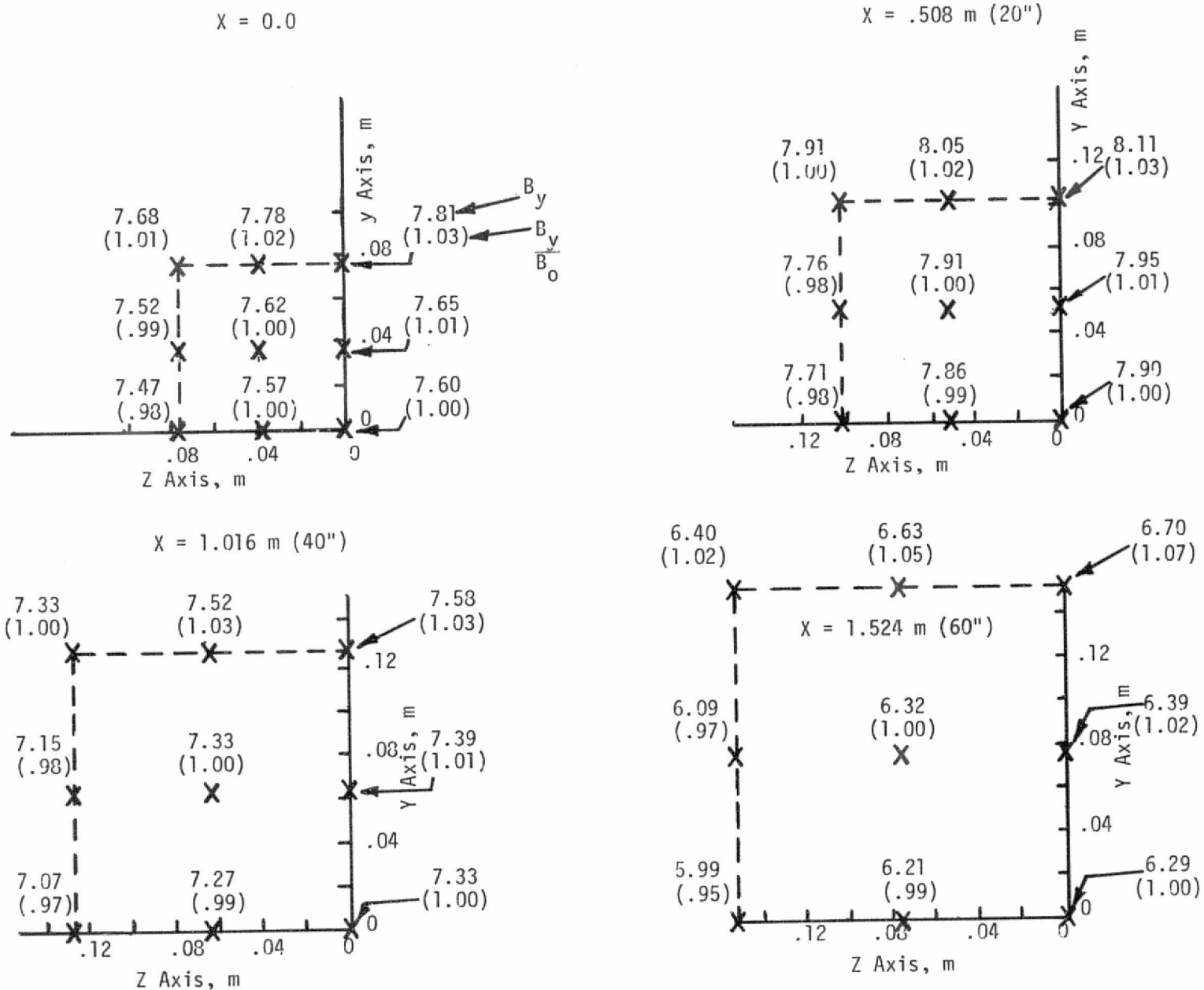


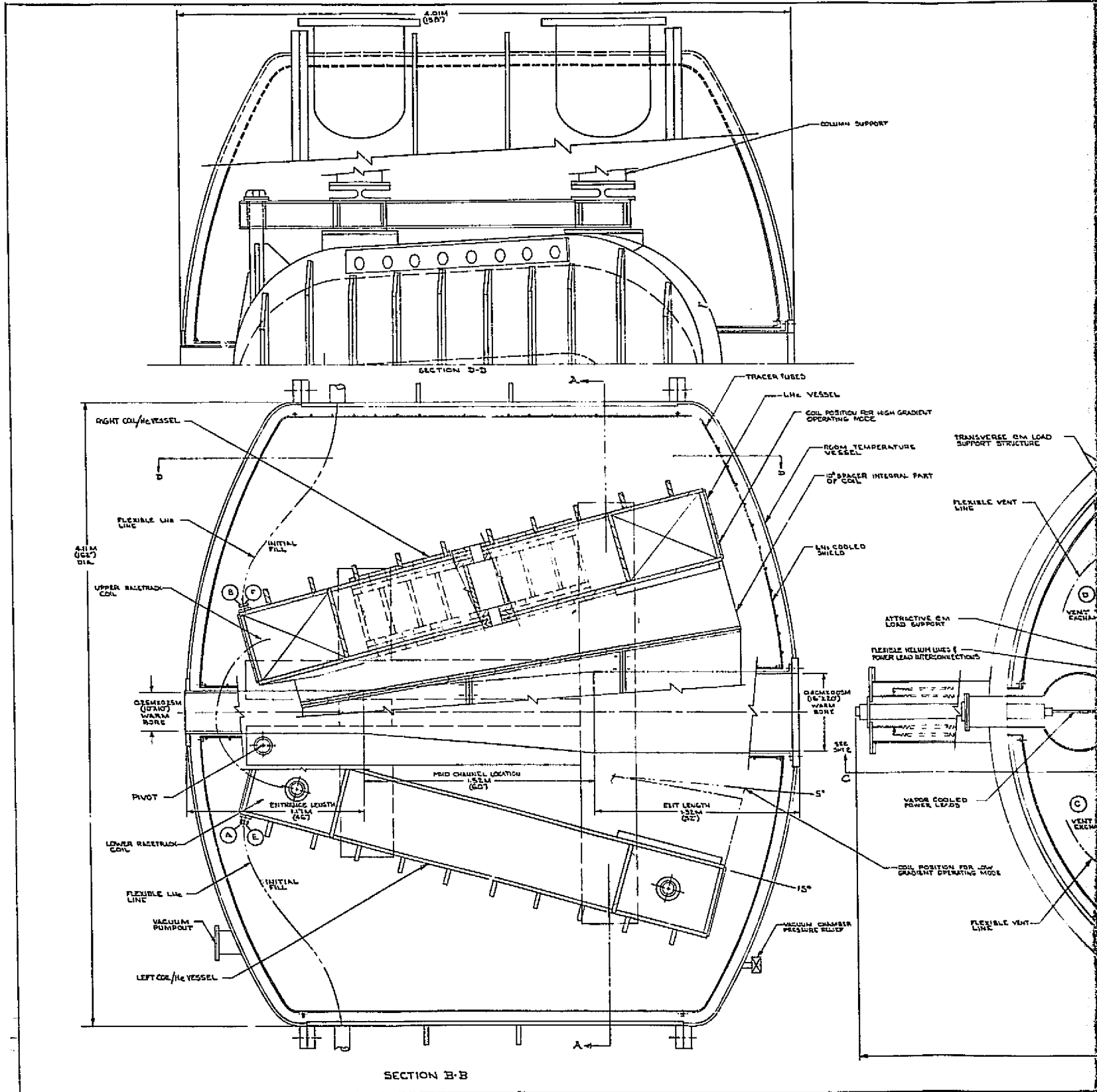
Figure V-5. Calculated Main Component of Field and Homogeneity in One Quadrant of the MHD Channel at Four Planes Along the Axis for the Low Gradient Operating Mode

Table V-3

Computed Field Components at Selected Points Throughout  
MHD Channel Volume for 5<sup>0</sup> Mode

Coordinate (m)			Field Component (T)			Field Magnitude (T)	
X	Y	Z	B <sub>X</sub>	B <sub>Y</sub>	B <sub>Z</sub>	/B/	
0.400	0.00	0.00	0.00	7.93	0.00	7.93	} Points on Axis
0.500	0.00	0.00	0.00	8.00	0.00	8.00	
0.600	0.00	0.00	0.00	7.99	0.00	7.99	
0.700	0.00	0.00	0.00	7.86	0.00	7.86	
-0.724	0.00	0.00	0.00	6.29	0.00	6.29	} Field Points at Duct Outlet
-0.724	0.00	0.076	0.00	6.21	0.00	6.21	
-0.724	0.00	0.152	0.00	5.99	0.00	5.99	
-0.724	0.076	0.00	0.28	6.39	0.00	6.40	
-0.724	0.076	0.076	0.28	6.32	-0.15	6.33	} Field Points 40" from Duct Inlet
-0.724	0.076	0.152	0.27	6.09	-0.29	6.10	
-0.724	0.152	0.00	0.55	6.70	0.00	6.72	
-0.724	0.152	0.076	0.55	6.63	-0.29	6.66	
-0.724	0.152	0.152	0.54	6.40	-0.59	6.45	} Field Points 20" from Duct Inlet
-0.216	0.00	0.00	0.00	7.33	0.00	7.33	
-0.216	0.00	0.064	0.00	7.27	0.00	7.27	
-0.216	0.00	0.127	0.00	7.07	0.00	7.07	
-0.216	0.064	0.00	0.08	7.39	0.00	7.39	} Field Points at Duct Inlet
-0.216	0.064	0.064	0.07	7.33	-0.12	7.33	
-0.216	0.064	0.127	0.07	7.15	-0.24	7.15	
-0.216	0.127	0.00	0.15	7.58	0.00	7.58	
-0.216	0.127	0.064	0.15	7.52	-0.24	7.53	} Field Points at Duct Inlet
-0.216	0.127	0.127	0.14	7.33	-0.49	7.35	
0.292	0.00	0.00	0.00	7.90	0.00	7.90	
0.292	0.00	0.051	0.00	7.86	0.00	7.86	
0.292	0.00	0.102	0.00	7.71	0.00	7.71	} Field Points at Duct Inlet
0.292	0.051	0.00	0.06	7.95	0.00	7.95	
0.292	0.051	0.051	0.06	7.91	-0.10	7.91	
0.292	0.051	0.102	0.05	7.76	-0.19	7.76	
0.292	0.102	0.00	0.12	8.11	0.00	8.11	} Field Points at Duct Inlet
0.292	0.102	0.051	0.11	8.05	-0.19	8.05	
0.292	0.102	0.102	0.11	7.91	-0.38	7.92	
0.800	0.00	0.00	0.00	7.60	0.00	7.60	
0.800	0.00	0.038	0.00	7.57	0.00	7.57	} Field Points at Duct Inlet
0.800	0.00	0.076	0.00	7.47	0.00	7.47	
0.800	0.038	0.00	-0.18	7.65	0.00	7.65	
0.800	0.038	0.038	-0.18	7.62	-0.06	7.62	
0.800	0.038	0.076	-0.18	7.52	-0.13	7.52	} Field Points at Duct Inlet
0.800	0.076	0.00	-0.36	7.81	0.00	7.82	
0.800	0.076	0.038	-0.36	7.78	-0.13	7.79	
0.800	0.076	0.076	-0.36	7.68	-0.26	7.69	

ORIGINAL PAGE IS  
OF POOR QUALITY



FOLDOUT FRAME /

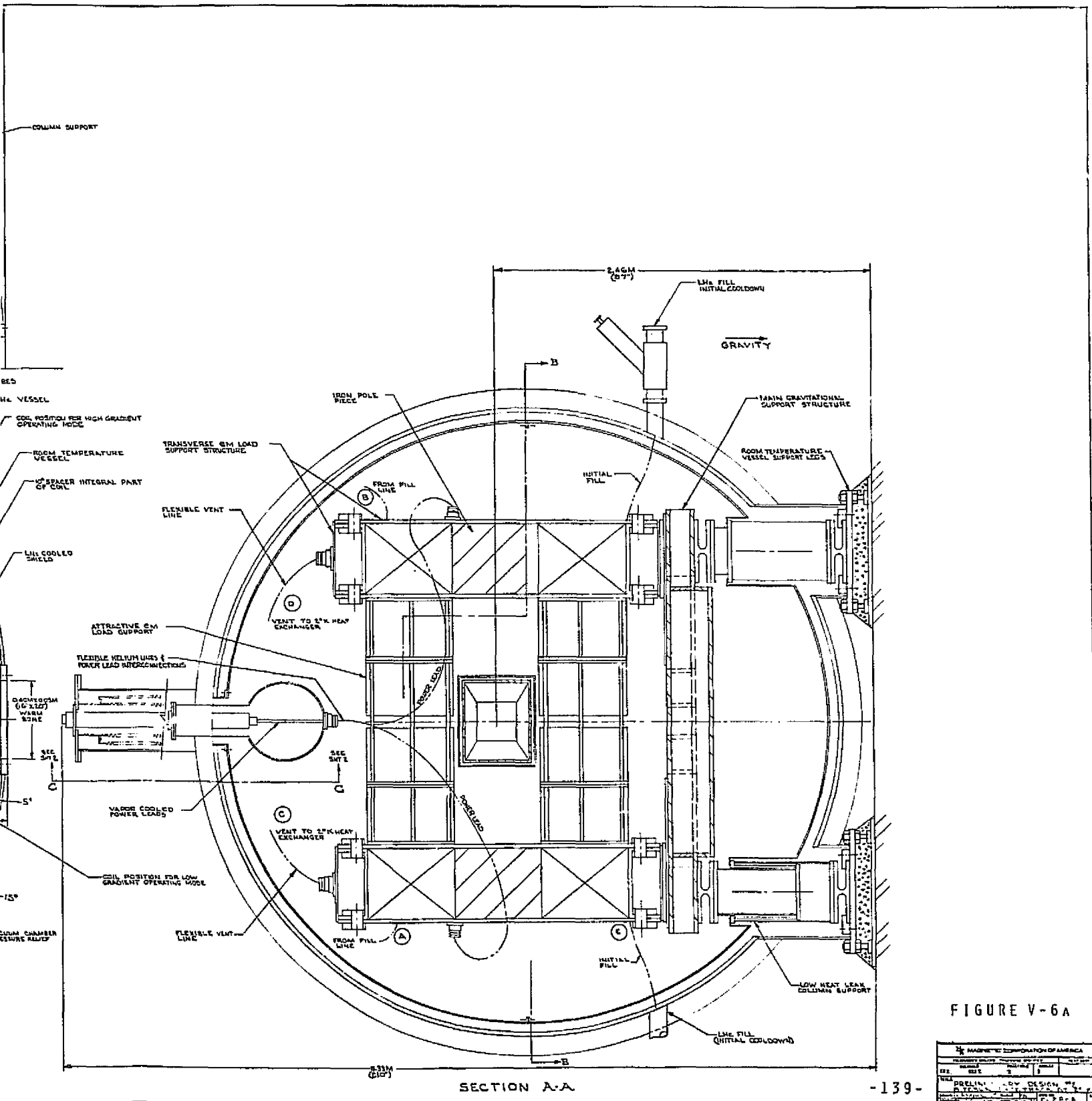
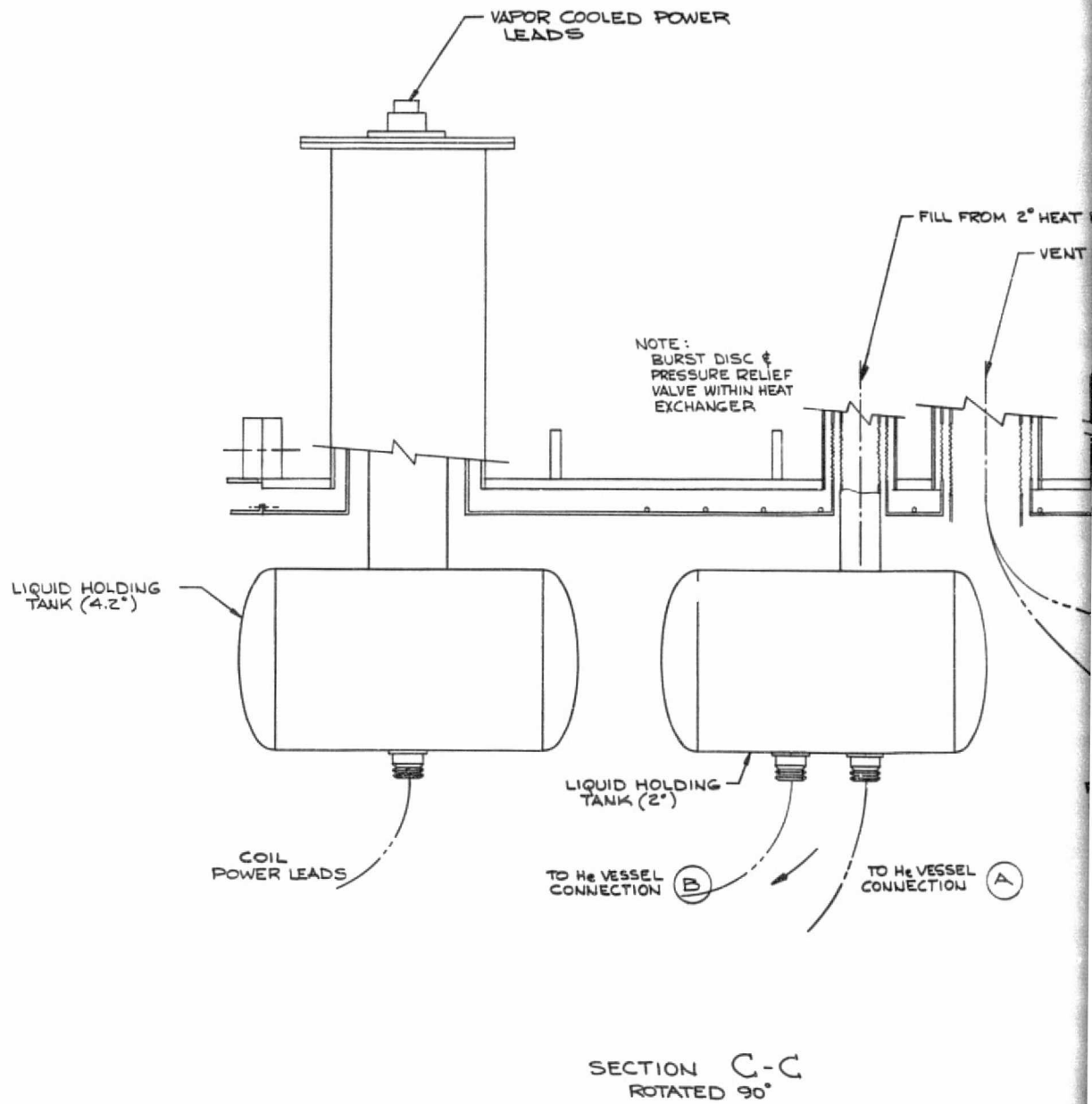


FIGURE V-6A

MAGNETIC CORPORATION OF AMERICA	
REV.	DATE
1	3/1/58
2	3/1/58
3	3/1/58
4	3/1/58
5	3/1/58
6	3/1/58
7	3/1/58
8	3/1/58
9	3/1/58
10	3/1/58
11	3/1/58
12	3/1/58
13	3/1/58
14	3/1/58
15	3/1/58
16	3/1/58
17	3/1/58
18	3/1/58
19	3/1/58
20	3/1/58
21	3/1/58
22	3/1/58
23	3/1/58
24	3/1/58
25	3/1/58
26	3/1/58
27	3/1/58
28	3/1/58
29	3/1/58
30	3/1/58
31	3/1/58
32	3/1/58
33	3/1/58
34	3/1/58
35	3/1/58
36	3/1/58
37	3/1/58
38	3/1/58
39	3/1/58
40	3/1/58
41	3/1/58
42	3/1/58
43	3/1/58
44	3/1/58
45	3/1/58
46	3/1/58
47	3/1/58
48	3/1/58
49	3/1/58
50	3/1/58
51	3/1/58
52	3/1/58
53	3/1/58
54	3/1/58
55	3/1/58
56	3/1/58
57	3/1/58
58	3/1/58
59	3/1/58
60	3/1/58
61	3/1/58
62	3/1/58
63	3/1/58
64	3/1/58
65	3/1/58
66	3/1/58
67	3/1/58
68	3/1/58
69	3/1/58
70	3/1/58
71	3/1/58
72	3/1/58
73	3/1/58
74	3/1/58
75	3/1/58
76	3/1/58
77	3/1/58
78	3/1/58
79	3/1/58
80	3/1/58
81	3/1/58
82	3/1/58
83	3/1/58
84	3/1/58
85	3/1/58
86	3/1/58
87	3/1/58
88	3/1/58
89	3/1/58
90	3/1/58
91	3/1/58
92	3/1/58
93	3/1/58
94	3/1/58
95	3/1/58
96	3/1/58
97	3/1/58
98	3/1/58
99	3/1/58
100	3/1/58

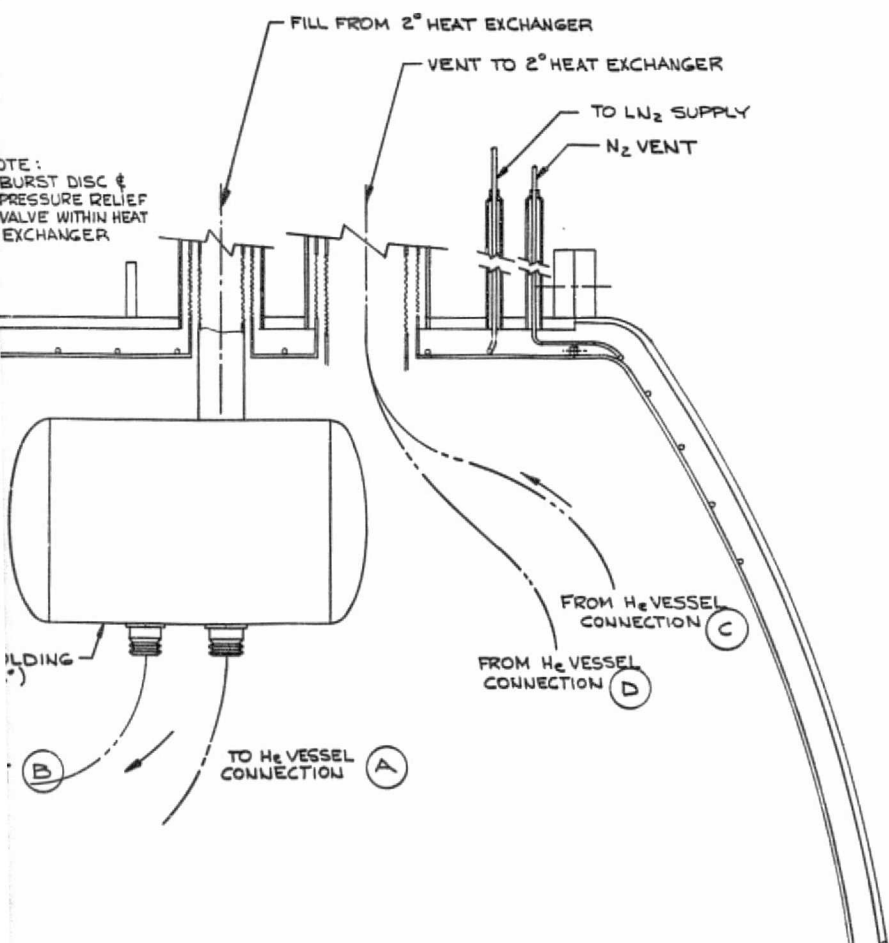
ORIGINAL PAGE IS  
OF POOR QUALITY





DATE	BY	REVISION RECORD	AUTH	DR	CR

POWER



ON C-C  
ROTATED 90°

FIGURE V-6B

TOLERANCES (EXCEPT AS NOTED)		MAGNETIC CORPORATION OF AMERICA	
DECIMAL		SCALE	DRAWN BY <i>[Signature]</i>
FRACTIONAL		1/8	CHECKED BY <i>[Signature]</i>
ANGULAR		TITLE PRELIMINARY DESIGN #2 8 TESLA RACETRACK AT 2°K	
	DATE	DRAWING NUMBER	
	7-16-76	E2808	SHT 2 OF 2

main field direction is horizontal. The warm bore tube measures 0.254 m x 0.254 m at the inlet and tapers to 0.406 m x 0.508 m (16 in. x 20 in.) at the outlet (i.e., the 0.406 m dimension is along the horizontal axis) over an "active" MHD channel length of 1.524 m (60 in.). The entrance length of the warm bore tube measures 1.17 m (46 in.), and the exit length measures 1.32 m (52 in.). The highest point (vapor-cooled power leads) of the completed assembly measures about 6.33 m (250 in.) above the foundation. The dewar outer diameter, 4.37 m (172 in.), is similar to that for Design No. 1, while the overall length of the dewar for Design No. 2 measures a little less than that for Design No. 1. The overall weight of the magnet system for Design No. 2 ranges from 66,335 kg (145,937 lbs.) to 57,525 kg (126,555 lbs.) based on the value of the allowable heat flux assumed in conductor design. As in Design No. 1, the dimensions given for Design No. 2 utilize the additional clearance available the the warm bore outlet.

The magnet coils are of a racetrack geometry and are designed to operate in the superconducting state at a temperature of 2° K and a pressure of ~ 0.03 atmospheres. A possible cryogenic support system is shown schematically in Figure V-7. The main magnet coils are refrigerated by a "2.0 K" heat exchanger. A helium liquefier system provides helium to a pressurized storage dewar which supplies liquid to be utilized in the heat exchanger. The storage dewar also provides He I for coolant to a separate dewar in which the vapor-cooled leads are mounted. Boiloff from the power lead coolant dewar and the return from the heat exchanger are passed back to the liquefier system.

A liquid helium flow schematic is shown in Figure V-8. Fill and vent points are labeled to correspond to points on the assembly drawing (Figure V-6). The initial cooldown to 4.2 K and fill would be accomplished by passing LHe I into the fill lines (E and F) at the bottom of each coil/He vessel and venting through C and D. During normal operation, the fill line would feed the 2 K reservoir from the heat exchanger and the vent lines would return flow to the heat exchanger.

A schematic for power flow in the system is shown in Figure V-9. With this concept the power would pass through the power lead dewar wall in a sealed feed through. The leads on the magnet side of the feed throughs would be a heavy, oversized cable or braid of superconductor and copper insulated from and mounted in a flexible line. Since one end of the line would be anchored at ~ 4.2 K on the power lead dewar and the other end at ~ 2.0 K on the main magnet dewar, it is clear that a small temperature gradient will exist along the line. Furthermore, a He I/He II interface will exist in the lines. A full-scale mock-up and test of this power feed system (as well as other selected system components) would be desirable following a detailed design phase.

An alternate system would involve a 2 K refrigerator directly coupled to the main racetrack dewars. The main advantage of the system shown is that the liquefier system may be temporarily shut down for maintenance without interfering with magnet operation as long as He I is available in the storage dewar.

Many of the aspects of the design which deal with em load support, gravitational load support, interconnections, and general descriptive functions of each major component of the magnet system that are discussed in Section IV-A-1 for Design No. 1 also hold true for Design No. 2 with the following exceptions:

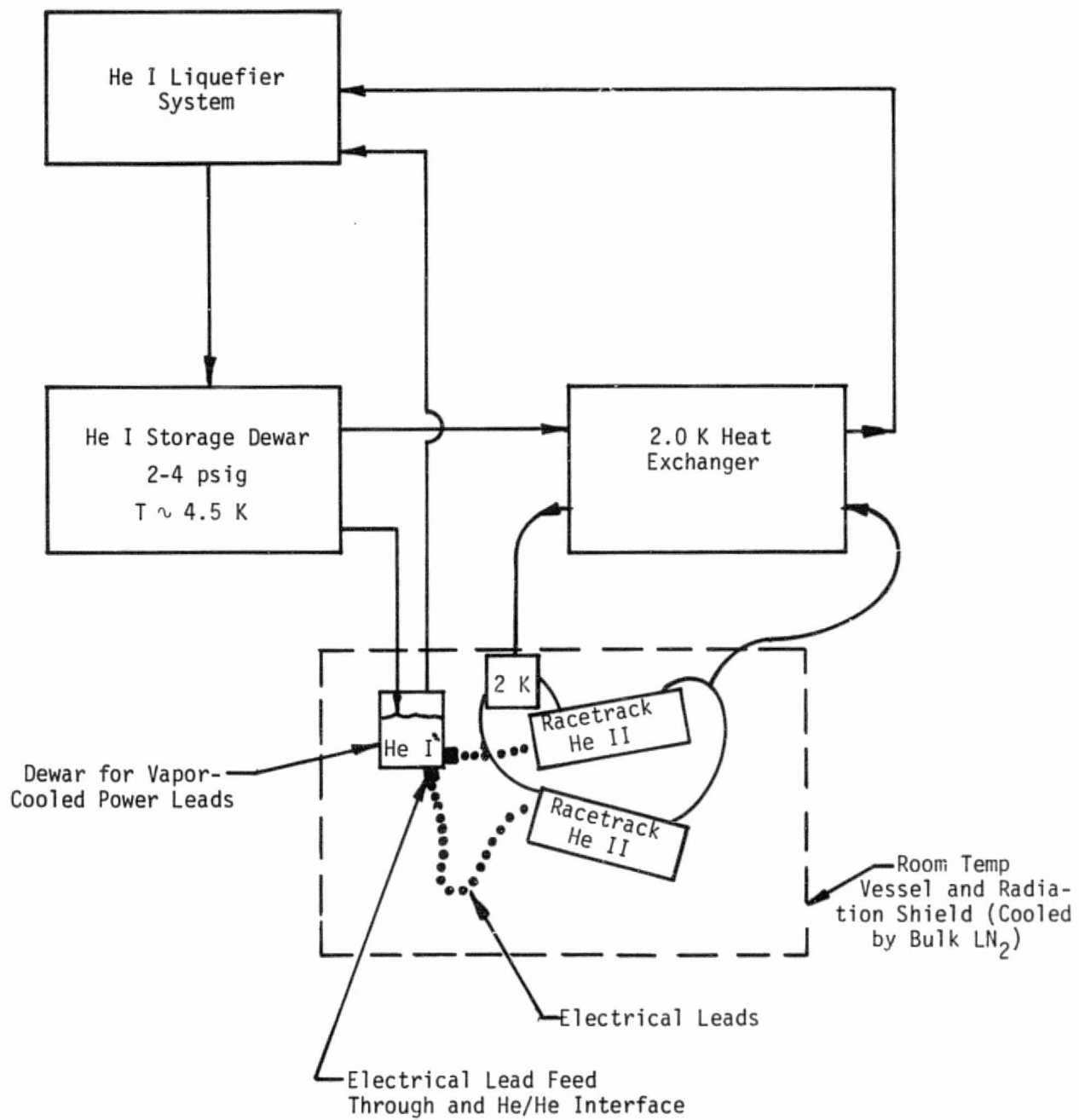


Figure V-7

Schematic for Possible Cryogenic Support System

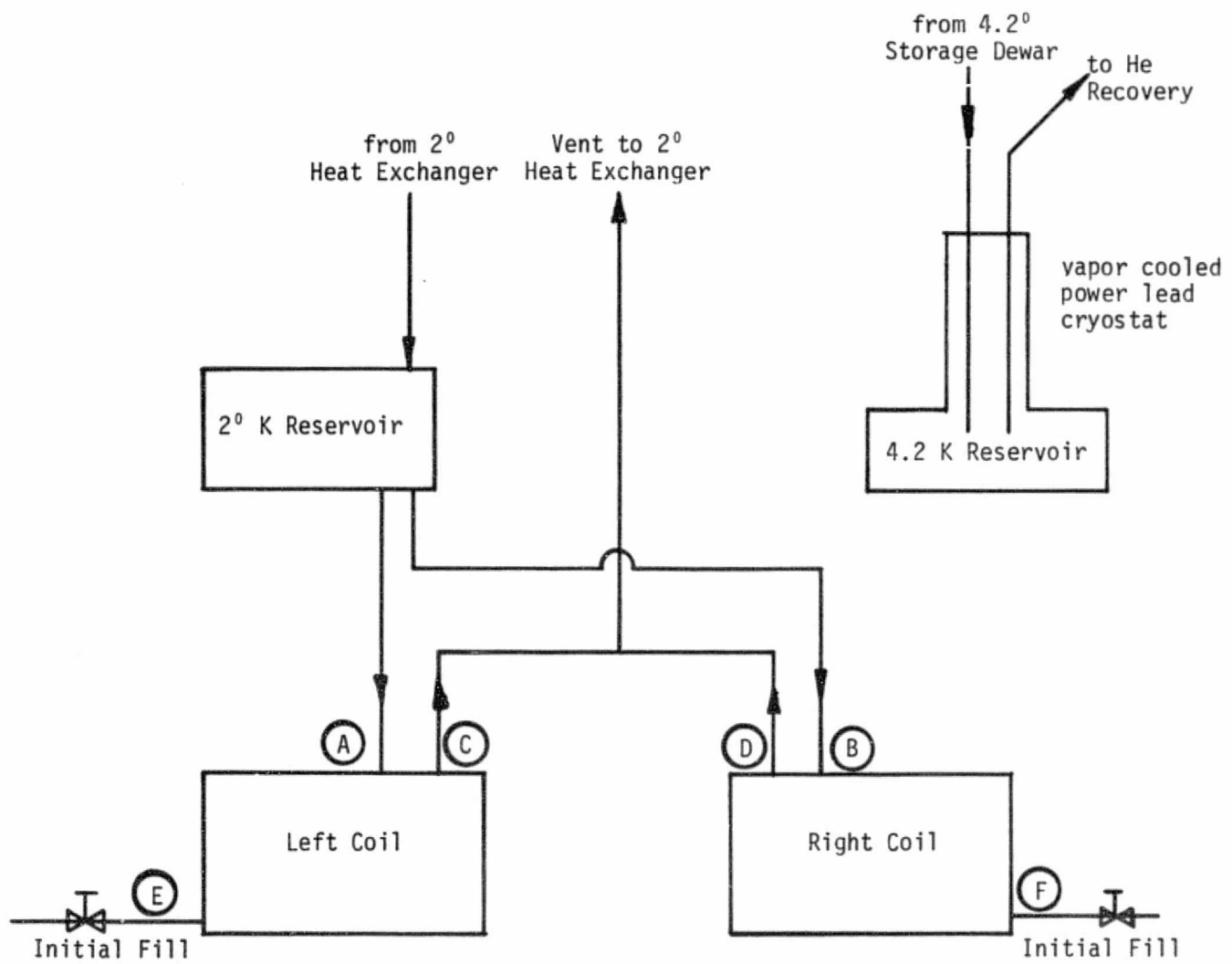


Figure V-8

Liquid Helium Flow Schematic for  
 Preliminary Design No. 2  
 (Ref: Figs. V-6, V-7)

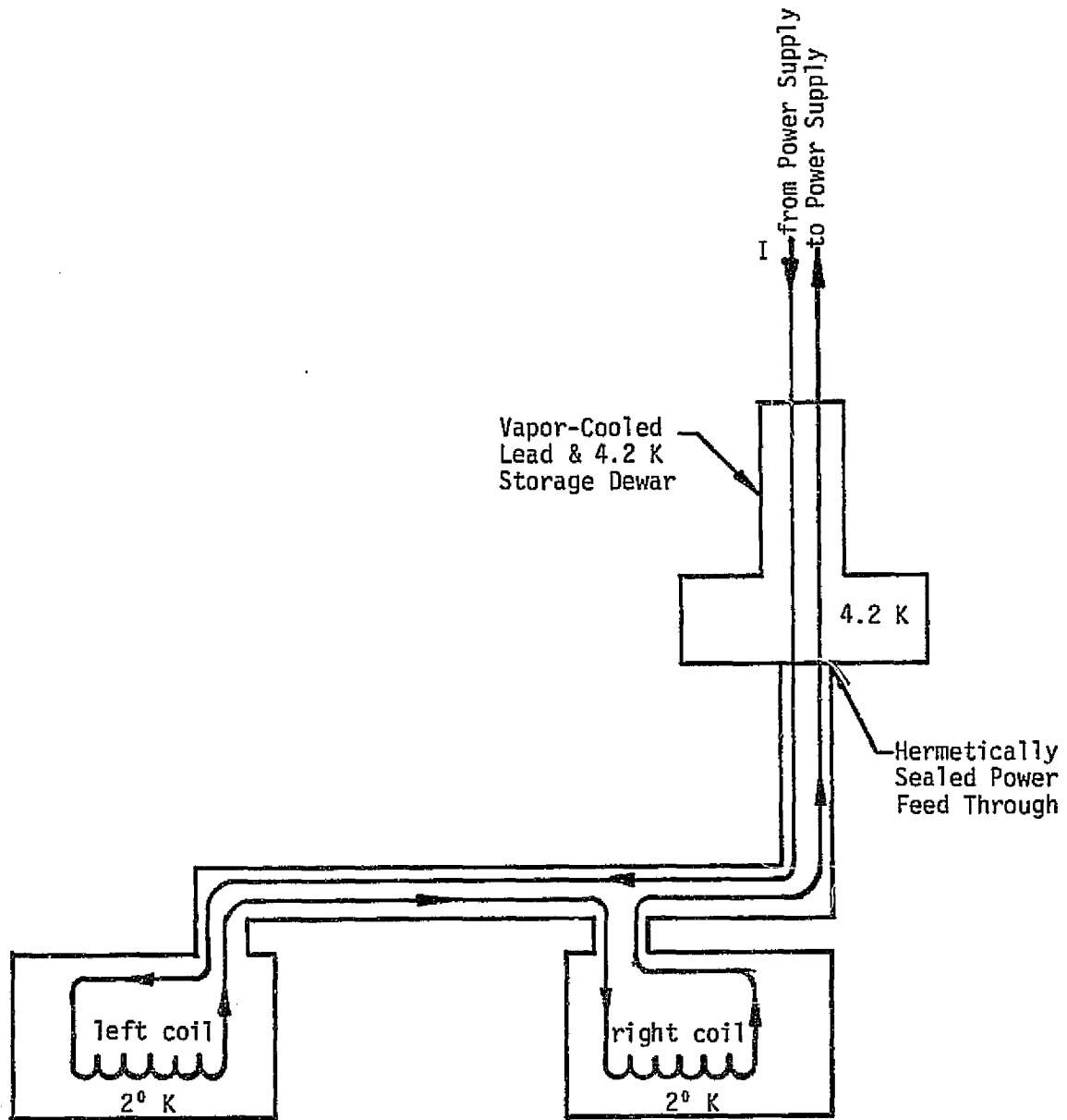


Figure V-9

Power Flow Schematic for Preliminary Design No. 2

1. The coil/He vessels, rather than being one atop the other as in Design No. 1, are side by side and are supported on their sides by a pivoted shaft at the inlet end and a rail support on the outlet end which has a low friction surface on which the coil/He vessels may slide during the coil angle change procedure. This also means that the main magnetic field component is horizontal and not vertical as it is for Design No. 1.
2. The main gravitational support is below the coil/He vessels; consequently, it does not transmit any em loads as the corresponding component must in Design No. 1. This also results in somewhat shorter low heat leak columns.
3. The spacers for the support of the attractive em loads for the low gradient profile (i.e.,  $5^\circ$  half-angle) are an integral part of the coil/He vessel. This is accomplished by welding plates, which have been shaped to the correct angle, to the bottom of the coil/He vessel. For the high gradient profile (i.e.,  $15^\circ$  half-angle) a spacer is required and bolts to each coil/He vessel. This is also a viable alternate for Design No. 1 which used two sets of spacers.

## 2. Alteration of Field Gradient

Table V-4 outlines the steps in the procedure for changing the coils from the high gradient mode (wide angle) to the low gradient mode (low angle). The main advantage Design No. 2 has over Design No. 1 with respect to changing coil angles is the fact that the large weights of the coil/He vessels are supported by the pivot shaft and the rail support; consequently, a much smaller jack can be used to move them.

Table V-4 is intended as an outline of the procedure and must be expanded to include a detailed step-by-step procedure and QC when a detailed design effort is performed.

## 3. Outline of System Assembly

Table V-5 outlines an assembly procedure for the magnet system described above. It shows the basic sequence of events that is required and indicates the complexity of the task and scope of the major erection equipment needed. The same assumptions and preface remarks as made in Section IV-A-4 for Design No. 1 apply here as well.

After dewar evacuation and successful completion of the steps in Table V-5, the magnet is ready to be cooled down and energized. This assumes that appropriate tests and quality control checks have been performed during the final assembly stage.

## B. WINDING GEOMETRY AND CONDUCTOR CHARACTERISTICS

The design of the winding envelope for Design No. 2 involved an iterative procedure, which began with the dimensions generated in the Phase I effort, proceeded through dimensional variations until the desired magnetic field characteristics were achieved in the channel, and proceeded through overall current density variations until the winding was graded and peak field reduced to an

Table v-4

Outline of Procedure to Alter Field Gradient for Design No. 2  
(High Gradient Mode to Low Gradient Mode)

De-energize the magnet, remove the LHe and allow the system to warm up to room temperature.

Apply a fixture to support the downstream end of the warm bore tube.

Release the dewar vacuum and remove the downstream room temperature vessel end cover.

Apply a fixture to support the downstream end of the bore tube radiation shield

Remove superinsulation as necessary and remove flexible helium lines from each coil to the fill and vent ports.

Attach a mechanical or hydraulic jack between coil/LHe vessels.

Remove the spacers.

Change the angle of the coils by jacking each coil/LHe vessel into place.

Bolt the He vessels together. Remove the jacks.

Replace the flexible helium lines to fill and vent ports.

Replace downstream radiation shield end cover.

Replace superinsulation and remove support fixture for downstream end of bore tube radiation shield.

Replace room temperature vessel end cover and remove warm bore tube and support fixture.

Evacuate vessel and prepare for cooldown.

Table V-5

Outline of Assembly Procedure for Design No. 2\*

Place the bottom half of the room temperature vessel in position on the foundation (reference: Figure V-10a).

Place the low heat leak columns inside the legs of the room temperature vessel and fasten them to the base of the legs (reference: Figure V-10a).

Attach the preassembled multilayered superinsulation blankets to the entire inside surface of the room temperature vessel (reference: Figure V-10a).

Place the lower half of the radiation shield in position and attach it to the low heat leak columns. Attach the multilayered superinsulation blankets to the entire inside surface of the radiation shield (reference: Figure V-10b).

Place the main gravitational structure on the low heat leak columns and fasten it in place (reference: Figure V-10c).

Place the coil/He vessels in position and fasten the pivot shaft to the rear rail support (reference: Figure V-10d).

Attach the preassembled multilayered superinsulation blankets to the entire inside surface of the upper half of the room temperature vessel. Place the latter in position on top of the lower half and weld them together along the mating surfaces (reference: Figure V-10d).

Position and dress the multilayered superinsulation blanket along the inside of the mating surfaces of the room temperature vessel halves (reference: Figure V-10d).

Attach the multilayered superinsulation blanket to the inside of the upper half of the radiation shield. Slide it into position from the end of the assembly and fasten it to the lower half of the radiation shield (reference: Figure V-10e).

Spread coil/He vessels apart, slide power lead assembly into place and mount, and slide 2 K reservoir into place and mount (reference: Figure V-10e and f).

Complete assembly of power lead system, connections to  $2^0$  K heat exchanger, and all internal electrical connections and plumbing (reference: Figure V-10e and f).

If high gradient mode operation is desired, slide attractive em load support spacers into place and fasten. If low gradient mode operation is desired, slide coil/He vessels together and fasten (reference: Figure V-10e and f).

---

\* Occasional reference to the assembly drawing, which is shown in Figure V-6, will aid in visualization of the procedure.



Table V-5 (Concluded)

Using a fixture to support one end, feed the warm bore tube radiation shield, which has multilayered superinsulation blankets attached to its outer wall, through the rectangular opening in the main gravitational support, position it in place, and support it at each end (reference: Figure V-10g).

Assemble the radiation shield end covers, which have multilayered superinsulation blankets attached to their inside surface, to each end of the magnet and bolt to bore tube radiation shield (reference: Figure V-10g).

Connect the tracer tubes of the warm bore tube radiation shield to those on the end covers at each end of the magnet as required (reference: Figure V-10g).

Position the room temperature vessel end covers, which have multilayered superinsulation blankets attached to their inside surfaces, in place and fasten them to the flanges of the center portion of the room temperature vessel (reference: Figure V-10h).

Using the same procedure as that used for installation of the warm bore tube radiation shield, feed the warm bore tube, which has multilayered superinsulation blankets attached to its outer wall, through the rectangular opening in the bore tube radiation shield and position it in place (reference: Figure V-10h).

Bolt the warm bore tube to the downstream end cover and weld warm bore tube to upstream end cover (reference: Figure V-10h).

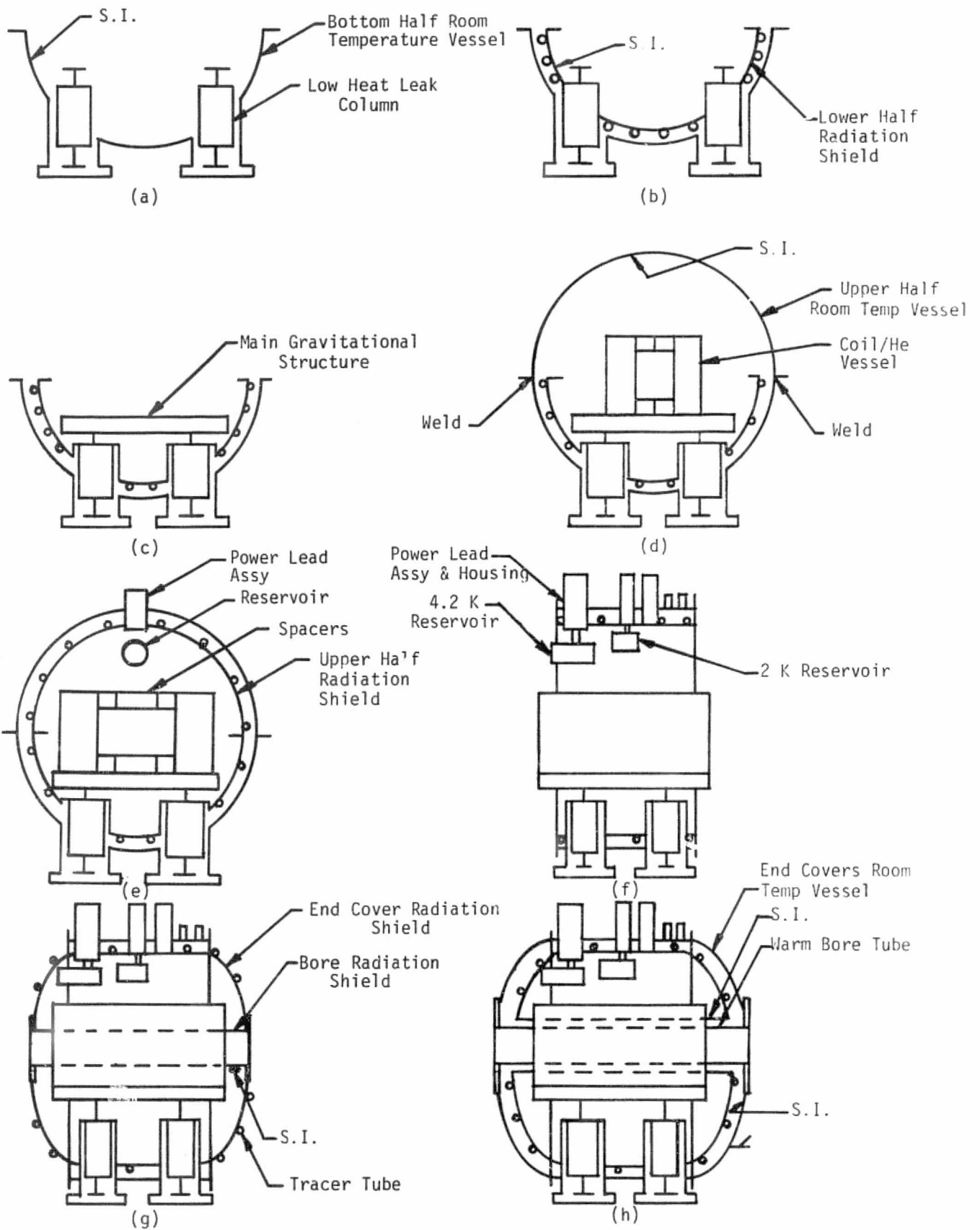


Figure V-10. Assembly Sequence for Design No. 2

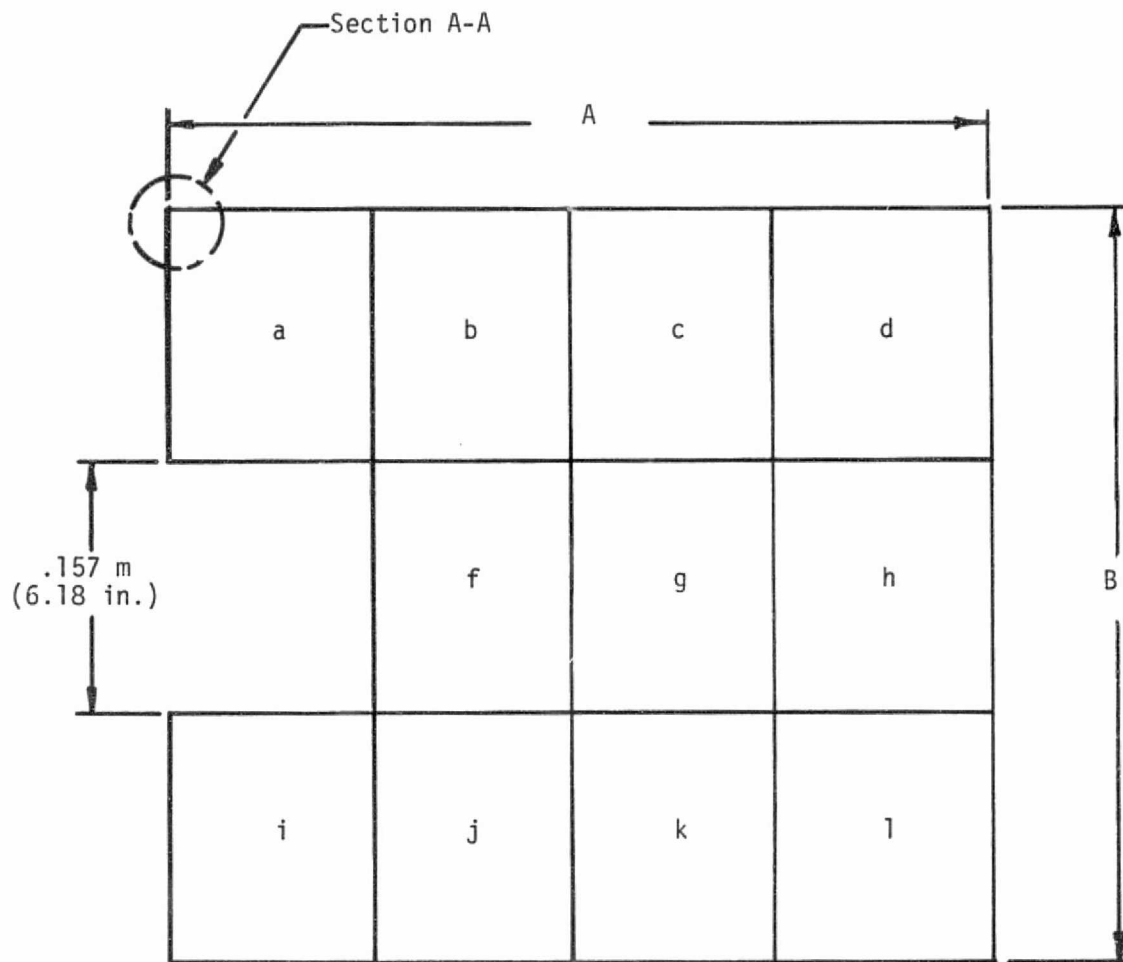
acceptable level. The final configurations are shown in Figure V-11, which is a cross section through the end turn region of the coil at the high field end in the  $Z=0$  plane. This design uses a "notch" in the winding envelope for the purposes of peak field reduction in a manner similar to that used for Design No. 1. The investigation of grading and field distribution within the windings utilized a model with 11 current filaments with one located at the center of each section labeled a, b, c ...  $\lambda$ . During a final detailed design phase, more filaments would be used and the shape of the rectangular notch would be altered somewhat. The model used was sufficient for purposes of this preliminary design.

Winding construction is illustrated in "Section A-A" of Figure V-11. It is similar to that used in Design No. 1 in that a spiral wrap of insulation has been used on the conductor and each turn is supported by the stainless steel channel section which carries the axial load on the coil system and also prevents turn to turn load accumulation. The thickness of the slats between layers has been altered in a manner consistent with stability requirements (see Appendix B).

Considerable uncertainty exists concerning superconducting magnet stability criterion for operation in sub-lambda LHe. To circumvent the present lack of information, two designs were generated for this 2° K system. They were based on successively larger allowable heat fluxes from the surface of the conductor. These were chosen as 2 and 4 watt/cm<sup>2</sup> and used in a model to size conductor for a design at each level. The overall dimensions of the winding which resulted for each "q" are presented in the table in Figure V-11 and related to the sketch through the dummy dimensions "A" and "B." This information is also presented in Figure V-12 which shows the envelope dimensions for Designs 2.1 ( $q = 2$  watt/cm<sup>2</sup>) and 2.2 ( $q = 4$  watt/cm<sup>2</sup>), drawn to scale relative to the original winding envelope boundary used for computation of field distributions.

Four conductors were used in each design for grading purposes. Stainless steel was sized for each conductor. The dimensional characteristics, lengths, and weights for the conductors and stainless steel channels are shown in Tables V-6 to V-9, and a summary is given in Table V-10. Note that there is little variation in length of conductor between the designs; however, the conductor weight decreases dramatically. The latter occurs because the increase in allowable surface heat flux ( $q$ ) reduces the copper to superconductor ratio required to achieve stability. The decrease in conductor weight as  $q$  increases leads to an increase in internal structure weight. This is due to the constraint imposed in the design whereby the stress in the conductor was limited to 10<sup>4</sup> psi. Consequently, when the conductor size decreases with increasing  $q$ , it is necessary to add more steel to carry the loads which remain essentially constant. The net result is that the conductor weight for  $q = 4$  W/cm<sup>2</sup> is equal to 55 percent of the value corresponding to a  $q = 2$  W/cm<sup>2</sup>, whereas the weight of conductor plus internal structure for  $q = 4$  W/cm<sup>2</sup> is equal to 82 percent of the value corresponding to a  $q = 2$  W/cm<sup>2</sup>.

In order to calculate the field distribution in the windings, 11 current filaments were used in a manner similar to that used for Design No. 1. This is illustrated in Figure V-13 in which the location of the iron is shown as well as a rectangular notch. As in the case of Design No. 1, the rectangular notch



Dimensions

	A	B
Design 2.1 ( $q=2 \text{ W/cm}^2$ )	0.552 m (21.73 in.)	0.471 m (18.54 in.)
Design 2.2 ( $q=4 \text{ W/cm}^2$ )	0.436 m (19.13 in.)	0.471 m (18.54 in.)

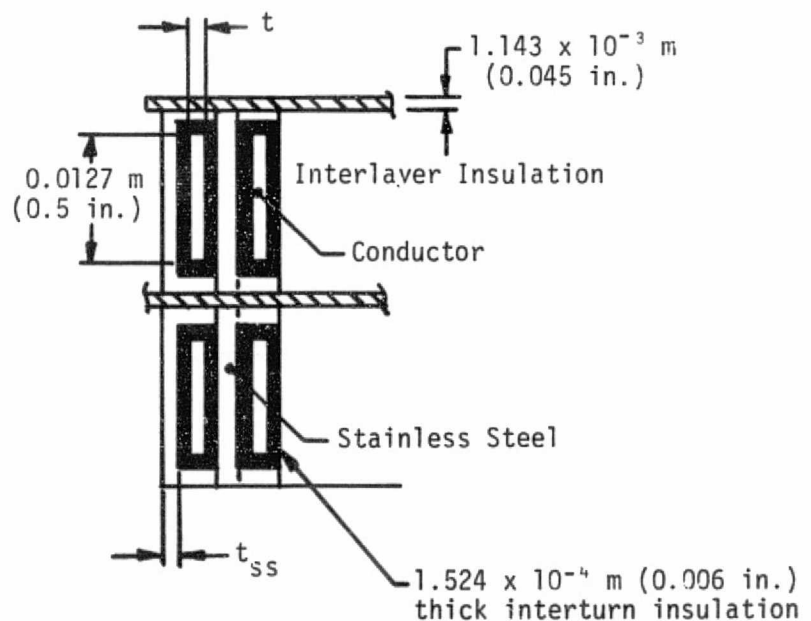


Figure V-11. Winding Final Dimensions and Constructional Detail for Preliminary Design No. 2

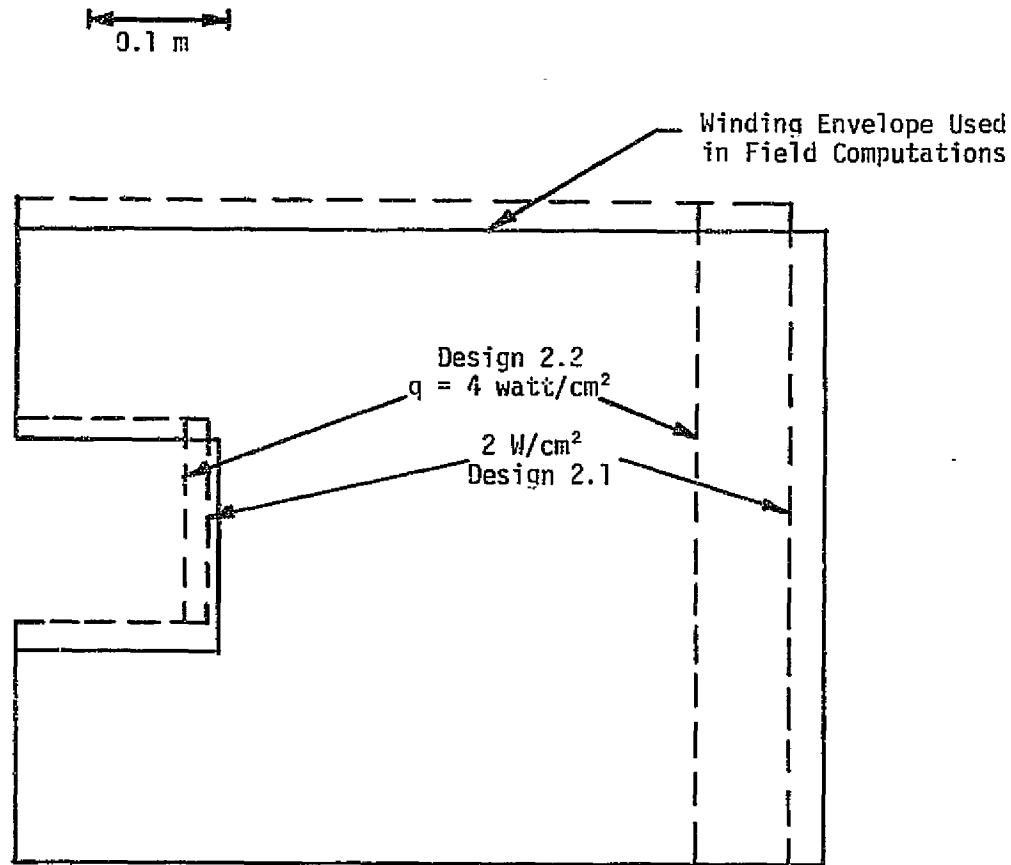


Figure V-12

Cross Section of Coil End Turn Region Showing Winding Envelopes Calculated for Two Different Values of Allowable Surface Heat Flux from Conductor ( $q$ ) for Preliminary Design No. 2 and Envelope Used for Field Computations

Table V-6

Estimated Conductor Requirements for Design No. 2.1

$q = 2 \text{ W/cm}^2$ ; Conductor Width = 0.0127 m = 0.5 in.

<u>Conductor Type</u>	<u>Region Where Used</u>	<u>Conductor Thickness m (in.)</u>	<u>Copper Superconductor</u>	<u>Length (m)</u>	<u>Weight (kg)</u>
1	a, f, i	$3.35 \times 10^{-3}$ (0.132)	7.5	3,585	1,665
2	b, j	$3.25 \times 10^{-3}$ (0.128)	9.3	4,145	1,475
3	c, g, k	$3.10 \times 10^{-3}$ (0.122)	12.0	9,480	3,240
4	d, h, l	$2.69 \times 10^{-3}$ (0.106)	16.7	<u>15,360</u>	<u>4,580</u>

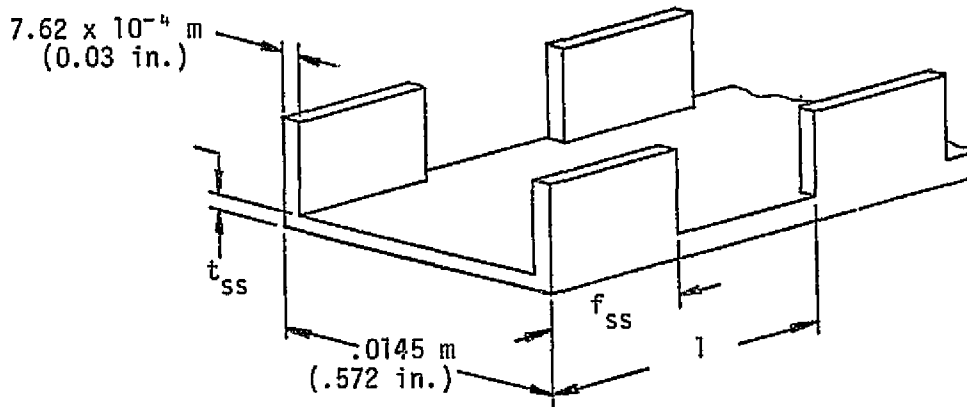
Total Length = 32,570 m

Total Weight = 10,960 kg

Table V-7

Internal Structural Requirements for Design 2.1

$q = 2 \text{ W/cm}^2; f_{ss} = 0.6$



<u>SS Type</u>	<u>Region Where Used</u>	<u><math>t_{ss}</math> m (in.)</u>	<u>Length (m)</u>	<u>Weight (kg)</u>
1	a, i	$1.07 \times 10^{-2}$ (0.422)	2,260	2,806
2	b, j	$5.26 \times 10^{-3}$ (0.207)	4,145	2,574
3	f	$9.04 \times 10^{-3}$ (0.356)	1,325	1,390
4	c, g, k	$1.7 \times 10^{-3}$ (0.067)	9,480	2,060
5	d, h, l	$7.62 \times 10^{-4}$ (0.030)	<u>5,360</u>	<u>1,660</u>

Total Length = 32,570

Total Weight = 10,490

Table V-8

Estimated Conductor Requirements for Design No. 2.2

q = 4 W/cm<sup>2</sup>; Conductor Width = 0.0127 m = 0.5 in.

<u>Conductor Type</u>	<u>Where Used</u>	<u>Conductor Thickness m (in.)</u>	<u>Copper Superconductor</u>	<u>Length (m)</u>	<u>Weight (kg)</u>
1	a, f, i	2.11 x 10 <sup>-3</sup> (0.083)	4.3	3,570	780
2	b, j	1.98 x 10 <sup>-3</sup> (0.078)	5.2	4,100	865
3	c, g, k	1.85 x 10 <sup>-3</sup> (0.073)	6.8	9,330	1,855
4	d, h, l	1.57 x 10 <sup>-3</sup> (0.062)	9.2	<u>14,820</u>	<u>2,520</u>

Total Length = 31,820 m

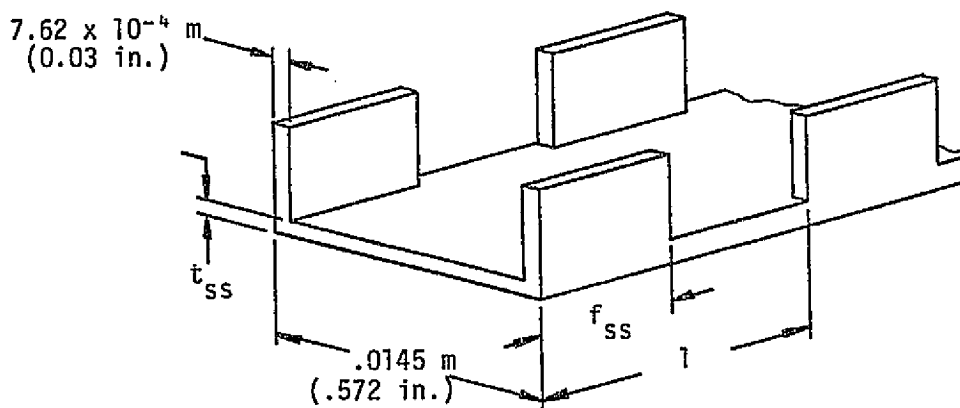
Total Weight = 6,020 kg



Table V-9

Internal Structural Requirements for Design 2.2

$q = 4 \text{ W/cm}^2; f_{ss} = 0.6$



SS Type	Region Where Used	$t_{ss}$ m (in.)	Length (m)	Weight (kg)
1	a, i	$1.15 \times 10^{-2}$ (0.451)	2,250	2,963
2	b, j	$6.05 \times 10^{-3}$ (0.238)	4,100	2,875
3	f	$9.8 \times 10^{-3}$ (0.386)	1,320	1,488
4	c, g, k	$2.46 \times 10^{-3}$ (0.097)	9,330	2,152
5	d, h, l	$7.62 \times 10^{-4}$ (0.030)	<u>14,820</u>	<u>1,492</u>

Total Length = 31,820

Total Weight = 11,560

Table V-10  
Summary of Requirements for Conductor and  
Internal Structure for Design No. 2

<u>Design</u>	<u>q</u> <u>(W/cm<sup>2</sup>)</u>	<u>Conductor</u> <u>Length</u> <u>(m)</u>	<u>Conductor</u> <u>Weight</u> <u>(kg)</u>	<u>Int. Struc.</u> <u>Weight</u> <u>(kg)</u>	<u>Wt. of Conductor</u> <u>and Int. Struc.</u> <u>(kg)</u>
2.1	2	32,570	10,960	10,490	21,450
2.2	4	31,820	6,020	11,560	17,580

FA 3683

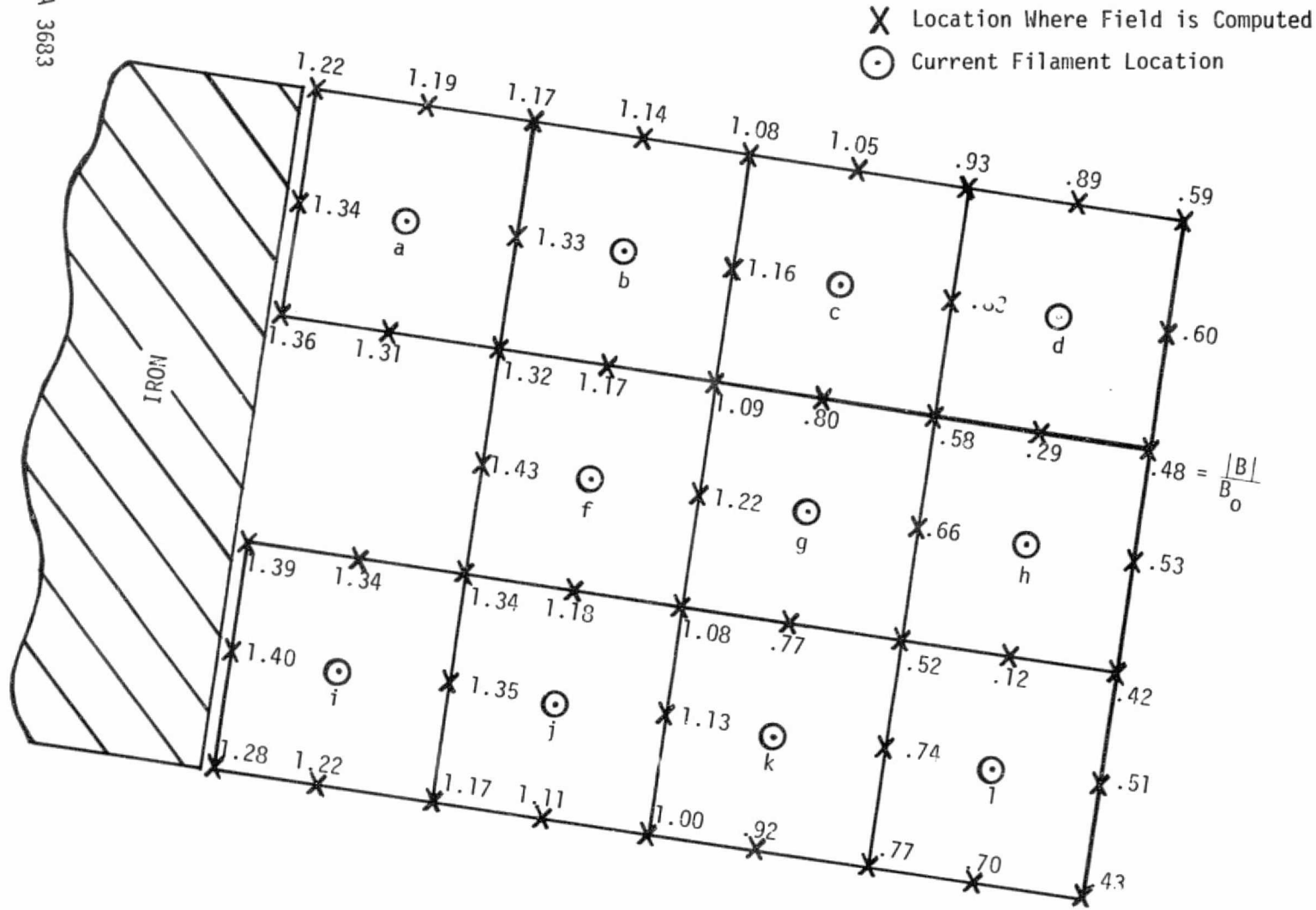


Figure V-13. View of Cross Section of End Turn Region for Design No. 2 Showing the Locations of the 11 Current Filaments Used to Determine the Peak Field Distribution in the Windings. The Field Distribution is Also Shown.

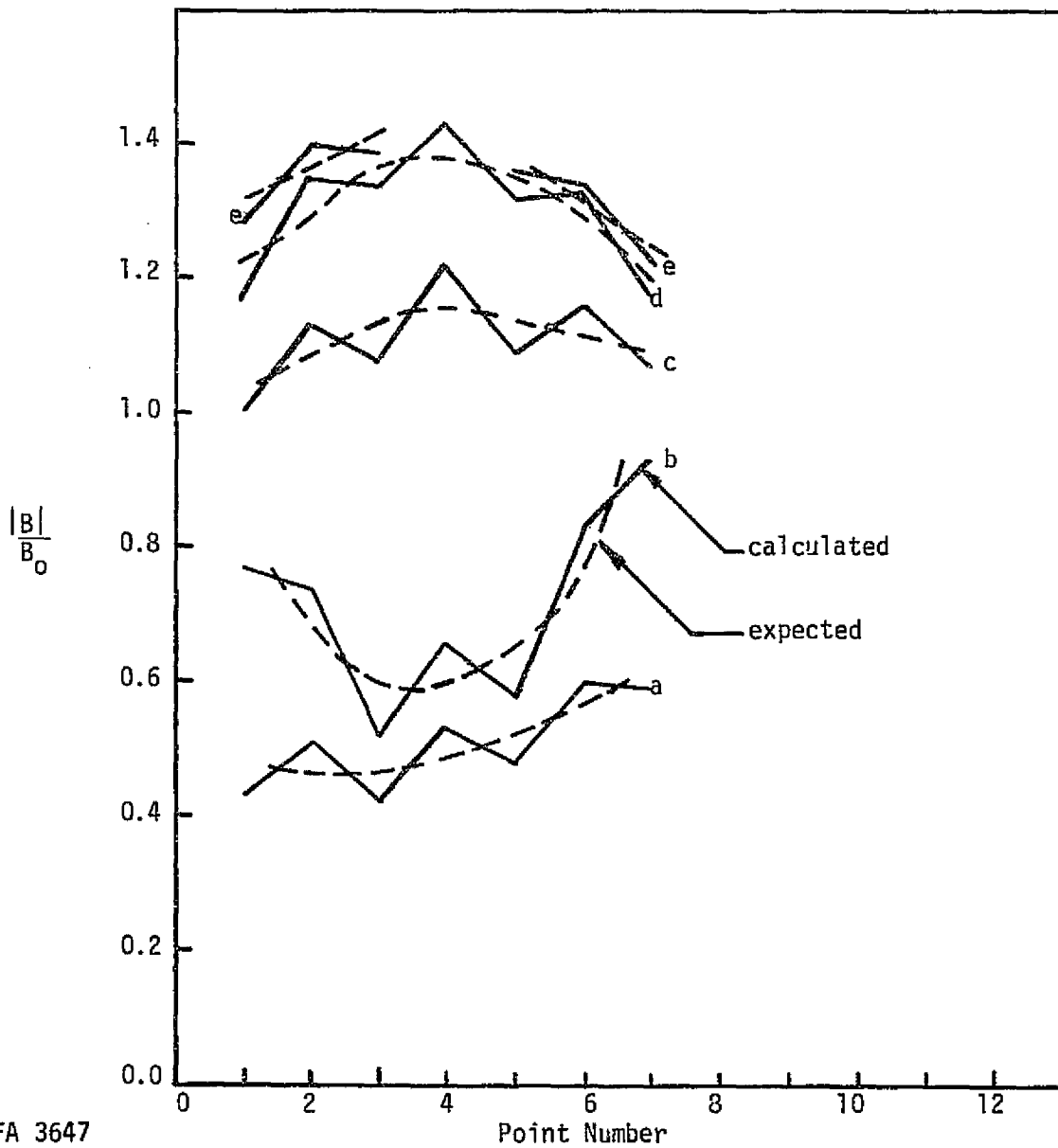
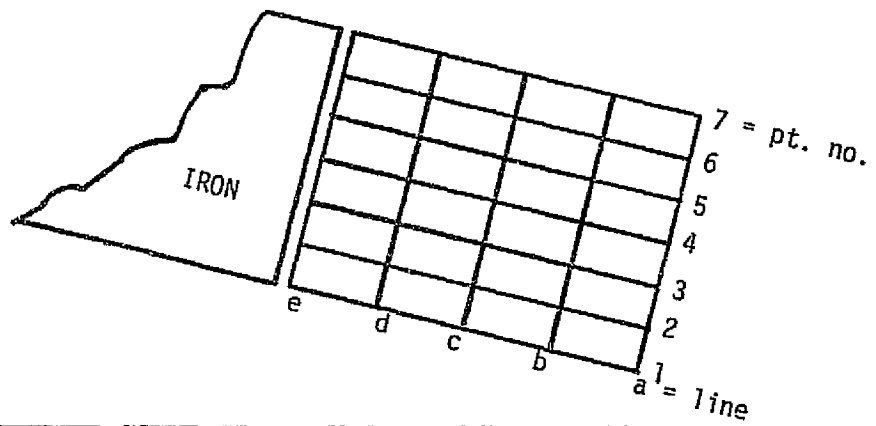
will most likely evolve into a more triangular region when a detailed design is performed using a model with more filaments. The model used was sufficient for the purposes of this effort. The calculated field distribution over the winding is given.

The manner in which the field varies along selected lines through the winding is shown in Figure V-14. The filament model used leads to an overestimate of field strength at points adjacent to filaments and an underestimate at points between filaments. Calculated curves therefore exhibit the "sawtooth" character shown. The actual field variation is not due to concentrated currents flowing in filaments but to current distributed over large areas; consequently, the actual field distribution will tend toward the average curves labeled "expected" in Figure V-14. Results have the same general character as with Design No. 1. The general decrease in overall level of field as the winding progresses from inside to outside allows for several conductors to be used in a graded design.

The initial goal of the grading process is to vary the overall current density in sections of the coil for the purpose of reducing the peak field concentration ratio. Conductors are then selected following a field computation throughout the winding. The results of successive iterations in search of a suitable current density distribution is shown in Figure V-15. Results are sawtooth in form for reasons discussed earlier and may be smoothed by considering lines (not shown) connecting averages between adjacent calculated points. The plot shows the field concentration ratio at successive points around the inside boundary of winding. The result of the grading procedure is to reduce the peak field concentration ratio from an initial of about 1.55 to about 1.37.

After specification of the winding components and overall winding dimensions, a preliminary investigation was carried out concerning the behavior of the coil during a quench transient. The model used was described earlier relative to Design No. 1 (see Figure IV-14 and the related text). Analyses were centered on Design 2.2 since this utilized the smallest conductor and, therefore, had the highest current density of the two alternates. Calculations were performed with the maximum permissible resistance in the dump circuit since this removes as much energy as possible from the coil. This resistor was taken as  $0.5 \Omega$  since this leads to an initial voltage of 2 kV across the coil terminals and higher values were considered impractical. Estimated results under these conditions indicated temperatures corresponding to possible burnout levels. Since the dump resistor level was already as high as possible, it was decided that the coil would have to be protected by an active system.

With this approach it is assumed that the initiation of quench is detected and that other normal regions are initiated in the coil system by heaters which are activated following detection. In this way the coil energy is dissipated over more material and the severity of the quench is reduced. Estimated results under these conditions are shown in Figures V-16, V-17, and V-18. In each figure two curves are shown which correspond to quench initiation at four and six locations in the magnet, respectively. Figure V-16 illustrates the current vs. time characteristics and the faster decay rates which arise as more normal regions are initiated. The temperature transients are shown in Figure V-17, which shows the maximum temperature decreasing as the number of propagating regions increase. Similarly, Figure V-18 illustrates the way in which the



FA 3647

Figure V-14. Variation of Magnetic Field Through the Winding in Design No. 2

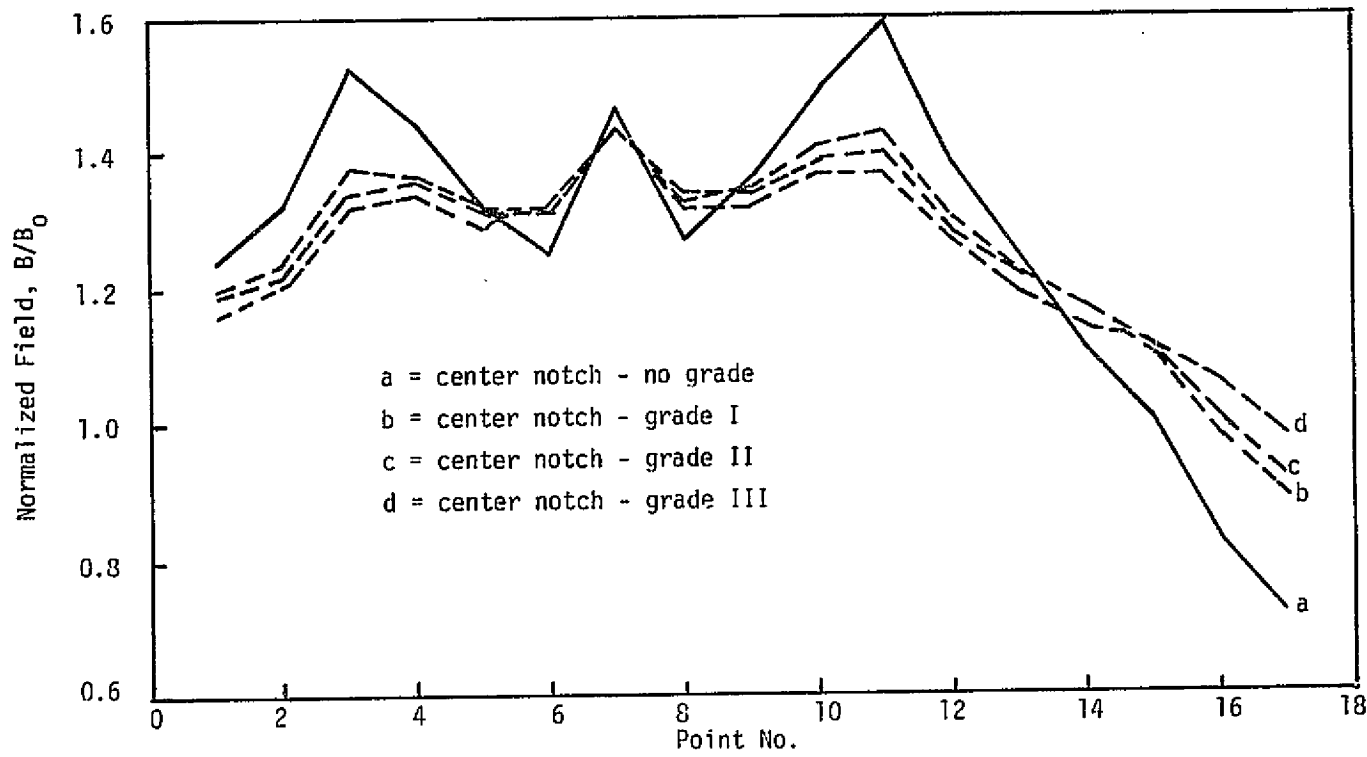
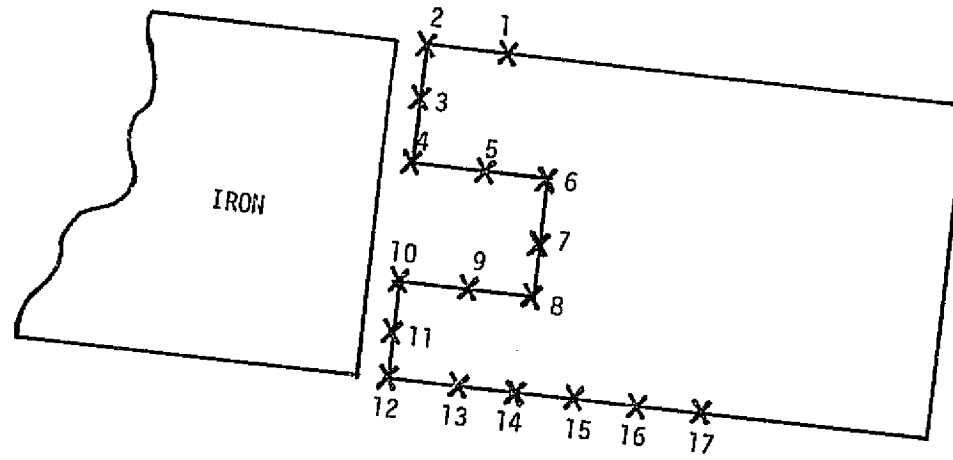
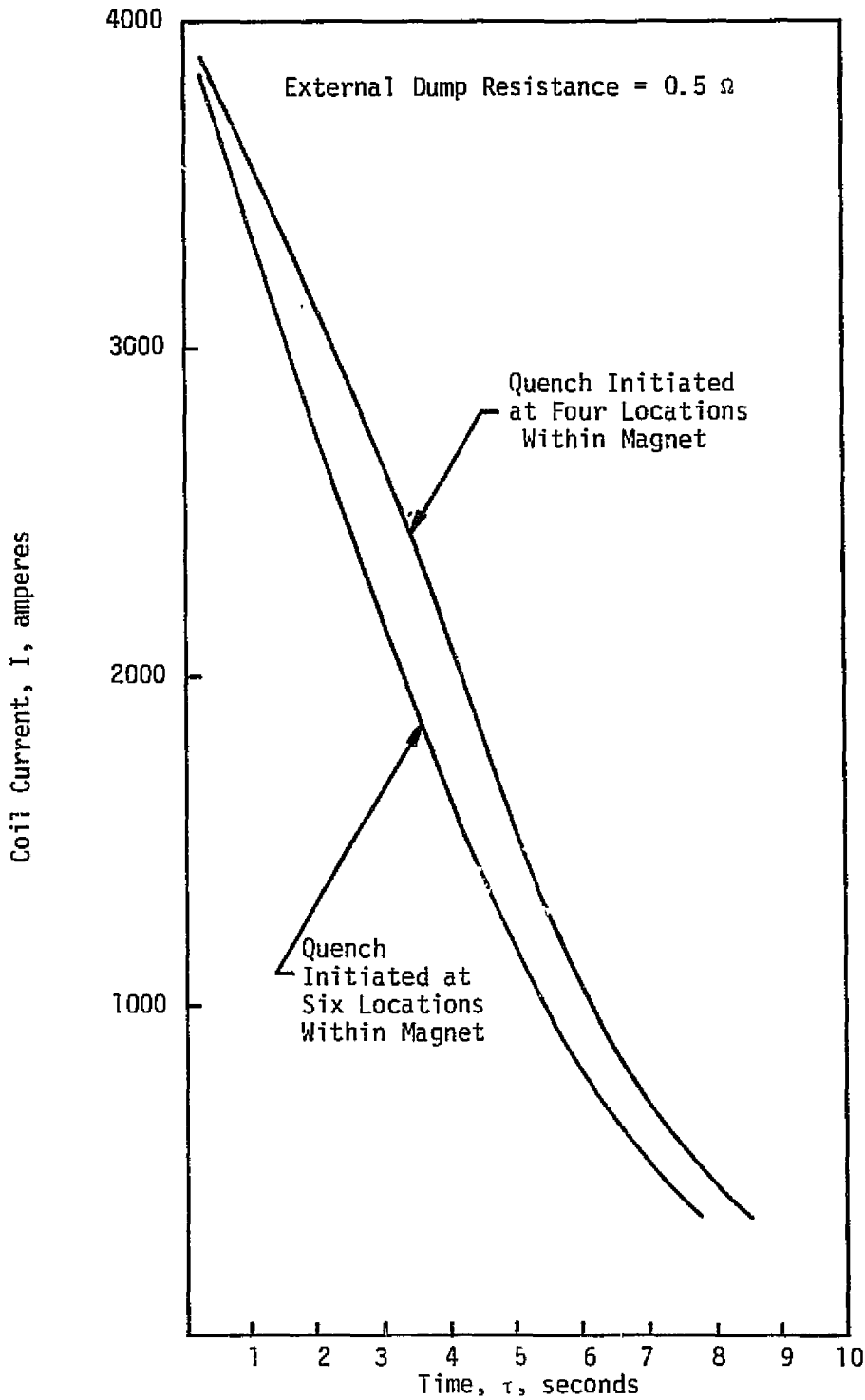


Figure V-15. Successive Iterations in Grading of Current Density Leading to the Final Configuration in Figures V-9 and V-10



FA 3660

Figure V-16

Coil Current Vs. Time for Preliminary Design No. 2 Quench Simulation

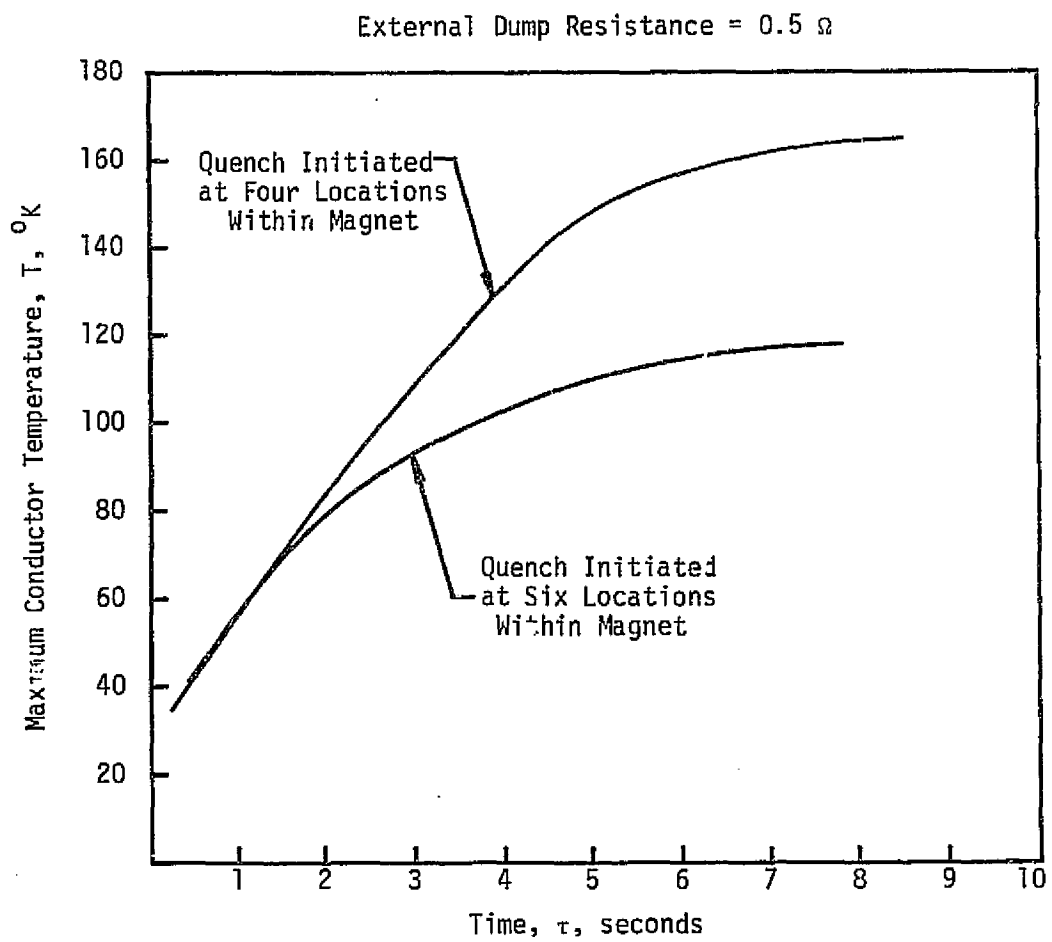


Figure V-17

Maximum Conductor Temperature Vs. Time for Preliminary Design No. 2  
Quench Simulation



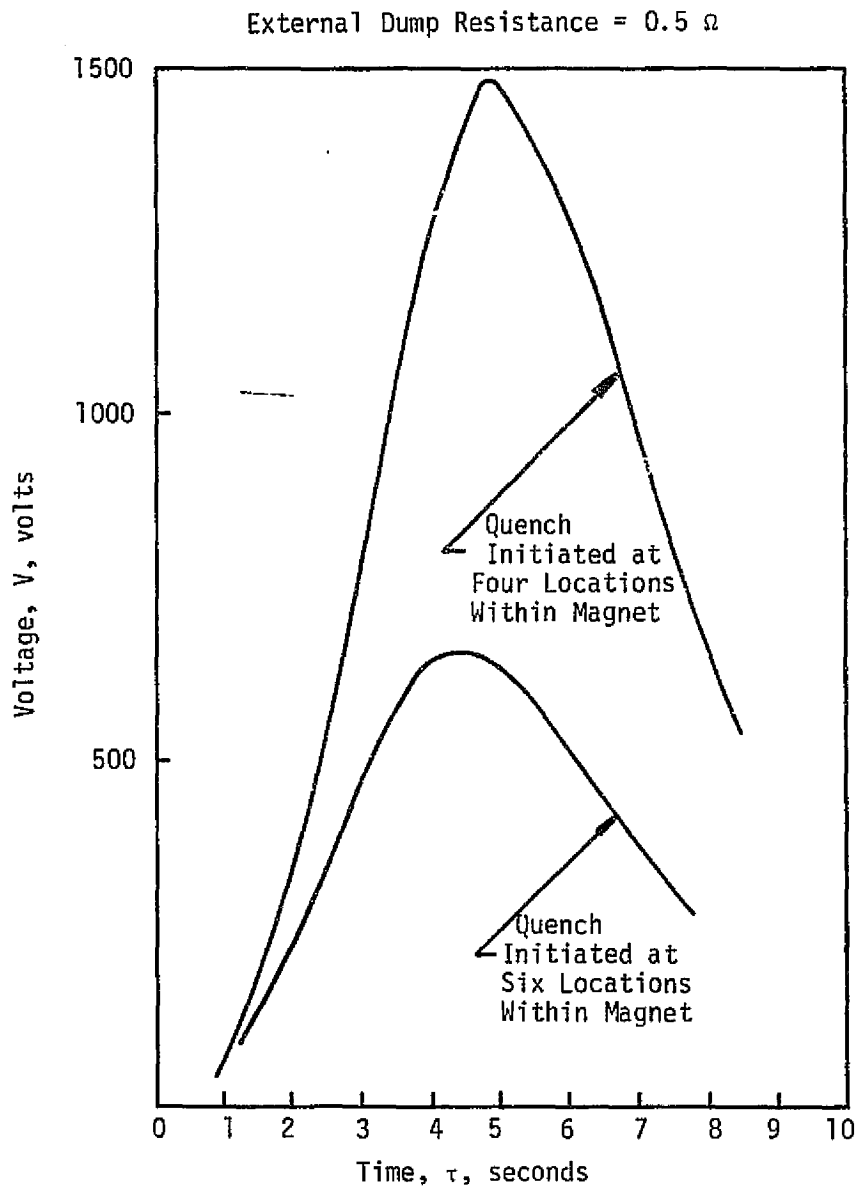


Figure V-18

Computed Voltage Across Normal Region for Preliminary Design No. 2

voltage level within the coil system is reduced as the number of normal regions propagating simultaneously increases.

The conclusion to be drawn from this initial study into the quench behavior for Preliminary Design No. 2 is that the current density is sufficiently high relative to Design No. 1 to lead to more severe quench conditions. A more detailed analysis and supporting effort will be required during detailed design. Furthermore, estimates indicate that a simple protection scheme consisting of a single dump resistor may not be adequate; consequently, more complex measures may be necessary. The initiation of multiple normal regions following the detection of the onset of a normal region is a relatively simple approach which may alleviate the high temperature, high voltage problem.

### C. STRUCTURE AND DEWAR DESIGN

The structure and dewar description and structural design criteria for Design No. 2 are similar to those utilized for Design No. 1. Exceptions are discussed in this section.

#### 1. em Forces

The basic geometry and field level for both Design Nos. 1 and 2 are identical. The main difference lies in the average overall current density in the windings and therefore in envelope dimensions. The latter may be expected to alter the distribution of loads of em origin somewhat; however, the net loads axially, in the transverse direction, and between coils for Design No. 2 would be expected to be close to those calculated for Design No. 1. As a result, the em loads calculated for Design No. 1 were used as the em loads for Design No. 2 in estimating the structural requirements. If either case is pursued, a more detailed force distribution and structural analysis would be necessary.

#### 2. Structure Description and Design Criteria

A summary of the mechanical characteristics of the structural components for Design No. 2 is given in Table V-11. This gives the design pressures, weights, materials, and overall sizes of the major structural components of the magnet system which includes the coil/He vessel, the support spacers for the attractive em loads, and the main gravitational structure.

##### a. Winding Internal Structure

The internal structure for Designs 2.1 and 2.2 consists of the stainless steel channel discussed earlier (see Tables V-7, V-9, V-10, and V-11). The sides of the stainless steel channel are intermittent to allow for helium circulation. Their primary purpose is to transmit load and prevent turn to turn load accumulation in the conductor in a direction perpendicular to the wide conductor face. The back of the stainless channel is continuous and is sized to limit the axial stress in the conductor to  $10^4$  psi as a result of the forces in the end turn region of the magnet. It is assumed that these loads result in a hoop stress in the steel and the conductor. The estimated hoop stress distribution in the winding for Preliminary Design No. 2 is shown in Figure V-19.

Table V-11

Summary of Mechanical Characteristics of the Major  
Structural Components for Design Nos. 2.1 and 2.2

I. Coil/He Vessel

A. Design Pressure

1.  $2.07 \times 10^5$  N/m<sup>2</sup> (30 psia) Internal
2.  $1.03 \times 10^5$  N/m<sup>2</sup> (15 psia) External

B. Weight

	<u>2.1</u>	<u>2.2</u>
1. Conductor	10,960 kg (24,112 lbs.)	6,020 kg (13,244 lbs.)
2. Iron	6,773 kg (14,900 lbs.)	6,773 kg (14,900 lbs.)
3. Structure	<u>18,955</u> kg (41,700 lbs.)	<u>18,468</u> kg (40,630 lbs.)
	36,688 kg (80,712 lbs.)	31,261 kg (68,774 lbs.)

C. Material

1. Conductor = MF NbTi/Copper
2. Iron = AISI 1008
3. Structure = 310S SS

D. Overall Size of Each Vessel

	<u>2.1</u>	<u>2.2</u>
1. Length	3.18 m (125 in.)	3.05 m (120 in.)
2. Width	2.51 m (99 in.)	2.51 m (99 in.)
3. Height	.76 m (30 in.)	.76 m (30 in.)

II. Support Spacers for Attractive em Load

A. Weight = 932 kg (2,050 lbs.); Total = 3,737 kg (8,200 lbs.)

B. Material = 310S SS

C. Overall Size

1. Length = 3.19 m (126 in.)
2. Width = 0.58 m (23 in.)
3. Inlet Height = 0.15 m (6 in.)
4. Outlet Height = 0.41 m (16 in.)

III. Main Gravitational Support Structure

A. Weight = 1,000 kg (2,200 lbs.)

B. Material - 310S SS

C. Overall Size

1. Length = 2.76 m (109 in.)
2. Width = 2.58 m (102 in.)
3. Height = 0.28 m (11 in.)

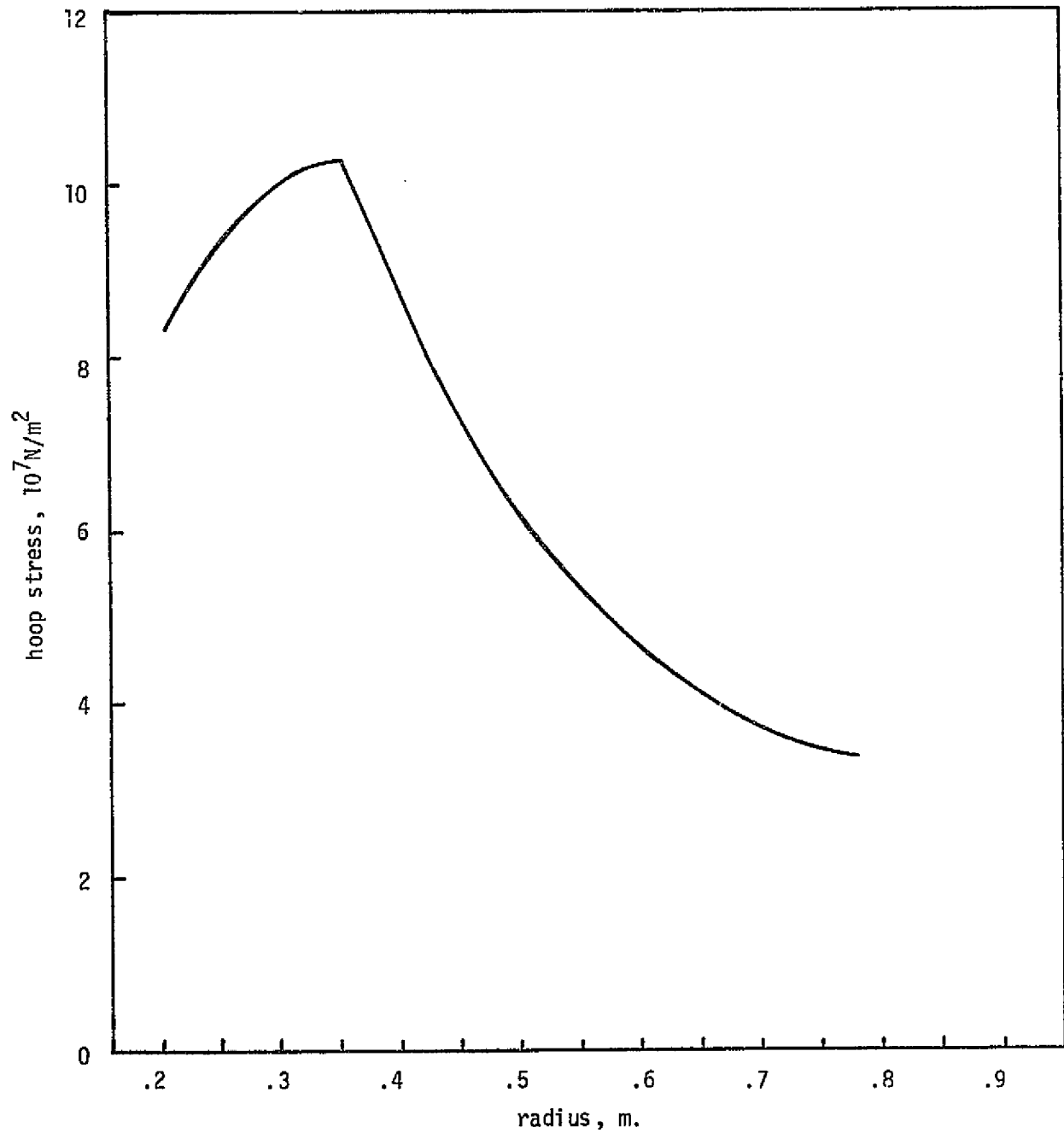


Figure V-19

Estimated Average Hoop Stress Distribution for Preliminary Design No. 2.

Note that the level is somewhat higher than for Design No. 1 (Figure IV-23). This arises from the higher current density in this case. These estimates are suitable for the purposes of this study; however, a detailed structural analysis will be necessary during the final design.

#### b. Coil/He Vessel

The coil/He vessels for Design No. 2 are supported on their sides and not their faces as was done for Design No. 1. However, this difference in gravitational orientation does not affect the coil/He vessel structure itself which carries the large transverse electromagnetic loads. Plates are welded to the bottom of the coil/He vessel and are shaped to conform to the angle required for low gradient mode operation.

#### c. Attractive em Load Support Spacers

Since the spacers for the low gradient profile mode for Design No. 2 are an integral part of the coil/He vessel, the only set of spacers required are those for the high gradient profile mode. Two wedge-shaped spacers are required for this case, and they fasten between the left and right coil/He vessels. The spacers are fabricated from 310S stainless steel and consist of a top plate, bottom plate, and two webs which have been sized from a compression stress, critical buckling stress, and elastic stability viewpoint. The fasteners which hold them in place have been sized to support the high shear forces that develop as a result of the attractive em loads acting on the tapered surface of the spacer.

#### d. Main Gravitational Support

The main gravitational support for Design No. 2 consists of a front rail, a rear rail, and two interconnecting beams which are welded together to form a single subassembly. A low friction material is located on the front and rear rails in the area underneath the coil/He vessels. It consists of a thin sheet of material which extends over the length of travel of the coil/He vessels as it moves from the low gradient mode to the high gradient mode. These rails and beams transmit the weight of the system to low heat leak column supports.

### 3. Dewar Description and Design Criteria

The dewar for Design No. 2 has been designed to withstand the gravitational loads of the magnet. It has also been designed to insulate the cold space sufficiently well to maintain the heat leak into the system at an acceptable level. The mechanical characteristics for the dewar for Design 2 are given in Table V-12. The dewar consists of a warm bore tube, warm bore tube radiation shield, outer room temperature vessel, outer radiation shield, and the column support system. The radiation shield is cooled by liquid nitrogen, which is assumed to be available in external storage dewars and fed through the tracer tubes on the radiation shield. The 2 K (nominal) heat exchanger of the cryogenic support subsystem which has been discussed earlier mounts on top of the room temperature

Table V-12

Summary of Mechanical Characteristics of Dewar  
for Design No. 2

- I. Room Temperature Vessel
  - A. Design Pressure
    - 1.  $1.03 \times 10^5 \text{ N/m}^2$  (15 psia) Internal
    - 2.  $1.03 \times 10^5 \text{ N/m}^2$  (15 psia) External
  - B. Weight = 18,636 kg (41,000 lbs.)
  - C. Material = 304L SS
  
- II. Radiation Shield
  - A. Design Pressure
    - 1.  $0 \text{ N/m}^2$  (0 psia) Internal
    - 2.  $0 \text{ N/m}^2$  (0 psia) External
  - B. Weight - 5,909 kg (13,000 lbs.)
  - C. Material = ETP Copper Annealed
  
- III. Column Support System
  - A. Configuration
    - 1. Four legs consisting of three concentric cylinders
    - 2. All columns have flexural hinges and are designed to compensate for thermal contraction of the He vessel and main support
  - B. Type
    - 1. Inner Cylinder = G10
    - 2. Intermediate Cylinder = Aluminum
    - 3. Outer Cylinder = G10
    - 4. Hinge Material = 6Al4V ELI Titanium
  - C. Weight = 71 kg (156 lbs.) ea x 4 = 284 kg (625 lbs.) total
  
- IV. 4,000 A Lead Assembly
  - A. Weight = 91 kg (200 lbs.)
  - B. Material = OFHC Copper and G10

vessel. The liquid helium vessel has been incorporated into the coil support structure and was discussed earlier.

a. Warm Bore Tube and Bore Radiation Shield

Figure IV-24, which shows the cross section of the warm bore tube and bore radiation shield at the inlet for Design No. 1, also applies for Design No. 2. At the outlet, the warm bore tube dimensions differ from those for Design No. 1 in that the largest dimension, 0.508 m (20 in.), lies along the horizontal axis. The orientation relative to the magnetic field is the same, however.

b. Room Temperature Vessel and Outer Radiation Shield

Other than the fact that the overall length of the room temperature vessel (and, consequently, that of the radiation shield) is slightly, 0.279 m (11 in.), shorter due to the smaller main gravitational support and coil/He vessel, all other aspects of the room temperature vessel and outer radiation shield for Design No. 2 are the same as Design No. 1, which is discussed in more detail in Section IV-C-3-b.

c. Column Support System

The low heat leak columns for Design No. 2 are approximately one half the height of those for Design No. 1. The shorter height means that the web of the hinge is thinner and the size of and thickness of the concentric cylinders remain the same. The  $2.2 \times 10^3$  N (500 lbs.) lateral load design criteria controls the thickness of the web of the hinges, and therefore, since the moment arm through which it acts is shorter, it follows that the web can be made thinner.

4. Radiation Heat Load Estimates

The total heat load on the magnet system consists of the sum of the conduction heat leak through the supports, the radiation heat leak, resistive heating in nonsuperconducting electrical joints, and the heat loss due to conduction through and heat generation in the energized leads. For the scale of magnet systems under consideration, thermal radiation and the vapor-cooled power leads are the largest heat load on the system.

The radiative heat load from the room temperature container to the radiation shield and from the radiation shield to the liquid helium container can be estimated by calculating the surface area exposed to thermal radiation and by estimating an equivalent heat flux per unit surface area for these two temperature ranges. The estimates have been performed for Design No. 2, and the results are presented in Table V-13. It was assumed that the radiation shield is cooled by liquid nitrogen and the equivalent heat flux through the superinsulation from room temperature was 100 milliwatts per square foot. The heat flux from the radiation shield to the superinsulated liquid helium container was assumed to be 5 milliwatts per square foot.

Table V-13

Estimated Cryogenic Characteristics for Preliminary Design No. 2  
8 T Racetrack with Iron - 2 K

- I. Temperature He Vessel - 2<sup>o</sup> K
- II. Temperature Radiation Shield - 77<sup>o</sup> K
- III. Total He Inventory - 245 liters
- IV. Boiloff Rate
  - A. Leads - 12 l/hr.
  - B. Radiation Shield, Column Supports, He Vessel - 8 l/hr.
- V. Superinsulation
  - A. Bore
    - 1. Cold Side -  $1.91 \times 10^{-2}$  m (.75 in.)
    - 2. Warm Side -  $2.54 \times 10^{-2}$  m (1.0 in.)
  - B. Outside
    - 1. Cold Side -  $5.08 \times 10^{-2}$  m (2.0 in.)
    - 2. Warm Side -  $5.08 \times 10^{-2}$  m (2.0 in.)



## VI. 8 T RECTANGULAR SADDLE, 4.2 K SYSTEM

This section will present results on the third of the three preliminary designs considered in Phase II of the program. This was a cryostatically stable, 8 T, 4.2 K magnet-dewar system as was Design No. 1 (see Section IV); however, Design No. 3 was based on a rectangular saddle winding geometry. The latter was chosen since the estimates performed in Phase I implied a substantial economic advantage for this winding shape. Even though the saddle is more complex to build than the racetracks (e.g., see Sections IV and V), it is substantially lighter and uses less conductor for a given central field because the conductor is used more efficiently from the standpoint of field production in the region of interest.

System No. 3 was designed such that the MHD channel axis was vertical and the main magnetic field horizontal. Note, however, that any of the three magnet designs considered could be used with any of the three dewar designs with minor alterations. The system to be discussed was also designed such that the field gradient along the MHD channel could be altered by variation of the angle between coils.

The subsections which follow will present an overall description of the system, a discussion of the winding geometry and conductor characteristics, and a description of the structure and dewar design.

### A. SYSTEM DESCRIPTION

#### 1. Overall Characteristics

The preliminary design characteristics for Design No. 3 are given in Table VI-1. The table gives overall dimensions of the system, electrical characteristics, and weights of the major components of the magnet system. Two modes are indicated and correspond to operation of the two racetrack/saddle coils with a  $2^\circ$  included half-angle (low gradient mode) or  $10^\circ$  included half-angle (high gradient mode). The maximum field at the winding is 9.5 T. This may be reduced somewhat upon further iteration of the graded design during a future detailed design phase. Overall current density and conductor density ranges are given. As with Design Nos. 1 and 2, the conductor is the heaviest major component and for this design represents about 14 percent of the total weight of the magnet system.

The magnetic flux density at the inlet for the high and low gradient operating modes is the same as for Design Nos. 1 and 2; i.e., 8.0 T. At the outlet the low gradient operating mode has a magnetic flux density of 6.4 T whereas the field at the outlet for the high gradient mode is 4.5 T. Uniformity requirements are  $\pm 5\%$  for the low gradient mode and  $\pm 8\%$  for the high gradient mode.

Top and side views of the racetrack/saddle coils are given in Figures VI-1 and VI-2. Figure VI-2 shows the two extreme coil positions from the viewpoint of field variation. Calculated field profiles along the channel axis for these coil positions are shown in Figures VI-3 and VI-4. The magnetic flux density variation from a linear profile on axis is  $\pm 5\%$  for the low gradient mode and  $\pm 8\%$  for the high gradient mode.

Table VI-1

Preliminary Design Characteristics for Design No. 3  
8 T Rectangular Saddle with Iron - 4.2 K

Dewar Dimensions

Inlet	0.2540 m x 0.2540 m (10 in. x 10 in.)
Outlet	0.4064 m x 0.4064 m (16 in. x 16 in.)
Overall Height	6.18 m (244 in.)
Outside Diameter	4.27 m (168 in.)

Electrical Characteristics

Field at Channel Inlet	
2 <sup>o</sup> Mode	8.00 T
10 <sup>o</sup> Mode	7.36 T
Field at Channel Outlet	
2 <sup>o</sup> Mode	6.41 T
10 <sup>o</sup> Mode	4.50 T
Max. Field on Channel Axis	
2 <sup>o</sup> Mode	8 T
10 <sup>o</sup> Mode	8 T
Max. Field at Winding*	9.12 T
Active Field Length	1.524 m (60 in.)
Stored Energy*	62.2 x 10 <sup>6</sup> J
Inductance*	7.77 H
Operating Current*	4000 A
Overall Current Density*	3.68 x 10 <sup>7</sup> A/m <sup>2</sup> - 4.53 x 10 <sup>7</sup> A/m <sup>2</sup>
Conductor Current Density*	6.02 x 10 <sup>7</sup> A/m <sup>2</sup> - 7.38 x 10 <sup>7</sup> A/m <sup>2</sup>
Total Turns	2,652
Ampere-Meters	7.83 x 10 <sup>7</sup>

Weights

Conductor (kg)	9,770
Structure (kg)	40,941
Dewar (kg)	<u>20,940</u>
TOTAL (kg)	71,651

\* Values for 2<sup>o</sup> Mode

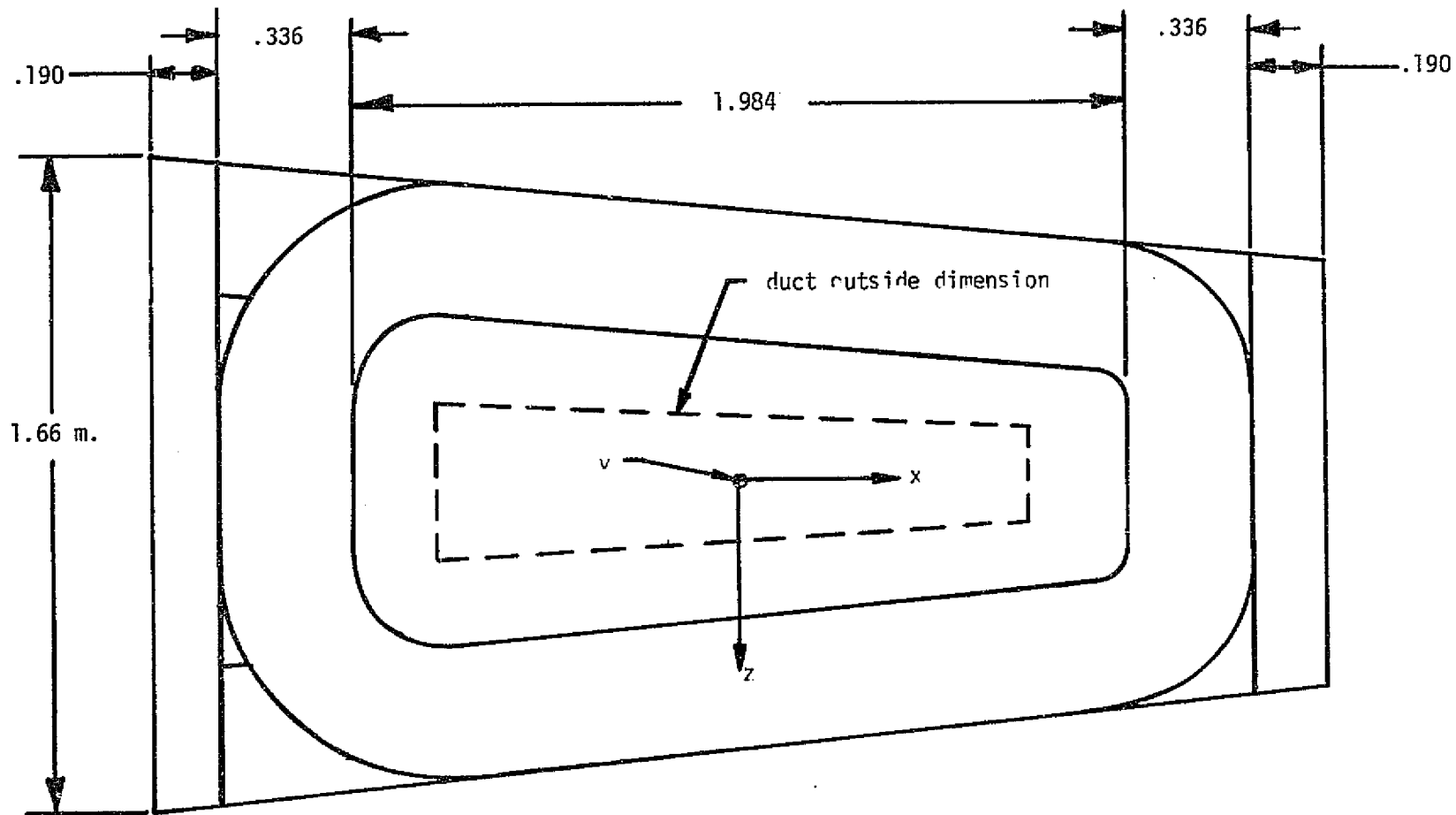


Figure VI-1

Top View of Racetrack and Saddle for Preliminary Design No. 3

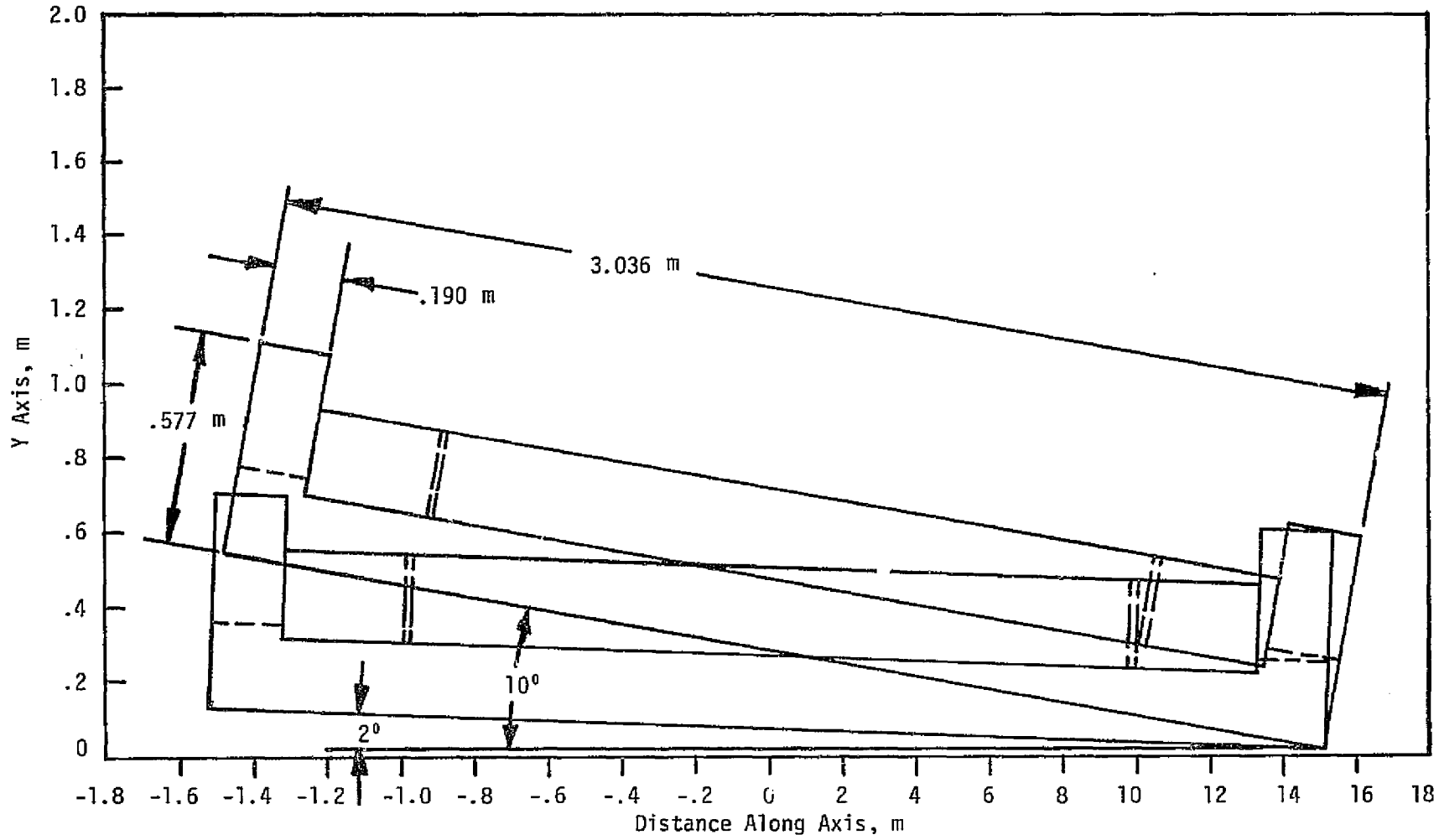


Figure VI-2

Side View of Racetrack and Saddle for Preliminary Design No. 3

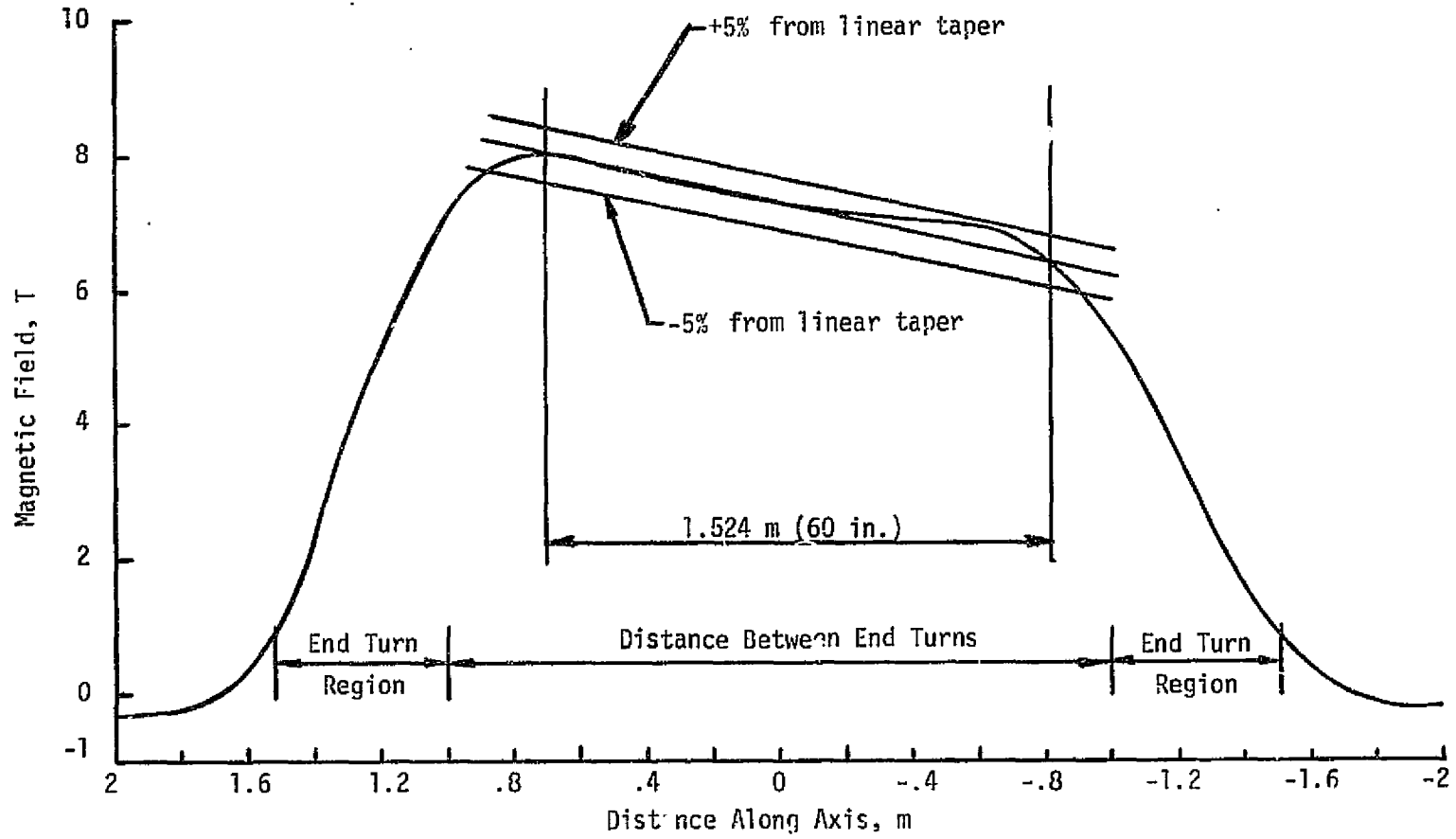


Figure VI-3

Field Profile Along Channel Axis for Design No. 3 in the Low Gradient Operating Mode

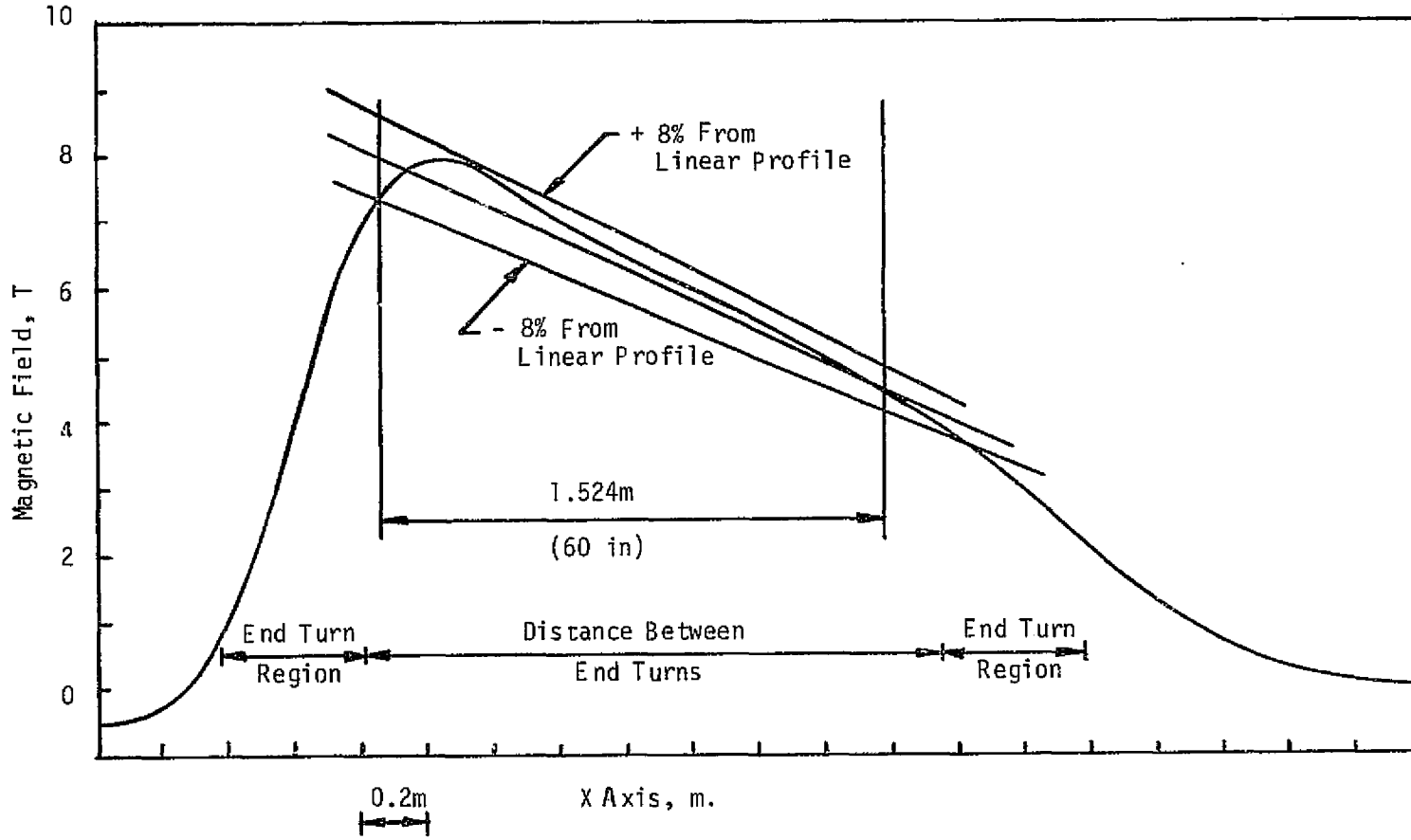


Figure VI-4  
Field Profile Along Channel Axis for Design no. 3 in the High Gradient Operating Mode

Figure VI-5 shows one quadrant of the cross section of the MHD channel inlet, channel exit, and at planes one quarter of the distance from each end of the channel. Two numbers are given at each point in the sections. One number is the Y component of field (i.e., main field direction), and the other number (in parentheses) is the ratio of the local Y component of field to the Y component of the field on axis in that plane. Table VI-2 gives results for the computed field components and magnitude with corresponding coordinates in the channel.

Figure VI-6 shows the assembly drawing (MCA Drawing E-2809) of the magnet-dewar system for this design. The magnet-dewar system consists of the same major components as Design Nos. 1 and 2. The basic differences in this design are as follows:

1. The basic coil geometry is that of a rectangular saddle, but consists of a racetrack coil nested inside the end turns of a rectangular saddle coil.
2. Internal coil structure for the racetrack is not required for hoop loads because of the different manner of coil support; i.e., the end turns of the racetrack coil are supported axially by the rectangular saddle end turns which in turn are supported by the coil/He vessel structure. Intermediate structural components between the racetrack and saddle end turns may be found to be necessary in the final design. Stainless steel banding in the windings has been used to prevent the accumulation of forces from layer to layer and from turn to turn as a result of the electromagnetic loads.
3. External structure in the form of straight beams and tension rods are required to support the transverse loads in the windings. This differs somewhat from the racetrack cases discussed earlier. Figure VI-7 shows that for racetrack coils, the bottom and top plates of the coil/He vessel can support the transverse em forces and because of their geometry they clear the warm bore tube and radiation shield. However, the rectangular saddle coil geometry disallows this; consequently, the transverse em loads must be supported in another manner such as the straight beams and tension rods which were utilized on this program. The straight beams transmit the load in bending to the tie rods, which in turn support the load in tension.
4. The axis of the MHD channel is vertical.
5. The main gravitational support structure carries gravitational loads only; i.e., it does not transmit attractive em loads in compression as is the case for Design No. 1.

The location of the MHD channel relative to the axis of the magnet remains the same as for the first two designs. The inlet and outlet dimensions of the warm bore tube and the "active" MHD channel length conform to the user requirements. The distance from the upstream end of the dewar to the channel inlet (entrance length) measures 1.06 m (42 in.), and the distance from the channel outlet to the downstream end of the dewar (exit length) measures 1.13 m (44 in.).

The magnet-dewar system is fastened to the foundation in four places and has a total weight of about 48,970 kg (107,730 lbs.). It measures 6.18 m (244

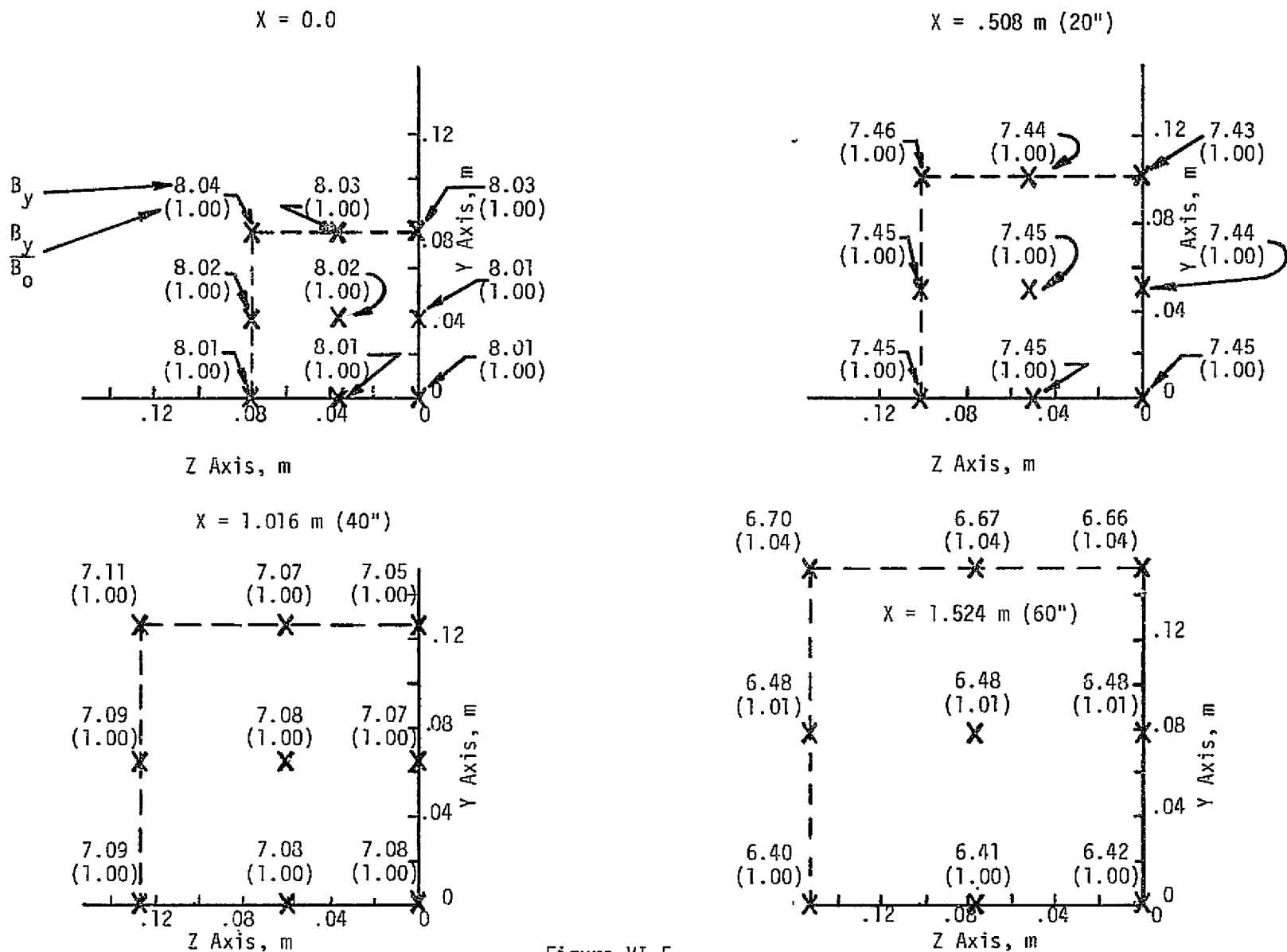


Figure VI-5

Calculated Main Component of Field and Homogeneity in One Quadrant of the MHD Channel at Four Planes Along the Axis for the Low Gradient Operating Mode



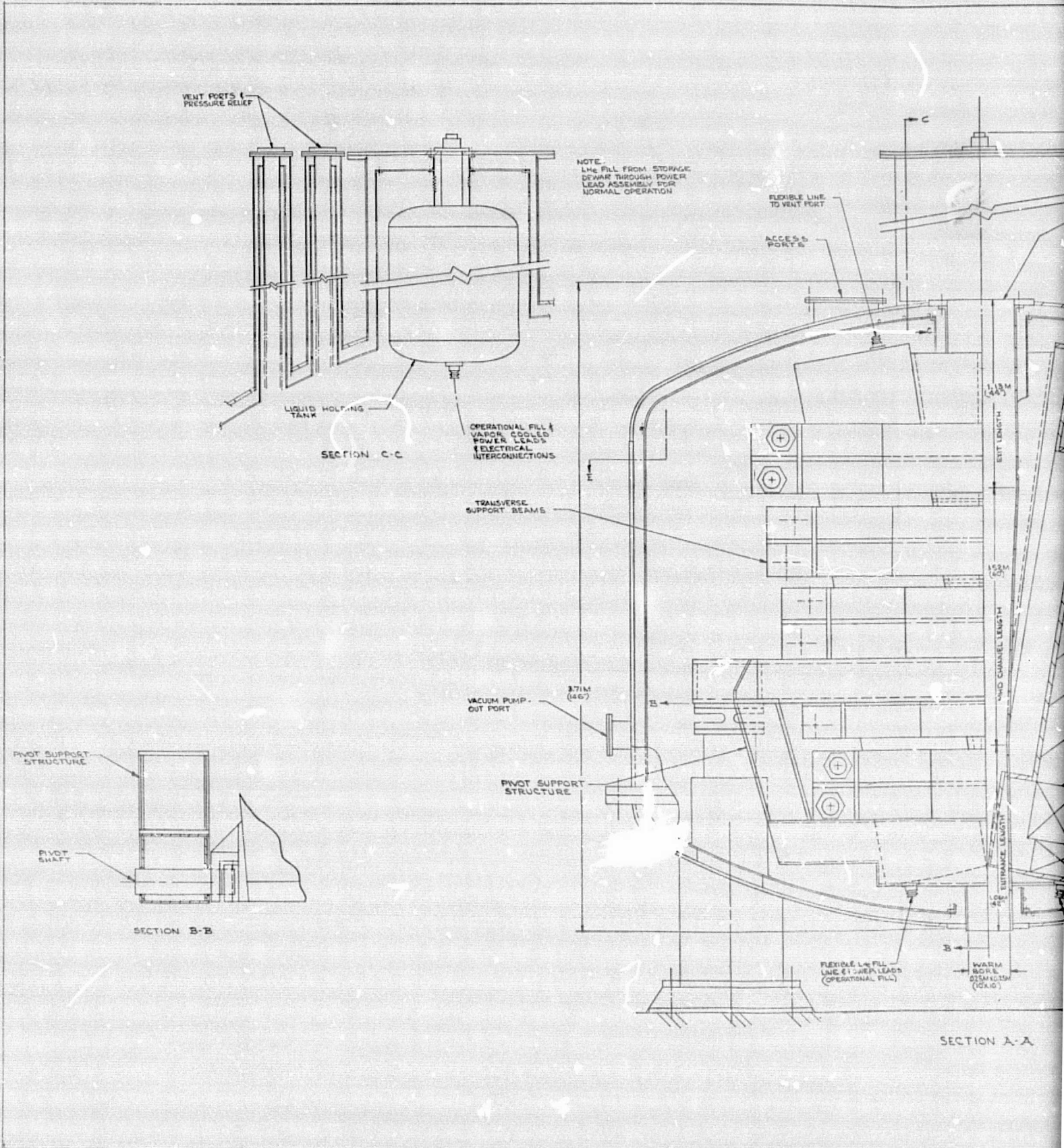
Table VI-2

Computed Field Components at Selected Points Throughout  
MHD Channel Volume for 5<sup>0</sup> Mode

Coordinate (m)			Field Component (T)			Field Magnitude (T)	
X	Y	Z	B <sub>X</sub>	B <sub>Y</sub>	B <sub>Z</sub>	/B/	
0.500	0.00	0.00	0.00	7.81	0.00	7.81	}
0.600	0.00	0.00	0.00	7.93	0.00	7.93	
0.700	0.00	0.00	0.00	8.01	0.00	8.01	
0.800	0.00	0.00	0.00	7.99	0.00	7.99	
-0.824	0.00	0.00	0.00	6.42	0.00	6.42	}
-0.824	0.00	0.076	0.00	6.41	0.00	6.41	
-0.824	0.00	0.152	0.00	6.40	0.00	6.40	
-0.824	0.076	0.00	0.29	6.48	0.00	6.48	
-0.824	0.076	0.076	0.29	6.48	0.00	6.49	}
-0.824	0.076	0.152	0.30	6.48	-0.03	6.48	
-0.824	0.152	0.00	0.53	6.66	0.00	6.68	
-0.824	0.152	0.076	0.54	6.67	0.01	6.69	
-0.824	0.152	0.152	0.56	6.70	-0.01	6.73	}
-0.316	0.00	0.00	0.00	7.08	0.00	7.08	
-0.316	0.00	0.064	0.00	7.08	0.00	7.08	
-0.316	0.00	0.127	0.00	7.09	0.00	7.09	
-0.316	0.064	0.00	0.03	7.07	0.00	7.07	}
-0.316	0.064	0.064	0.03	7.08	0.01	7.08	
-0.316	0.064	0.127	0.03	7.09	0.00	7.09	
-0.316	0.127	0.00	0.06	7.05	0.00	7.05	
-0.316	0.127	0.064	0.06	7.07	0.03	7.07	}
-0.316	0.127	0.127	0.06	7.11	0.03	7.11	
0.192	0.00	0.00	0.00	7.45	0.00	7.45	
0.192	0.00	0.051	0.00	7.45	0.00	7.45	
0.192	0.00	0.102	0.00	7.45	0.00	7.45	}
0.192	0.051	0.00	0.05	7.44	0.00	7.44	
0.192	0.051	0.051	0.05	7.45	0.00	7.45	
0.192	0.051	0.102	0.05	7.45	0.00	7.46	
0.192	0.102	0.00	0.10	7.43	0.00	7.43	}
0.192	0.102	0.051	0.10	7.44	0.01	7.44	
0.192	0.102	0.102	0.10	7.46	0.02	7.46	
0.700	0.00	0.00	0.00	8.01	0.00	8.01	
0.700	0.00	0.038	0.00	8.01	0.00	8.01	}
0.700	0.00	0.076	0.00	8.01	0.00	8.01	
0.700	0.038	0.00	0.02	8.01	0.00	8.01	
0.700	0.038	0.038	0.02	8.02	0.00	8.02	
0.700	0.038	0.076	0.02	8.02	0.00	8.02	}
0.700	0.076	0.00	0.04	8.03	0.00	8.03	
0.700	0.076	0.038	0.04	8.03	0.01	8.03	
0.700	0.076	0.076	0.04	8.04	0.01	8.04	

Points on Axis  
Field Points at Duct Outlet  
Field Points 40" from Duct Inlet  
Field Points 20" from Duct Inlet  
Field Points at Duct Inlet

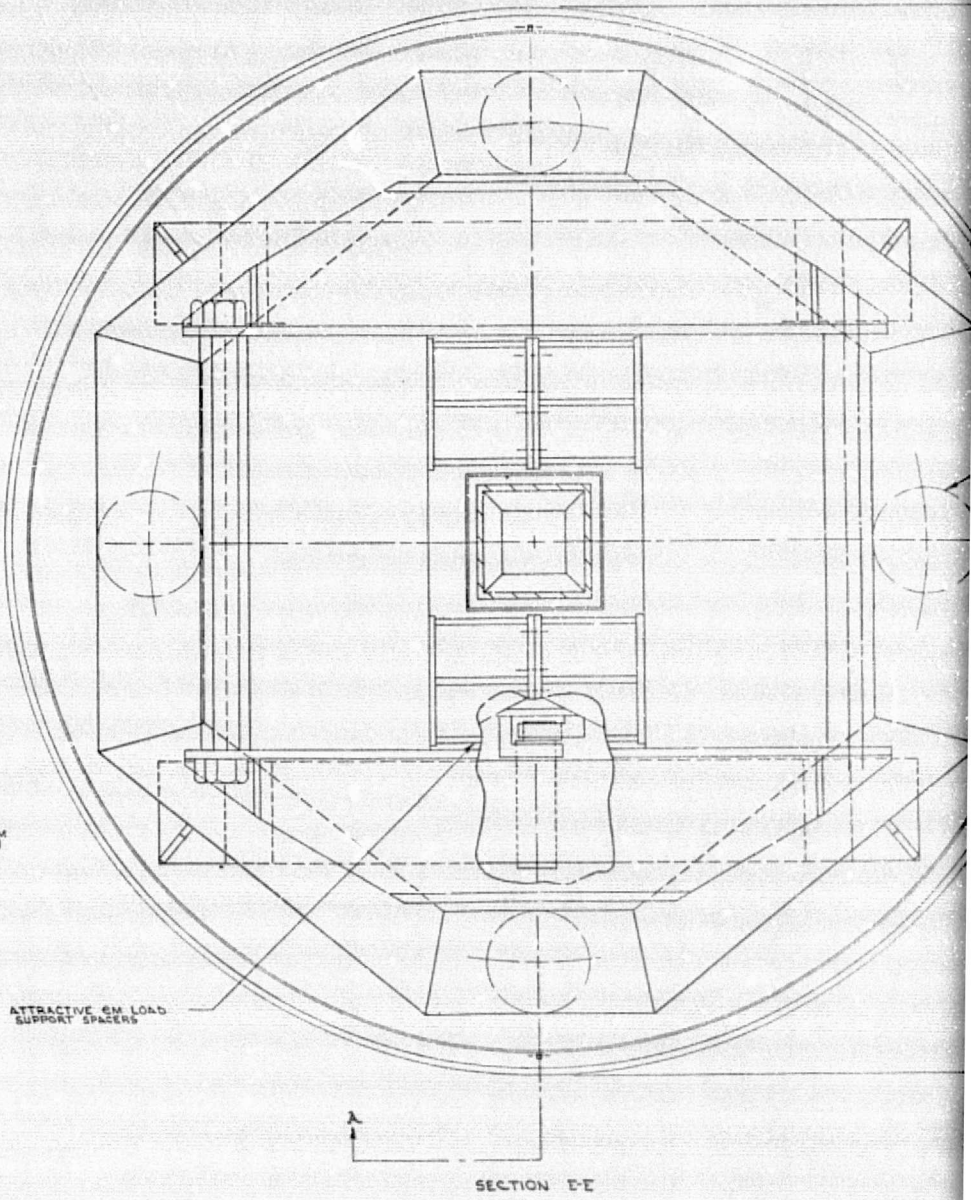
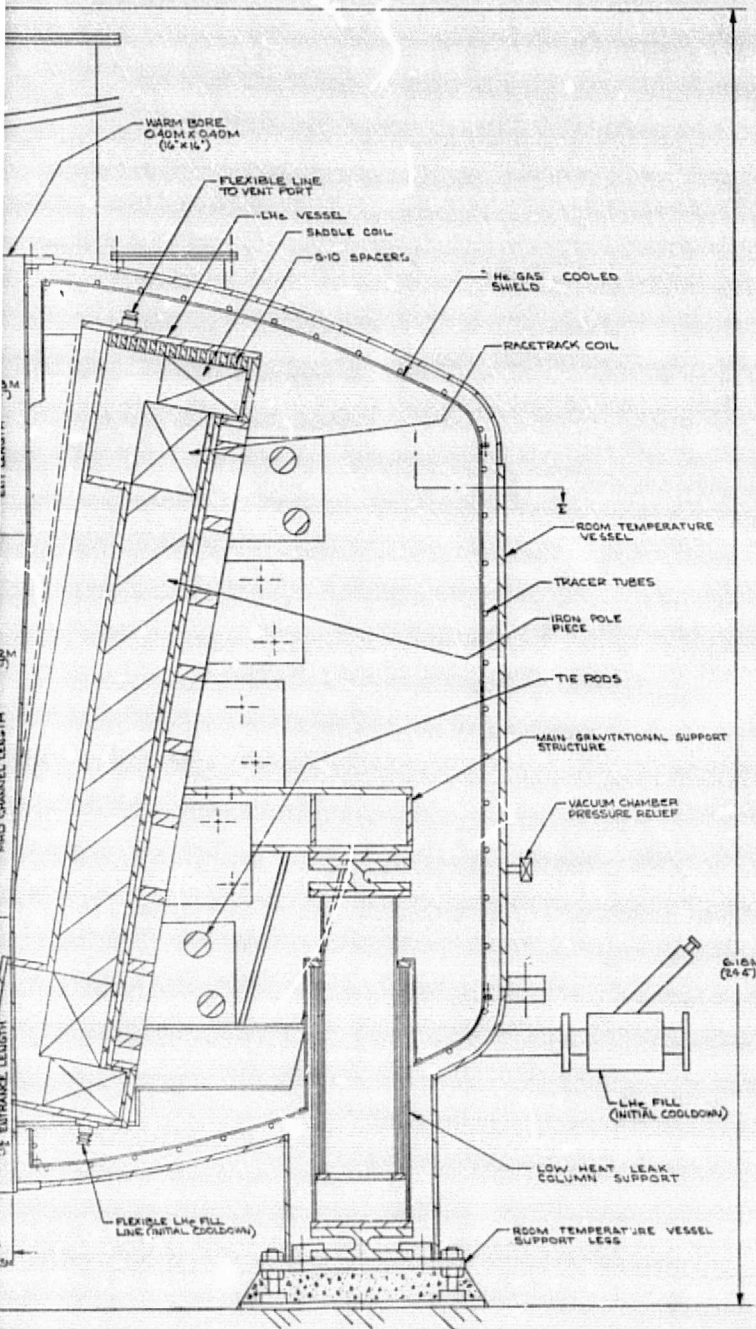
PRECEDING PAGE BLANK NOT FILMED



FOLDOUT FRAME

ORIGINAL PAGE IS OF POOR QUALITY

FOLDOUT



A-A

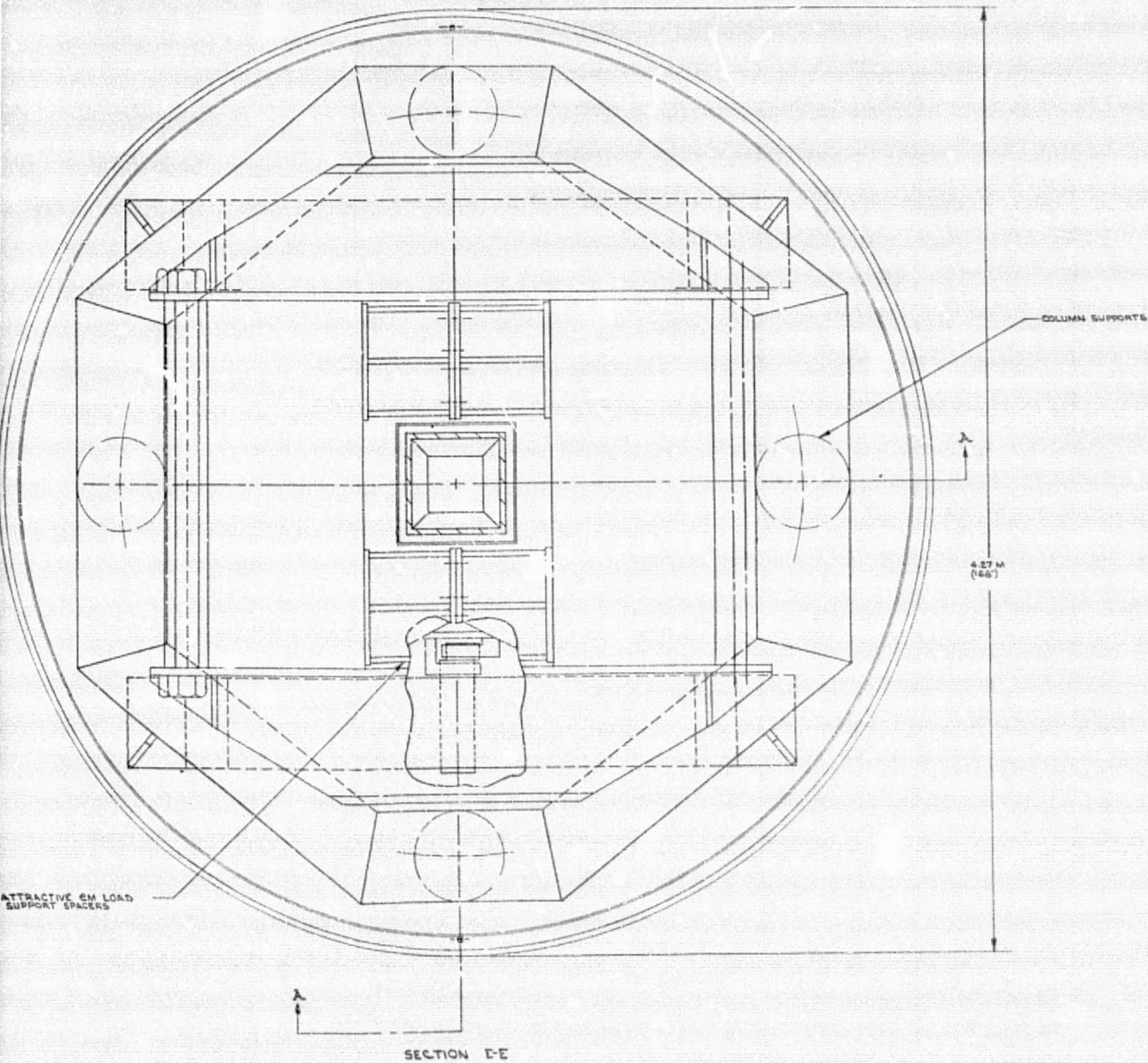
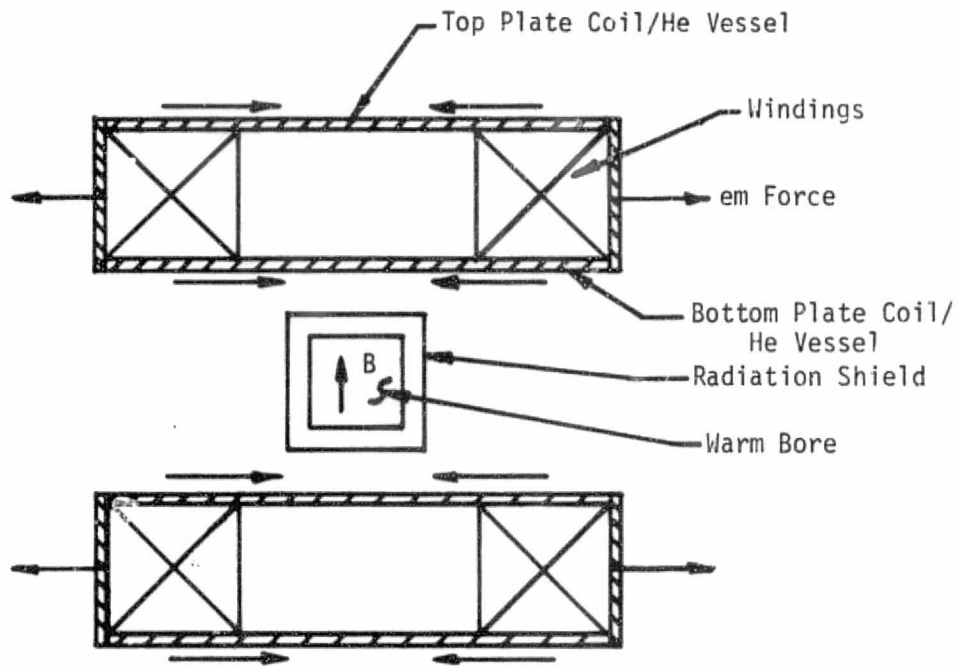
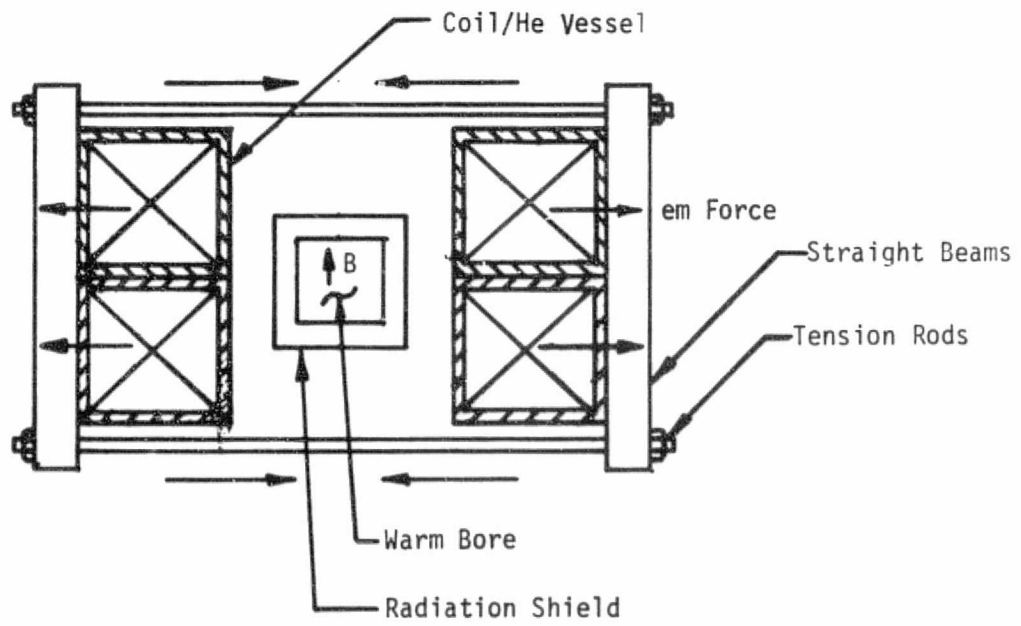


FIGURE VI-6

REVISIONS	
NO.	DESCRIPTION



Racetrack



Saddle

Figure VI-7

Comparison of Transverse Support Structure for Racetrack Coil Geometry and Rectangular Saddle Coil Geometry

in.) from the foundation to the highest point on the magnet, which is the top of the vapor-cooled lead assembly housing, and has an outside diameter which measures approximately 4.27 m (168 in.). The overall height measurement was based on a clearance of .470 m (18.5 in.) between the inlet end of the dewar and the foundation. Consideration must be given to alteration of this dimension to allow for MHD system components or to provide for a "pit" beneath the inlet section which will allow for components. The magnet could sit on raised concrete piers as an alternate method to allow for adequate clearance for MHD system hardware.

During operation, the MHD flow direction will be from the bottom of the magnet to the top. As with the first two designs, the fill and vent ports, in addition to the relief valve, are located at the top of the magnet, while the initial fill LHe valve and the vacuum chamber relief valve are located near the bottom. Access ports are provided at the top of the magnet to facilitate final connections to the vent lines.

The dewar utilizes a Helium gas-cooled radiation shield between the warm vessel and cold vessel walls. Superinsulation is used between the warm vessel and radiation shield and between the radiation shield and cold vessel at all locations except where penetrations are necessary for the gravitational supports, power leads or fill and vent lines. The warm bore tube and bore radiation shield are concentric and supported by connections to their corresponding elements at the ends.

The axial em loads are supported by the coil/He vessel structure. A series of straight beams and tension rods bear the transverse em loads. The straight beams extend across the faces of the sides of both coil/He vessels and are tied together with the tension rods. The attractive em loads between coils are supported by wedge-shaped spacers, which also set the coil angles, in the same fashion as that for Design Nos. 1 and 2.

The main gravitational support structure, which is supported by four (4) low heat leak columns spaced 90° apart from each other, carries the dead weight of the coil/He vessels, the spacers, the straight beams and tension rods, and the radiation shield. It does not experience any em loads. Verticality of the coil/He vessel is maintained by means of the transverse support beam bearing on the main gravitational support and thus acting as an "outrigger". The coils pivot at one end on a shaft, which is an integral part of the main gravitational support structure, to allow the angle between them to be changed.

The electrical interconnections and vapor-cooled power lead connections are made in a similar manner to that described for Design No. 1 (see Section IV-4).

## 2. Alteration of Field Gradient

Each coil is located in an integral coil/He vessel which has been designed to allow rotation to a new included half-angle between coils. Table VI-3 outlines the steps in the procedure for changing the coil angle from a high

gradient mode (wide angle) to the low gradient mode. This procedure must be reviewed and considered in detail during a final design of the system.

### 3. Outline of System Assembly

The following will outline an assembly procedure for the magnet system described above. It shows the basic sequence of events that is required and indicates the complexity of the task and scope of the major erection equipment needed. A final procedure is beyond the scope of the present effort and would result from a detailed design program.

The procedure assumes that each coil and its main coil/He vessel structure is subassembled off-site. The main components of the dewar are also assumed to be subassembled off-site. In addition, it is assumed that the facility, foundation, utilities, and component handling fixtures are available. It is essential that measures be taken to ensure a "clean room" atmosphere about the immediate area in which the final assembly takes place. This will minimize the possibility of foreign matter, dust, etc. gathering on critical surfaces such as the superinsulation. Several ports for viewing or accessibility would be necessary. The quantity, size, and location of these ports will be determined during the final design phase.

After dewar evacuation and successful completion of the procedure as outlined in Table VI-4, the magnet is ready to be cooled down and energized. This assumes that appropriate tests and quality control checks have been performed during the final assembly stage.

Table VI-3

Outline of Procedure to Alter Field Gradient for Design No. 3

De-energize the magnet, remove the LHe and allow the system to warm up to room temperature.

Release the dewar vacuum, open the access ports at the top of the magnet, and disconnect the flexible vent lines internal to the system.

Apply a fixture to horizontally support the downstream end of the warm bore tube and remove bolts between bore tube and upper dewar end cover.

Remove bolts in flange at room temperature end of power lead assembly; remove bolts at interface between lower end cover and main room temperature vessel; lift and remove upper dewar end cover and main room temperature vessel as a unit.

Apply a fixture to horizontally support the downstream end of the bore tube radiation shield.

Remove superinsulation and unbolt the downstream, radiation shield end cover from the main radiation shield, bore tube radiation shield and radiation shield within the power lead assembly; disconnect tracer tubes as required, then lift and remove the radiation shield end cover.

Apply a fixture to vertically support all tie rods and transverse support beams in position; loosen tie rods.

Attach a mechanical or hydraulic jack between each coil/LHe vessel and the main gravitational structural support near the mechanical snims that maintain coil verticality.

Unbolt attractive em load support spacers and remove.

Change the angle of the coils by jacking each coil/LHe vessel into place.

Bolt the He vessels to each other and position the transverse support beam on the main gravitational support to maintain verticality of the coil/He vessel.

Remove the jacks.

Tighten all tension rods and remove fixtures holding transverse support beams.

Replace the downstream radiation shield end cover and bolts to main shield, bore tube shield and shield in power lead assembly.

Replace superinsulation and remove support fixture for downstream end of bore tube radiation shield.

Replace room temperature vessel end cover and main vessel, bolt as required, and remove warm bore tube end support fixture.



Table VI-3 (Concluded)

Connect internal vent line by using access parts.

Evacuate vessel and prepare for cooldown.

Table VI-4

Outline of Assembly Procedure for Design No. 3\*

Position the lower dish section of the room temperature vessel on the foundation (reference: Figure VI-8a).

Mount the low heat leak support columns in the section (reference: Figure VI-8a).

Apply superinsulation to the inside surface of the room temperature vessel (reference: Figure VI-8a).

Apply superinsulation to inside surface of lower radiation shield dish and mount on support columns (reference: Figure VI-8b).

Lift the main gravitational support structure into place on support columns and fasten (reference: Figure VI-8c).

Stack loosely assembled transverse support beams and tension rods on gravitational support structure (reference: Figure VI-8d).

Preassemble the two coil/LHe vessels and attractive em load support spacers. Lift and lower into position between transverse support beams onto pivot shafts. Also interconnect coils electrically at lower end (reference: Figure VI-8d).

Sequentially position transverse support beams and tighten tension rods (reference: Figure VI-8e).

Connect initial fill lines to initial fill port

Apply superinsulation to outside of cylindrical outer radiation shield and then lift and position over assembly onto lower radiation shield dish. Bolt at periphery and connect tracer tubes (reference: Figure VI-8f).

Apply superinsulation to outside of bore tube radiation shield. Lower into bore. Bolt at lower end and connect tracer tubes (reference: Figure VI-8f).

Position LHe holding tank and power lead assembly. Complete power lead and fill connections to coil/LHe vessels (reference: Figure VI-8f).

Apply superinsulation to inside of upper radiation shield dish. Lower into position. Bolt and connect tracer tubes at periphery, at bore, and at power lead assembly. Lower warm bore tube into position and support at upper end. (reference: Figure VI-8g).

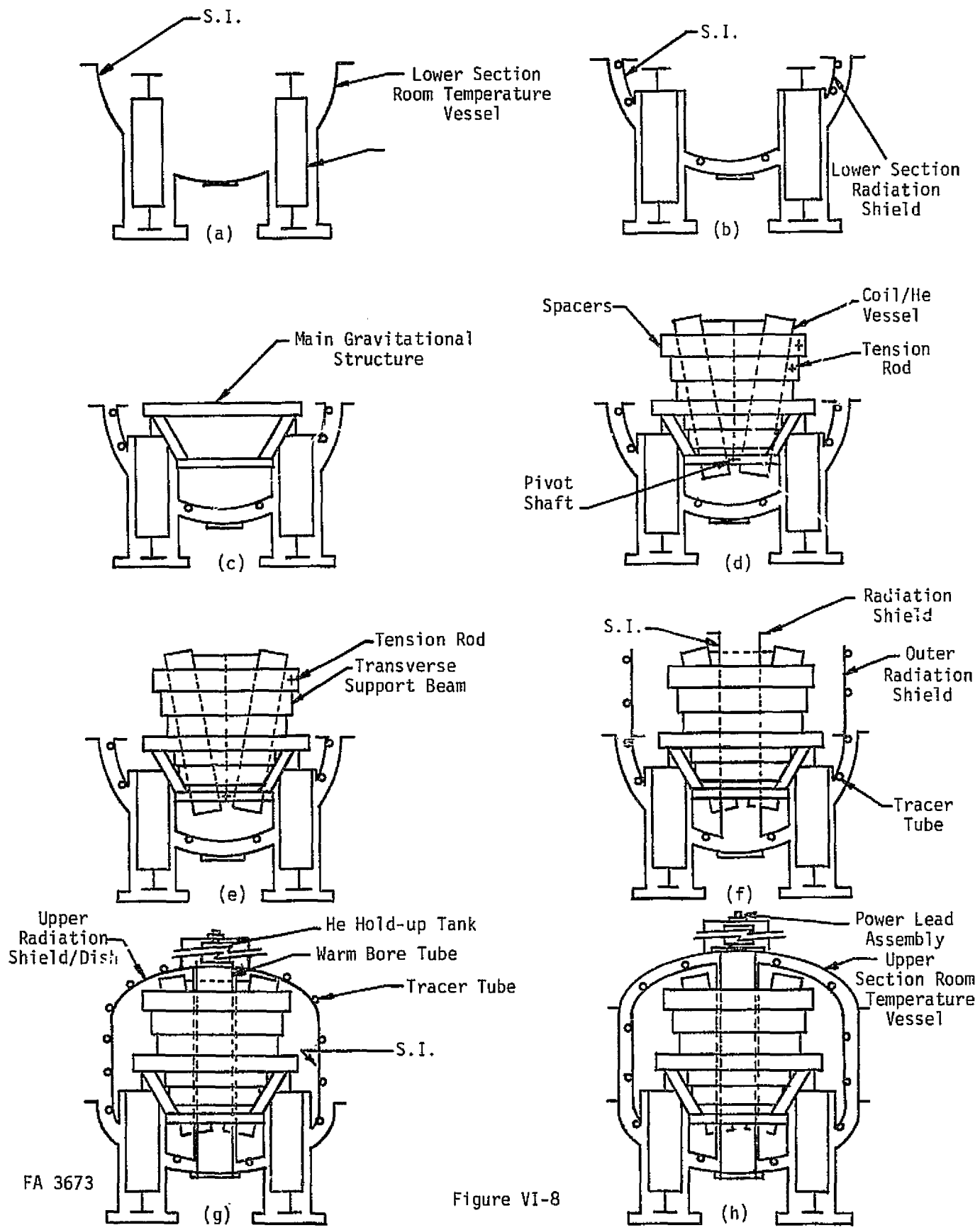
Apply superinsulation to inside of room temperature vessel subassembly consisting of cylindrical shell, upper dish, and power lead housing. Lift and lower into position onto lower dish and bolt. Complete vent port assembly via access ports (reference: Figure VI-8h).

---

\* Occasional reference to the assembly drawing, which is shown in Figure VI-6, will aid in visualization of the procedure.

Table VI-4 (Concluded)

Bolt upper room temperature dish to warm bore tube and weld lower end of bore tube to lower dish (reference: Figure VI-8h).



FA 3673

Figure VI-8

Assembly Sequence for Design No. 3

## B. WINDING GEOMETRY AND CONDUCTOR CHARACTERISTICS

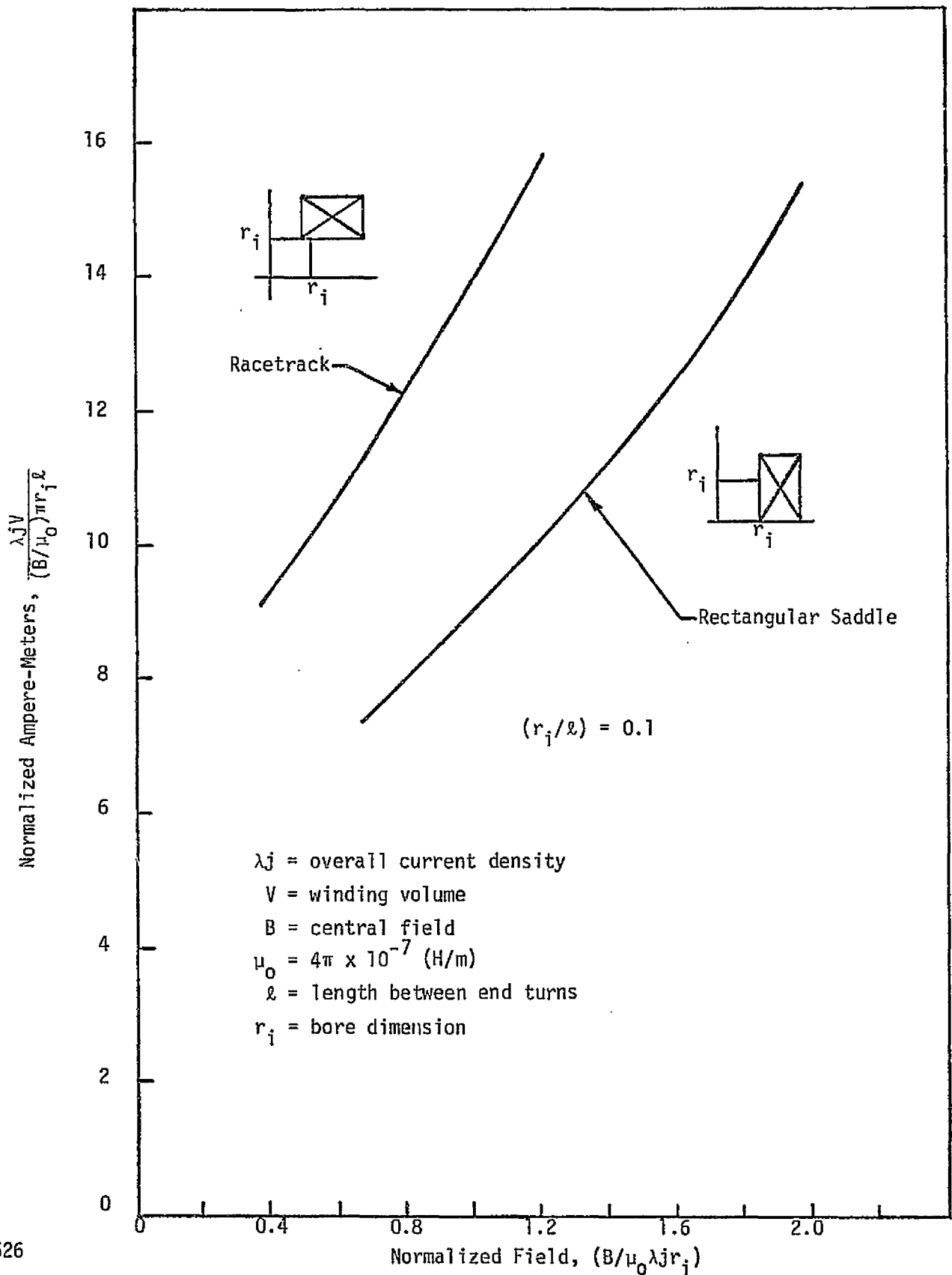
The rectangular saddle geometry was chosen to be carried through Phase II because of the relatively low cost estimate generated in Phase I in comparing candidate coil shapes. This arises primarily from the more efficient placement of the conductor in a saddle in terms of magnetic field production for a given number of amp-turns or amp-meters. The effect is illustrated in Figure VI-9, which is a plot in normalized form of dimensionless ampere-meters vs. dimensionless magnetic field for the racetrack and saddle geometries for magnets with bore dimensions which do not vary with length. The inserts on the figure define the geometric variable  $r_i$  as the distance from channel axis to winding. "B" is the desired magnetic field on axis, " $\ell$ " the distance between coil end turns, and " $\lambda j$ " the overall current density. It is clear that the rectangular saddle requires less ampere-meters than the racetrack for any given  $r_i$ , B,  $\lambda j$ , and  $\ell$ . The figure was calculated for a specific value of  $(r_i/\ell)$ ; however, the trend between geometries is essentially the same for all relatively long systems.

A drawing of one quadrant of the rectangular saddle winding used in Design No. 3 is illustrated in Figure VI-10. The winding envelope is shown as well as the location of the warm bore and channel. At the level of overall current density utilized, the winding cross section extends above the level of the bore. An option exists, therefore, to design each of the windings in the system either as: (1) a single rectangular saddle where all turns must be bent up and over the channel in the end turn regions or (2) a pair of coils consisting of a racetrack nested within a saddle. The latter was chosen (see Figures VI-1 and VI-2) since the system size will require modular coil fabrication and since it requires slightly less conductor than the first option. The racetrack is formed from those turns in the cross section (see Figure VI-10) which are high enough to be passed directly over the bore tube without first being bent up; the saddle is formed from those turns which lie alongside the bore tube. The system is, strictly speaking, a hybrid consisting of both racetracks and rectangular saddles; however, it will be referred to as the latter to avoid confusion with systems 1 and 2 which consist of racetracks alone.

The process of winding design for system 3 was iterative and similar to that used for Design Nos. 1 and 2. The starting point was again the set of coil dimensions and uniform overall current density found in Phase I for the 8 T, 4.2 K rectangular saddle with iron. The design proceeded through a process of grading which was again limited to a small number of different conductor sizes.

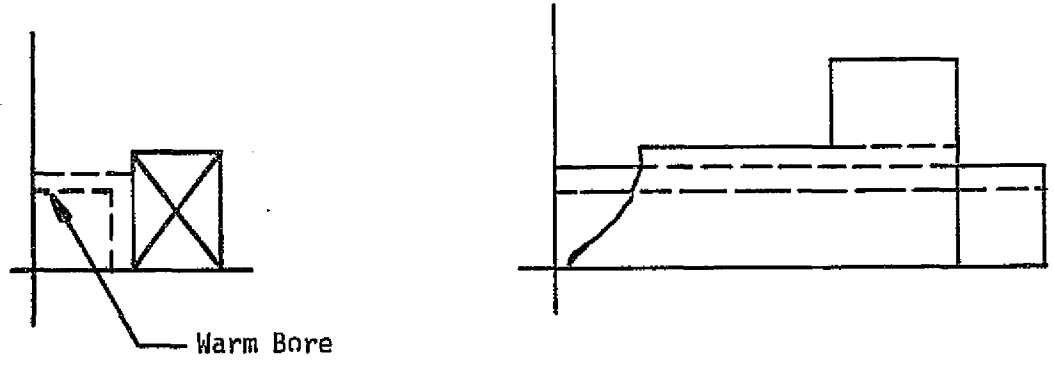
The manner in which the conductor and internal structural support is utilized in the rectangular saddle design is illustrated in Figure VI-11. Final dimensions are given for a transverse section of the winding and the end turn region. The racetrack has been divided into two regions which use two different conductors (regions "A" and "B"), each of which is 0.0254 m (1 in.) wide. The rectangular saddle uses the same 0.0127 m (0.5 in.) wide conductor throughout. Further grading may be found to be desirable during the detail design phase.

As indicated in Figure VI-11, the design assumes that the conductor will be insulated via a 60 percent coverage of spiral wrap insulation. The conductor is wound in parallel with and nested in a stainless steel channel section. The sides of the channel are sized to prevent turn to turn load accumulation

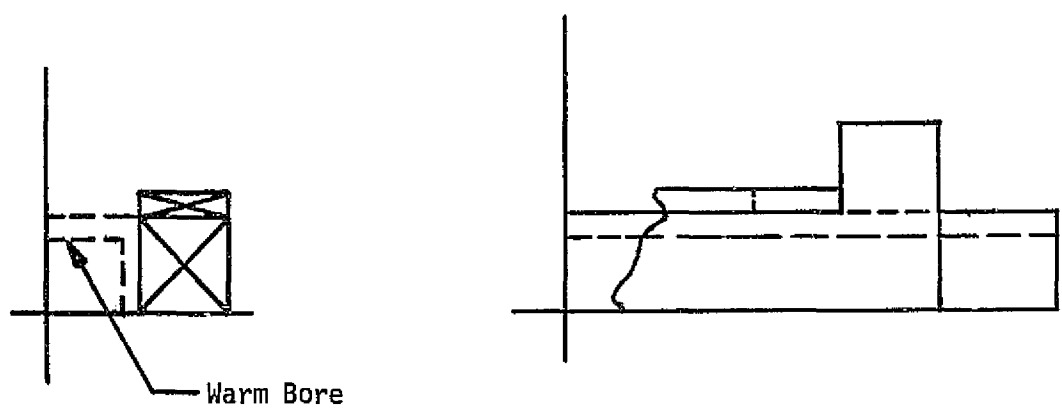


FA 3626

Figure VI-9 Normalized Amp-Meters Vs. Normalized Field for Optimized Racetrack and Rectangular Saddle Winding Geometries



Option 1 - Bend All Turns Up and Over the Bore Tube

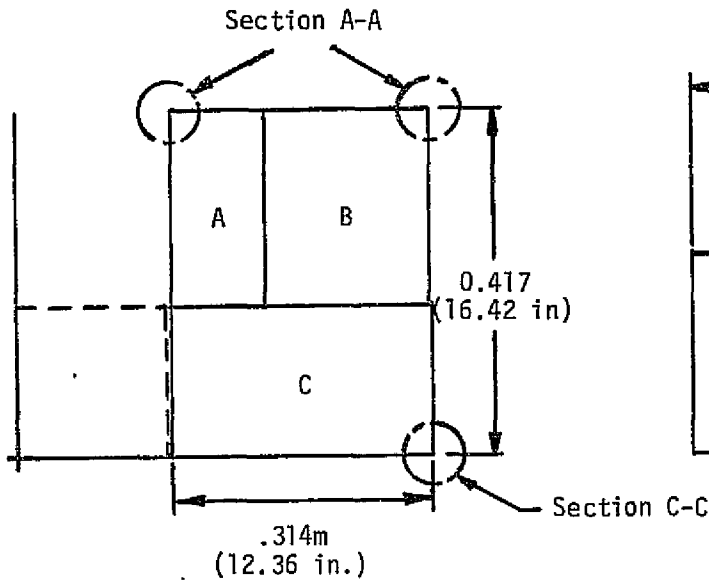


Option 2 - Racetrack Nested in Saddle

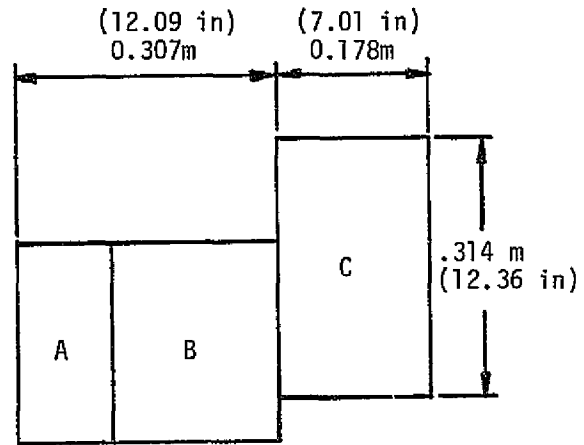
Figure VI-10

Comparison of Optional End Turn Configuration for a Rectangular Saddle

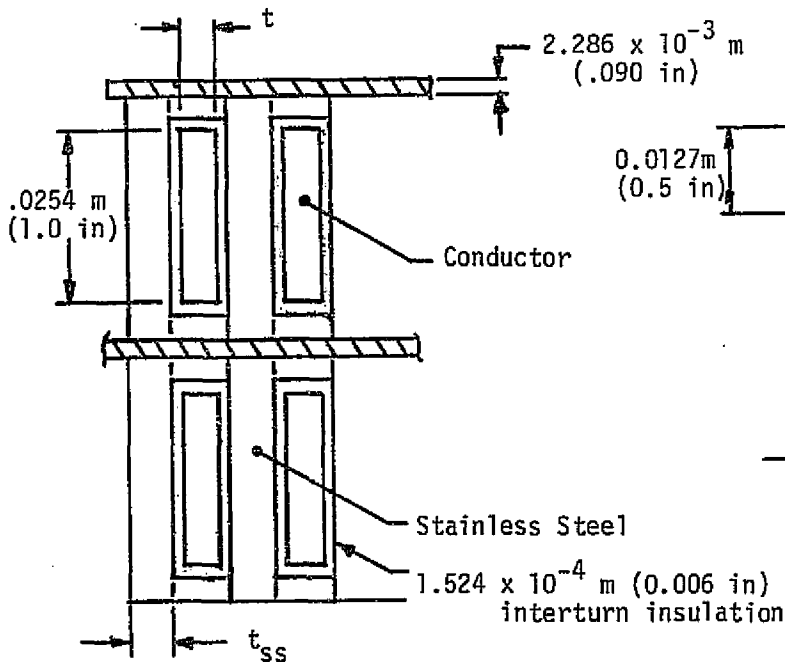
Transverse Cross-Section



End Turn Region Cross-Section



Section A-A



Section C-C

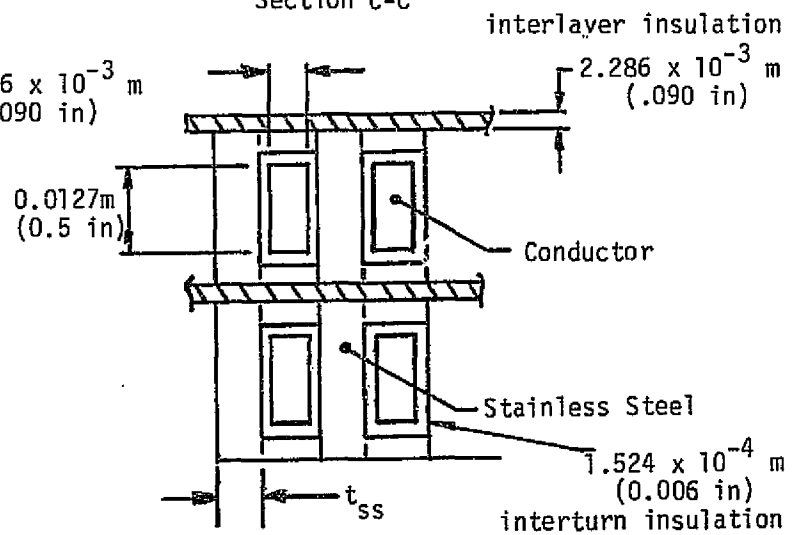


Figure VI-11

Winding Final Dimensions and Cross-Sectional Detail for Preliminary Design No. 3.



perpendicular to the wide face of the conductor. The stainless steel channel sides are also intermittent to allow for helium circulation around each conductor. Epoxy fiberglass slats are used between layers (60 percent coverage) to allow for helium circulation and to act in conjunction with the back of the stainless steel channel to prevent turn to turn load accumulations parallel to the wide face of the conductor.

The dimensional characteristics of the three conductors and required stainless steel banding are given in Tables VI-5 and VI-6. Conductors were designed to be cryostatically stable at 4.2 K according to criteria discussed in Appendix B. The size was also based on the maximum field experienced in the winding sections in which it was utilized.

Figure VI-12 shows a cross section of the winding for Design No. 3 in the end turn region. The solid lines indicate the winding boundary assumed for field computation purposes to provide input information to size conductor. The dashed lines show the "final" winding boundary for Design No. 1 on the basis of the conductor and steel chosen as a result of the previous step. The next step in the iterative design process would be to recompute the field distribution in the new winding envelope and re-grade the conductor. This process would be continued in the final design phase.

The model used for field calculations in the windings for Preliminary Design No. 3 is shown in Figure VI-13, which is a cross section of the nested racetrack/saddle in the midplane ( $Z=0$ ) of the end turn region. The location of the iron is shown as well as the 12 current filaments used to model the coil to generate the field profiles for use in grading studies. As discussed earlier, the field may be expected to be overestimated at points adjacent to current filaments and underestimated at points between filaments. However, the model is suitable for preliminary design purposes and may be expected to provide a reasonable field estimate if values at adjacent points are averaged and applied midway between the points used. For this preliminary design the peak field search was limited to the  $Z=0$  plane shown, a transverse section close to the ends, and a plane ( $Z = 0.192$  m) just inside the curve of the end turns. Peak field concentration ratios for the latter are the most severe and are shown in Figure VI-14. A graph of the variation of the peak field concentration ratio along several lines through the section at  $Z = 0.192$  is shown in Figure VI-15. A similar plot is given in Figure VI-16 for a plane in the transverse section close to the end turn region at the high field end. Note that the fields experienced by the winding in this section are somewhat lower. In the final design phase a more extensive search should be performed, and a model with more filaments would be used. Results, however, would not be expected to substantially alter the conclusions reached in this preliminary design effort.

Following specification of the coil and conductor characteristics, a preliminary investigation into the quench characteristics for magnet design no. 3 was begun. The model used was described earlier relative to Design No. 1 (see Figure IV-14 and the related text). Results were somewhat more favorable than with Design No. 1 primarily because the rectangular saddle of Design No. 3 has a lower stored energy than the racetrack of Design No. 1 and, therefore, less energy to be dissipated during a quench. Results of the quench calculations

Table VI-5

Estimated Conductor Requirements for Design No. 3;  $q = 0.7 \text{ W/cm}^2$

<u>Conductor Type</u>	<u>Region Where Used</u>	<u>Conductor Thickness m (in.)</u>	<u>Conductor Width m (in.)</u>	<u>Copper Superconductor</u>	<u>Length (m)</u>	<u>Weight (kg)</u>
1	A	$2.62 \times 10^{-3}$ (0.103)	.0254 (1.0)	8.2	2,717	1,519
2	B	$2.13 \times 10^{-3}$ (0.084)	.0254 (1.0)	12.9	6,396	3,025
3	C	$4.57 \times 10^{-3}$ (0.18)	.0127 (0.5)	24.9	<u>10,452</u>	<u>5,226</u>

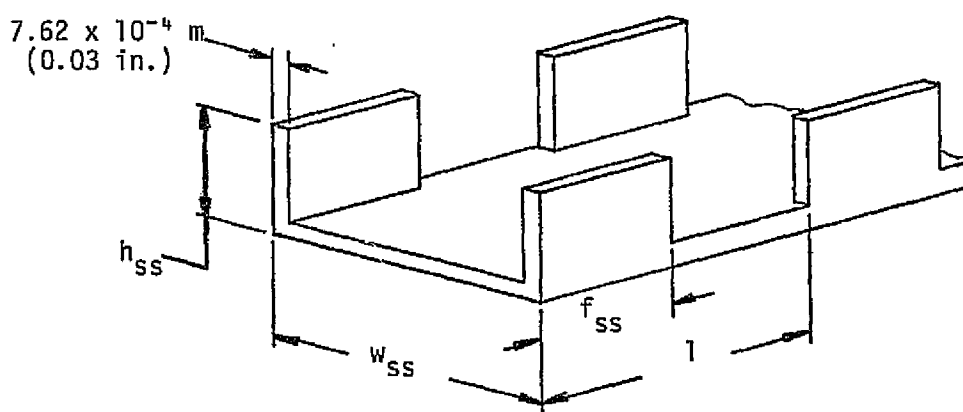
Total Length = 19,565

Total Weight = 9,770

Table VI-6

Internal Structural Requirements for Design No. 3

$q = 0.7 \text{ W/cm}^2; f_{ss} = 0.6$



<u>SS Type</u>	<u>Region Where Used</u>	$w_{ss}$ <u>m (in.)</u>	$h_{ss}$ <u>m (in.)</u>	<u>Length (m)</u>	<u>Weight (kg)</u>
1	A	0.0272 (1.072)	$3.68 \times 10^{-3}$ (.145)	2,717	495
2	B	0.0272 (1.072)	$3.2 \times 10^{-3}$ (.126)	6,396	1,145
3	C	0.0145 (0.572)	$5.64 \times 10^{-3}$ (.222)	<u>10,452</u>	<u>1,265</u>

Total Length = 19,565 m

Total Weight = 2,905 kg

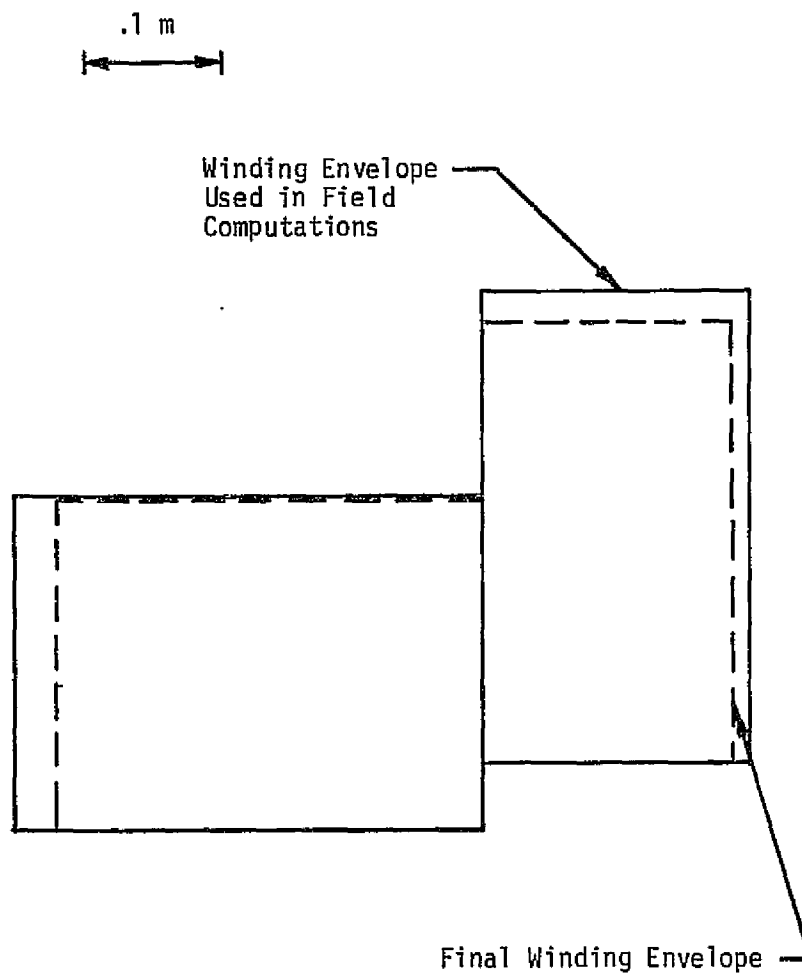
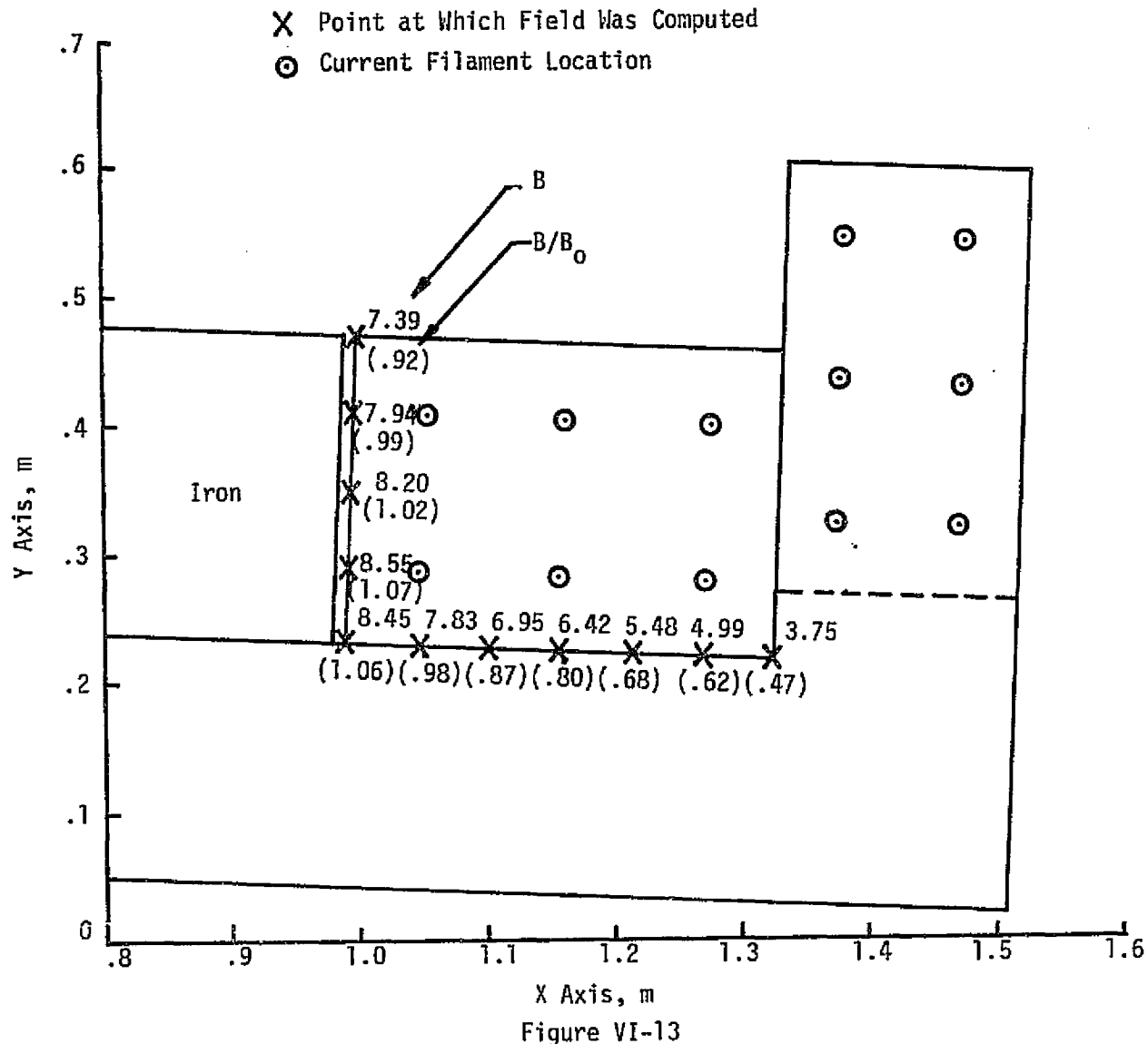


Figure VI-12

Cross-Section of Coil End Turn Showing Initial Winding Envelope for Field Computations and Final Winding Envelope Based on Selected Conductors.



Cross Section of Coil at High Field End Showing Current Filament Location for Peak Field Search and Field Magnitudes at Selected Points in the End Turn Midplane (Z = 0.0) for Design No. 1

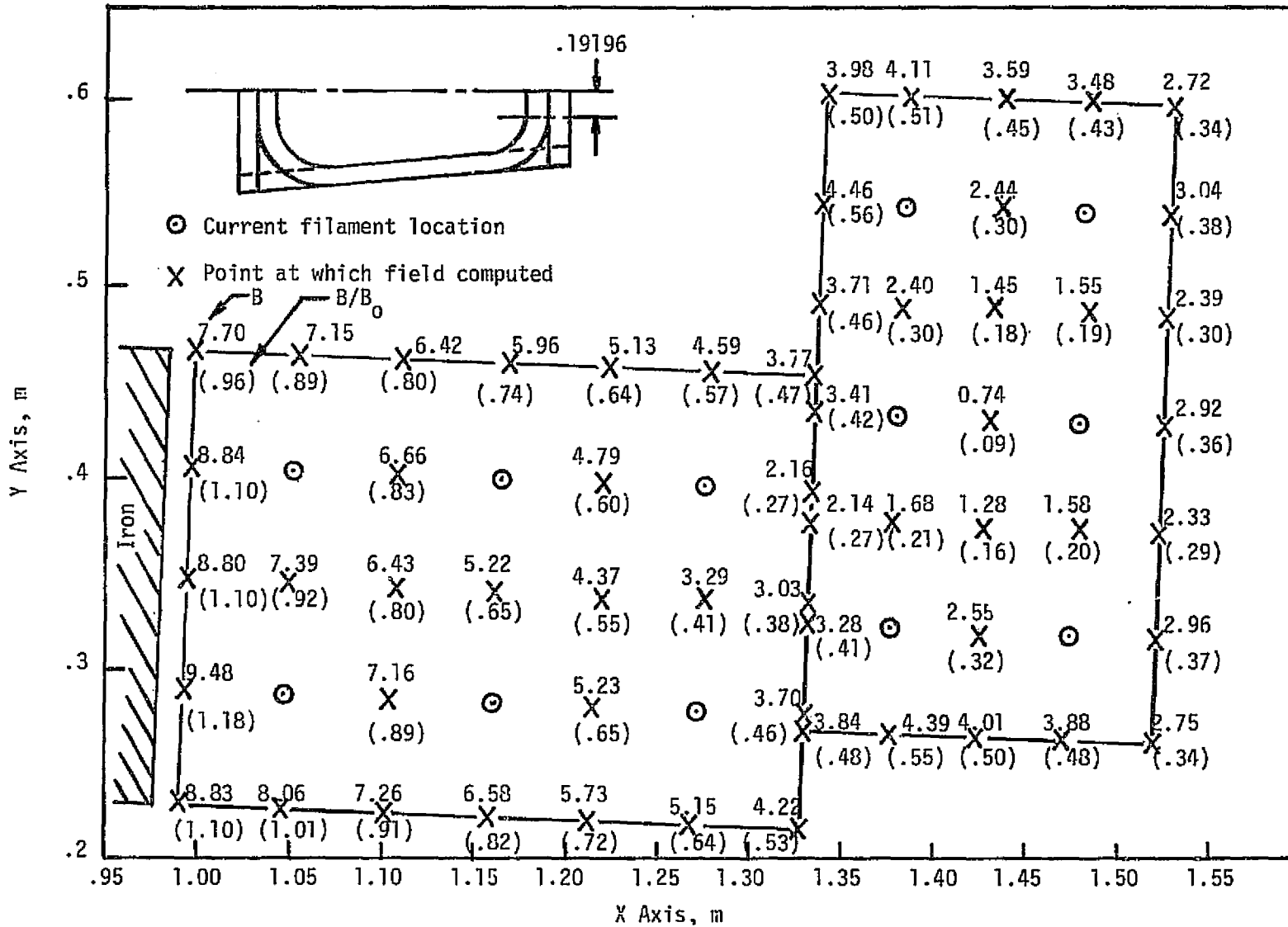


Figure VI-14. Computed Values for Field and Field Concentration Ratio in a Selected Plane in the End Turn Region for Preliminary Design No. 3 (Z = 0.192)

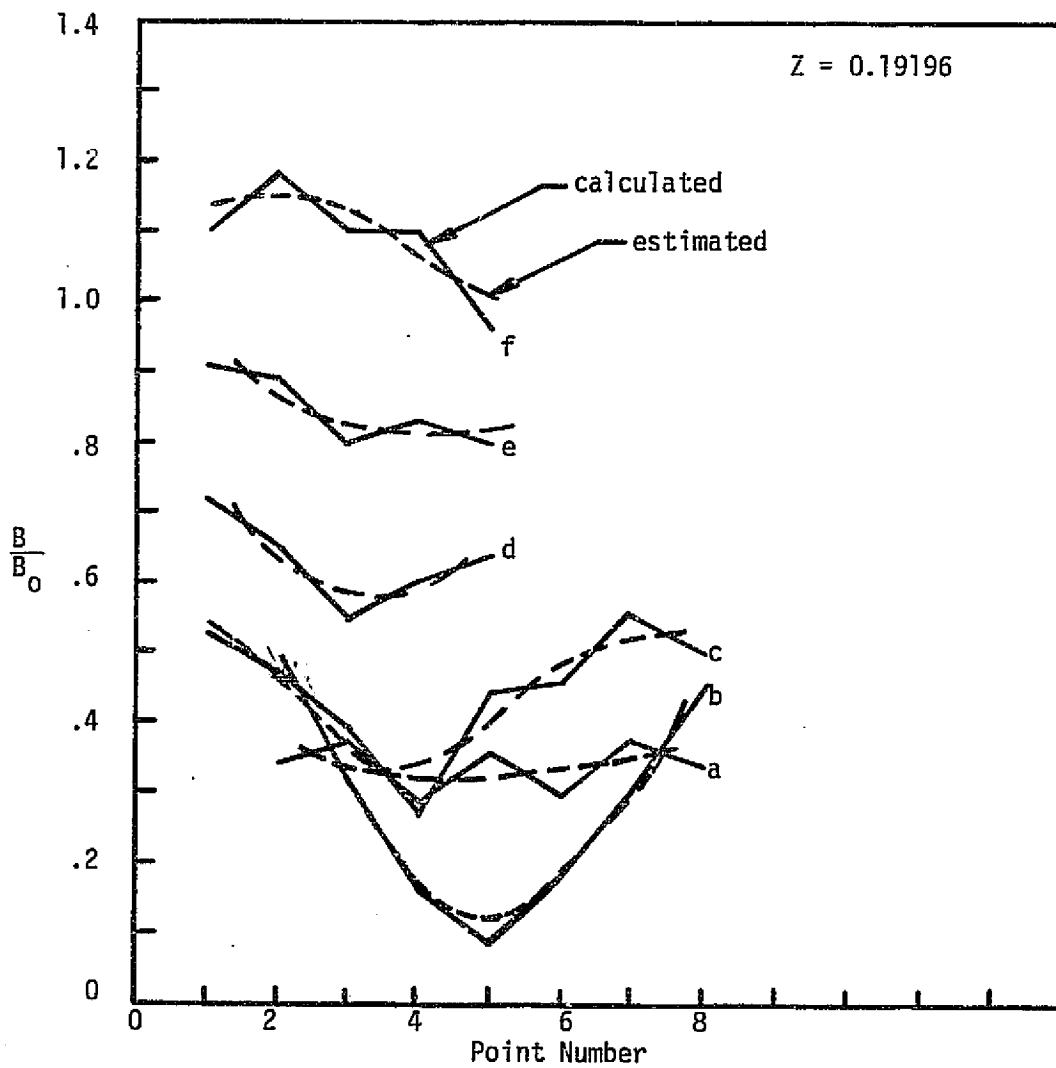
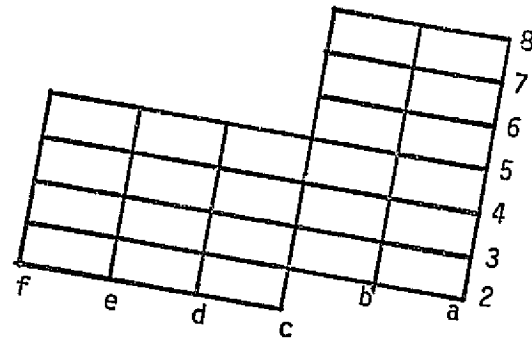
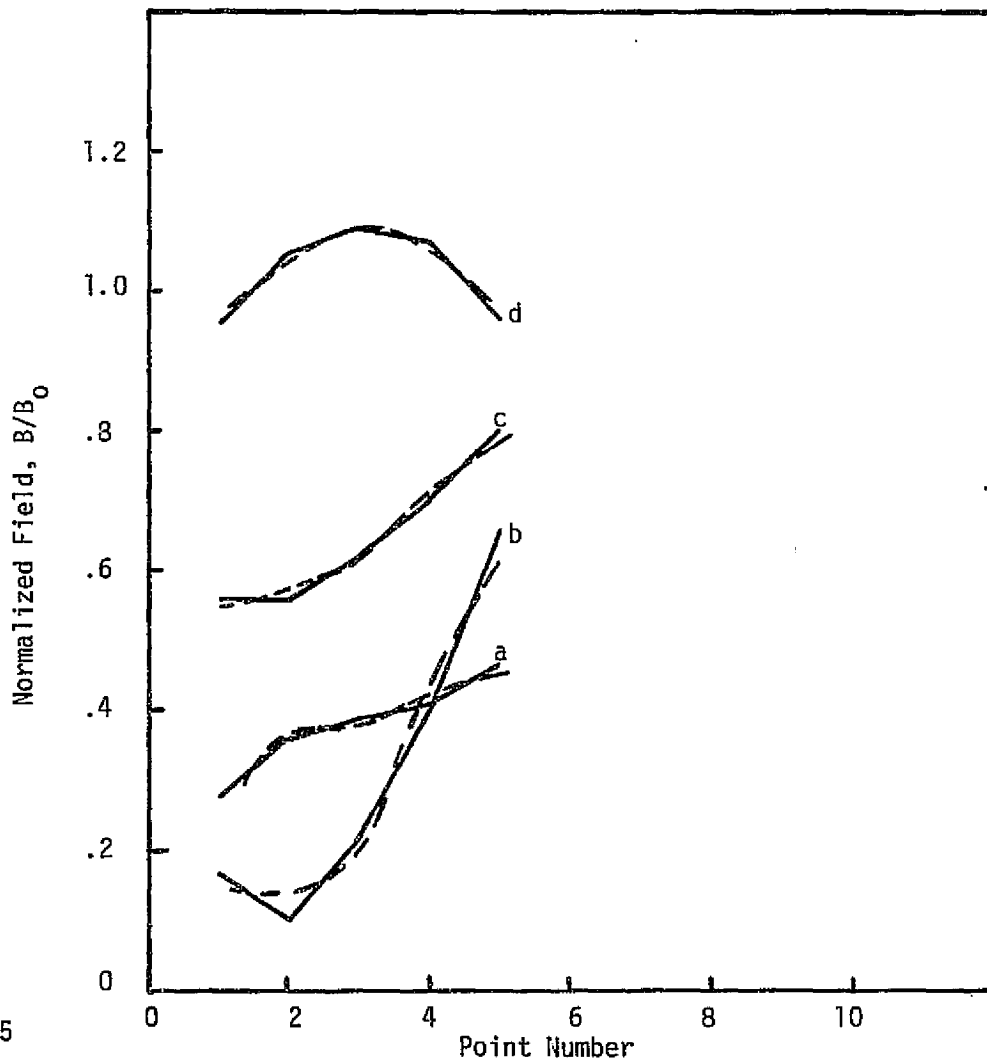
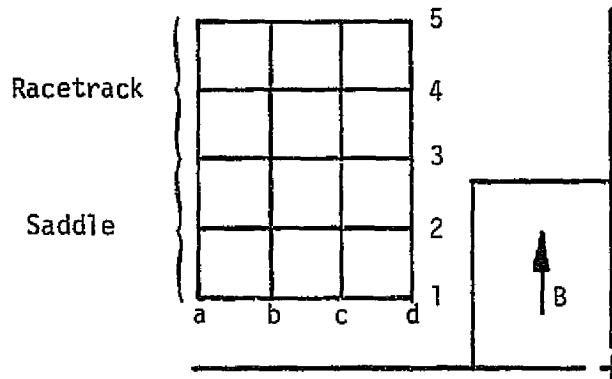


Figure VI-15. Variation of Field Concentration Ratio Along Several Lines Through the Winding in the  $Z = 0.192$  Plane in the End Turn Region



FA 3645

Figure VI-16. Variation of Field Concentration Ratio Along Several Lines Through the Winding in a Transverse Section Close to the End Turn Region



are shown in Figures VI-17 through VI-19 for two values of the dump resistor and are summarized in Table VI-7. These estimates indicate that layer to layer and terminal voltages are somewhat more favorable than with Design No. 1 and that a simple protection circuit involving a dump resistor value of about 0.25 to 0.50  $\mu$  will probably be adequate for quench protection. More detailed analysis will be required during specification of the protection system following a detail design phase.

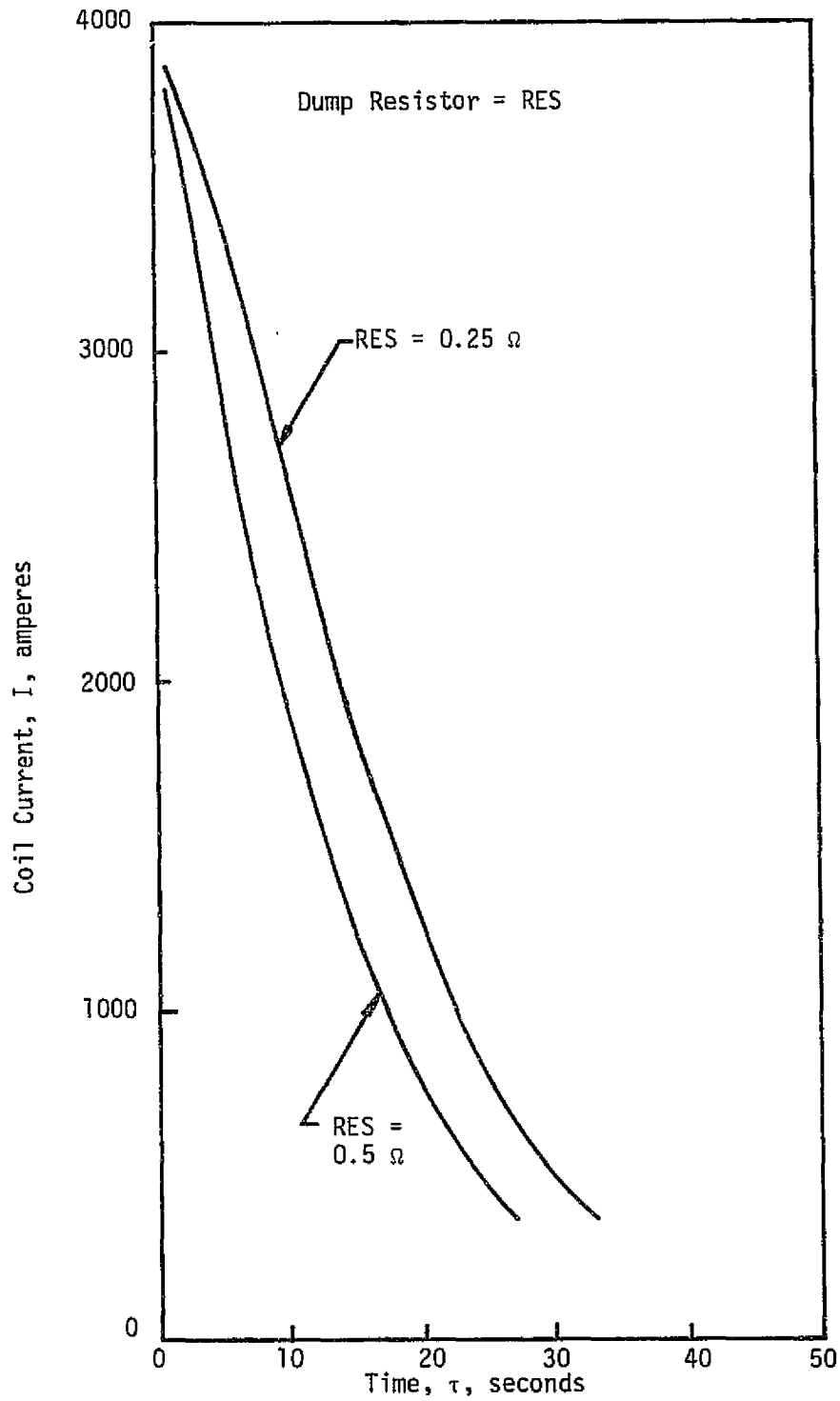


Figure VI-17

Computed Current Vs. Time During Quench Transients for Preliminary Design No. 3

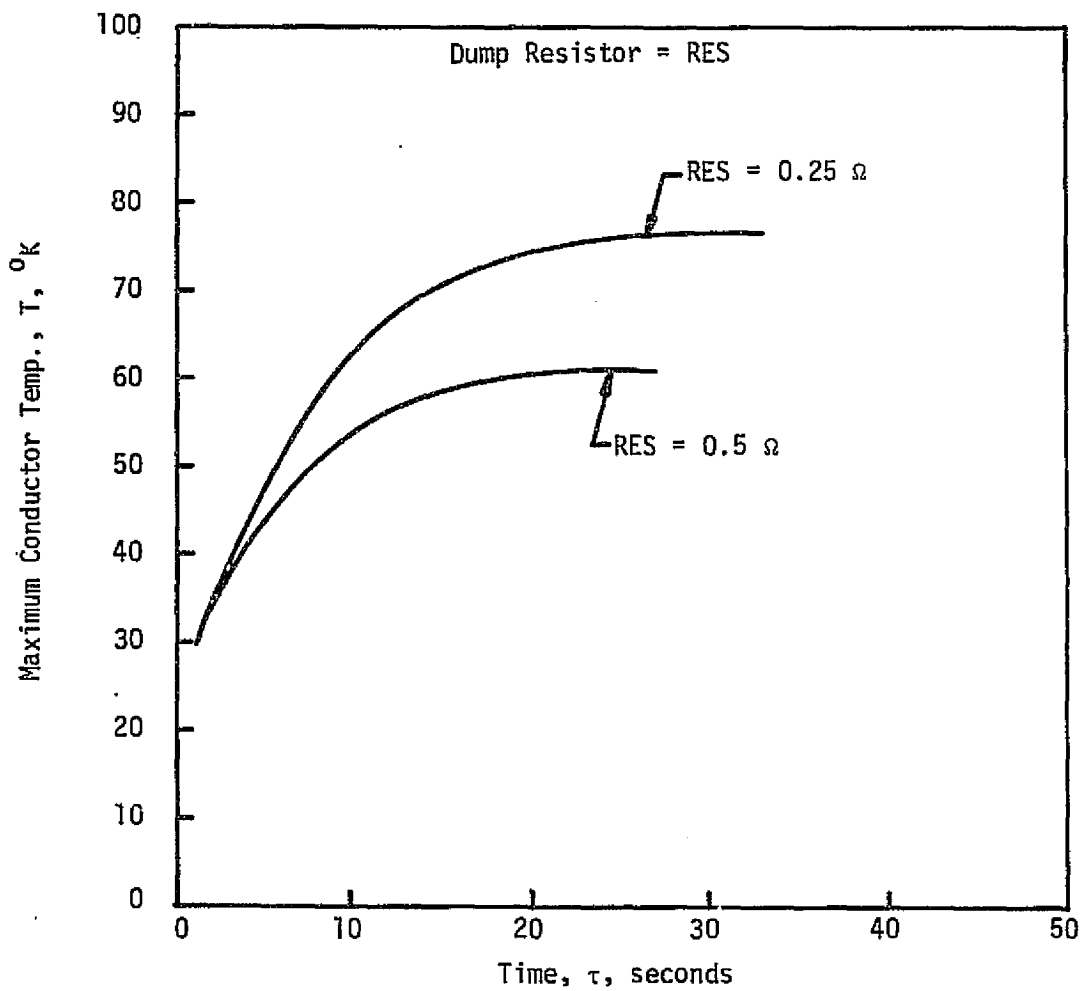


Figure VI-18

Computed Maximum Conductor Temperature Vs. Time for Preliminary Design No. 3 Quench Simulation

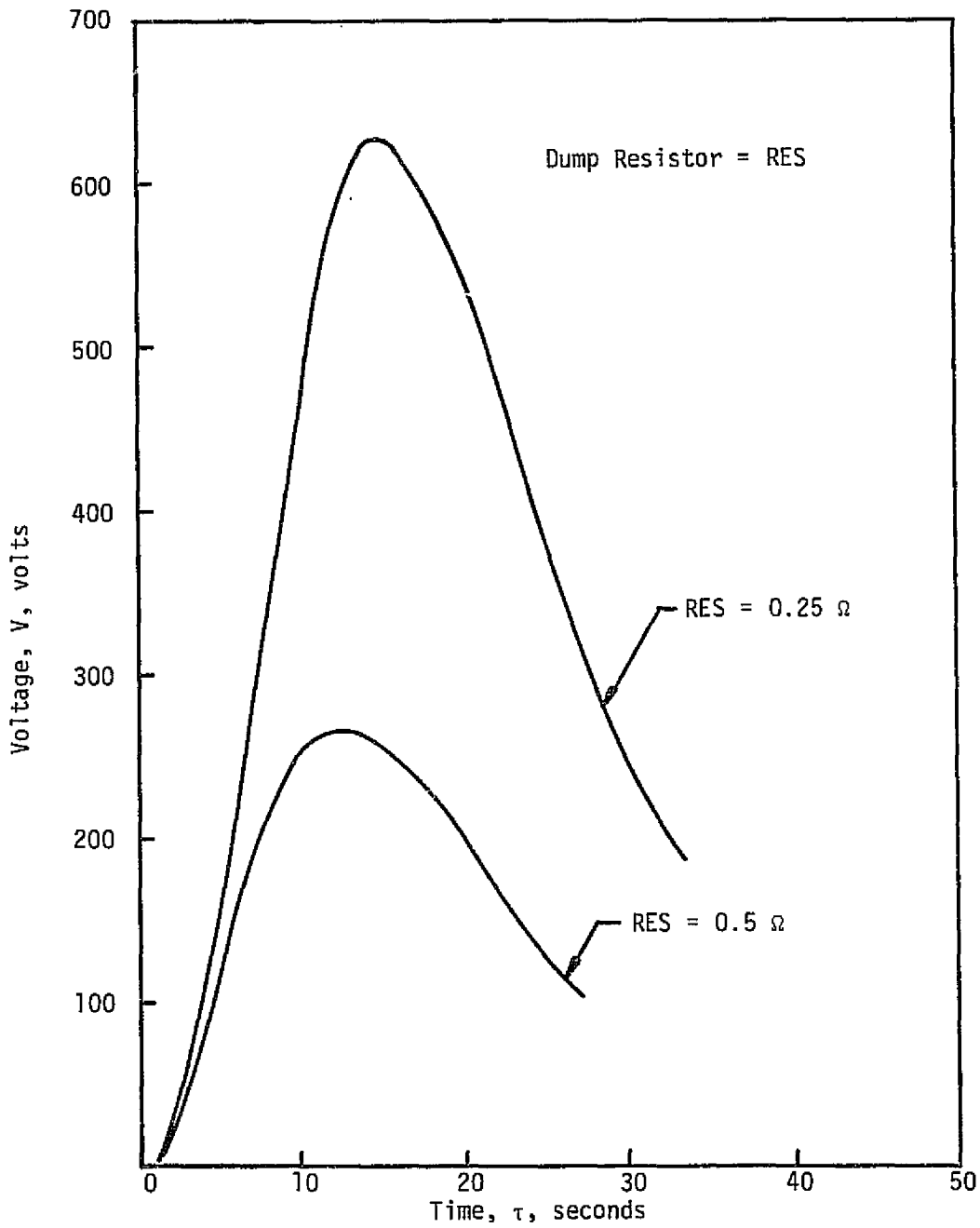


Figure VI-19

Computed Conductor Voltage Across Normal Region During Quench Transient for Preliminary Design No. 3

Table VI-7

Summary of Estimated Quench Characteristics for Design No. 3

<u>Dump Resistor (<math>\Omega</math>)</u>	<u>Decay Time Constant (sec)</u>	<u>Maximum Temperature (<math>^{\circ}</math> K)</u>	<u>Maximum Voltage Across Normal Region (V)</u>	<u>Maximum Voltage At Coil Terminals (V)</u>
.25	19.09	77	615	1000
.50	11.83	61	265	2000

## C. STRUCTURE AND DEWAR DESIGN

This section discusses the components of the structure and dewar for System No. 3 and the design criteria on which the design was based. The method for calculation of applied forces, as discussed in Section IV-C for Design No. 1, can be directly applied to Design No. 3 as well, and therefore, only the results of the em load computations, including a sketch of the current filament model which was used in the analysis, are presented in this section.

### 1. em Forces

The current filament location used for force computation in this preliminary design is illustrated in Figure VI-20. This is again a coil cross section in the end turn region in the  $Z=0$  plane. Forces of electromagnetic origin for the purposes of this preliminary design were computed using four current filaments in each coil. The amp turns for each filament are indicated. Two views of the current sticks for the model are given in Figures VI-21 through VI-25 together with force vectors drawn to scale to illustrate the load distribution and magnitude at rated field.

The force components parallel to the X axis are the axial load components on the coils and for this design are supported by the coil/He vessel, while the Z axis force components are called the transverse load components on the coils and for this design are supported by the straight beams and tension rods. The Y axis force components are the attractive components between coils and are supported by wedge-shaped spacers.

### 2. Structure Description and Design Criteria

A summary of the mechanical characteristics of the structural components for Design No. 3 is given in Table VI-8. This gives the design pressure, weights, materials, and overall sizes of the major structural components of the magnet system which includes the coil/He vessel, the support spacers for the attractive em loads, the main gravitational support structure, and the straight beams and tension rods. The design was based on a maximum allowable working stress of  $2.75 \times 10^3 \text{ N/m}^2$  (40,000 psi) which was based on a margin of safety of two (2) applied to the allowable yield strength of the 310S stainless steel material.

#### a. Winding Internal Structure

The internal structure for Preliminary Design No. 3 consists of the stainless steel channel section which encloses each turn as described earlier. Estimates indicate that the conductor alone would be able to mechanically withstand the bearing stress due to em load accumulation in the windings. However, for the purposes of preventing the onset of instability due to conductor motion, the stainless steel was included to collect and transmit the loads through the winding to the external structure and thus prevent turn to turn load accumulation on the conductor.

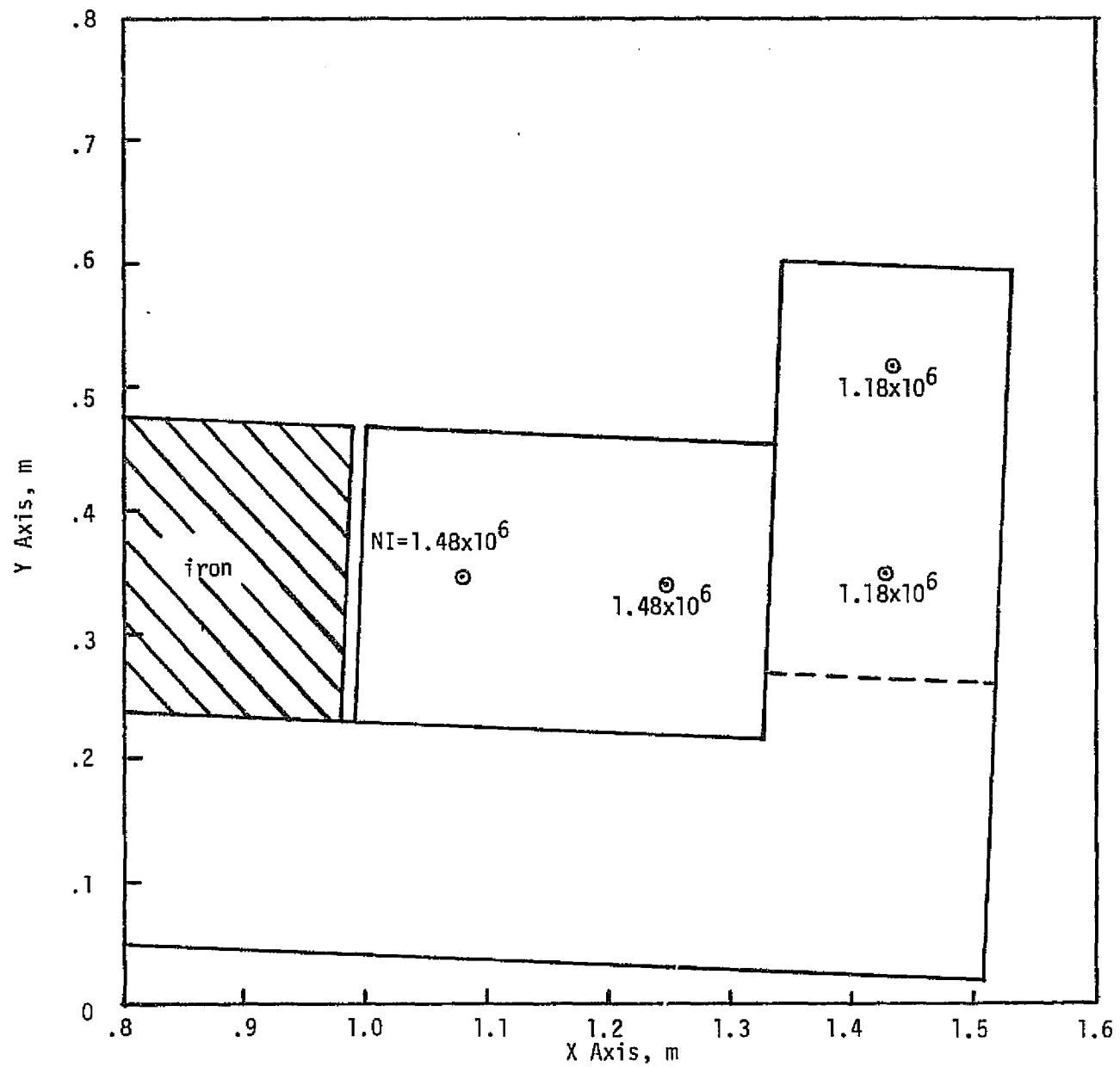


Figure VI-20. Location of Current Filaments in Winding Section in End Turn Region for Design No. 3.

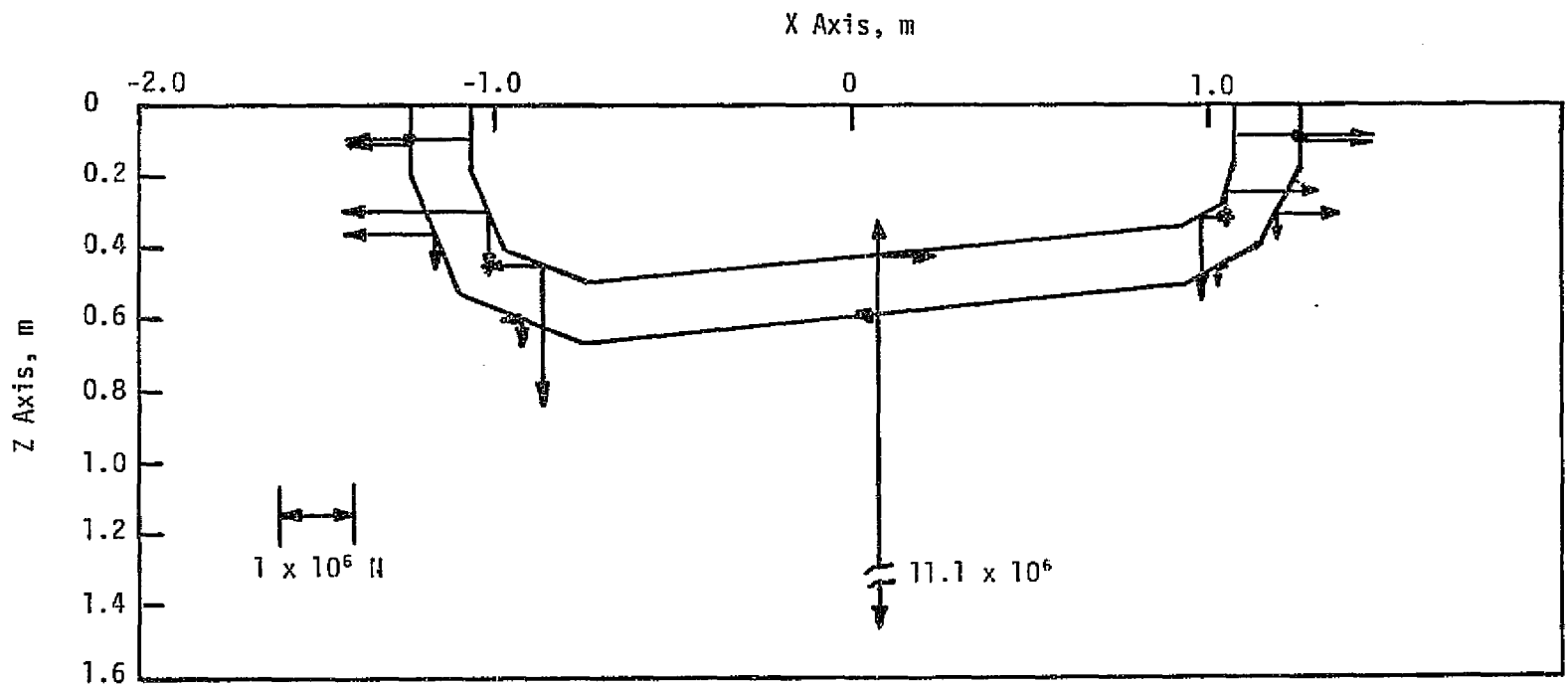


Figure VI-21

Top View of the Two Current Filaments which Represent One Half of the Upper Racetrack. Also Shown Are Electromagnetic Force Components on the Racetrack Parallel to the X and Y Axes.



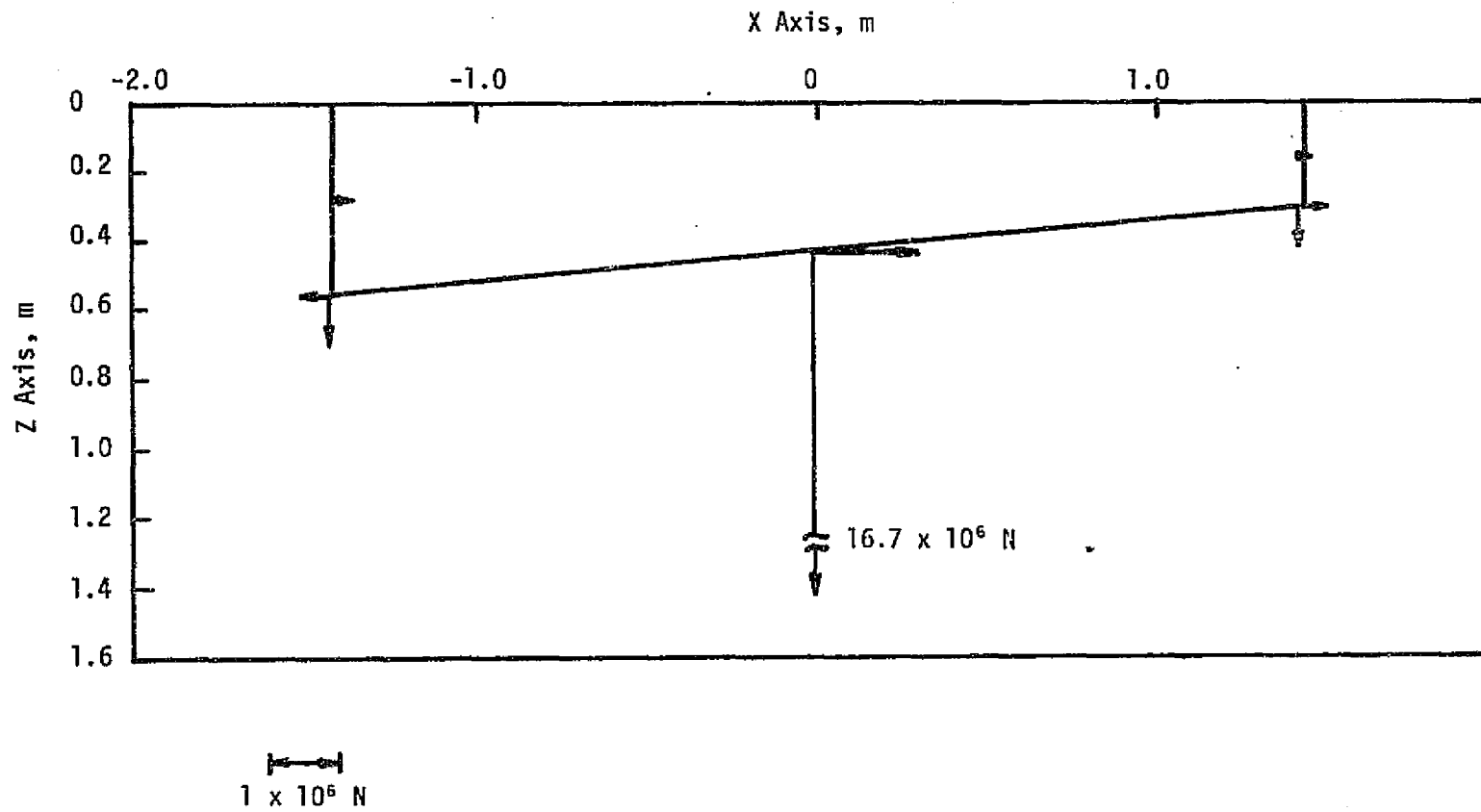


Figure VI-22

Top View of the Current Filament which Represents One Half of the Inner Section of the Upper Saddle. Also Shown Are Electromagnetic Force Components on the Filament Parallel to the X and Z Axes.

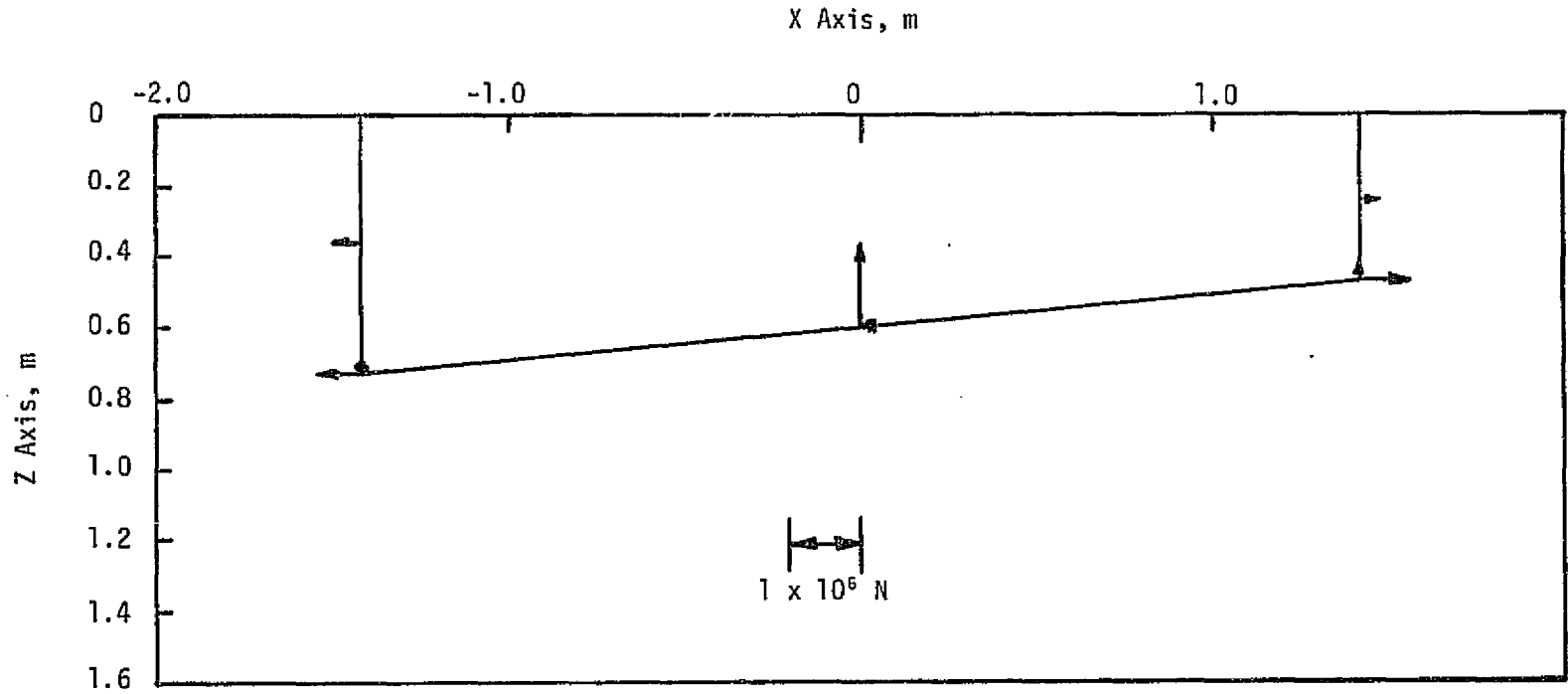


Figure VI-23

Top View of the Current Filament Which Represents One Half of the Outer Section of the Upper Saddle. Also Shown Are Electromagnetic Force Components on the Filament Parallel to the X and Z Axes.

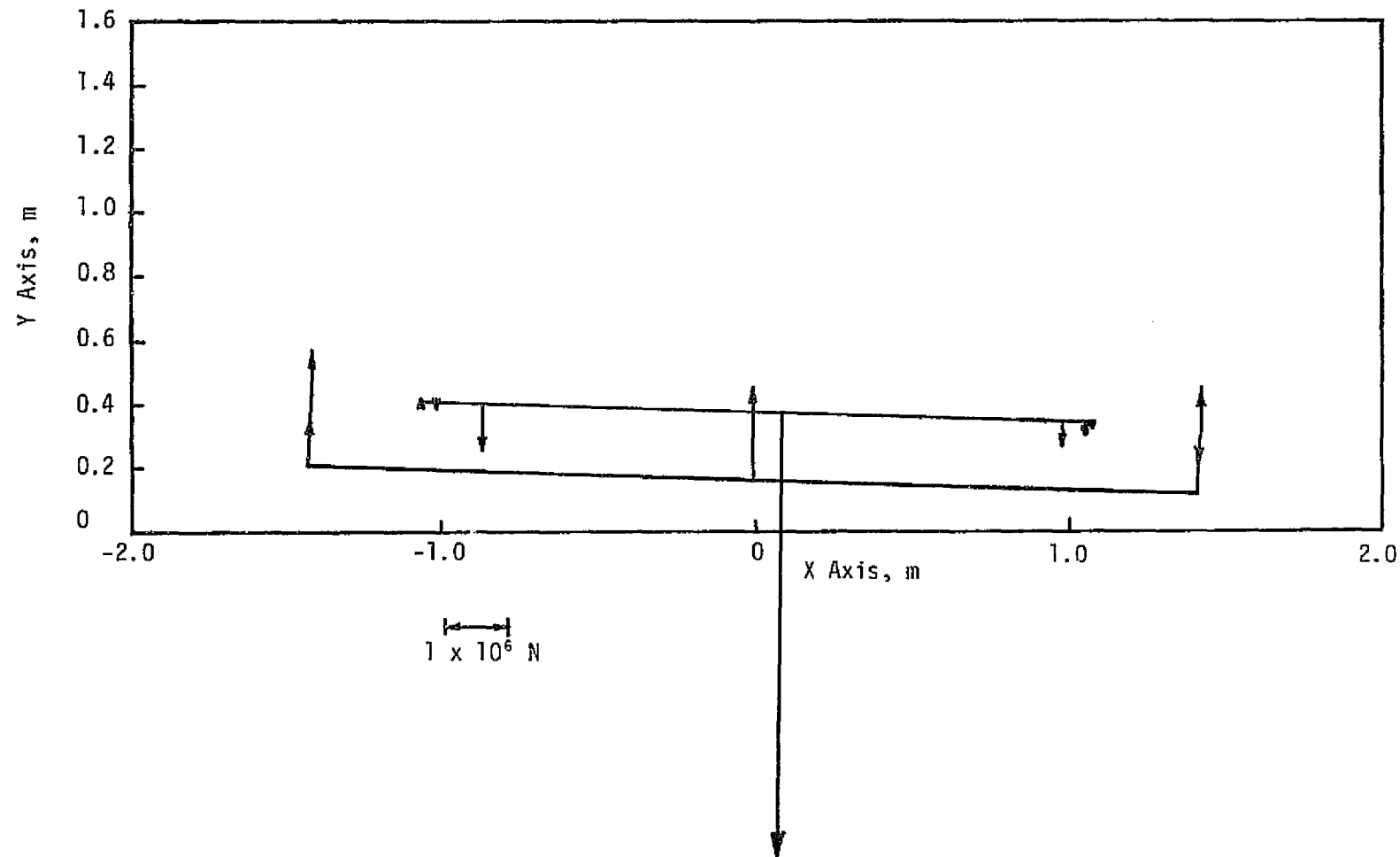


Figure VI-24. Side View of the Two Current Filaments which Represent One Half of the Inner Section of the Upper Racetrack and Saddle Coils. Also Shown Are the Electromagnetic Force Components on the Filaments Parallel to the Y Axis.

FA 3638

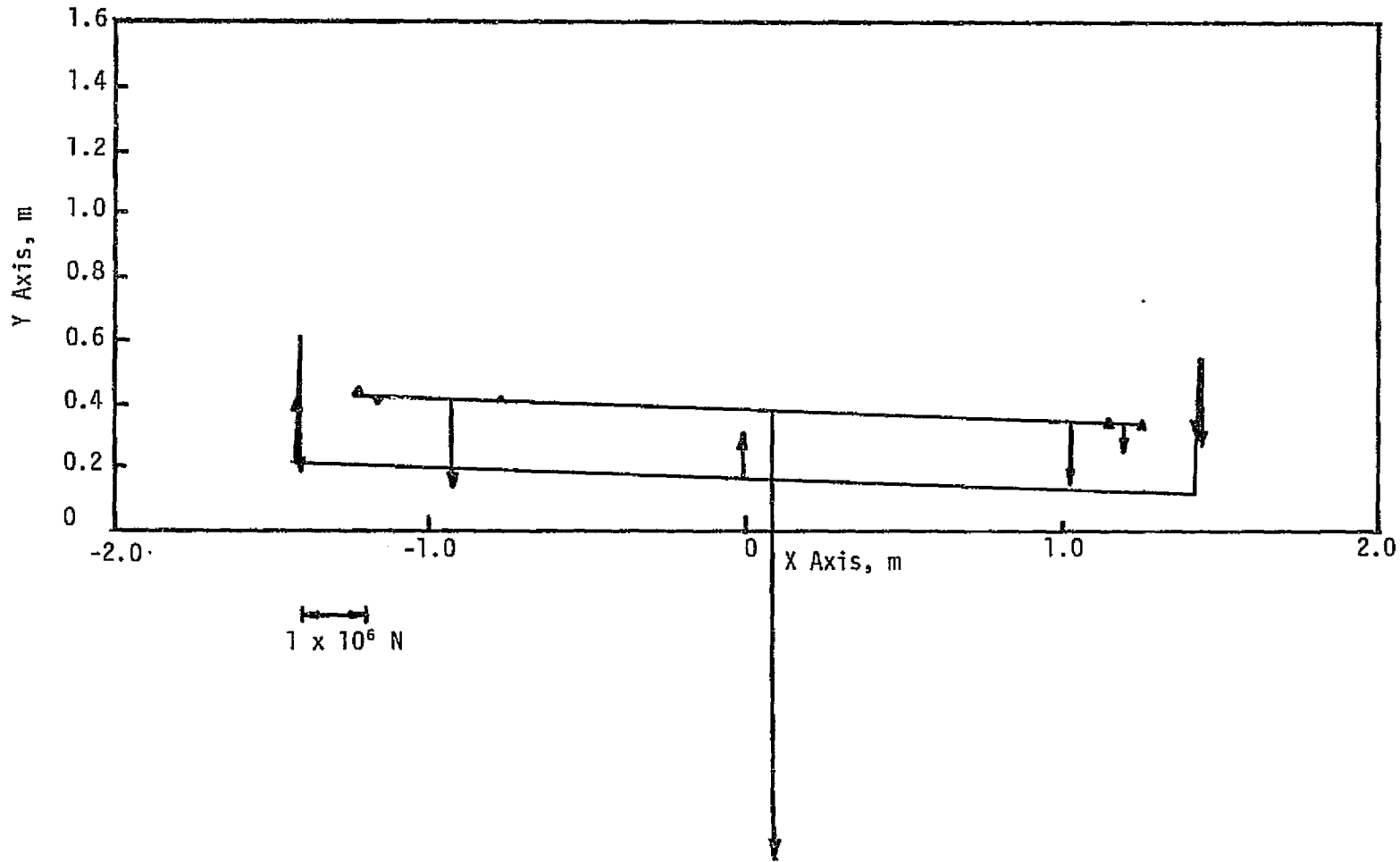


Figure VI-25. Side View of the Two Current Filaments which Represent One Half of the Outer Section of the Upper Racetrack and Saddle Coils. Also Shown Are the Electromagnetic Force Components on the Filaments Parallel to the Y Axis.

Table VI-8

Summary of Mechanical Characteristics of the Major  
Structural Components for Design No. 3

- I. Coil/He Vessel
  - A. Design Pressure
    - 1.  $2.07 \times 10^5 \text{ N/m}^2$  (30 psia) Internal
    - 2.  $1.03 \times 10^5 \text{ N/m}^2$  (15 psia) External
  - B. Weight
    - 1. Conductor = 9,770 kg (21,444 lbs.) (2)
    - 2. Iron = 10,350 kg (22,770 lbs.) (2)
    - 3. Structure = 14,545 kg (32,000 lbs.) (2)
    - TOTAL = 34,665 kg (76,264 lbs.)
  - C. Material
    - 1. Conductor = MF NbTi/Copper
    - 2. Iron = AISI 1008
    - 3. Structure = 310S SS
  - D. Overall Size of Each Vessel
    - 1. Length = 3.15 m (124 in.)
    - 2. Width = 2.44 m (96 in.)
    - 3. Height = .76 m (30 in.)
- II. Support Spacers for Attractive em Load
  - A. Weight = 734 kg (1,615 lbs.) ea; total = 2,936 kg (6,460 lbs.)
  - B. Material = 310S SS
  - C. Overall Size (each)
    - 1. Length = 2.74 m (108 in.)
    - 2. Width = 0.51 m (20 in.)
    - 3. Inlet Height = 0.10 m (4 in.)
    - 4. Outlet Height = .81 m (32 in.)
- III. Main Gravitational Support Structure
  - A. Weight = 3,455 kg (7,600 lbs.)
  - B. Material = 310S SS
  - C. Overall Size
    - 1. Length = 3.76 m (148 in.)
    - 2. Width = 3.50 m (138 in.)
    - 3. Height = .25 m (10 in.)
- IV. Straight Beams and Tension Rods
  - A. Total Weight = 9,655 kg (21,240 lbs.)
  - B. Material = 310S SS
  - C. Overall Size - varies (see assembly drawing, Figure IV-6)

#### b. Coil/He Vessel

The coil/He vessel contains the racetrack and rectangular saddle coils, iron pole piece, and LHe and is shaped in the form of a "U" which wraps around the warm bore tube. It also tapers along the "active" MHD channel length and maintains a constant clearance between itself and the bore radiation shield. Basically speaking, the coil/He vessel structure consists of top, bottom, and side plates which are fabricated from 310S stainless steel plate. Ribs are welded to the top plate for additional stiffness. The assembly and fabrication procedure of the coil/He vessel is as follows. After the sides and bottom have been welded together to form an open box structure, the saddle coils (which have previously been wound and tested) are first placed into the structure on epoxy-glass spacers, followed by the racetrack coil (which also has been previously wound and tested) which nests inside the end turns of the rectangular saddle coil. Shims of epoxy-glass material are added to ensure a tightly packed container. After this, the top cover is added and seal welded. After a thorough mechanical and electrical check, the coil/He vessel subassembly is ready for installation in the magnet system.

The coil/He vessel has been designed to withstand a maximum internal pressure of  $2.07 \times 10^5 \text{ N/m}^2$  (30 psia) which is the release pressure for pressure relief valves on the system and also has been designed to support the axial forces of the coil windings. In addition, the unsupported area of the bottom of the vessel which bridges the warm bore tube and bore radiation shield has been designed to withstand the em loads and the internal pressure. The bottom plate has also been sized to support the em loads exerted on it by the iron pole piece. Ribs are welded to the bottom of the vessel for additional stiffness and are tapered to correspond to the low gradient mode half-angle for the coils. "U" shaped supports are provided near the bottom of the coil/He vessel structure to accept the pivot shaft, which is an integral part of the main gravitational support.

#### c. Attractive em Load Support Spacers

Since the low gradient mode half-angle is built into the bottom of the coil/He vessels for this design, spacers to support the attractive em loads between coils are required for the high gradient mode only. For Design No. 3, one (1) set of spacers having four (4) spacers per set is provided and fastened between the coil/He vessels in a similar fashion as for Design Nos. 1 and 2. There are two wedge-shaped spacers per side with each spacer having one tapered side and one straight side. The tapered side of the spacers fastens to the bottom of the coil/He vessel, while the straight side mates with the other spacers' straight side along the centerline of the magnet. Each welded spacer consists of a top, bottom, and two center webs and is fabricated from 310S stainless steel plates. The spacers have been designed to support the attractive em loads that exist between coils during normal operation and have been analyzed from a compression stress, critical buckling load, and elastic stability viewpoint. The fasteners that hold the spacers in place have been sized to support the high shear loads that develop as the em loads tend to squeeze the tapered sections out from in between the coils.

#### d. Main Gravitational Support

The gravitational support is an octagonal welded structure which is fabricated from 310S stainless steel. It fastens to the top of the four low heat leak columns of the dewar and has two (one on each side) welded U-shaped trusses which are fabricated from 310S stainless steel plate stock, extending below it into the domed head of the bottom of the dewar. The pivot shafts, on which the coil/He vessels rotate to facilitate the changing of the coil angle, are welded to these trusses. Basically speaking, the octagonal structure and trusses are box shaped beams.

This structure has been designed to support only gravitational loads because the magnet axis is vertical and as a result the support spacers for the em loads do not transmit any of the em load to it. The gravitational loads consist of: the weight of the coil/He vessels, the attractive em load spacers, the straight beams and tension rods, and the weight of the gravitational support itself. As with Design Nos. 1 and 2, the main gravitational support will probably be made in two pieces and welded together on-site in order to satisfy shipping requirements.

### 3. Dewar Description and Design Criteria

The dewar for Design No. 3 has been designed based on the same applied loadings and design criteria as that for Design Nos. 1 and 2. These are discussed in Section IV-C. A summary of the mechanical characteristics of the dewar for Design No. 3 is given in Table VI-9. This gives the design pressures, weights, materials, and overall sizes of the major dewar components for the magnet system. These components include the room temperature vessel, the radiation shield, the column support system, and the vapor-cooled power lead assembly.

#### a. Warm Bore Tube and Bore Radiation Shield

The warm bore tube size at the entrance and exit is as specified by the customer; i.e., 0.254 m x 0.254 m (10 in. x 10 in.) at the inlet and 0.406 m x 0.406 m (16 in. x 16 in.) at the outlet. The exit dimensions for Design Nos. 1 and 2 were increased in one direction to 0.508 m (20 in.) because there was adequate room to do so. However, this is not the case with Design No. 3 because the coil geometry is a rectangular saddle shape and as a result it engulfs or wraps around the warm bore tube and bore radiation shield. The other aspects of the warm bore tube and bore radiation shield are the same as Design Nos. 1 and 2 with respect to wall thickness, shapes, clearances, and materials. (See Figure IV-24 for the cross section of the warm bore tube and radiation shield at the inlet to the magnet; i.e., it is the same as that for Design Nos. 1 and 2. The warm bore tube and the radiation shield for Design No. 3 were based on the same loadings, design criteria, and method of analysis as that for Design Nos. 1 and 2.

#### b. Room Temperature Vessel and Outer Radiation Shield

The room temperature vessel for this design consists of two parts, one of which is the stationary lower end cover and the other is the removable main

Table VI-9

Summary of Mechanical Characteristics of Dewar for Design No. 3

- I. Room Temperature Vessel
  - A. Design Pressure
    - 1.  $1.03 \times 10^5 \text{ N/m}^2$  (15 psia) Internal
    - 2.  $1.03 \times 10^5 \text{ N/m}^2$  (15 psia) External
  - B. Weight = 16,622 kg (36,570 lbs.)
  - C. Material = 304L SS
- II. Radiation Shield
  - A. Design Pressure
    - 1.  $0 \text{ N/m}^2$  (0 psia) Internal
    - 2.  $0 \text{ N/m}^2$  (0 psia) External
  - B. Weight = 3,659 kg (8,050 lbs.)
  - C. Material = ETP Copper Annealed
- III. Column Support System
  - A. Configuration
    - 1. Four legs consisting of three concentric cylinders
    - 2. All columns have flexural hinges and are designed to compensate for thermal contraction of the He vessel and main support
  - B. Type
    - 1. Inner Cylinder = G10
    - 2. Intermediate Cylinder = Aluminum
    - 3. Outer Cylinder = G10
    - 4. Hinge Material = 6A14V ELI Titanium
  - C. Weight = 142 kg (312 lbs.) ea 3 4 = 568 kg (1,250 lbs.) total
- IV. 4,000 A Lead Assembly
  - A. Weight = 91 kg (200 lbs.)
  - B. Material = OFHC Copper and G10



section and upper end cover. Unlike Design Nos. 1 and 2, the assembly procedure for Design No. 3 (as outlined in Section VI-A) allows the main section of the room temperature vessel to be a single weldment. The main section consists of the top end cover and the midsection, which are welded together to form a single weldment. Depending on the mode of shipping, it can either be fabricated as a single weldment off-site (in which case it could be shipped by rail) or made in two pieces which would then be welded together at the site (in which case it could be shipped by truck). As with Design Nos. 1 and 2, the mating flanges of the main section and the removable end cover would have to be machined in order to obtain a vacuum tight seal. The material, design criteria, and method of analysis of the room temperature vessel for Design No. 3 are the same as that for Design Nos. 1 and 2 and are explained in Section IV-C.

The outer radiation shield is designed to be fabricated in the same fashion as the room temperature vessel. However, additional precautions to prevent damage during shipment must be taken with the outer radiation shield; e.g., temporary braces could be added to the open ends to prevent distortion. The material, design criteria, and method of analysis of the outer radiation shield for Design No. 3 are the same as that for Design Nos. 1 and 2 and are explained in Section IV-C.

#### c. Column Support System

The design of the low heat leak columns for Design No. 3 has been performed in the same manner as that for Design Nos. 1 and 2. Since the overall height and load is essentially the same as that for Design No. 1, the sizes of the cylinders and hinges are the same. See Section IV-C for a more detailed discussion of the column support system proposed for use in this preliminary design.

#### 4. Radiation Heat Load Estimates

The total heat load on the magnet system consists of the sum of the conduction heat leak through the supports, the radiation heat leak, resistive heating in nonsuperconducting electrical joints, and the heat loss due to conduction through and heat generation in the energized leads. For the scale of magnet systems under consideration, thermal radiation and the loss associated with the power leads are the largest heat loads on the system.

The radiative heat load from the room temperature container to the radiation shield and from the radiation shield to the liquid helium container can be easily estimated by calculating the surface area exposed to thermal radiation and by estimating an equivalent heat flux per unit surface area for these two temperature ranges. These estimates have been performed for Design No. 3, and the results are presented in Table VI-10. It was assumed that the radiation shield is cooled by liquid helium boiloff and the equivalent heat flux through the superinsulation from room temperature was 100 milliwatts per square foot. The heat flux from the radiation shield to the superinsulated liquid helium container was assumed to be 5 milliwatts per square foot.

Table VI-10

Estimated Cryogenic Characteristics for Preliminary Design No. 3  
Rectangular Saddle with Iron - 4.2 K

- I. Temperature He Vessel - 4.2° K
- II. Temperature Radiation Shield - 98° K
- III. Total He Inventory - 240 liters
- IV. Boiloff Rate
  - A. Leads - 12 l/hr.
  - B. Radiation Shield, Column Supports, He Vessel - 8 l/hr.
- V. Superinsulation
  - A. Bore
    - 1. Cold Side -  $1.91 \times 10^{-2}$  m (.75 in.)
    - 2. Warm Side -  $2.54 \times 10^{-2}$  m (1.0 in.)
  - B. Outside
    - 1. Cold Side -  $5.08 \times 10^{-2}$  m (2.0 in.)
    - 2. Warm Side -  $5.08 \times 10^{-2}$  m (2.0 in.)

## VII. DISCUSSION OF RESULTS

The main goal of this program was to generate preliminary design characteristics for a superconducting magnet system to be used in an MHD test facility.

### A. PHASE I RESULTS

Alternate conceptual designs were evaluated in Phase I (see Section III) with emphasis on variations in winding geometry, magnetic field level, operating temperature, superconducting material and the use of iron for magnetic field enhancement. Thirteen conceptual designs were generated and considered relative to three combinations of operating temperature and superconducting material. Relative cost estimates were then determined for the 39 combinations which resulted.

The geometric variations considered in Phase I consisted of the solenoid, racetrack, and two saddle configurations. Of the three basic types, the saddle is most efficient in material utilization, followed by the racetrack and the solenoid. This was clearly reflected in material requirements and in relative cost; hence the saddle was retained for consideration in Phase II. Of the two saddle geometries (annular section versus rectangular saddle), the rectangular saddle was less costly and was considered less complex and more suited to the square bore requirements of the MHD system. Phase II was, therefore, to consider the rectangular saddle geometries. The racetrack was significantly higher in relative cost than the saddles; however, it was retained for investigation because of its more simple geometry. Solenoids were attractive from the standpoint of cost for magnets on this scale but were discounted since future large MHD systems would require saddles or racetracks and it was felt that this system should be a step in the development of full-scale systems.

Estimates during Phase I further showed that material requirements increased dramatically with field level over the range considered (5 T to 8 T). After consideration of the potential future requirements for the MHD test facility, the decision was made to concentrate on the 8 T field level in Phase II. At this field level, Phase I estimates showed that the use of iron for field enhancement in the channel was warranted, consequently, iron pole pieces were used in all three Phase II designs.

Review of the Phase I estimates on maximum field levels in the windings combined with estimates on conductor cost for several conductor and operating temperature options indicated that Phase II should concentrate on the use of NbTi superconductor at 4.2 K. In addition, the decision was made to evaluate the potential impact of operation in sub-lambda helium, hence, the operating temperature for one of the Phase II systems was selected as 2.0 K.

The net result of the Phase I effort was the decision to develop preliminary designs for the following 8 Tesla systems using NbTi superconductor and using iron for field enhancement:

1. Racetrack Geometry at an Operating Temperature of 4.2 K
2. Racetrack Geometry at an Operating Temperature of 2.0 K
3. Rectangular Saddle Geometry at an Operating Temperature of 4.2 K

The operating temperatures given should be interpreted as nominal values. For example, 4.2 K is the saturation temperature for liquid helium at one atmosphere. If the system were operated with a liquefier or refrigerator, however, the magnet dewar pressure would probably be slightly above one atmosphere with a corresponding temperature of about 4.5 K. This possibility was accounted for in the designs by selecting an operating current level for the nominal temperature at 70% of the critical current level for the nominal temperature. Operation at a slightly higher temperature is, therefore, not discounted but would result in an operating current to critical current ratio above 70%.

A further constraint was imposed after considering the future requirements of an MHD test facility. All systems were designed such that they could be periodically disassembled to allow alteration of the field profile in the channel. This field profile flexibility may prove invaluable in development of MHD system components.

#### B. CHARACTERISTICS OF PHASE II PRELIMINARY DESIGNS

The magnetic field and dimensional characteristics for the warm bore in each of the preliminary designs are given in Table VII - 1. Note that all systems achieve 8.0 T on the MHD channel axis and that two operating modes are given. The first is a low gradient mode corresponding to a relatively small angle between coils in the system and the other is a high gradient mode with a relatively large angle between coils in the system. The active field lengths are the same for the three systems and the warm bore requirements are satisfied. Note, however, that the racetrack geometry allows the warm bore requirements to be exceeded without penalty in the sense that the outlet dimensions may be opened up to 0.4064 x 0.508 m. (16 in. x 20 in.) even though the requirement is for 0.4064 x 0.4064 m. (16 in. x 16 in.). This arises from the difference in relative conductor position for the racetrack and for the saddle. In the former case, additional bore divergence may occur without alteration of conductor position whereas the rectangular saddle geometry would require an increase in conductor requirements under the same dimensional increase.

The overall dimensions for the three systems are summarized in Table VII - 2. The dimensions for the three cases are similar and, it should be noted, that any of the three magnets could be mounted in any of the cryostats shown with minor alterations. Designs No. 1 and No. 2 are both racetrack coil systems with the main axes of the dewar and MHD channel mounted horizontally. The basic difference is that the main field direction is vertical with system No. 1 and horizontal for system No. 2. The latter case allows for a somewhat less complex procedure to be used in alteration of the angle between coils to change the field gradient. The least complex procedure is believed to result with the cryostat used for design No. 3 since all major pieces may be lifted vertically for disassembly as opposed to being cantilevered as in designs No. 1 and No. 2. The main disadvantage in the third approach is that the MHD channel axis is vertical and, therefore, many components of the MHD system would have to be located below the dewar or suspended above it. Design No. 2 is shown with a 2 K heat exchanger in outline on the top of the system. This heat exchanger could be used on the other system as well if one of those dewar orientations was preferred. A more detailed description of the three systems is presented in the assembly drawings (Figures IV - 6, V - 6, VI - 6) and the related text.

TABLE VII-1

MAGNETIC FIELD AND DIMENSIONAL CHARACTERISTICS IN THE WARM BORE  
FOR PRELIMINARY DESIGN NOS. 1, 2 AND 3

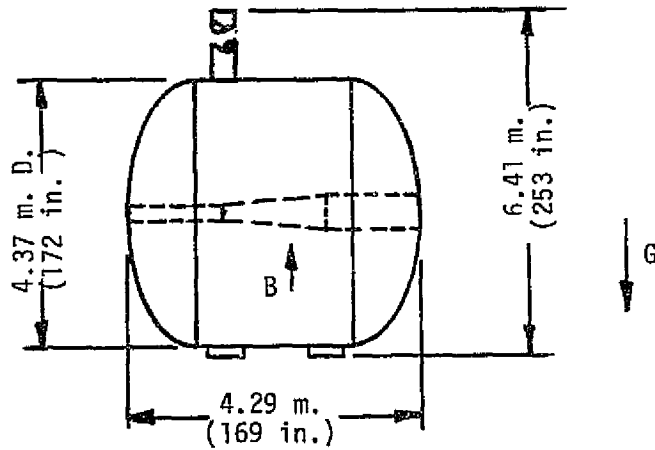
	<u>System</u>		
	<u>1</u>	<u>2</u>	<u>3</u>
Max. Field on Channel Axis (T.)	8.0	8.0	8.0
Magnetic Field at Inlet* (T.)	7.6/7.9	7.6/7.85	8.0/7.36
Magnetic Field at Outlet* (T.)	6.08/4.65	6.29/4.5	6.4/4.5
Active Field Length	1.524 m. (60 in.)	1.524 m. (60 in.)	1.524 m. (60 in.)
Warm Bore Inlet Dimensions	0.254 x 0.254 m. (10 x 10 in.)	0.254 x 0.254 m. (10 x 10 in.)	0.254 x 0.254 m. (10 x 10 in.)
Warm Bore Outlet Dimensions	0.4064 x 0.508 m. (16 x 20 in.)	0.4064 x 0.508 m. (16 x 20 in.)	0.4064 x 0.4064 m. (16 x 16 in.)

\*values given are for low gradient/high gradient operating modes

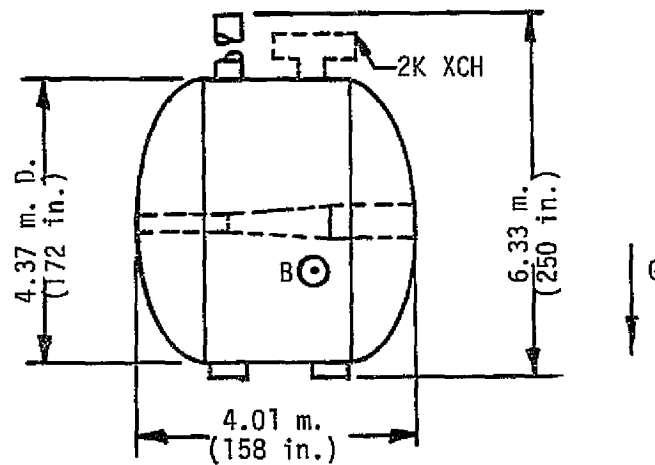
TABLE VII-2

OVERALL SYSTEM DIMENSIONS FOR PRELIMINARY DESIGNS 1, 2 AND 3

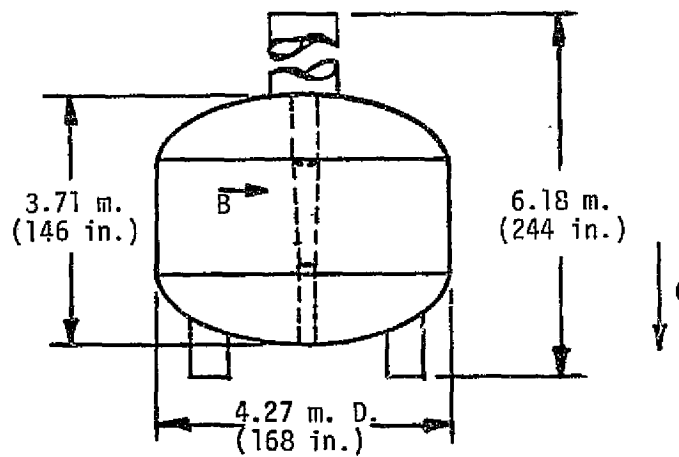
Preliminary  
Design No. 1  
(8 T Racetrack, 4.2 K)



Preliminary  
Design No. 2  
(8 T Racetrack, 2K)



Preliminary  
Design No. 3  
(8 T Rectangular  
Saddle, 4.2 K)



One of the critical areas in superconducting magnet design is the selection of the conductor. In the preliminary design phase this may be done on the basis of past experience. However, in the final design phase to be performed in the future, experimental verification will be necessary. Sufficient experience with design and operation of superconducting magnets in He I at 4.2 K exists to allow stability criterion to be chosen for preliminary design purposes. This hinges on the selection of an allowable heat flux from the surface of the conductor to the liquid helium in the windings and this value was chosen as 0.7 watt/cm<sup>2</sup> for designs No. 1 and No. 3. Design No. 2 operates in He II, however, and considerable uncertainty exists over the selection of a corresponding criterion. As a result two alternates were considered. Design No. 2.1 was based on a choice of allowable heat flux from the conductor surface of 2 watt/cm<sup>2</sup> and design No. 2.2 was based on a value of 4 watt/cm<sup>2</sup>. It is clear that a more detailed analyses and an experimental program would be desirable to verify the choice for designs No. 1 and No. 3, but a supporting program is absolutely essential for design No. 2. The logical time for this effort to be performed would be in a detailed design phase for the system configuration finally selected.

A comparison of the weights of the major components of the preliminary designs is given in Table VII - 3. The effect of geometry is evident through a comparison of designs No. 1 and No. 3. This clearly shows that the rectangular saddle satisfies the user requirements on field and active volume with less conductor because the system is more compact. Structural weight totals for the two systems are comparable. If the designs were carried out for the low gradient mode alone, however, the structural weight for the saddle would be somewhat lower since the transverse support beams could be substantially shorter. Designs No. 2.1 and No. 2.2 illustrate the potential impact of operation at 2.0 K. Depending on the attainable heat flux from the surface of the conductor, designs No. 2.1 and No. 2.2 show a considerable saving in conductor required. This is compensated somewhat by the increase in internal structure required to carry the em loads.

The electromagnetic characteristics of the systems are outlined in Table VII - 4. The lower level of maximum magnetic field at the winding for the rectangular saddle (design No. 3) relative to design No. 1 is a definite advantage and has impact on conductor cost. The racetracks for designs No. 2.1 and No. 2.2 have a somewhat higher value for maximum field at the winding than design No. 1 (also a racetrack) because their average overall current density is higher. A range of current densities is given for the designs to correspond to the maximum and minimum values achieved through grading of the conductor. The total ampere meters required (a measure of conductor cost) for all the racetracks are similar; however, the conductor for designs No. 2.1 and No. 2.2 may be expected to be successively less expensive than design No. 1 because they are substantially smaller due to the high values for heat flux which was assumed. Note that the amp meter requirement for the saddle (design No. 3) is substantially lower than for the comparable racetrack (design No. 1).

After completion of the preliminary designs, cost estimates for the systems were prepared. These are summarized in Table VII - 5. The method of cost estimation is discussed in Section VII - C. Relative values may be expected to be more accurate than the absolute values given.

TABLE VII-3  
 COMPONENT WEIGHT COMPARISON FOR  
 PRELIMINARY DESIGNS 1, 2 AND 3

	<u>1</u>	<u>System</u>		<u>3</u>
		<u>2.1</u>	<u>2</u> <u>2.2</u>	
Geometry	racetrack	racetrack	racetrack	saddle
Operating Temp. ( <sup>o</sup> K)	4.2	2.0	2.0	4.2
Conductor (Kg)	15,900	10,960	6,020	9,770
Structure				
Internal (Kg)	8,770	10,490	11,560	2,905
External (Kg)	31,096	19,965	15,025	38,036
Dewar (Kg)	25,204	24,920	24,920	20,940
Total Wt. (Kg)	80,970	66,335	57,525	71,651



TABLE VII-4

ELECTROMAGNETIC CHARACTERISTICS FOR PRELIMINARY DESIGNS 1, 2 AND 3  
(LOW GRADIENT OPERATING MODE)

	System			
	<u>1</u>	<u>2</u>		<u>3</u>
		<u>2.1</u>	<u>2.2</u>	
Max. Field on Channel Axis (T.)	8.0	8.0	8.0	8.0
Max. Field at Winding (T.)	10.3	11.4	11.4	9.12
Operating Current (A.)	4000	4000	4000	4000
Operating Temp. ( <sup>0</sup> K)	4.2	2.0	2.0	4.2
Stored Energy (10 <sup>6</sup> J.)	171	138	138	62.2
Inductance (H.)	21.5	17.3	17.3	7.77
Overall Current Density (10 <sup>7</sup> A/m <sup>2</sup> )	1.97 - 4.52	1.78 - 6.79	1.84 - 9.66	3.68 - 4.53
Conductor Current Density (10 <sup>7</sup> A/m <sup>2</sup> )	5.21 - 8.16	9.39 - 11.7	14.9 - 20.0	6.03 - 7.38
Total Turns	4894	4824	4824	2652
Total Ampere-Turns (10 <sup>6</sup> A)	19.58	19.3	19.3	10.6
Total Ampere Meters (10 <sup>7</sup> A·m)	12.7	13.03	12.73	7.83

TABLE VII-5  
SUMMARY OF COST ESTIMATES FOR PHASE 2 PRELIMINARY DESIGNS (10<sup>3</sup> DOLLARS)

<u>Designation</u>	<u>1</u>	<u>2</u>	<u>3</u>	
		<u>2.1</u>	<u>2.2</u>	
<u>Geometry</u>	racetrack	racetrack	racetrack	saddle
<u>Central Field (T.)</u>	8.0	8.0	8.0	8.0
<u>Operating Temperature (K)</u>	4.2	2.0	2.0	4.2
<u>Labor Costs:</u>				
<u>Design</u>	325	325	325	385
<u>Fabrication and Installation</u>	484	482	480	509
<u>Labor Subtotal</u>	809	807	805	894
<u>Material Costs:</u>				
<u>Conductor</u>	575	304	267	233
<u>Support Structure</u>	254	254	254	196
<u>Dewar</u>	248	268	268	215
<u>Iron Plug</u>	12	12	12	8
<u>Tooling</u>	194	194	194	181
<u>Miscellaneous and Shipping</u>	231	186	179	150
<u>Subtotal</u>	1514	1218	1174	983
<u>Administrative Expenses</u>	455	365	352	295
<u>Material Subtotal</u>	1969	1583	1526	1278
<u>TOTAL COST</u>	2778	2390	2331	2172

The total cost estimates in Table VII - 5 imply that the saddle system (design No. 3) is substantially less costly than the corresponding racetrack (design No. 1) at the same temperature. Results also indicate that the racetracks at 2.0 K (designs No. 2.1 and 2.2) will be somewhat less costly than the 4.2 K racetrack. Note, however, that no allowance has been made for the cost of refrigeration at either temperature or for supporting development.

The design, fabrication and installation labor costs are essentially the same for all racetracks and are lower than the corresponding line items for the saddle because the latter is a more complex winding and structure. The saddle is, however, much more compact and this is reflected in its relatively low material costs for all line items.

The main differences in material costs between designs No. 1, 2.1 and 2.2 are in the conductor which shows a substantial difference in favor of No. 2.1 and 2.2 and in the dewar where the latter is slightly more expensive to allow for the more complicated interface with the subsystem providing 2 K refrigeration (not a cost component in this study).

#### C. ESTIMATION OF COSTS FOR PRELIMINARY DESIGNS NO. 1, 2 AND 3

The purpose of this section is to outline the manner in which the cost components were estimated for use in Table VII - 5.

##### 1. Labor Costs

###### a. Design

In generating labor costs for the design of the different systems under consideration, it was assumed that the design effort required was primarily dependent on basic geometry. In addition, it was assumed that the results of Phase II could be used as the basis of the design for the next phase which means that the field level, MHD channel "active" length and channel sizes will not change. The design effort was broken into a list of design tasks for the racetrack and saddle systems. For each task the manhours were estimated for engineering, drafting, and engineering assistant labor categories. Manhours in each category were totaled for each system geometry, and a total design cost was generated under the assumption that the unit labor cost to the program was \$30/manhour for engineering, \$20/manhour for drafting, and \$12/manhour for engineering assistants. An allowance was also included for a direct material charge for computer usage.

###### b. Fabrication and Installation

In generating labor costs for fabrication and installation, manhours were estimated for engineering, quality control and technician labor categories for four general tasks for each system. The four tasks included: superconducting coil module fabrication, module and structural assembly, coil-dewar assembly, and assembly to subsystems (e.g., power supply, quench protection circuitry, refrigeration system, etc.).

No allowance was made for initial system shakedown and test nor for site preparation (e.g., foundation, building, utilities, etc.). Manhours were totaled and costs were generated under the assumption that the unit labor cost to the program was \$30/manhour for engineering, \$20/manhour for quality control and \$12/manhour for technicians.

## 2. Material Costs

### a. Conductor

Conductor dimensions and the required copper to superconductor ratio were determined as part of the design effort. Figure VII - 1 illustrates the "built-up" construction which was chosen. This may be expected to be economical for the high copper to superconductor ratios and large quantities required for the magnets under consideration. It consists of a basic multifilament conductor which is then soldered to sufficient copper to achieve the necessary total copper to superconductor ratios. A cost estimate for a unit length of conductor was determined as a function of magnetic field by first estimating the cost per kiloamp-meter for the basic conductor and then incrementing the cost to allow for the additional copper required and for the soldering operation. The cost per kiloamp-meter for the base conductors was estimated as discussed in Section III. No attempt was made to consider the cost or fabrication implications of large quantity production or the need to develop handling techniques. These unit cost estimates were combined with the requirements generated in each design to arrive at a cost estimate for the conductor in each configuration.

### b. Support Structure

Costs for support structure were determined by estimating the weight of structural components and then multiplying by an estimated cost/unit weight. In addition, cutting, machining, welding and fabrication costs were estimated. Structural weights were based on preliminary designs for support sized on the basis of calculated loads of electro-magnetic origin for each case. Components were divided into external structure and internal structure. External structure was defined as coil He vessel, main gravitational, and attractive em load spacers, rods and built-up stainless steel sections such as I beams applied to the outside of the winding envelope. Internal structure was defined as stainless steel strip wound within the windings in parallel with the conductor for internal winding support. Following estimation of weights for external and internal structure, structural material costs were generated assuming unit costs of 1.65 \$/lb. for external structure and 1.0 \$/lb. for internal structure. Structural fabrication costs were then generated in the following manner: \$.10/lb. was used for cutting estimates and was based on a typical cut in a 1" thick stainless steel plate using a plasma arc cutting process. The linear footage of weld was estimated and the following rates per foot were used to estimate the welding costs:

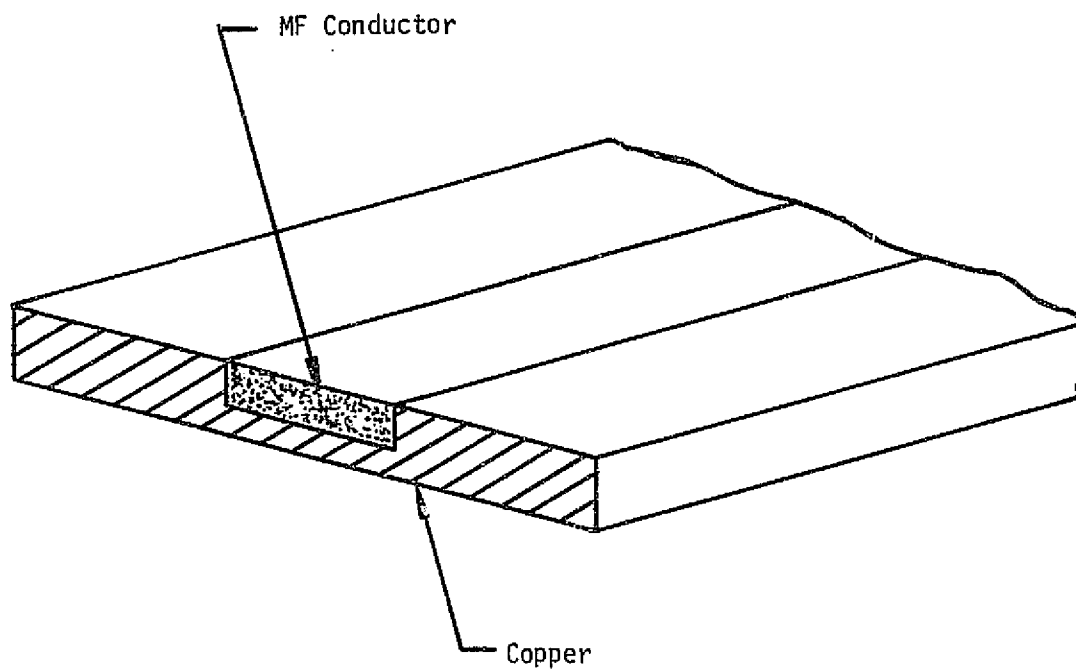


Figure VII-1

"Built-up" Conductor Construction for Multifilament Superconductor in Preliminary Designs 1, 2, and 3.

1" Plate or greater - \$50/ft.  
3/4" Plate or greater - \$40/ft.  
1/2" Plate or greater - \$20/ft.

It was assumed that the cost for the welding jigs are included in the above rates. Machining costs were based on \$20/Hr. for small work and \$200/Hr. for large work. Labor rates were based on \$12/Hr., and \$1/lb. was used for the stainless steel banding to estimate the costs to cut the notches.

c. Dewar

Dewar weights were estimated on the basis of the overall size of the windings plus support structure together with preliminary design calculations involving the necessary shell, plate, and rib thicknesses to support the atmospheric loads with a suitable safety factor. Dewar material and fabrication costs were then determined in the same manner as that used for the support structure.

d. Iron Plug

For each case involving the use of iron, the weight of the iron plugs was determined on the basis of the system dimensions. A cost estimate was then found on the basis of a unit cost assumed to be 0.75 \$/lb.

e. Tooling

For each case (racetrack and rectangular saddle) estimates were made for the cost of tooling in four categories. This included winding fixtures, coil and module handling fixtures, winding machine requirements, and on-site handling and dewar assembly fixtures. Material and fabrication costs were generated in the same manner as that used for support structure. Costs to engineer and design the tooling have been included at \$30/manhour for engineering and \$20/manhour for draftsmen.

f. Miscellaneous

The cost for miscellaneous material items was assumed to be 15 percent of the sum of the material cost estimates for conductor, support structure, dewar, iron plugs, and tooling. Shipping costs were included as miscellaneous costs and were assumed to be 3% of the material cost estimates.

g. Administrative Expenses

Administrative expenses are those costs which arise in procurement of the material and in administering the contracts for each material item. These were assumed to be 30 percent of the subtotal for conductor, support structure, dewar, iron plugs, tooling and miscellaneous.

## VIII. SUMMARY

The following conclusions may be drawn as a result of the preliminary design evaluation performed under this program:

1. The satisfaction of user requirements concerning field level, field profile and field volume may be accomplished with a superconducting magnet system.
2. The concept of alteration of field profile by occasional disassembly of the system to change the angle between coils appears feasible for a test facility on this scale.
3. The racetrack and rectangular saddle winding geometries seem most suitable for this application. The former because of its simplicity and the latter because of its efficient use of material.
4. Cost estimates indicate that superconducting magnet systems on this scale are material intensive.
5. Stabilized NbTi superconductor is the most economical conductor for use at the field and temperature levels of interest to this program.
6. For operation at 4.2 K, the rectangular saddle (Preliminary design No. 3) may be expected to be substantially less expensive than the racetrack system (Preliminary design No. 1). It is also estimated to be less costly than the 2.0 K racetrack designs (Preliminary designs Nos. 2.1 and 2.2).
7. There is little information available concerning design of stable superconducting magnets in He II. Conditions may be expected to be substantially better than in He I. As a result, alternate designs (Preliminary Design Nos. 2.1 and 2.2) were considered for the second configuration at 2.0 K assuming that an improved thermal environment would exist from the stability standpoint. Results indicated that the 2.0 K designs (Preliminary Design Nos. 2.1 and 2.2) would require considerably less conductor than the 4.2 K design (Preliminary Design No. 1); however, this was offset by a requirement for more internal structure in order to limit the stress induced in the conductor by the loads of electromagnetic origin. The net impact was to yield a moderate cost savings for the 2.0 K systems over the 4.2 K system. The cost of refrigeration and of supporting development was not considered.
8. Preliminary design No. 1 utilized a horizontal MHD channel axis with vertical magnetic field; design No. 2 used a horizontal MHD channel axis with horizontal magnetic field; design No. 3 used a vertical MHD channel axis with horizontal magnetic field. All three magnet configurations appear interchangeable in orientation with minor dewar modifications. From the standpoint of alteration of field profile, all configurations

are feasible; however design No. 3 is the least complex, followed by design No. 2 and design No. 1. Design No. 3, however, has the MHD channel axis oriented vertically and this may present more serious interface problems with other components of the MHD generator than the designs with channel axis horizontal.



#### APPENDIX A. EFFECT OF ACCESS PORTS ON THE FIELD IN THE MHD CHANNEL

During the program, interest was expressed in the provision for access into the MHD duct area for instrumentation through ports placed parallel or transverse to the main field direction. The parallel ports must pass through the iron plugs in the bore of each coil. The presence of the hole in the iron produces a field perturbation because of the lack of iron. Estimates of the size of this perturbation were generated for a typical case. The hole dimensions for the case analyzed are shown in Figure A-1. A hole with a .0762 x .1524 m. (3" x 6") cross section was chosen with a gap typical of port location at the magnet system center. A coordinate system is also shown for use in conjunction with results plotted in Figures A-2 to A-5. Each plot is taken in a plane of constant Z and is a plot of the Y component of field as a function of X for several values of constant Y. The field shown is the perturbation profile or the profile which must be subtracted from the actual field present to account for the absence of iron in the hole. In general, the perturbation is small when compared to the expected background field levels of 6 to 8 T.

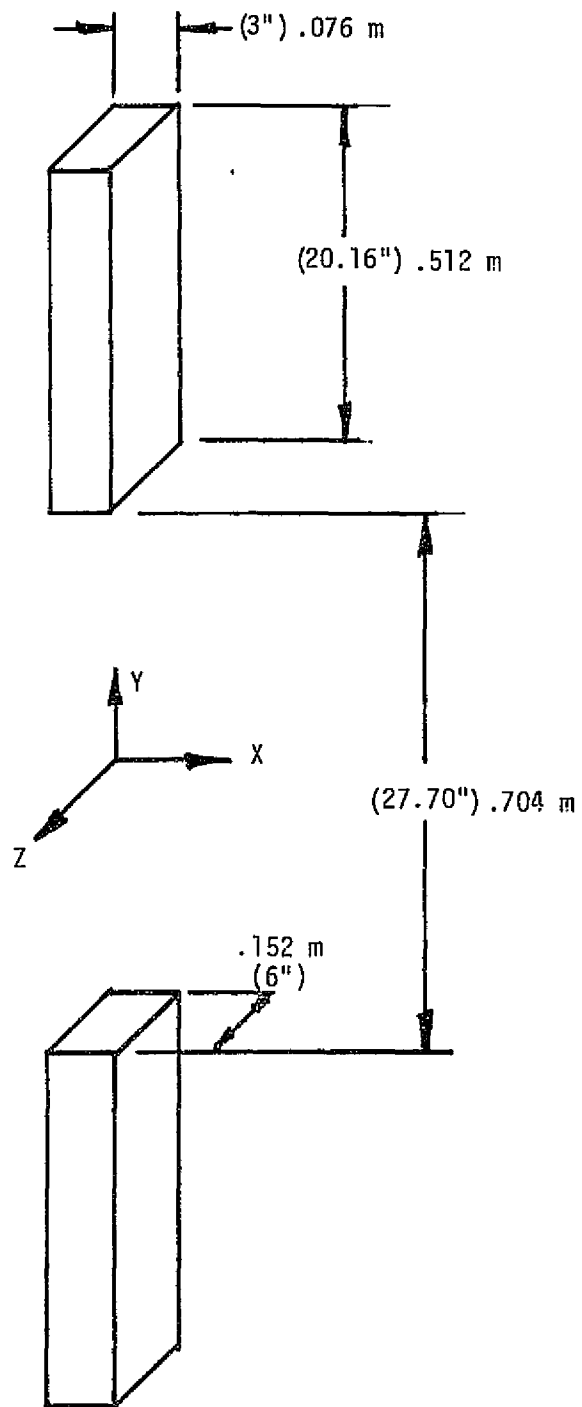


Figure A-1

Sketch of the Dimensions of a Typical Access Hole Through the Iron at the Magnet Center

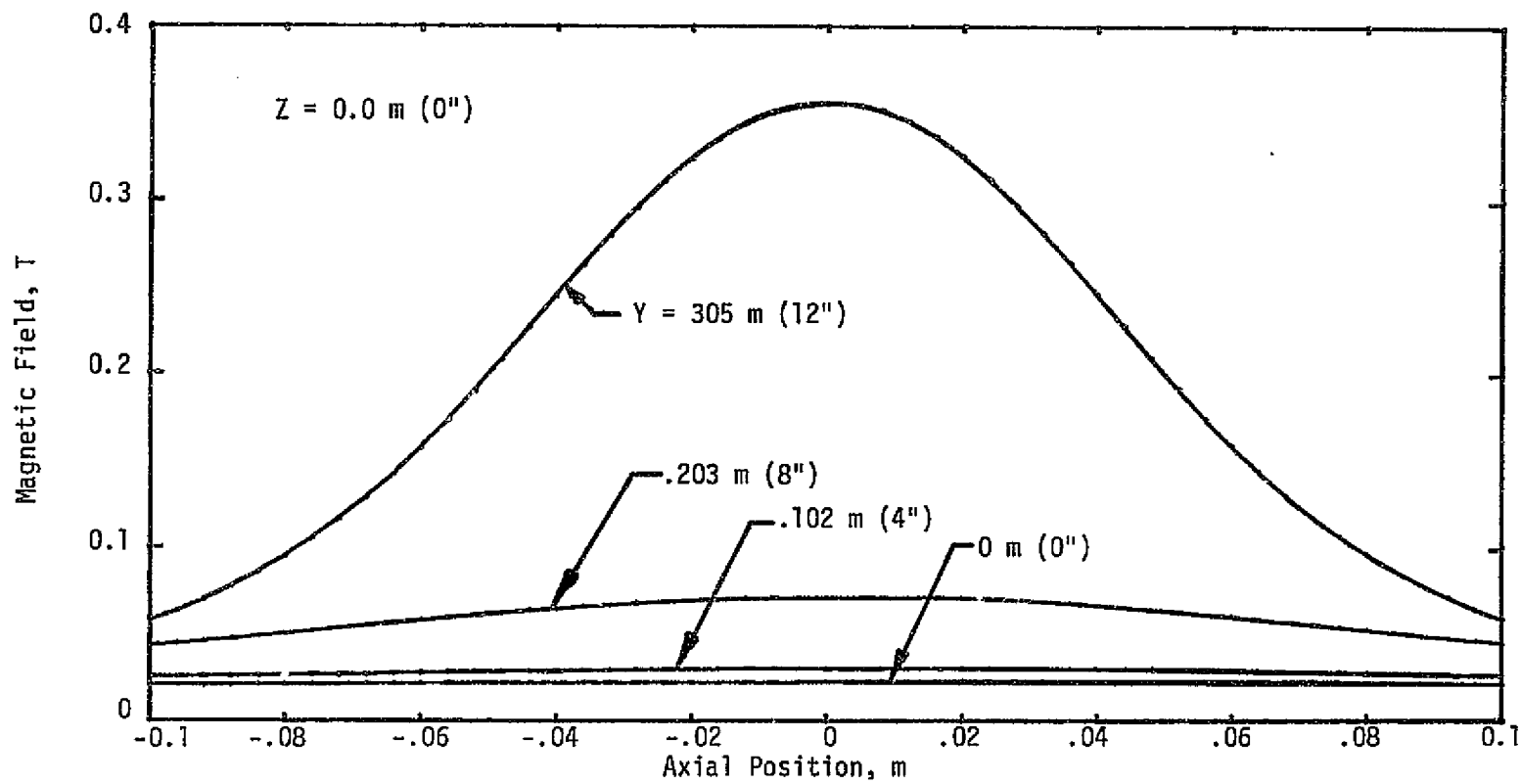


Figure A-2. Plot of Field Perturbation in the Z = 0.0 Plane Arising from an Access Hole with Dimensions as Shown in Figure A-1

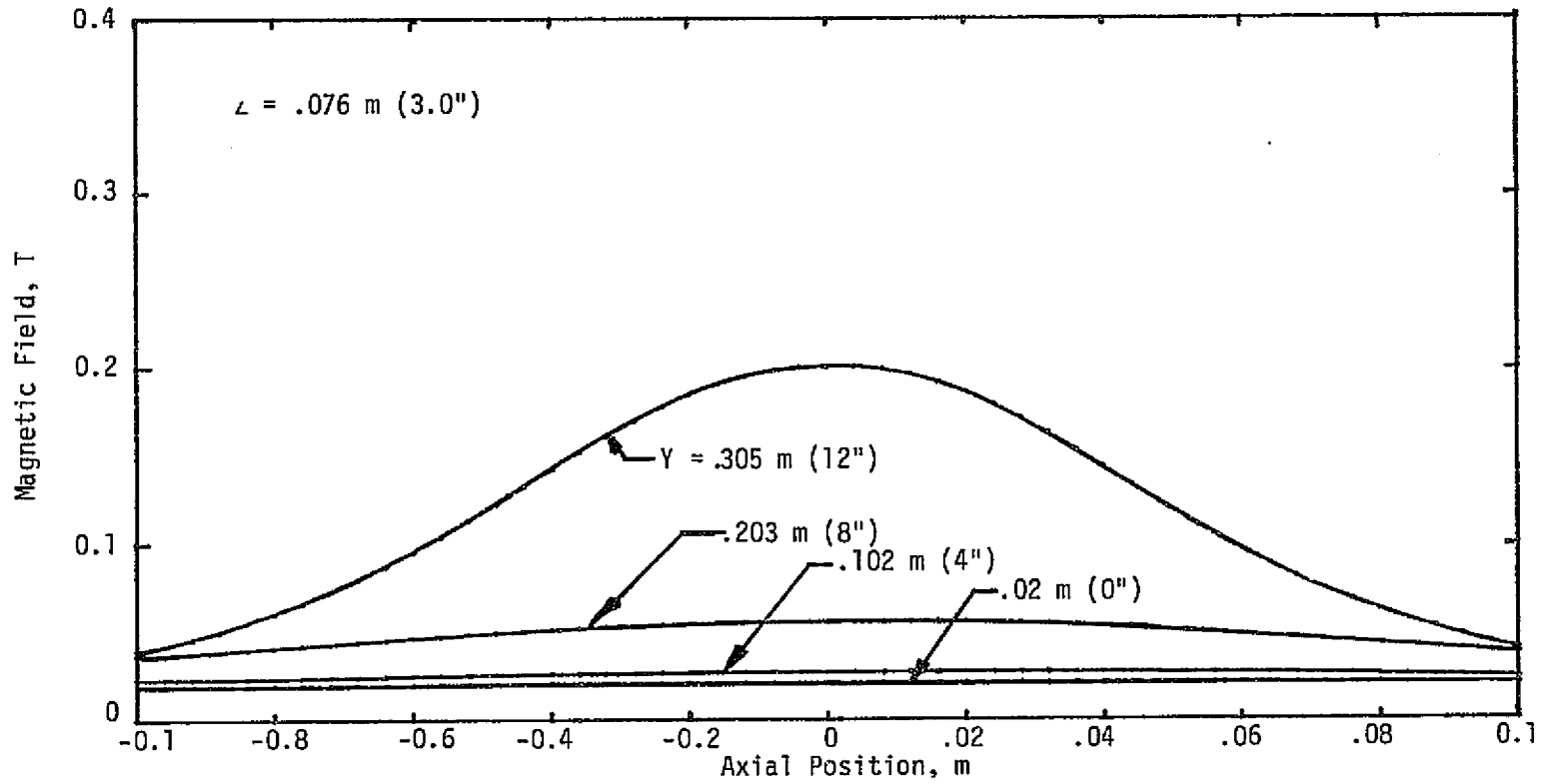


Figure A-3. Plot of Field Perturbation in the Z = .076 m Plane Arising from an Access Hole with Dimensions as Shown in Figure A-1

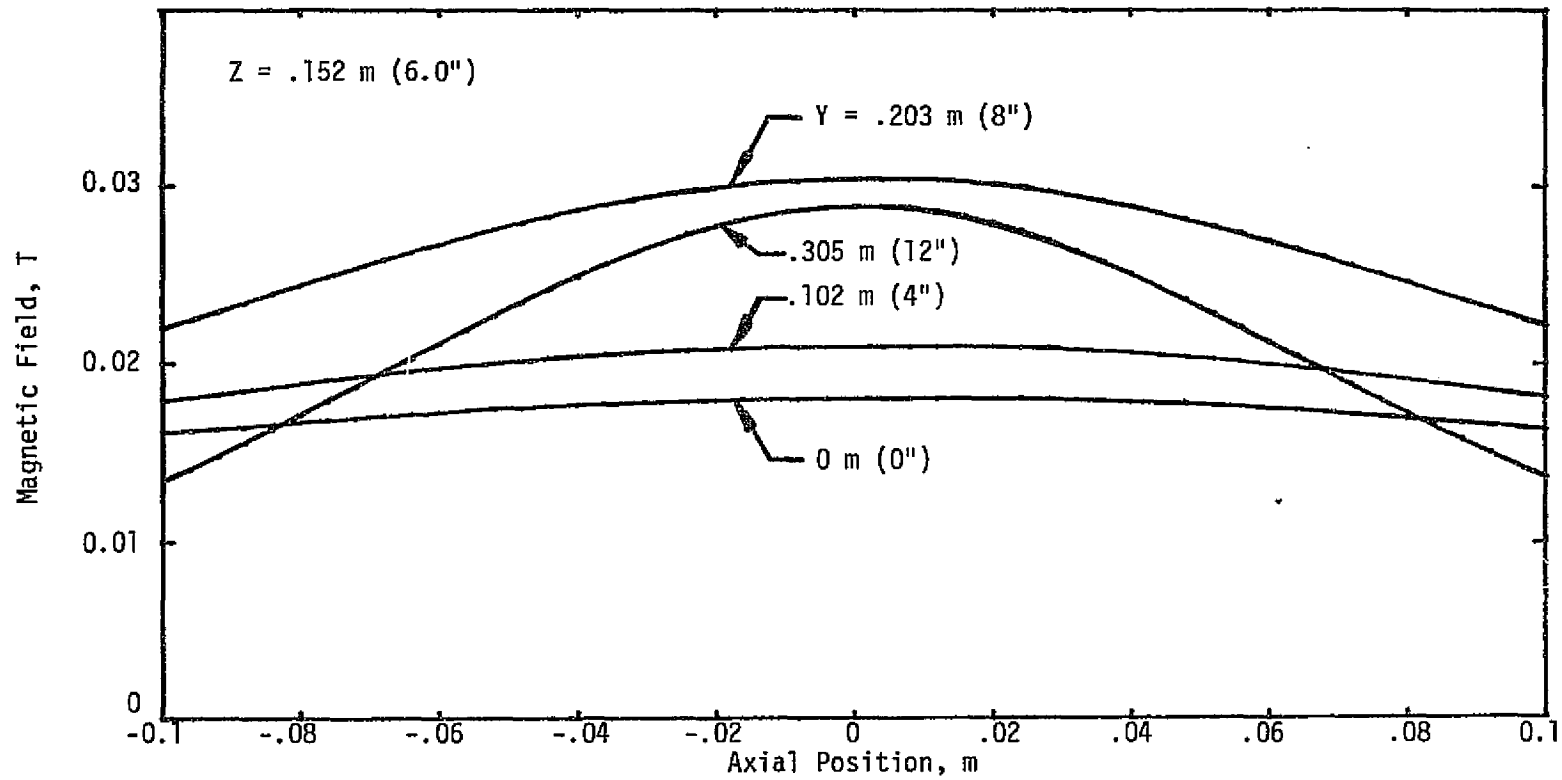


Figure A-4. Plot of Field Perturbation in the  $Z = .152$  m Plane Arising from an Access Hole with Dimensions as Shown in Figure A-1

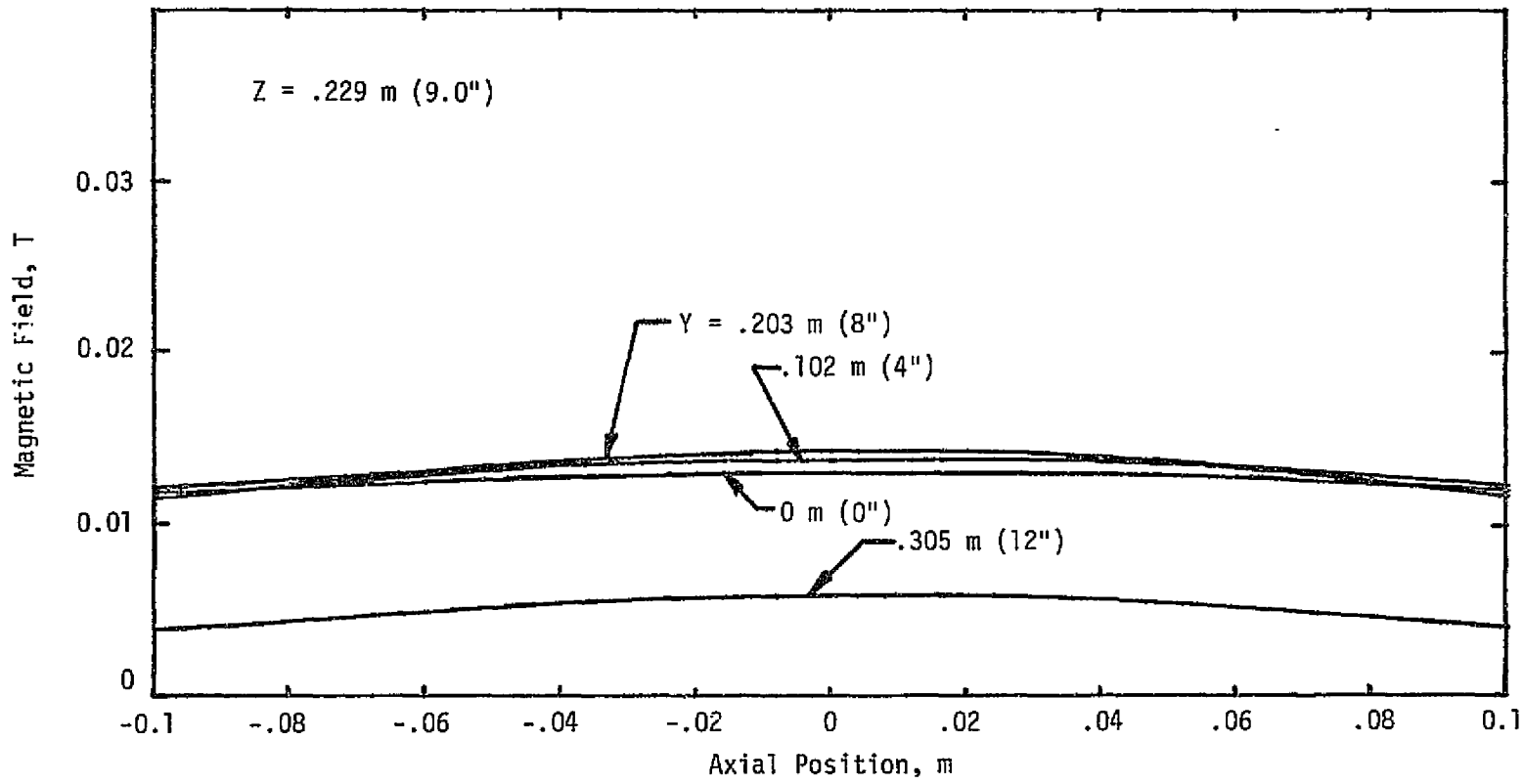


Figure A-5. Plot of Field Perturbation in the Z = .229 m Plane Arising from an Access Hole with Dimensions as Shown in Figure A-1

## APPENDIX B. STABILITY CRITERION

The purpose of this section is to present a brief discussion of stability criteria and the methods used in sizing conductors for use in this preliminary design program. During the final design phase an experimental effort is essential to provide data to verify stability of operation. This may be accomplished with a carefully controlled series of tests employing models of the windings.

### A. ADIABATIC AND DYNAMIC STABILITY

The basic concepts and theory behind adiabatic and dynamic stabilization are well understood; however, the generation of accurate design criteria is hampered by geometrical complexity and the difficulty of including the effects of the temperature dependence of material properties. In many instances data on material properties are scarce or nonexistent.

The basis for adiabatic (sometimes called intrinsic) stability lies in limiting superconductor strand size to the point where the magnetization energy of the superconductor is restricted to a level which would not raise the temperature above the critical value if the energy were dissipated adiabatically within the superconductor. The magnetization energy arises from shielding currents on the filament surface which prevent an applied field from penetrating the bulk of the superconductor.

Limiting size also limits the magnitude of the shielding currents and the energy dissipated when the applied field finally penetrates (i.e., when a "flux jump" occurs). Several discussions<sup>1-4</sup> are available on the subject and generally conclude that it is necessary for the diameter of a superconducting filament,  $d$ , to be less than a critical value, i.e.,

$$d < \frac{\pi}{2j_{ch}} \left[ \frac{\gamma C (T_{ch} - T_b)}{\mu_0} \right]^{1/2} \quad (B-1)$$

where:

$T_{ch}$  = critical temperature at zero current in the presence of a magnetic field

$T_b$  = bath temperature

$j_{ch}$  = superconductor critical current density in the presence of a magnetic field

$\mu_0$  =  $4\pi \times 10^{-7}$  (H/m)

$\gamma$  = density of the superconductor

$C$  = specific heat of the superconductor

Refinements are possible but the above illustrates the basic functional dependence of the properties involved.

The adiabatic stability criterion given above implicitly assumes that, in a multifilament conductor, the superconducting filaments are decoupled (i.e., they act independently in an electromagnetic sense). For this to be achieved it is necessary that the conductor be twisted, otherwise the filaments toward the outside of the conductor will shield an applied field from the inner filaments and the characteristic size for stability is much larger than the diameter of a single filament. Twisting a given conductor is only effective until the rate of change of applied field exceeds a limiting value.

This is best understood by referring to the simplified model in Figure B-1 which shows the cross section of a conductor containing only two superconducting strands in an electrically conducting substrate. The conductor is exposed to a uniform time varying magnetic field (transport currents are neglected). The picture shows the field distribution for the actual geometry as well as for an equivalent developed geometry which shows the magnetic field perpendicular to the plane of the two strands. The induced current is a shielding current and flows in opposite directions in each of the two strands. Only the component of magnetic field perpendicular to the plane of the strands induces circulating currents. The magnitude of the circulating current density in each superconducting strand is:

$$j_s = \frac{\ell^2 \left( \frac{dB}{dt} \right)}{\pi^2 \rho d_s} \quad (B-2)$$

where:

$j_s$  = induced current density in each superconducting strand

$\ell$  = length for 180° of twist

$\rho$  = resistivity of the substrate\*

$d_s$  = diameter of the superconducting strand

B = magnetic field

\*The above equations are the results derived from simplified models which assume a one component matrix with uniform resistivity,  $\rho$ . Refinements are possible to account for geometrical effects and effects of multi-component matrices. The basic concepts are unchanged, however, and would not alter this general discussion.

Note the dependence on rate of change of field. If the induced current density is comparable to the critical current density then the effective current carrying capacity is reduced. The induced eddy currents decay after the magnetic field stops varying in time. This decay-time constant may be interpreted in an alternate fashion as a limiting time in which the external field may change and still not be shielded from the interior filaments. This characteristic time may be shown to be:



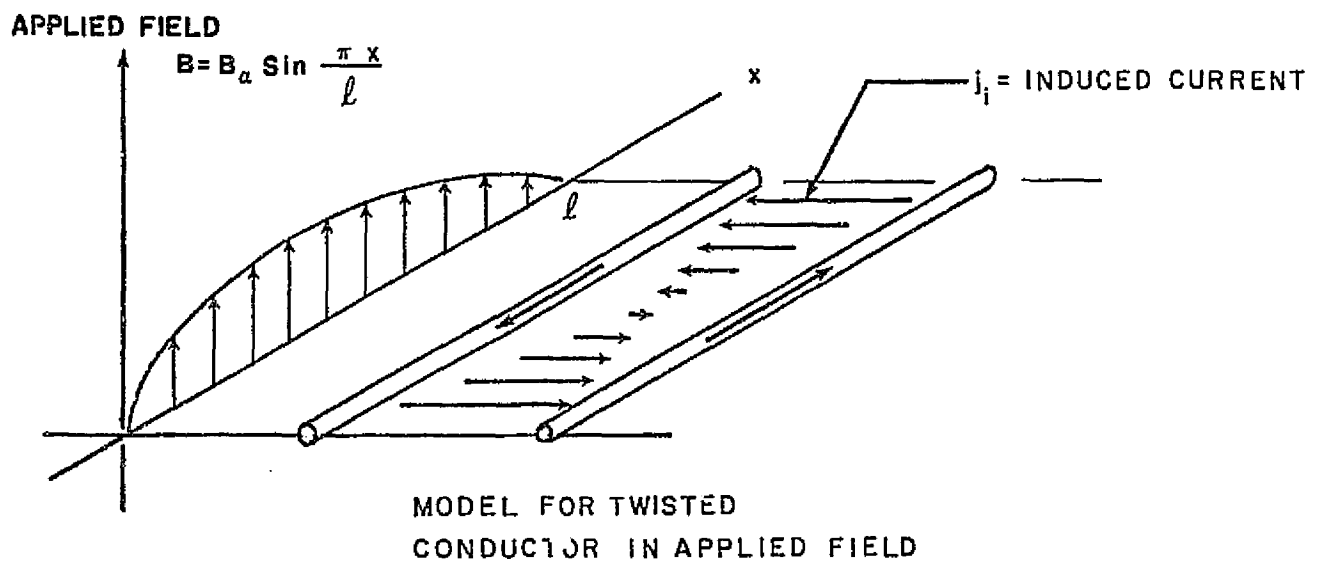
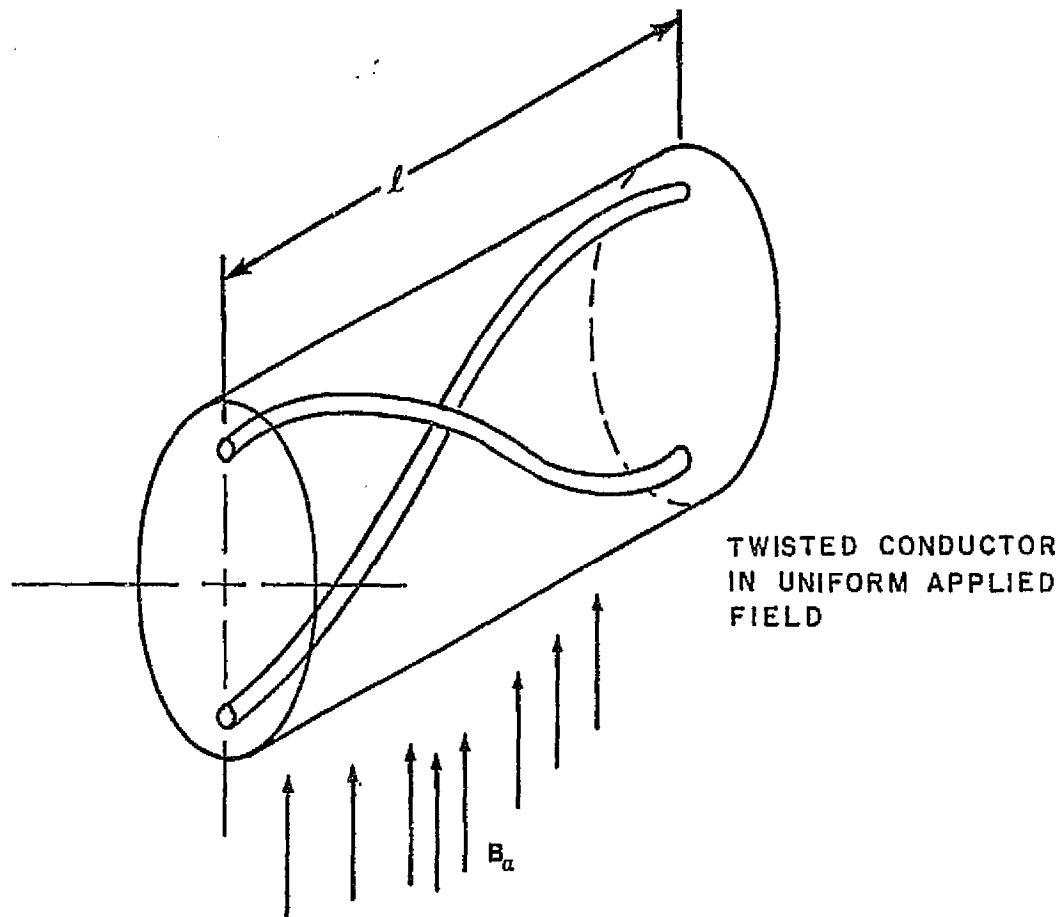


Figure B-1  
Effect of Twist on the Superconductor

$$\tau = \frac{\mu_0 \ell^2}{\pi^2 \rho} \quad (B-3)$$

It can be concluded that untwisted conductors ( $\ell \rightarrow \infty$ ) have shielding currents that do not decay in time. On the other hand, even twisted conductors behave as though they were not twisted for high rates of change of magnetic field. An effectively twisted conductor allows the current to distribute evenly among all the individual strands in the composite and contributes very significantly to the overall stability.

The basic concept underlying dynamic stability was a natural outgrowth of adiabatic stability theory. In the latter it is assumed that the magnetization energy dissipation is localized in the sense that no heat transfer is allowed away from the volume element in which the dissipation occurs. Relaxation of this stringent condition takes into consideration the transient thermal and electromagnetic character of the problem and rapidly becomes mathematically complex. It may be concluded for the purposes of this discussion that a conductor with filaments small enough to be stable in an adiabatic sense will also be stable in a dynamic sense.

For this application, the magnet operates in a dc mode and charge times may be expected to be relatively long (a substantial fraction of an hour). The production of a twisted, multifilament NbTi superconductor with sufficiently high twist rates and sufficiently small filaments to assure adiabatic stability is well within the state of the art of manufacture for this type of conductor. This, however, is stability relative to dissipation of magnetization energy. Other destabilizing sources may exist in a winding and the main thrust of cost effective winding design must aim at nullifying or reducing the destabilizing influence of these sources.

## B. CRYOSTATIC STABILITY

The simplest and most conservative stability criterion is based on a steady state analysis of the conductor terminal characteristics as determined by the superconductor, the stabilizing substrate, and the heat transfer from the conductor to the liquid helium. The terminal characteristics are derived by equating the heat generated by the conductor to the heat transferred from the conductor to liquid helium.<sup>5-9</sup> The main result of this approach is that the temperature in the conductor with all the current flowing in the substrate must be less than the critical temperature (at zero current and at the operating magnetic field) of the superconductor itself. Due to the non-linear character of heat transfer to liquid helium, this requires that conductors and windings be designed for a limit on maximum heat flux per unit area of conductor exposed to liquid helium, assuming that all the current is in the substrate.

In simplified form, this requires that the following be satisfied for a conductor with rectangular cross-section,  $t \times w$ :

$$\text{Heat Balance: } \rho j_{sc} I = 2fq(t+w)(csc) \quad (B-4)$$

$$\text{Geometry: } j_{sc} tw = I(1+csc) \quad (B-5)$$

where:

$\rho$  = resistivity =  $\rho(B,T)$

$B$  = magnetic flux density

$T$  = temperature

$j_{sc}$  = superconductor current density =  $j_{sc}(B,T)$

$I$  = operating current

$q$  = heat flux per unit area

$f$  = fraction of exposed area

$csc$  = copper to superconductor ratio

A refinement of the analysis considers temperature variation across the conductor and leads to the conclusion that the diameter of the superconductor (e.g., for round superconducting filaments) should be less than a certain size so that the temperature drop within the superconductor is small and recovery to the superconducting state is assured if a normal region develops. This size is given by:

$$d < \frac{2}{j_{ch}} \left[ \frac{k(T_{ch} - T_b)}{\rho} (csc) \right]^{1/2} \quad (B-6)$$

where:  $k$  = thermal conductivity of the superconductor

$\rho$  = resistivity of the substrate material

$(csc)$  = ratio of substrate area to superconductor area

Further refinements to the model are possible; however, the above result derived from a relatively simple model indicates the important conductor properties and the sensitivity of the strand size limit to property variation. For example, note that "d", the strand size limit, would vary inversely as the superconductor critical current density but is less sensitive to the other variables because of the fractional power dependence. Again, the satisfaction of equation (B-6) is well within the state of the art of conductor manufacture.

The cryostatic stability criteria (i.e., Equations (B-4) to (B-6)) or their equivalent have been used in the design of the largest superconducting magnets now in existence. The source of uncertainty in design involves the choice of  $q$ , the allowable heat flux from the surface, and whether or not strictly steady state criteria should be utilized since most destabilizing influences may be expected to be transient in nature.

The steady state heat transfer characteristics of liquid helium (i.e., He I) are such that small temperature differences between the surface and the bulk helium are possible only when operating in the nucleate boiling range. The upper limit of the nucleate boiling range is usually defined in terms of the maximum heat flux which can be transferred across a liquid helium-solid interface. If the heat flux exceeds this maximum, transition to film boiling occurs, and there is generally a large increase in the interface temperature difference. The results of experiments carried out to determine the peak nucleate boiling heat flux (PNBF) in small channels are summarized by Johannes.<sup>10</sup> He presents the results in the form of a correlation between the PNBF and the ratio of the length to diameter of the channel. Unfortunately, if this correlation is used for magnets having channel lengths of the order of those of the magnets proposed in this program, it leads to extremely large channel diameters for reasonable heat fluxes. The reason for this is that the experiments from which the data correlation was derived involved heating at the specified flux over the whole length of the channel. Consequently, the quality of the helium progressively worsened in traveling from the inlet to the outlet. Eventually the quality was so poor at the outlet that there was insufficient liquid at the outlet to support nucleate boiling, and it was here that the transition to film boiling first occurred. The quality at which this occurs has been shown to be about 30 percent vapor.<sup>11</sup>

Protection against heating throughout the length of the channel in a real magnet is unrealistic; the object of stabilization is to prevent this extreme situation from happening. Therefore, rather than use the unnecessarily restrictive  $l/d$  versus  $q$  correlation, it is reasonable to base the choice of  $q$  (for conductor sizing purposes) on past experience involving winding models and stability tests, then to proceed to a verification of the design through model testing in the preliminary design phase.

In this program a value of  $q = 0.35$  watt/cm<sup>2</sup> was selected for use in Phase I. This level is quite conservative, but was utilized in Phase I to assure that sufficient winding volume would be allotted to allow for the addition of internal structure during Phase II. Past measurements on winding models have exhibited effective  $q$ 's of about 0.8 - 1.2 watt/cm<sup>2</sup> for local disturbances, primarily because of two and three dimensional effects. As a result, a level of  $q = 0.7$  watt/cm<sup>2</sup> was used to size conductors for use in the He I, 4.2 K, preliminary designs (i.e., Preliminary designs Nos. 1 and 3). The conductor thickness versus magnetic field which results from estimates on this basis are shown in Figures B-2 and B-3.

Preliminary design No. 2 was based on an operating temperature of 2 K which corresponds to He II. In this state, the helium exhibits an essentially infinite thermal conductivity and very little information is available concerning suitable criteria for stability. As a result, conductors were sized for two

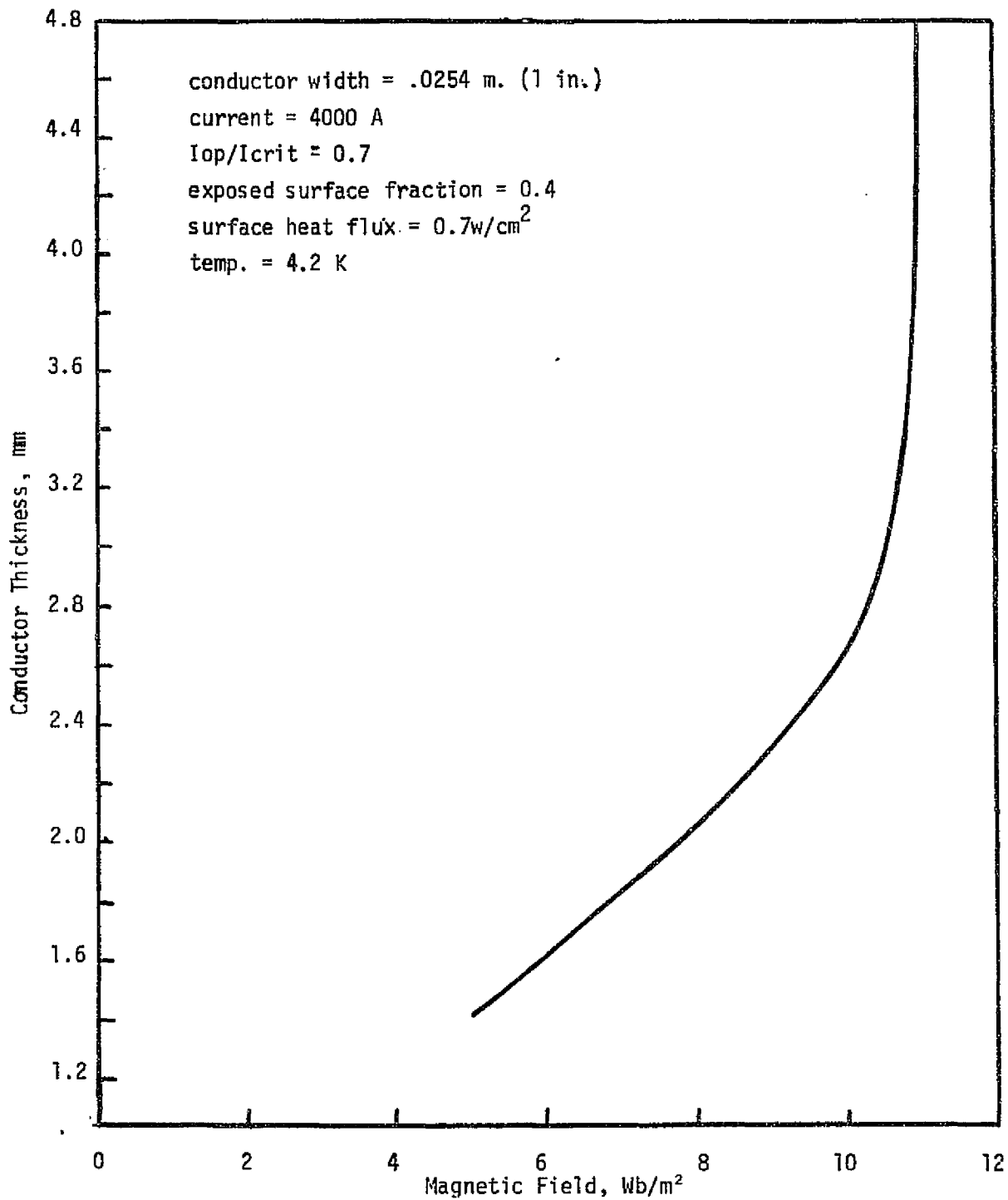


Figure B-2

Conductor Thickness vs. Magnetic Field for Preliminary Designs 1 and 3.

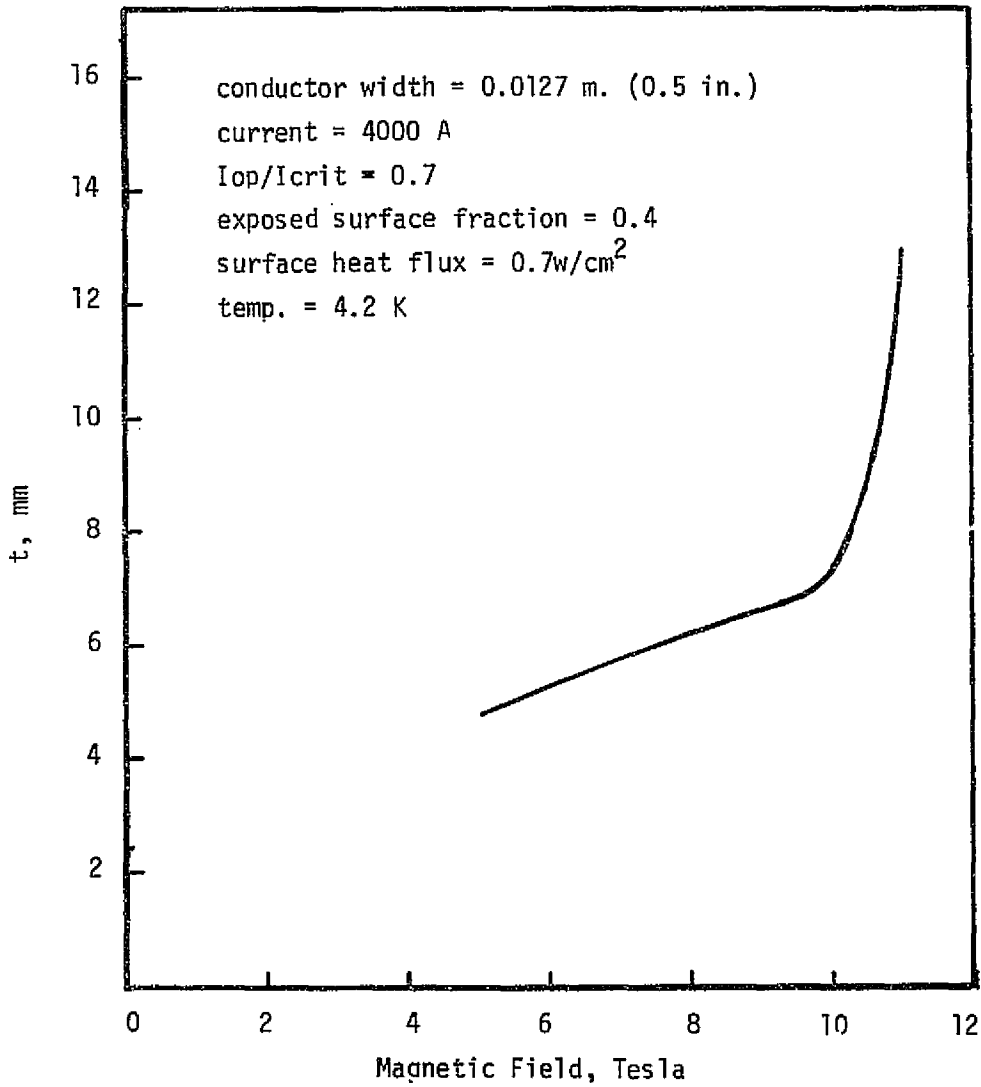


Figure B-3

Conductor Thickness vs. Magnetic Field for Preliminary Design No. 3.

design alternates (i.e., Preliminary designs Nos. 2.1 and 2.2) where it was assumed that the effective  $q$  which could be achieved in each case was 2 watt/cm<sup>2</sup> and 4 watt/cm<sup>2</sup>, respectively. Conductor sizes which result under these assumptions are shown in Figure B-4 which was used for preliminary design No. 2. It must be emphasized that empirical verification is essential in this case and criteria modification may be necessary.

The entire area of stability criteria is in a continuous state of review. The assumptions made have a strong impact on conductor size, copper to super-conductor ratio and overall winding dimensions. This, in turn, has a major effect on cost. Recent efforts on sizing cooling passages have centered on the provision of sufficient liquid helium within the winding to allow a high enough thermal capacity locally to absorb a transient disturbance (e.g., frictional heating due to relative conductor motion). Very little experimental data is available. In the preliminary designs carried out in this effort, the decision was made to provide a minimum local liquid helium volume equal to 10 percent of the local conductor volume. Actual values in the designs range from a low of 10 percent to a high of 34 percent. This may be altered by changes in thickness of conductor insulation or thickness of cooling spacers between layers and should be investigated experimentally during the final design phase.

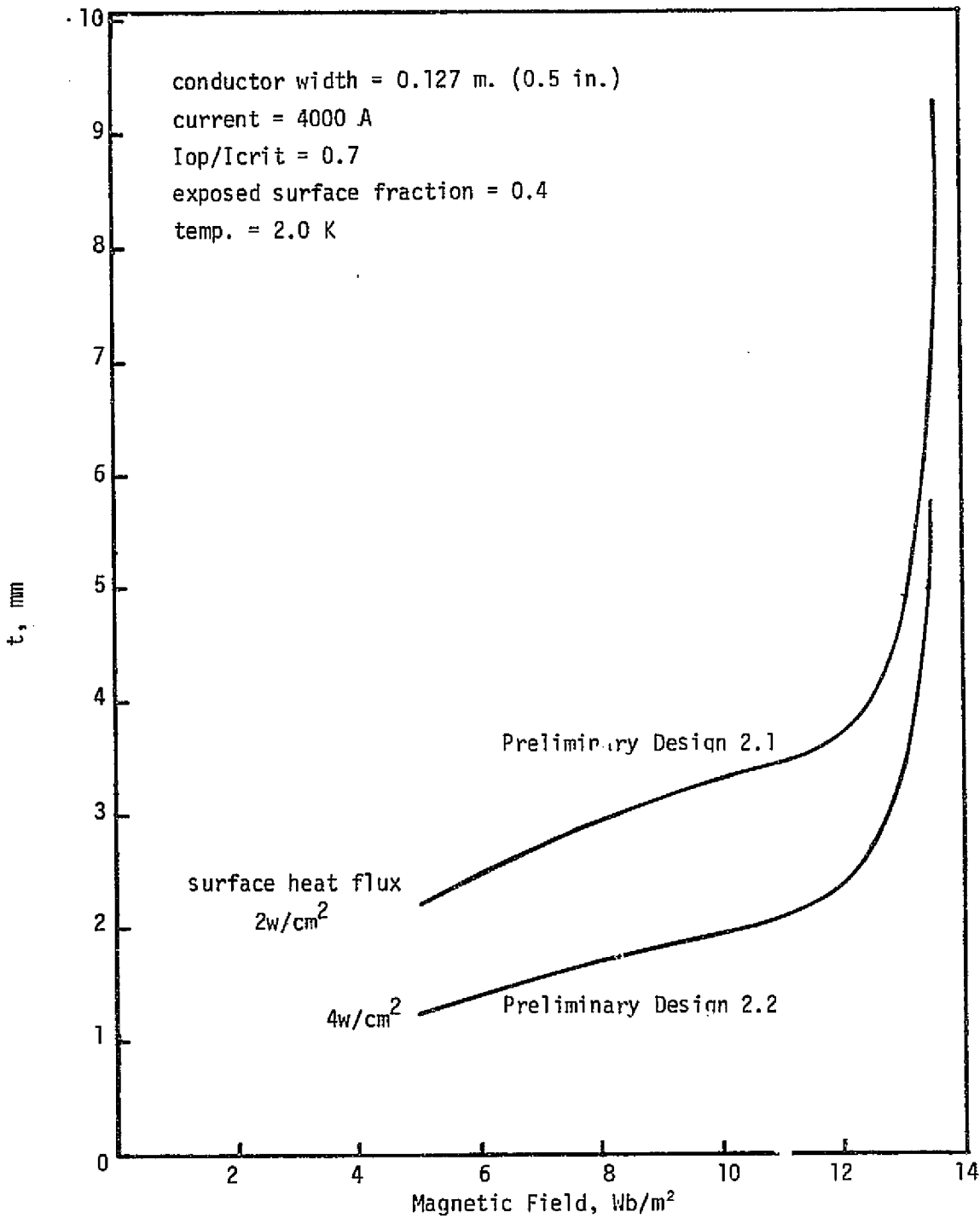


Figure B-4

Conductor Thickness vs. Magnetic Field for Preliminary Design 2.



REFERENCES FOR APPENDIX B

1. Chester, F.F., Rep. Progr. Phys., Vol. 30, p. 561, 1967.
2. Hart, H.R., Jr. Proc. 1968 Summer Study, "Superconducting Devices and Accelerators," Brookhaven National Laboratory, BNL 50155, p. 571, 1968.
3. Wilson, M.N., Walters, C.R., Lewin, J.D., and Smith, P.F., J. Phys.D. Appl. Phys., Vol. 3, p. 1517, 1970.
4. Stekly, Z.J.J., "The Science and Technology of Superconductivity", Vol. II, Ed. by Mathews, W.N. and Edelsack, E.A., Plenum Pub., N.Y. 1971.
5. Kantrowitz, A.R. and Stekly, Z.J.J., "Appl. Phys. Letters," 6, 56, 1965.
6. Stekly, Z.J.J., Thome, R.J., Strauss, B., 1968 Summer Study, "Superconducting Devices and Accelerators," Brookhaven National Laboratory, BNL 50155, p. 748, 1968.
7. Gauster, W.F. and Hendricks, J.B., "Journal of Applied Physics", Vol. 39, p. 2572, 1968.
8. Maddock, B.J., et al, Cryogenics, Vol. 9, No. 4, p. 261, August 1969.
9. Kremlev, M.G., Cryogenics, Vol. 7, p. 267, 1967.
10. C. Johannes, Recent Advances in Heat Transfer to Helium I, ICEC 3, Berlin, 1970.
11. M. N. Wilson, "Heat Transfer to Boiling Liquid Helium in Narrow Vertical Channels," Liquid Helium Technology, Pergamon Press, 1956.